HUDSON-LAMB, D L

THE THERMAL DECOMPOSITION REACTIONS OF GYPSUM, LIME AND LIMESTONE COMPOUNDS

PhD UP 1997

The thermal decomposition reactions of Gypsum, Lime and Limestone compounds

by

Denise Lindy Hudson-Lamb

A dissertation presented in partial fulfilment of the requirements for the degree

Doctor of Philosophy

in

Chemistry

in the Faculty of Science

University of Pretoria

Pretoria, South Africa

October 1997

Promoter: Professor C.A. Strydom

Dedicated to my husband

DAVE

my children

GAVIN, NICOLE AND EDWIN

and my parents

EDDIE AND MAUREEN KRUGER

for their love, support and understanding

CONTENTS

PAGE

PAGE

PAGE

PAGE

PAGE

PAGE

ACKNOWLEDGEMENTS

The author would like to express sincere thanks to:

PROFESSOR C.A. STRYDOM for her guidance, motivation and unfailing support.

MR J.H. POTGIETER for his support of the project and for the XRF analyses.

MRS S. VERRYN for performing all the X-ray diffraction analyses.

The ELECTRON MICROSCOPY UNIT of the University of Pretoria for all their assistance in taking the electron micrographs.

The FRD for their financial support.

PPC for providing all the various samples for this project.

The PERSONNEL of the Chemistry Department of the University of Pretoria for their assistance and support.

MRS H. DE BEER for helping with the typing.

The HAVEMANN family for the linguistic editing.

AND TO ALL who were involved in performing any of the supplementary analyses required for the completion of this dissertation.

SUMMARY

A thermogravimetric study has been undertaken of the thermal decomposition of naturally-occurring Southern African gypsum, pure calcium sulphate dihydrate, synthetically prepared gypsum as well as naturally-occurring Southern African lime, limestone and their pure compounds.

The decomposition reactions proceed without any evidence of detectable melting and the reaction products are identified by using X-ray diffraction analysis and the mass loss percentages on the thermogravimetric curves. Atmospheres used are air, air/water, nitrogen, CO_2, CO_2/air and CO_2/water.

Mass loss versus time curves of the decomposition reactions of the compounds are used to obtain the activation energy values at different heating rates and fractions decomposed. The shape of the curve of the activation energy versus fraction decomposed yields important information on the complexity of the reaction. This information together with the kinetic data, is used to select a kinetic equation which gives the best mathematical description of the individual decomposition reactions. The kinetic description of the individual decomposition reactions differs in the different atmospheres. The partial pressures of CO_2 and water vapour, also influence the thermal decomposition of the compounds.

Keywords: thermogravimetric, dehydration, gypsum, calcium sulphate dihydrate, kinetics, calcium carbonate, limestone, calcium hydroxide, calcium oxide, decarbonation, recarbonation, activation energy.

OPSOMMING

'n Termogravimetriese ondersoek, wat handel oor die termiese ontbinding van natuurlike Suider-Afrikaanse gips, suiwer kalsiumsulfaatdihidraat, sinteties-vervaardigde gips, asook natuurlike Suider-Afrikaanse kalk, kalksteen en hulle ooreenstemmende suiwer verbindings, is onderneem.

Die ontbindingsreaksies verloop sonder enige bewyse van smelting en reaksieprodukte is geidentifiseer deur X-straal diffraksie analise en die massa verlies persentasies op die termogravimetriese kurwes te gebruik. Atmosfere wat gebruik is, is lug, 'n lug/waterdamp mengsel, stikstof, CO_2, 'n CO_2/lug mengsel en 'n CO_2/waterdamp mengsel.

Massa verlies teenoor tyd kurwes van die ontbindingsreaksies van die verbindings is gebruik om die aktiveringsenergie waardes by verskillende verhittingstempos en omsettingsfraksies te verkry. Die vorm van die kurwe van die aktiveringsenergie versus fraksie ontbind lewer belangrike inligting oor die kompleksiteit van die reaksie. Hierdie inligting tesame met die kinetiese data, is gebruik om 'n kinetiese vergelyking te selekteer wat die beste wiskundige beskrywing van die afsonderlike ontbindingsreaksies gee. Die kinetiese beskrywings van die onderskeie ontbindingsreaksies verskil in die verskillende atmosfere. Die parsiële druk van CO_2 en waterdamp beinvloed ook die termiese ontbinding van die verbindings.

Sleutelwoorde: termogravimetriese, dihidrasie, gips, kalsiumsulfaatdihidraat, kinetika, kalsiumkarbonaat, kalk, kalksteen, kalsiumoksied, kalsiumhidroksied, ontkarbonering, herkarbonering, aktiveringsenergie.

CHAPTER ONE

INTRODUCTION

Gypsum (mainly calcium sulphate dihydrate) is used extensively in many industries, especially in cement production. The cement manufacturers add between 3 % and 6 % gypsum to avoid flash (immediate) setting of the cement [1; 2]. Gypsum, which acts as a retarder during the setting reaction of cement, also affects strength development and volume stability in the cement [3]. Gypsum is a mixture of mainly calcium sulphate dihydrate ($CaSO_4 \bullet 2H_2O$), calcium sulphate hemihydrate ($CaSO_4 \bullet 0.5H_2O$) and anhydrous calcium sulphate (anhydrite ($CaSO_4$)). A high hemihydrate content results in false setting of the cement, thus a maximum percentage of the hemihydrate is permitted in gypsum samples for cement manufacture [3]. With a high hemihydrate content, the cement sets too fast and the workers find that the cement mix is not manageable.

It is shown in the literature that the dehydration of calcium sulphate dihydrate proceeds via two reactions [4; 5]

$$CaSO_4 \bullet 2H_2O\ (s) \rightarrow CaSO_4 \bullet 0.5H_2O\ (s) + 1.5\ H_2O\ (g)$$
$$CaSO_4 \bullet 0.5H_2O\ (s) \rightarrow CaSO_4\ (s) + 0.5H_2O\ (g)$$

The investigation of the dehydration of gypsum was undertaken to observe the kinetic differences, if any, between naturally-occurring Southern African gypsum, synthetic gypsum (which is prepared via the reaction of limestone with sulphuric acid as described in the literature [6]) and pure calcium sulphate dihydrate in different atmospheres. The cement silos in Port Elizabeth experience moisture and build-up problems. Cement lumps and build-ups are found on the internal surfaces. This leads to blockages in the silos. Naturally-occurring gypsum is used in the manufacturing of the cement in Port Elizabeth while a synthetically-prepared gypsum is used in Johannesburg. The cement manufacturers may use synthetic gypsum if the

factories are not situated near a gypsum quarry. The kinetics of the dehydration of the various gypsum samples was followed using different atmospheres.

The investigation also includes a kinetic study of the thermal decomposition of naturally-occurring Southern Africa calcium carbonates as well as of pure calcium carbonate, calcium hydroxide and calcium oxide. Calcium carbonate is used as a filler (function is more physical) and lime is used as a cementitious material and plasticiser in order to make the cement more workable (function is more chemical) [8, page 95 and 380]. The limestone and lime also act as water retention agents to prevent too rapid drying when the cement is used for plastering purposes [1, page 38]. Calcium hydroxide is a hydration by-product of cement and it increases initially as the cement fraction hydrates. The calcium hydroxide reacts with additives to form a cement that is sulphate-resistant as it is less easily available for the formation of calcium sulphate.

The major limestone deposits used by the cement industry in South Africa are either primary or secondary deposits [9, page 14]. The primary limestones of South Africa are thought to have been formed in sea water and accumulated in deeper waters. The limestone which concentrated on the sea bed was formed as a result of organic and chemical processes. The formation of chemically deposited limestone, contributed to the formation of primary limestones [9, page 14]. Secondary limestone on the other hand was formed over periods of millions of years by the leaching action of rain water on host rocks such as dolomites and dolorites. Both calcium and magnesium carbonates were dissolved and wherever this solution accumulated in depressions the calcium carbonate crystallised out, but most of the magnesium carbonate, being more soluble, was removed with the water overflowing from the depressions. If the water was completely trapped then both calcium and magnesium carbonate crystallised out, giving rise to secondary dolomites or high magnesia limestones [9, page 15]. Pretoria Portland Cement (Cleveland) uses a mixture of South African

secondary limestone that is quarried at Beestekraal and at Pienaars River. The Beestekraal limestone has a higher magnesium oxide content and the Pienaars River limestone has a much higher silicon dioxide content. A mixture of the two gives a limestone that can be used as a filler in cement with a more acceptable magnesium oxide and silicon dioxide content. The kinetic study was performed to observe the thermal decomposition of pure calcium carbonate, Pienaars River - and Beestekraal limestone and limestone obtained from Lime Acres (which has a low silicon dioxide and magnesium oxide content but some manganese(III) oxide) in various atmospheres, namely air, carbon dioxide, a mixture of carbon dioxide and air, and "wet" atmospheres. The carbonation reactions were also studied as these undesired reactions between cement and carbon dioxide in a humid atmosphere may affect the flowability and strength of the cement and may cause other setting problems [7].

Among the techniques used in this study was, firstly, thermal analysis. The thermal decomposition reactions and reaction mechanisms of the above-mentioned compounds were investigated using thermogravimetry. The purity of the samples can be determined from the mass losses observed.

X-ray powder diffraction and electron microscopy techniques were used to identify the compounds and any impurities that may be present. X-ray fluorescence analyses were performed to obtain the percentage component analysis of each compound. Surface areas were also determined for each sample since the size of the particles may also influence the kinetics of the decomposition reactions. This investigation was performed on ground, mixed and sifted powdered samples with diameters between 45 and 106 μm.

CHAPTER TWO

KINETIC ANALYSIS

The aim of kinetic analysis is to determine the kinetic model and its parameters for the decomposition reaction which describes the experiment in the best way. Kinetic analysis comprises:

a) the choice and significance test of a model, and
b) the determination of the kinetic parameters.

Isothermal methods are not employed here as some of the reactions proceeded for more than 25 days without reaching a final constant mass loss. Also dynamic methods allow for the model-free approximation of the activation energy to be carried out by applying the Ozawa-Flynn-Wall analysis. Dynamic, non-isothermal methods were thus used to obtain the information on the kinetic model and its parameters [10]. The simultaneous kinetic analysis of several scans obtained with different heating rates with the Netzsch Thermokinetic Software Program overcomes the obvious shortcomings of single-step analysis [10; 11; 12].

The thermal decomposition of a solid is represented by

$$A(s) \rightarrow B(s) + C(g)$$

where A is the reactant in the solid phase
and B is the product in the solid phase
and C is the product in the gaseous phase [13, page 43].

The selection of the proposed reaction mechanism depends on the processes controlling the rate of product formation [13, page 6]. Reactions are generally controlled by:

1) Nucleation and growth of nuclei and interference - the nucleation

process involves conversion of a small volume of reactant into a stable particle of product and continued reaction (growth) occurs at the interfacial zone of contact between these two phases [13, page 42]. The initially generated germ nucleus develops into a growth nucleus, which increases in size through the advance of the reactant - product interface into the bulk of the solid [14, page 59].

2) Diffusion - in these reactions the phase boundary is present with all its limitations on the rate. The overall rate is determined by the movement of one or more reactant species to, or a product from, a reaction interface; alternatively, heat transfer may also play a role [12, page 68]. The diffusion rate through the product makes a significant contribution to the rate of the reaction [14, page 64].

3) Complete or partial liquifaction - where the interface boundary disappears and any diffusion problems are drastically altered [14, page 66].

In Table 2.1 is the list of the solid state decomposition reaction types where α is the fraction decomposed and t is the time of heating [13, page 74].

Table 2.1: Reaction types and the corresponding reaction equations

TYPE OF REACTION	Integral form (kt=)
Power law	α^n
1-Dimensional diffusion controlled	α^2
Power law	$\alpha^{1/2}$
Power law	$\alpha^{1/3}$
Power law	$\alpha^{1/4}$
Mampel intermediate law	$[1-(1-\alpha)^{1/2}]$
Phase boundary (spherical symmetry)	$[1-(1-\alpha)^{1/3}]$
First order	$-\ln(1-\alpha)$
Diffusion	$[-\ln(1-\alpha)]^{1/1,5}$
Erofe'ev random nucleation	$[-\ln(1-\alpha)]^{1/n}$ where n = 2;3;4
2-Dimensional diffusion controlled	$(1-\alpha)\ln(1-\alpha) + \alpha$
3-Dimensional diffusion controlled (Ginstling-Brounshtein)	$1 - 2/3\alpha - (1-\alpha)^{2/3}$
Jander	$[1-(1-\alpha)^{1/3}]^2$
Second order	$(1-\alpha)]^{-1} - 1$
One-and-half order	$(1-\alpha)^{-1/2} - 1$
Prout-Tompkins	$\ln[\alpha/(1-\alpha)]$
Exponential law	$\ln\alpha$

Most reactions do not occur as single-step processes, but as multiple-step reactions. The programme offers combinations of the single reactions for complex models - see table 2.2.

Table 2.2: Combining types of single-step reactions to form complex reactions

KEY: s = single; d = double; t = triple; f = following; c = consecutive; p = parallel; i = independent.

A → B	s	A→B→C→D	t;f;f
A → B → C	d;f		t;f;c
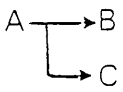	d:c		t:f;p
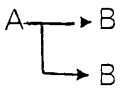	d:p	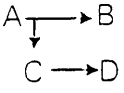	t:c;f
A → B C → D	d:i	A → B C→D → E	t:i;f
A → B C → D E → F	t:i;i	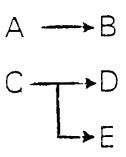	t:i;f

The determination of kinetic data involves a series of thermogravimetric decomposition curves using different heating rates. In solid state decomposition various stages can be identified [14, page 41]. They are:

First stage - nucleation

Second stage - nuclei growth and interface advancement

Third stage - a process of decay where the reaction interface decreases with time.

Kinetic parameters are obtained with the application of the Arrhenius equation:

$$k = A \exp(-E_a/RT)$$

where

A is the pre-exponential factor,

E_a is the activation energy,

R is the gas constant,

k is the rate constant at temperature

T on the absolute temperature scale.

The reactions controlled by (1) growth of nuclei and interface and their corresponding kinetic equations are given by the -

(a) Power law ($kt = \alpha^n$):

Reactions are described up to the point where $d\alpha/dt$ is a maximum. The equation takes into account the possibility of overlapping decomposition zones in the initial stages of decomposition. A constant rate of nuclei growth is superimposed upon nucleation according to the power law. The integer, n, is $n = \beta + \lambda$ where β is the nucleation stage and λ is the dimension of nuclei growth [13, page 50; 14, page 62).

(b) Exponential law ($kt = \ln \alpha$):

This reaction is also described up to where $d\alpha/dt$ is a maximum. This expression is denied for a "chain type" reaction where there is no overlap but only a possibility of branching nuclei. The important factor is the growth of the length of nuclei which is assumed to be at a constant rate and not the formation of new germ nuclei [14, page 62].

(c) Prout-Tompkins law ($kt = \ln[\alpha/(1-\alpha)]$):

This law considers the mechanism of the appearance of branching nuclei with interference between the nuclei during growth. The formation of nuclei is not considered to be important here, since the formation of new nuclei at a large number of potential sites appears at a constant rate ($\beta = 1$) [14, page 62]. Branching varies inversely with time.

(d) Erofe'ev Equation ($[-\ln(1-\alpha)]^{1/n}$ where n = 2; 3; 4):

This equation is valid for the range : $0.05 < \alpha < 0.9$. n = 2 corresponds to two dimensional growth; n = 3, implies three-dimensional growth and n = 4 corresponds to two stage nucleation [14, page 63].

The interface remains intact. Compact nuclei overlap leading to a contracting interface of a complex shape. Particle size distribution will influence the kinetic characteristics.

(e) Mampel intermediate law ($kt = [1-(1-\alpha)^{1/2}]$):

This law describes a system where the decomposition rate is continually decreasing. The law is related to the radius of the particles being decomposed. The equation is based on surface nucleation, surface growth and interface advancement towards the centre of spherical particles ("contracting sphere model"). For two-dimensional growth, the model becomes the contracting area law [14, page 63].

(f) First order decay law ($kt = -\ln(1-\alpha)$):

This law also holds for $d\alpha/dt$, a maximum and generally at the end of the decomposition reaction. It can be seen as a special case of the Erofe'ev equation with n = 1. Mampel deduced that this equation should hold over the decay period of decomposition, where it is dealing with relatively small particles. It is based on the nucleation of particles by an exponential law, followed by rapid two-dimensional growth . These smaller particles may also be produced by strain imposed on the system caused by change in the molecular volume of the reactant and product [14, page 64].

The reactions controlled by (2) diffusion. In this case a phase boundary is present and the rate of diffusion influences the overall rate of the reaction [14, page 64] -

(a) Parabolic law or 1-dimensional diffusion controlled law ($kt = \alpha^2$):
The surface area remains constant and it is characteristic that as the reaction rate decreases the barrier thickness increases.

(b) 2-dimensional diffusion ($kt = (1-\alpha)\ln(1-\alpha) + \alpha$):
This law allows for the product volume to differ from that of the reactant.

(c) 3-dimensional diffusion ($kt = [1-(1-\alpha)^{1/3}]^2$) :
This law allows for a spherical particle to be represented by the modified contracting cube equation (Jander equation).

(d) Ginstling Brounshtein (3-dimensional diffusion law) ($kt = 1 - \frac{2}{3}\alpha - (1-\alpha)^{2/3}$):
This is a more detailed form of the Jander equation. Temperature is very important for diffusional processes [14, page 65]. As the temperature increases, the following three phenomena are influenced:
(1) adhesion between the particles
(2) surface diffusion and
(3) bulk diffusion [14, page 65].

For the reactions where (3) liquefaction takes place, the interface boundary disappears and the rate of diffusion can be drastically altered. Two or three kinetic processes can be expected [14, page 66]. The overall reaction may be complicated by the fact that only partial liquefaction may occur in a certain restricted zone and decomposition may be occurring in other parts of the crystal by phase boundary controlled mechanisms.

CHAPTER THREE

CALCIUM SULPHATE

This study differentiates between calcium sulphate dihydrate which is pure $CaSO_4 \bullet 2H_2O$ and naturally-occurring gypsum (referred to as gypsum) which contains some dihydrate, hemihydrate and anhydrite of calcium sulphate as well as other impurities.

3.1 CRYSTAL STRUCTURES OF CALCIUM SULPHATES

In the $CaSO_4$ - H_2O system, three types of compounds have been recognised namely, $CaSO_4 \bullet 2H_2O$; $CaSO_4 \bullet 0.5H_2O$ and $CaSO_4$ [15]. Several different structural forms have been postulated for each of these three compounds in the literature.

At least three forms of $CaSO_4 \bullet 0.5H_2O$ and four forms of anhydrous $CaSO_4$ have been proposed [16; 17]. There has also been an extended argument as to whether the water in the hemihydrate is combined in a definite proportion, as in ordinary hydrates such as those of copper sulphate, or in continuously varying proportions, as in certain hydrated silicates [15]. The structural forms will be discussed later in this chapter.

3.1.1 Dihydrate ($CaSO_4 \bullet 2H_2O$)

The dihydrate usually occurs in nature as a fine-grained, compact mass of small crystals. It also occurs as large transparent crystals of selenite [18]. Synthetic gypsum can be prepared by mixing $CaCO_3$ (limestone) with diluted H_2SO_4 [6] as is done at PPC Cleveland's Jupiter cement plant:

$$CaCO_3(s) + H_2SO_4(aq) \rightarrow CaSO_4 \bullet 2H_2O(s) + CO_2(g)$$

The crystal structure of $CaSO_4 \bullet 2H_2O$ (see Figure 3.1.1) is described as being monoclinic prismatic in form with 4 or 8 molecules in the unit cell [19].

The crystal lattice is made up of calcium atoms and sulphate groups

separated by sheets of water molecules. The water molecules occupy important positions in the lattice and it is almost impossible to remove any water without destroying the lattice. Thus any lower hydrate should have a different structure from that of the dihydrate form [18].

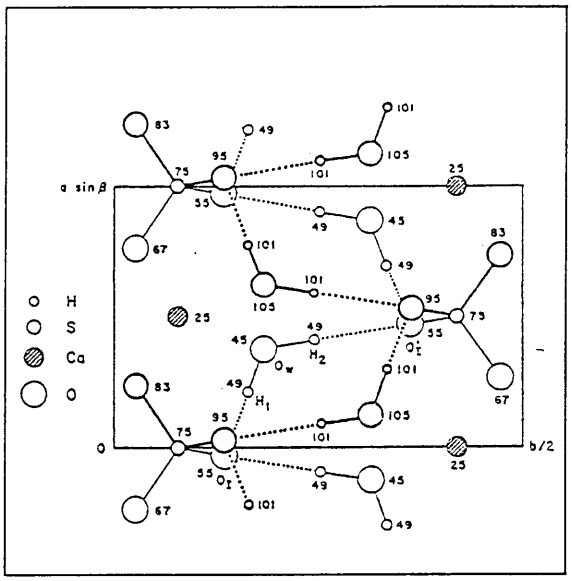

Figure 3.1.1 The crystal structure of $CaSO_4 \bullet 2H_2O$

3.1.2 Hemihydrate ($CaSO_4 \bullet 0.5H_2O$)

$CaSO_4 \bullet 0.5H_2O$ has been described as being a deformed monoclinic structure with 12 molecules of $CaSO_4 \bullet 0.5H_2O$ in a unit cell [20]. The cell dimensions are a = 12.691 Å; b = 6.932 Å; c = 12.028 Å; β = 90.18° [21].

The lattice is very stable because the calcium atoms and sulphate tetrahedrons are arranged in such a way that there are strong forces between the calcium ions of one layer and the SO_4^{2-} groups of the adjacent layers. The lattice has channels in which the water molecules are situated. The forces between the water molecules in these channels and the calcium ions and sulphate groups are weaker than the forces between the calcium ions and sulphate groups. Thus, part of the water of the hemihydrate can be removed without seriously disrupting the crystal structure [14, page 4]. The hemihydrate (α- $CaSO_4 \bullet 0.5H_2O$) crystal lattice can accommodate greater or smaller amounts of water than required by the formula without serious alteration of the crystal structure. There is also evidence for the

existence of a less stable form called ß-$CaSO_4$•$0.5H_2O$ [15, page 5]. The α- and ß-$CaSO_4$•$0.5H_2O$ have the same X-ray powder diffraction pattern. According to Kuntze [22], ß-hemihydrates have an exothermic peak at approximately 350 °C and in α-hemihydrate, an exothermic peak is observed below 250 °C. Kuntze [22] did not offer an explanation for this observation. In another study, it was reported that α-hemihydrate gives a sharp exothermic peak at about 200 °C, while ß-hemihydrate shows no sharp exothermic peak at this temperature but a broad exothermic curve at 250 °C [23].

α-Hemihydrate is prepared by dehydration methods which permit recrystallisation i.e. by solution processes or autoclaving. ß-Hemihydrate is prepared by atmospheric dehydration independent of the ambient water vapour pressure [22]. The water molecules are located within the coordination sphere of the Ca^{2+} ion (nine- coordinated) and exhibit long-range ordering. This is for both forms of hemihydrate. To minimise the electrostatic repulsion, only 67 % of the available water sites are occupied on the average [24].

3.1.3 Anhydrite ($CaSO_4$)

Three structural forms of anhydrous calcium sulphate have been reported. The structural forms are soluble anhydrite (γ-$CaSO_4$), insoluble anhydrite (ß-$CaSO_4$) [25] and monoclinic α-$CaSO_4$ [26]. Some authors reported that monoclinic α-$CaSO_4$ is the stable form from about 1200 °C to 1245 °C, where sulphate decomposition starts [26]. γ-$CaSO_4$ forms at temperatures between 75 ° and 105 °C [16]. According to Flörke [25], ß-$CaSO_4$ is stable over an extensive temperature range (< 1000 °C) and α-$CaSO_4$ is present at temperatures above 1100 °C.

Contradictory reports exist on the existence of ß-$CaSO_4$. Kelley [15] reported an α- and ß-soluble anhydrite and Gay [16] and Flörke [25] reported only one soluble polymorphic phase, γ-$CaSO_4$.

The unit cell of hexagonal γ-$CaSO_4$ contains 4 molecules (figure 3.1.3).

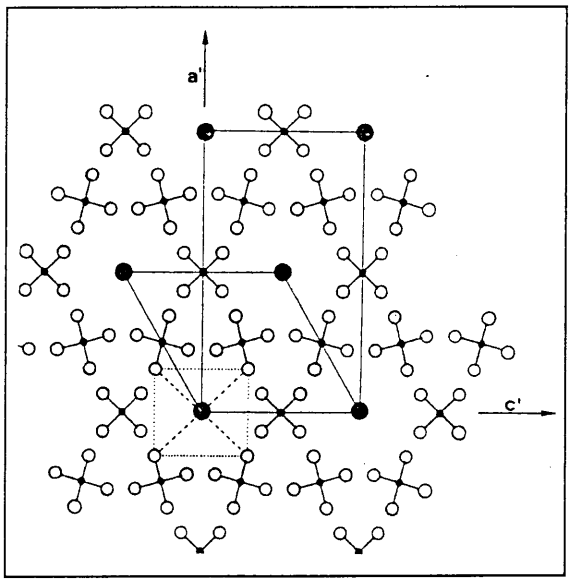

Figure 3.1.3 **The [001] projection of the γ-$CaSO_4$ structure. The possible positions for the water molecules in the hemihydrate structure are represented by the large black circles. The dashed lines from the water molecule indicate the four oxygens and the small black circle indicates the sulphur**

Reports on the crystal structures of α- and β-$CaSO_4$ could not be found. The lattice of γ-$CaSO_4$ has the closest packing, highest density and is the most stable arrangement of any of the calcium sulphates, which explains in part its low reactivity [16].

Hexagonal γ-$CaSO_4$ (proposed by Flörke [25]) and $CaSO_4 \bullet 0.5H_2O$ have very similar crystal structures in which the Ca^{2+} and SO_4^{2-} ions form diamond-shaped channels which contain the water molecules of the hemihydrate [25].

3.2 DECOMPOSITION AND KINETICS OF THE DECOMPOSITION OF CALCIUM SULPHATE AND ITS HYDRATES

3.2.1 Calcium sulphate hydrate

Depending on conditions (temperature, pressure), the dehydration of calcium sulphate dihydrate yields the following products: hemihydrate (plaster of Paris), γ-calcium sulphate (soluble anhydrite, hexagonal calcium sulphate), ß-calcium sulphate (insoluble anhydrite) and monoclinic α-calcium sulphate [16]. However, according to other sources [27; 28] no insoluble anhydrite is formed during the dehydration of the dihydrate or hemihydrate.

Isothermal dehydration and rehydration studies have been carried out on the $CaSO_4$ - H_2O systems. The dehydration of calcium sulphate can be represented by the following reactions:

$$CaSO_4 \bullet 2H_2O(s) \rightarrow CaSO_4 \bullet 0.5H_2O(s) + 1.5\ H_2O(g)$$
$$CaSO_4 \bullet 0.5H_2O(s) \rightarrow CaSO_4(s) + 0.5\ H_2O(g) \qquad [7]$$

The dehydration of calcium sulphate dihydrate begins at 112 °C and reaches its maximum rate at 135 to 145 °C [29]. Satava [29] refers to the calcium sulphate dihydrate as gypsum. It is not clear whether the calcium sulphate dihydrate is pure. Adams et. al. [25] found that when a sample of calcium sulphate dihydrate was subjected to differential thermal analysis (DTA), the DTA curves exhibited a marked endothermal peak starting at 250 °C and passing into an elongated exothermal one ending at ≈ 350 °C.

Borisenko [30] and Molony [4] suggested that the dehydration of calcium sulphate dihydrate (gypsum) is a diffusion - controlled process where the reaction begins at nuclei on the surface of single crystals. This process is represented by the equation, $1-(1-\alpha)^{1/3} = kt$, which suggests diminishing sphere kinetics, or a contracting volume progression of the reaction. Ball and Norwood [5] found the activation energy to be 96.2 kJ mol^{-1} for the

dehydration of α-calcium sulphate hemihydrate and suggested that at lower temperatures, nucleation is the rate-controlling process. At temperatures above 110 °C, the decomposition obeys the parabolic law, $\alpha^2 = kt$, which describes a one-dimensional diffusion mechanism. If the temperature increases above 110 °C, the reaction can be expressed by contracting disc kinetics, i.e. $1-(1-\alpha)^{1/2} = kt$. Later Ridge et. al. [31] and Gregg et. al. [32] found that the ß-hemihydrate has a number of micropores which makes the outward diffusion of water molecules relatively easy at very low partial pressures, i.e. the dehydration will have a low activation energy.

McAdie [33] found that the decomposition could be described by the equation, $\alpha = kt$, for the decomposition of calcium sulphate dihydrate. McAdie also found that the activation energy increases with pressure. The activation energy determined at 760 mmHg is 201.7 kJ mol^{-1}. The dehydration reaction has been shown by many investigators to be represented by a sigmoid curve if the fraction reaction is plotted against time. A kinetic interpretation of the sigmoidal form [33; 34; 35] suggests that the reaction rate below the inflexion point is controlled by the rate of nucleation, whereas the rate above the inflexion point is governed by a growth process. According to Gardet et. al. [34], the appropriate rate law ($V = k\, f(\alpha)$), is the interface advance kinetic law $V = k\,(1-\lambda)^n$, where $\frac{2}{3} < n < 1$ applies above the inflexion point. According to Molony and Ridge [4] the diminishing sphere model fits the experimental data the best with a value for $n = \frac{2}{3}$, while the diminishing cylindrical model implies a value for $n = \frac{1}{2}$.

The dehydration of calcium sulphate dihydrate to the hemihydrate involves the loss of chemically combined water and a lattice structure change. In the growth of the hemihydrate crystal on the dihydrate substrate there must always be a boundary region separating the two phases [17]. Fowler et. al. [17] suggests that it is the behaviour of this region which is regarded as fundamental to an understanding of the existence of the α- and ß-forms. Two types of crystal growth "coherent and incoherent" are determined by the lattice being strained. In the case of metals, incoherent nuclei form and

grow by crystallisation from the melt. α-Crystals grow incoherently and ß-crystals coherently. When the boundary region separating the two phases is continuous and it has a higher surface energy, there is an increase in the area of the separating surface. This results in coherent crystal growth. Coherent nuclei grow much more slowly than incoherent ones for the same rate of energy output.

Table 3.2.1 A summary of published results of the dehydration mechanism and activation energy values of calcium sulphate dihydrate

Author	Kinetic Model	Activation Energy in kJ mol^{-1}	Experimental Method
McAdie 1964 [33] $CaSO_4 \bullet 2H_2O$ (s) → $CaSO_4 \bullet 0.5H_2O$ (s) → $CaSO_4$ (s)	Rate law (α = kt)	201.7	Isothermal Gravimetry
Molony and Ridge 1968 [4] $CaSO_4 \bullet 2H_2O$ (s) → $CaSO_4 \bullet 0.5H_2O$ (s) → $CaSO_4$ (s)	Boundary control	----------	X-ray Diffraction
Ball and Norwood 1969 [5] $CaSO_4 \bullet 0.5H_2O$ (s) → γ-$CaSO_4$ (s)	< 110 °C Avrami-Erofe'ev nucleation and boundary control > 110 °C parabolic (α^2 = kt) law	246 ≥ E_a ≥ 144.7	Isothermal Gravimetry
Gardet et. al. 1976 [34]	The interface advance kinetic law	--------	--------

3.2.2 Gypsum

Natural gypsum used for cement production contains mostly dihydrate, but often impurities, such as calcite, insoluble anhydrite and clay are found [36; 37]. Dihydrate and insoluble anhydrite are stable materials found in nature, while hemihydrate and soluble anhydrite are highly unstable, and readily react with water. When dihydrate is heated, it dehydrates in two steps to the hemihydrate and soluble anhydrite:

$$CaSO_4 \bullet 2H_2O(s) \rightarrow CaSO_4 \bullet 0.5H_2O(s) + 1.5\ H_2O(g)$$
$$CaSO_4 \bullet 0.5H_2O(s) \rightarrow CaSO_4(s) + 0.5\ H_2O(g) \qquad [7]$$

The degree of gypsum dehydration is dependent on the origin of the gypsum as well as on exposure time, temperature and humidity [7]. Dehydration increases with exposure time to elevated temperatures and the rate of dehydration increases with temperature. The dehydration of the gypsum present in cement will usually proceed at a higher rate than dehydration of gypsum by itself as the humidity increases [7].

Investigators, Satava and Sestak [35, 38], found that α- and ß-hemihydrate decomposed thermally to anhydrite without an induction period. The activation energy obtained was 125 ± 12 kJ mol^{-1} and the reaction mechanism was given as the Mampel model; $-\log(1-\alpha) = Z.e^{-E/RT}.t$ (with Z as the pre-exponential factor). Khalil [39] suggested that the dehydration reaction of gypsum to the soluble anhydrite can be represented by

$$ln\ t = \frac{kT\ \alpha^{1/2}}{r^{1/2}}$$

where T is the heating time, k is the reaction constant, α is the fraction decomposed and r is the grain size. Heide [40] found that the dehydration reaction suggested an Avrami-Erofe'ev nuclei growth mechanism with an

activation energy of 130.5 kJ mol^{-1}, for the dehydration of calcium sulphate to γ-$CaSO_4$. Murat and Comel [41] presented three varying activation energies corresponding to three parts of the reaction during decomposition. The energy values obtained were 251 - 502 kJ mol^{-1} for the nucleus formation; 104 - 251 kJ mol^{-1} corresponding to nucleus propagating mechanism and 58 - 62 kJ mol^{-1} which corresponds to the diffusion of water vapour. The results obtained by Negro and Stafferi [42] corresponded to those obtained by Ball and Norwood [33] (for calcium sulphate dihydrate) and they found an activation energy of 112 - 126 kJ mol^{-1} for the dehydration of α-calcium sulphate hemihydrate to $CaSO_4$. Vakhlu et. al. [43] concluded that the dehydration of gypsum to the hemihydrate follows the Avrami-Erofe'ev nuclei-growth mechanism and obeys the model relation $[-\ln(1-\alpha)]^{½} = kt$, with an activation energy of 130.4 kJ mol^{-1}.

Bright and Ridge [44] found that dehydration nuclei in general did not occur at the same sites as etch pits of natural gypsum crystals. The etch pits were formed when the faces which were produced by cleaning were washed with distilled water. Patel and Raju [45] found that dehydration takes place preferentially at dislocation sites. Using photomicrographs, Patel and Raju [45] found that the thermal decomposition of crystals is initiated at dislocation sites.

Table 3.2.2 A summary of published results of the dehydration mechanism and activation energy values of gypsum

Author	Kinetic Model	Activation Energy in kJ mol^{-1}	Experimental Method
Bright and Ridge 1961 [44]	Dehydration at etch pits of gypsum crystals	----------	----------
Piecé 1965 - 1970 [46]	Diffusion of water molecules	$71 \leq E_a \leq 163.15$	Thermogravimetry
Patel and Raju 1969 [45]	Dehydration at dislocation sites	----------	----------
Satava and Sestak 1973 [38] $CaSO_4 \bullet 0.5H_2O$ (s) → $CaSO_4$ (s)	----------	110 - 378	----------
Vakhlu 1985 [43] $CaSO_4 \bullet 2H_2O$ (s) → $CaSO_4 \bullet 0.5H_2O$ (s)	Avrami-Erofe'ev nuclei-growth mechanism	130.4	----------
Negro and Stafferi 1972 [42] $CaSO_4 \bullet 2H_2O$ (s) → $CaSO_4$ (s)	----------	112 - 126	----------
Murat and Comel 1970 [41] $CaSO_4 \bullet 2H_2O$ (s) → $CaSO_4$ (s)	Nuclei formation Nuclei growth Diffusion of water molecules	351-502 104 - 251 58 - 62	Micro and Macro DTA

3.3 THE THERMODYNAMICS OF THE DECOMPOSITION OF CALCIUM SULPHATE HYDRATES

The following thermodynamic data was obtained for the thermal dehydration of calcium sulphate dihydrate at 298 K. For the reaction

$$CaSO_4 \bullet 2H_2O(s) \rightarrow CaSO_4 \bullet 0.5H_2O\ (\alpha)(s) + 1.5\ H_2O(g)$$

the heat of dehydration is 81.4 kJ mol^{-1} [15, page 53]. The dehydration to the ß-hemihydrate gives a heat of dehydration of 83.4 kJ mol^{-1} [15, page 53]. According to Kelley et. al. [15], the dehydration to insoluble anhydrite at 298 K is $\Delta H^\circ = 103$ kJ mol^{-1} and $\Delta G^\circ = +17.7$ kJ mol^{-1} [15, page 53]. The heat of dehydration of ß-hemihydrate to the ß-soluble anhydrite at 298 K is 32.5 kJ mol^{-1} and the free energy is + 12.3 kJ mol^{-1} [15, page 53].

The entropy, S°, values obtained by Kelley et. al. [15] for dihydrate, α- and ß-hemihydrate and insoluble anhydrite are respectively : 194.1 [15, page 19]; 130.5 [15, page 51]; 134.3 [15, page 51] and 106.7 J K^{-1} mol^{-1} at 298 K [15, page 19]. The entropy values of α- and ß-anhydrite(soluble) are respectively: 108,34 and 108,34 J K^{-1} mol^{-1} [15, page 23] at 298 K. Kelley et. al. [15, page 33] concluded from the dissociation-equilibrium measurements, that the ß-hemihydrate dissociates to a compound containing at least 0.069 mole water per mole $CaSO_4$, and that the dihydrate is in equilibrium with α-hemihydrate and liquid water in the region of 100 °C.

The values of the thermodynamic constants for the dehydration of gypsum would probably differ from that of pure $CaSO_4 \bullet 2H_2O$, as a result of the influence of the impurities on the reaction mechanisms. There is also a large difference in the thermodynamic constants with differing grain sizes.

CHAPTER FOUR

CALCIUM CARBONATE

4.1 STRUCTURAL FORMS OF CALCIUM CARBONATE

4.1.1 Pure calcium carbonate

Calcium carbonate ($CaCO_3$) is found in calcite (rhombohedral form) and in aragonite (orthorhombic form) [8, page 21]. Aragonite has a smaller molecular volume and is not as hard as calcite [8, page 8].

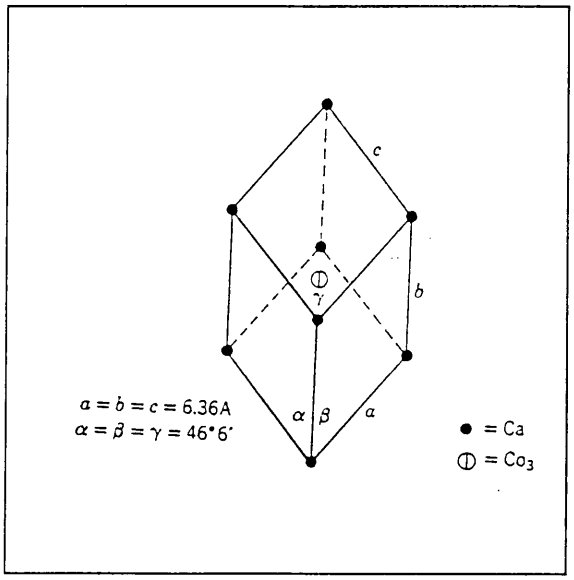

Figure 4.1 The crystal structure of calcite, $CaCO_3$

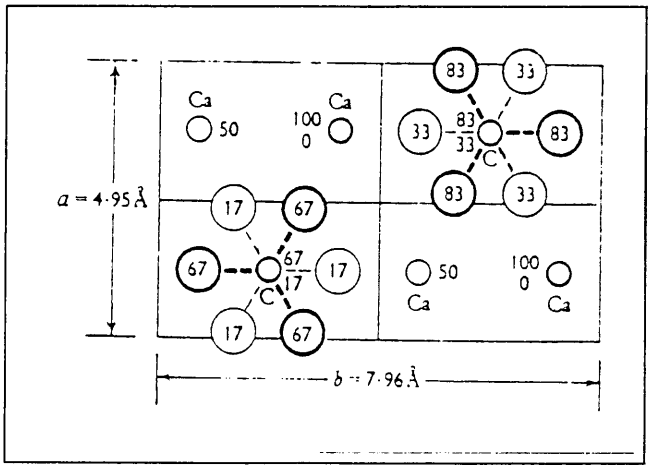

Figure 4.2 The crystal structure of aragonite

4.1.2 Limestone

Limestone is a term that includes calcium carbonate rocks or fossils. It is composed mainly of calcium carbonate with varying amounts of impurities, the most common of which are silica and alumina. Lime (CaO), which is generally derived from limestone, is a calcined or burned form of limestone [8, page 2].

Limestone may be composed of the following four minerals; calcite (rhombohedral $CaCO_3$); aragonite (orthorhombic $CaCO_3$); dolomite (rhombohedral $CaMgCO_3$) and magnesite (rhombohedral $MgCO_3$) [51; 52]. Vaterite (μ-$CaCO_3$) also occurs in small, scattered amounts. Vaterite is unstable, converting rapidly to calcite when subjected to temperatures above 65 °C [8, page 8].

There are many varieties of limestone in use, of which high-purity limestone and dolomite are the most common. High-purity limestone contains 97 - 99 % $CaCO_3$ and dolomite contains 40 - 43 % $MgCO_3$, with the $CaCO_3$ component 54 - 58 % and 1 - 3 % impurities [8, page 9].

The bulk density of limestone ranges between approximately 2000 - 2800 kg m^{-3} because of the difference in porosity. On an average the bulk density of dolomite is 2.5 % higher than pure calcium carbonate [8, page 22].

4.2 DECOMPOSITION AND KINETICS OF THE DECOMPOSITION OF CALCIUM CARBONATE

4.2.1 Calcium carbonate

The thermal decomposition of calcium carbonate

$$CaCO_3(s) \rightarrow CaO(s) + CO_2(g) \quad [8]$$

has been investigated by numerous investigators. There still is no consensus on the published results and mechanisms. The authors' opinions

on the rate-controlling steps range from that the chemical reaction is the rate-controlling step, [53; 54; 55; 56], to that with small particles, the decomposition is controlled only by the heat transfer [Gallagher and Johnson [57] and Caldwell et. al. [58]]. Other investigators [49; 59] reported that compacted pellets of calcium carbonate decompose by reactions controlled by both the heat and mass transfer rates. Hedin [50] and Koloberdin et. al. [60] found that for small particles the reaction is controlled by the heat transfer rate to the reaction surface and by a chemical reaction step on the surface.

There are thus numerous reports concerned with kinetic studies of the thermal decomposition of calcium carbonate under isothermal and non-isothermal conditions, as summarised in table 4.1.

Table 4.1 Some reported activation energy values for the thermal decomposition of calcium carbonate

Author	Activation Energy in kJ mol^{-1}	Sample form and mass (mg)	Reaction Order
Slonim 1930 [61]	159	powder -	1
Kappel et. al. 1940 [62]	205	powder -	0 - 1
Britton et.al. 1952 [63]	147 - 176	powder 500	0.58 - 0.74
Satterfield et. al. 1959 [53]	1506.3	compacted -	-
Ingraham et. al. 1963 [64]	170	- 455	0.67
Sharp et. al. 1969 [65]	180 - 193	pellet and powder 1000	0.7
Draper et. al. 1970 [66]	173	- 300 - 450	-
Beruto et. al. 1973 [55]	205	single crystal	-
Gallagher et. al. 1976 [57]	837 - 4184	powder 1 - 16	-

4.2.2 Limestone

Calcite (calcium carbonate) when decomposed isothermally at temperatures of 700 °C, 800 °C and 900 °C shows large differences in the decomposition rate [67; 68]. Greater resistance occurs in larger particles to decomposition [68]. Lee et. al. [68] found that under similar conditions, the

decomposition rate obtained for 7 mm particles was much less than that obtained for 2 mm particles. This was attributed to the fact that 2 mm particles decompose more rapidly than 7 mm particles and they have a longer time in which to sinter. The surface area produced by the decomposition of small particles will be greater than that from the decomposition of larger particles [68]. Lee et. al. [68] used the shrinking core model of a spherical particle, namely :

$$f(\alpha) = 3[1-(1-\alpha)^{1/3}].$$

Asaki et. al. [69] expressed the thermal decomposition of limestone as

$$CaCO_3\ (s) \rightarrow CaO\ (s) + CO_2\ (g).$$

Splichal et. al. [70] used the stathmographic method (method whereby change in weight is recorded on photographic paper) to study the rate of decomposition of limestone. They found that the rate of the decomposition of calcium carbonate and limestone, is a reaction of the ⅓ order. This is analogous to evaporation of CO_2 from the limestone sample.

4.3 THE THERMODYNAMICS OF THE DECOMPOSITION OF CALCIUM CARBONATE

4.3.1 Calcium carbonate

Calcium carbonate decomposes to calcium oxide and carbon dioxide via the following reaction at 600 - 950 °C using a heating rate of 5 °C min^{-1}: $CaCO_3(s) \rightarrow CaO(s) + CO_2(g)$. Hills [49] found the heat of decomposition of calcium carbonate to be about 167.4 kJ mol^{-1}. The heat of decomposition calculated from the thermochemical data available at 298 K is 178.5 kJ mol^{-1} and the entropy is 163.2 J K^{-1} mol^{-1} [71].

4.3.2 Limestone

Asaki et. al. [69] found the heat of decomposition for limestone to be 162.4 kJ mol^{-1}. The heat of activation obtained by Splichal et. al. [70] for the decomposition of limestone was 162.26 kJ between 700 °C and 795 °C.

CHAPTER FIVE

CALCIUM HYDROXIDE

5.1 CRYSTAL STRUCTURES OF CALCIUM HYDROXIDE

Calcium hydroxide is usually a fine powder [8, page 199]. Fineness varies, and particles may be microcrystalline or of colloidal size (submicron). The crystal is a hexagonal-shaped prism [8, page 200]. The calcium atoms are octahedrally, and the oxygen atoms tetrahedrally, co-ordinated [3, page 125].

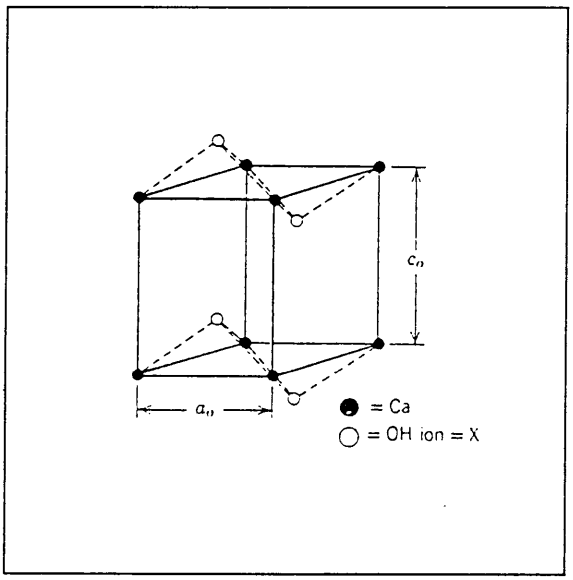

Figure 5.1 The crystal structure of calcium hydroxide

Calcium hydroxide has a layered structure. The inter-layer forces are weak, with negligible hydrogen bonding [3, page 125]. Calcium hydroxide occurs as a natural mineral, known as portlandite.

5.2 DECOMPOSITION AND KINETICS OF THE DECOMPOSITION OF CALCIUM HYDROXIDE

Calcium hydroxide decomposes as follows:

$$Ca(OH)_2(s) \rightarrow CaO(s) + H_2O(g)$$

in the temperature range 300 - 550 °C [72].

Published studies show a great variation in the activation energy values of the $Ca(OH)_2$ decomposition [73; 74]. The probable reason is the difference in the degree of crystallinity of the calcium hydroxide used.

Table 5.1: Some activation energy values for calcium hydroxide

Author	Activation Energy in kJ mol^{-1}	Mechanism
Chen et. al. [72]	96.03 - 107.32	Avrami-Erofe'ev with n = 1.5
Criado & Morales [73]	117.2	-
Maycock & Skalny [74]	176	-
Dave & Chopra [75]	146 - 188	-
Murthy et. al. [76]	45.72	-
Fujii & Tschiya [77]	13400	First order
Halstead & Moore [78]	104.2	-
Mikhail et. al. [79]	62.4	-
Dollimore et. al. [80]	109.2	-

5.3 THE THERMODYNAMICS OF THE DECOMPOSITION OF CALCIUM HYDROXIDE

Cazorla-Amaros [81] reported the heat of formation of $Ca(OH)_2$ to be 105 kJ mol^{-1} at 573 K. Published data gives the heat of decomposition for the reaction:

$$Ca(OH)_2(s) \rightarrow CaO(s) + H_2O(g)$$

as 788.2 kJ mol^{-1} and the entropy for the reaction as 325.3 J K^{-1} mol^{-1} at 298 K [71].

CHAPTER SIX

CALCIUM OXIDE

6.1 CRYSTAL STRUCTURES OF CALCIUM OXIDE

Pure calcium oxide has the sodium chloride structure that crystallizes in the cubic system as shown in Figure 6.1. The edges of the cube are 4.797 Å in length with calcium atoms located midway in between [8, page 195].

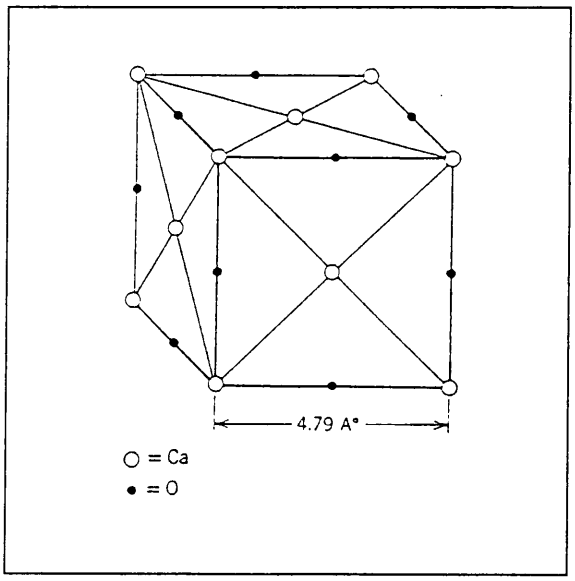

Figure 6.1: Crystal structure of calcium oxide

6.2 KINETICS OF CO_2 ADSORPTION ON CALCIUM OXIDE

The amount of CO_2 chemisorbed on CaO particles is a function of the pressure of carbon dioxide, temperature and time. The reaction is as follows:

$$CO_2(g) + CaO(s) \rightarrow CaCO_3(s)$$

Cazorla-Amoros et. al. [81], suggested that the reaction takes up two CO_2 molecules for each of the CaO i.e.

$CO_2(g) + CaO(surface) \rightarrow CaCO_3(surface)$

$CO_2(g) + CaCO_3(surface) \rightarrow CaCO_3(surface) + CO_2(s)$

nett: $2CO_2(g) + CaO(surface) \rightarrow CaCO_3(surface) + CO_2(s)$.

Cazorla-Amoros [81] suggested the following mechanism of formation of bulk $CaCO_3$:

(a) At $T < 573$ K, CO_2 interacts with the CaO surface, leading to the formation of C - O bonds, and subsequently to the formation of a layer of $CaCO_3$ on the surface.

(b) For $573 < T < 623$ K, after the formation of a monolayer of superficial carbonate, the thermal energy of this species is sufficient for a second layer of CO_2 to enter the CaO lattice (CO_2 (s)), initiating the formation of a new interface $CaCO_3$ - CaO. It is assumed that the molecule CO_2(s) left in the second layer does not form a new C - O bond. Thus, the fixation of two CO_2 molecules on each CaO.

(c) At $T > 623$ K, more CO_2 molecules enter CaO through the preceding mechanism. The formation of carbonate in the bulk occurs because this compound is obviously the final product of the reaction.

6.3 THE THERMODYNAMICS OF THE REACTIONS OF CALCIUM OXIDE

Boynton [8, page 199] reported the heat of formation of CaO at 298 K to be 653.2 kJ mol^{-1}.

CHAPTER SEVEN

EXPERIMENTAL

The thermal characteristics of the solid state decomposition reactions of gypsum, lime and limestone were investigated by means of thermogravimetry (TG), X-ray powder diffraction (XRD) and X-ray fluorescence (XRF).

7.1 THERMOGRAVIMETRIC AND CALORIMETRIC ANALYSIS

A Netzsch STA 409 simultaneous TG/DSC instrument was used to collect thermogravimetric and calorimetric data. Experiments were carried out in nitrogen (N_2), air, carbon dioxide (CO_2), air/water (H_2O), 50% CO_2/ 50 % air and 99.99% CO_2/ H_2O atmospheres. These carrier gases were of high purity (between 98.50% and 99.99%). In order to investigate the influence of water vapour pressure on the dehydration reactions of the compounds, air and CO_2 were bubbled through water in a closed glass funnel. See figure 7.1.

The temperature of the water in the glass tube was kept constant at 293 K. The carrier gas was fed through the water and the system was allowed to stabilise over a 24 hour period. The flow rate employed was approximately 20 cm^3 min^{-1}. Platinum pans were used as the sample and reference containers. Temperature and enthalpy calibration of the TG/DSC were achieved by making use of the ICTAC (International Confederation for Thermal Analysis and Calorimetry) recommended DTA (differential thermal analysis) [82]. Sample masses varied between 5 and 15 mg.

The software module for the kinetic analysis of thermal measurements by means of multivariant non-linear regression developed by Netzsch was used to investigate the kinetic behaviour of the dehydration of the samples.

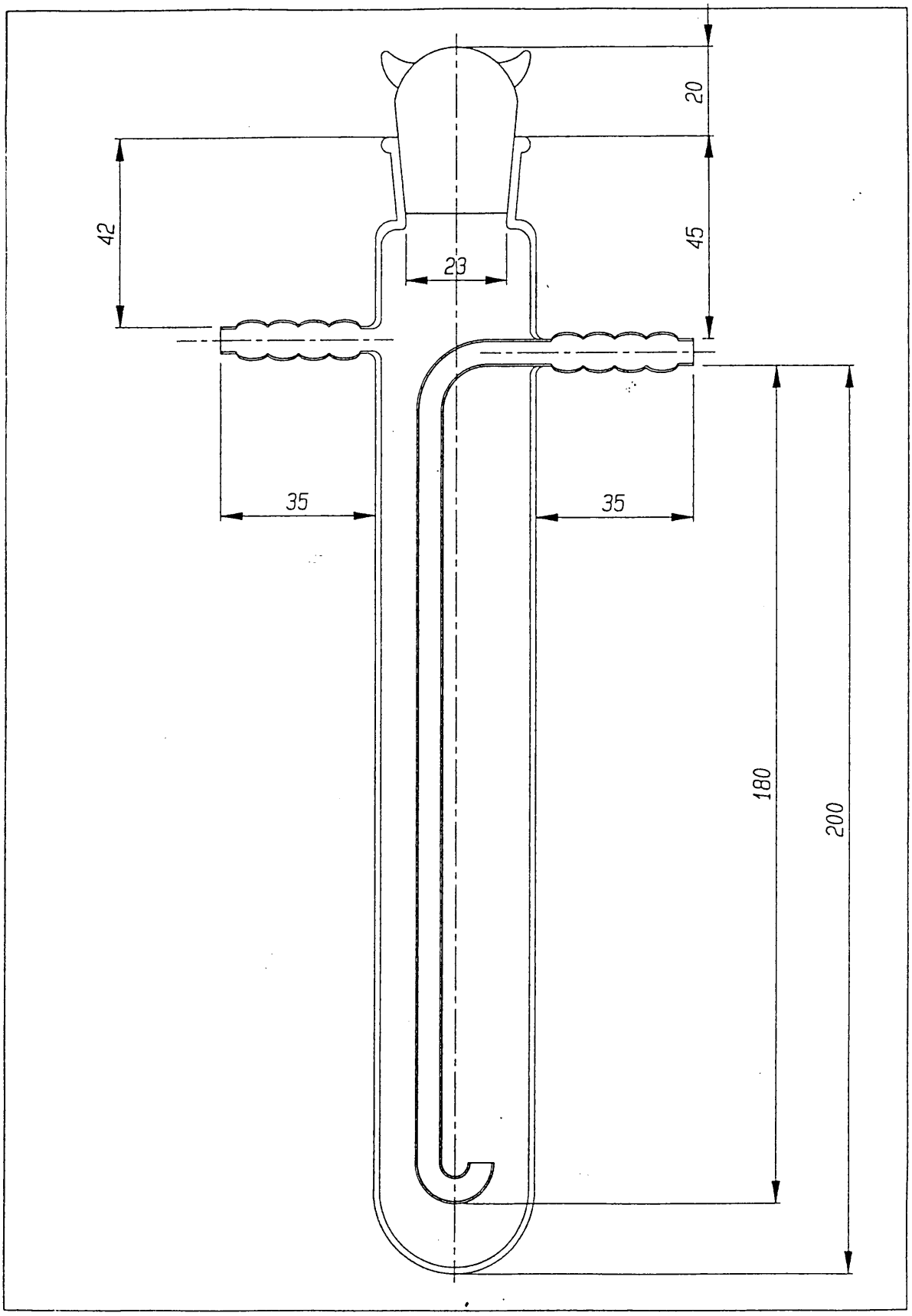

Figure 7.1: Glass funnel (measurements in mm) designed for water vapour measurements

7.2 X-RAY POWDER DIFFRACTION ANALYSIS

X-ray powder diffraction analyses were performed on an automated Siemens D501 XRD spectrometer with a 40 position sample changer and monochromated Cu K_α radiation. The results were analysed with the use of the International Centre Diffraction Data for PDS database sets 1-44. The results are given in table 7.1.

Table 7.1. XRD results of compounds investigated

Pure CSD	Syn Gyp	Nat Gyp	Pure Lime/s	Bees Lime/s	Pien Lime/s	Lime Acres Lime/s	$Ca(OH)_2$	CaO
CSD $CaSO_4$	CSD $CaSO_4$	CSD SiO_2 $CaSO_4$	$CaCO_3$	$CaCO_3$ SiO_2 dolomite	$CaCO_3$ SiO_2 dolomite	$CaCO_3$ dolomite	$Ca(OH)_2$ $CaCO_3$	CaO

Key for table 7.1 and table 7.2: CSD = calcium sulphate dihydrate ($CaSO_4 \bullet 2H_2O$); Syn Gyp = synthetic gypsum; Nat Gyp = natural gypsum; Lime/s = limestone; Bees Lime/s = Beestekraal limestone; Pien Lime/s = Pienaars River limestone; Lime Acres = Lime Acres limestone; $Ca(OH)_2$ = pure calcium hydroxide; CaO = pure calcium oxide and dolomite = $CaMg(CO_3)_2$.

7.3 OTHER ANALYSES

a] XRF analyses were performed on a Siemens MRS 400 MP wavelength dispersive XRF spectrometer. The results are given in table 7.2.

Table 7.2: XRF results of compounds investigated

	Pure CSD	Syn Gyp	Nat Gyp	Pure Lime/s	Bees Lime/s	Pien Lime/s	Lime Acres Lime/s	$Ca(OH)_2$	CaO
SiO_2	6.7	5.6	33.3	0.5	0.7	26.2	0.4	0.3	⟨0.1
Al_2O_3	3.3	0.7	8.3	0.1	0.1	6.1	0.1	0.0	⟨0.1
Fe_2O_3	0.0	0.4	4.6	0.1	0.1	2.5	0.1	0.2	0.1
Mn_2O_3	0.0	0.1	0	0.7	0.7	0.1	0.6	0.0	0.1
TiO_2	0.3	0.1	0.3	⟨0.1	0.0	0.3	⟨0.1	⟨0.1	⟨0.1
CaO	33.6	31.4	13.8	54.9	54.8	32.9	54.4	74.0	92.3
MgO	1.3	0.5	1.5	0.6	0.6	1.9	0.7	0.9	0.6
P_2O_5	0.1	<0.1	0.2	⟨0.1	⟨0.1	0.1	⟨0.1	0.1	0.0
SO_3	34.4	40.6	18.8	⟨0.1	⟨0.1	0.0	⟨0.1	0.0	⟨0.1
Cl	0.0	0	0	0.0	0.0	⟨0.1	0.0	⟨0.1	0.0
K_2O	0.2	<0.1	1.9	⟨0.1	0.1	0.6	⟨0.1	0.0	⟨0.1
Na_2O	0.0	<0.1	0.3	⟨0.1	0.1	0.1	0.0	0.1	0.1
LOI @ 1000°C	20.0	20.6	16.5	43.3	43.7	29.8	43.7	25.3	6.7
Total	99.9	100.3	99.5	100.2	100.9	100.6	100.0	100.9	99.9

b] Surface areas of the sifted samples were determined on a Micromeritics Flow Sorb II 2300 BET surface analyser by determining the quantity of nitrogen that adsorbs as a single layer of molecules, a so-called monolayer, on a sample. The surface areas for the compounds were determined three times and the averages are listed in table 7.3.

Table 7.3: Surface areas of the ground and sifted compounds investigated

Compound	Surface Area (m^2 g^{-1})
Pure calcium sulphate dihydrate	0.8
Synthetic gypsum	0.7
Natural gypsum	11.0
Pure calcium carbonate	0.2
Beestekraal limestone	0.9
Pienaars River limestone	13.5
Lime Acres limestone	0.6
Pure calcium hydroxide	2.0
Pure calcium oxide	2.6

c] Secondary electron micrographs were obtained on a JEOL 840 scanning electron microscope of the different compounds studied. The photographs of each compound are shown in figure 7.2.

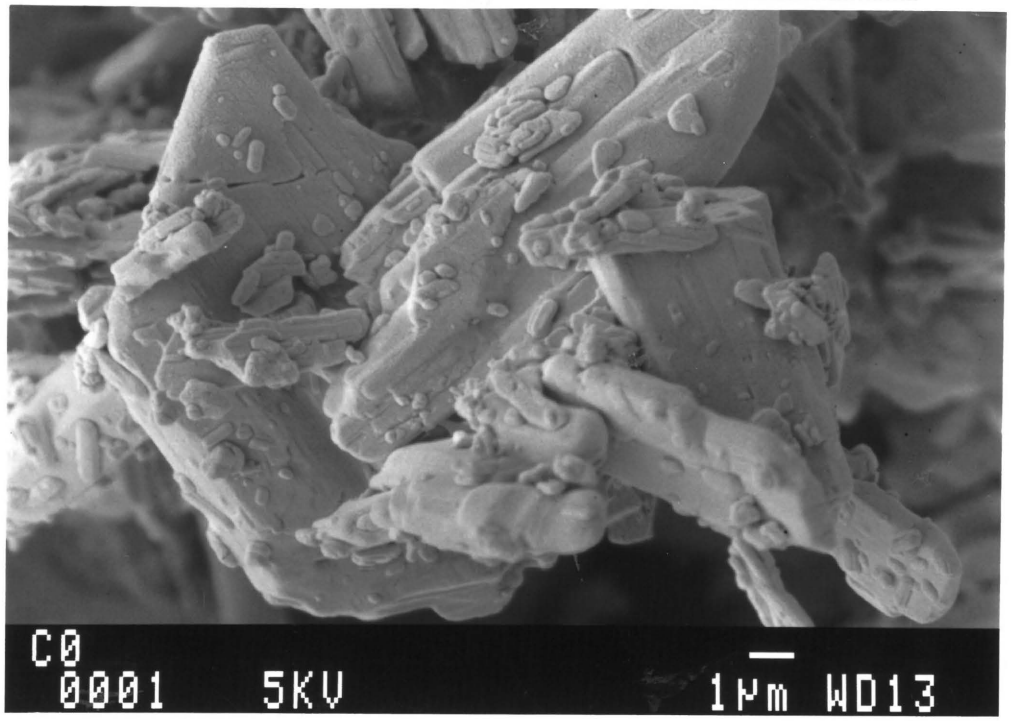

Figure 7.2 (a): Electron micrograph of calcium sulphate dihydrate

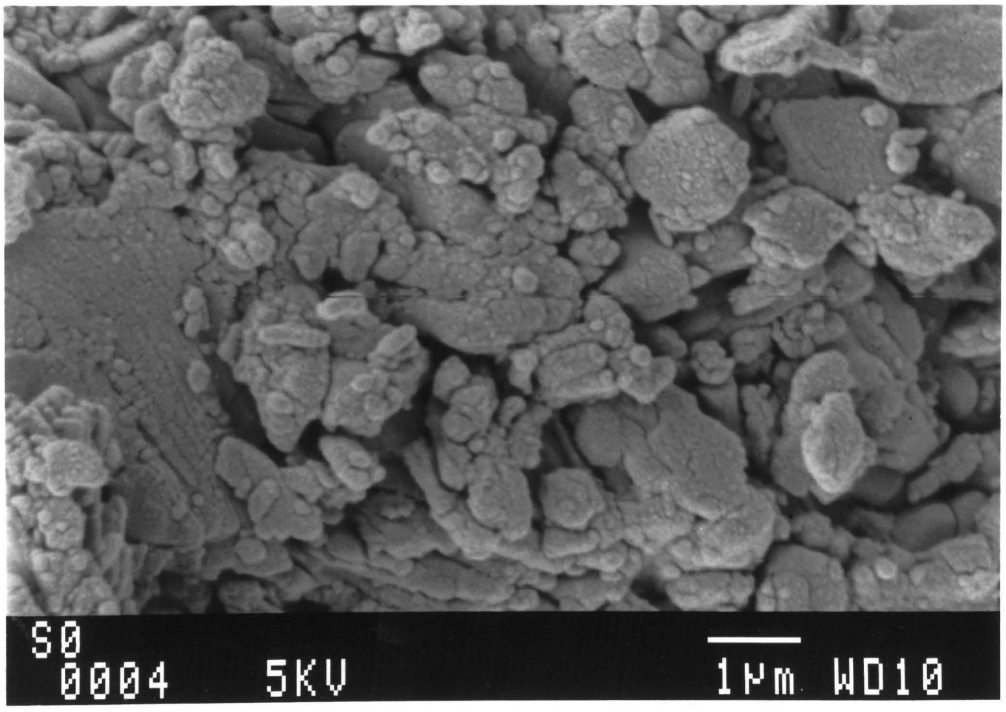

Figure 7.2 (b): Electron micrograph of synthetic gypsum

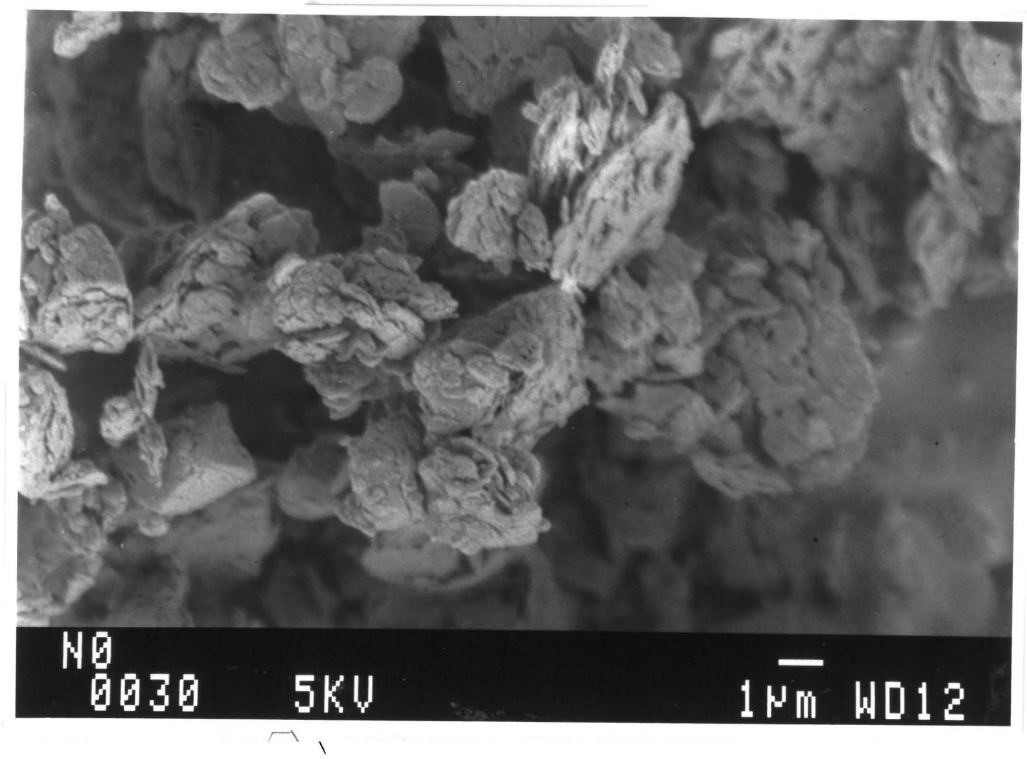

Figure 7.2 (c): Electron micrograph of natural gypsum

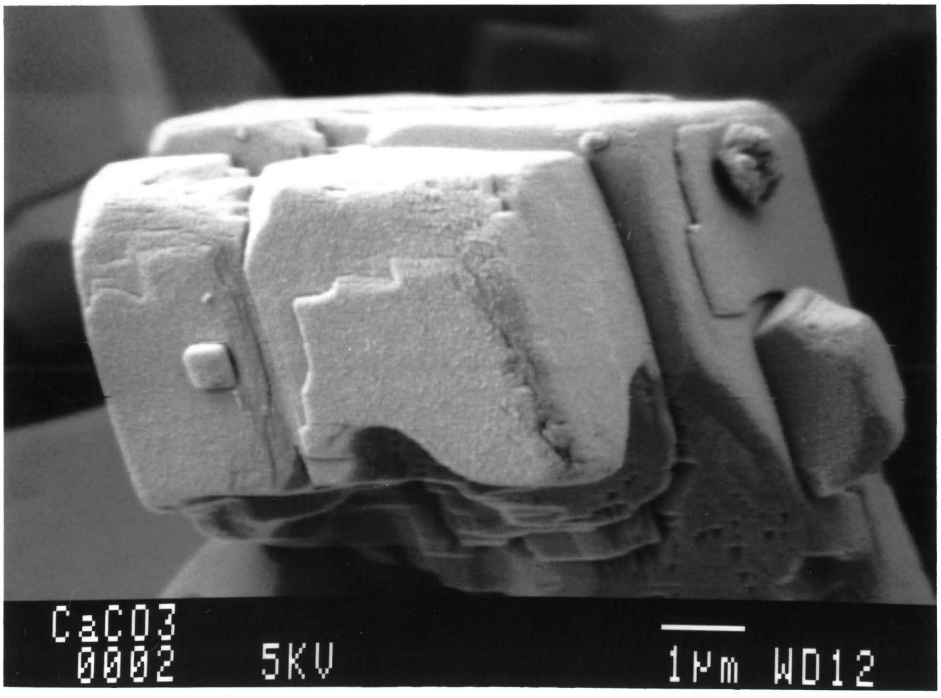

Figure 7.2 (d): Electron micrograph of calcium carbonate

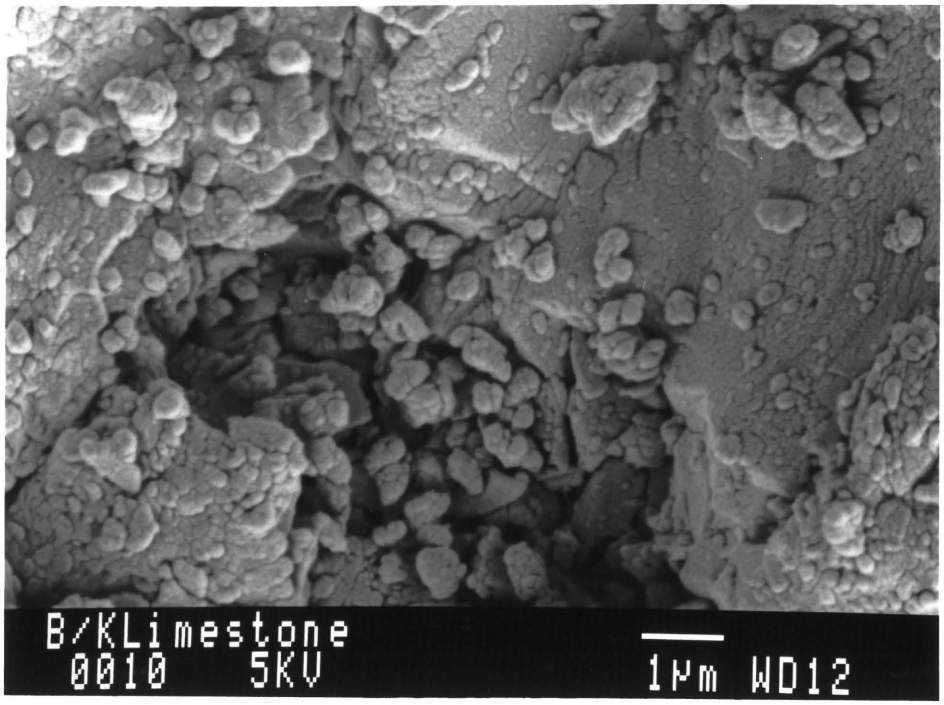

Figure 7.2 (e): Electron micrograph of Beestekraal limestone

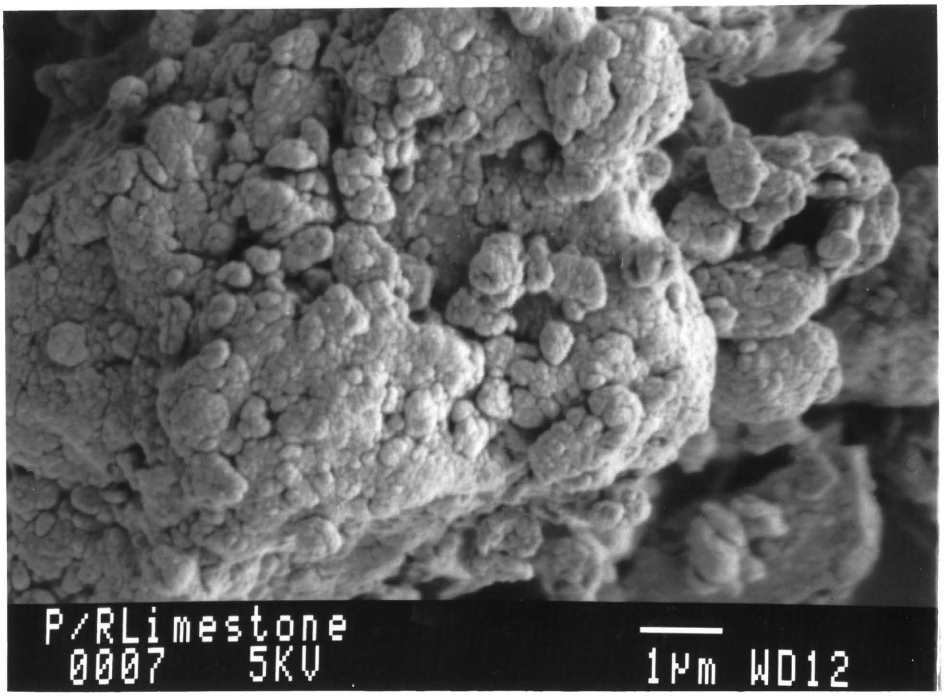

Figure 7.2 (f): Electron micrograph of Pienaars River limestone

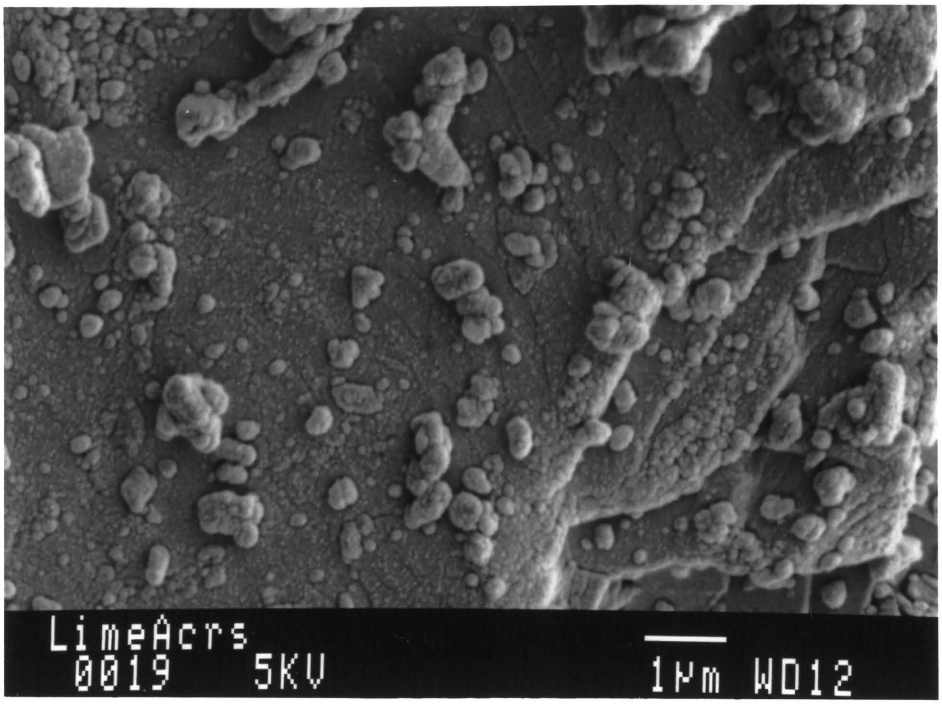

Figure 7.2 (g): **Electron micrograph of Lime Acres limestone**

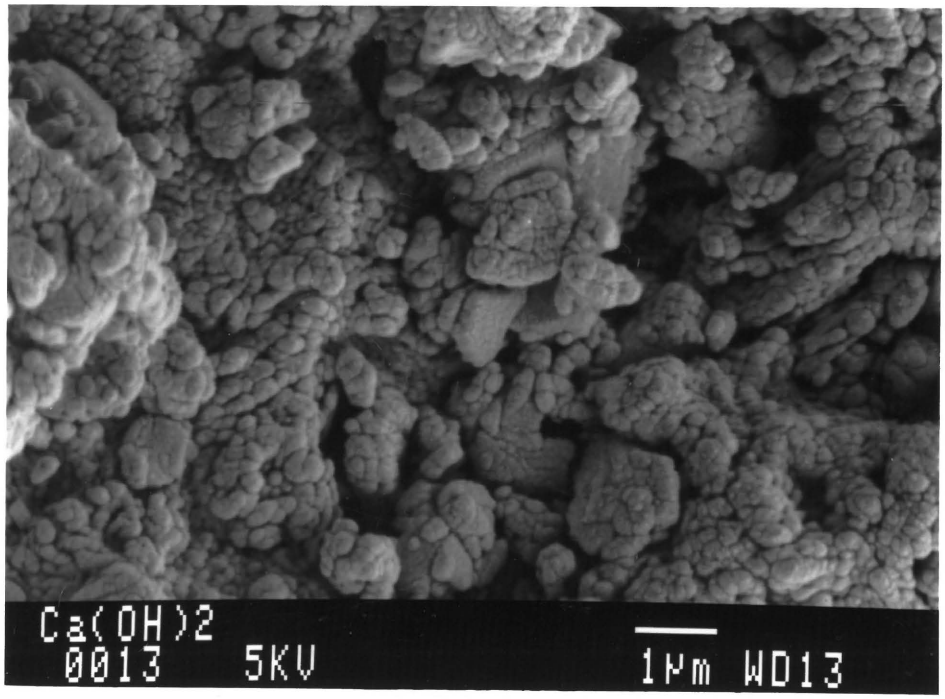

Figure 7.2 (h): **Electron micrograph of calcium hydroxide**

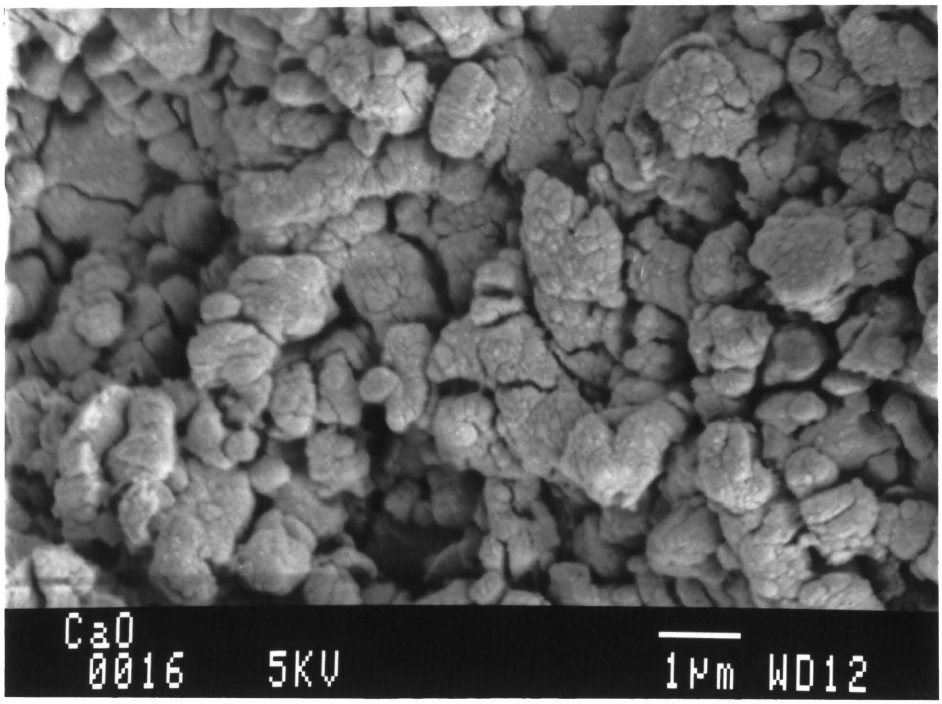

Figure 7.2 (i): Electron micrograph of calcium oxide

7.4 SAMPLE PREPARATION

Natural gypsum was obtained from PPC Technical Services in Cleveland, Johannesburg. The natural gypsum is mined in the Eastern Cape and is used by PPC, Port Elizabeth. The samples were ground to a fine powder with a ball grinder and thoroughly mixed in order to obtain a homogeneous sample.

Pure calcium sulphate dihydrate, pure calcium carbonate, calcium oxide and calcium hydroxide were obtained from PAL Chemicals as analytically pure reagents.

Limestone was obtained from the quarries where they are mined, namely Beestekraal, Pienaars River and Lime Acres. These samples were ground to a fine powder and each individual powder was thoroughly mixed. All the above samples were sifted and only the fraction with diameters between 45 and 106 μm were used.

7.5 DATA PROCESSING OF KINETIC STUDIES

The thermogravimetric data is used to calculate the activation energy at different α-values, using the isoconversional method described by Ozawa [83] and Flynn and Wall [84]. Ozawa [83] and Flynn and Wall [84] developed a method for the determination of the activation energy, independently of each other. The method includes several scans and these scans are performed at different but constant heating rates, β. The activation energy values obtained are plotted against α (reaction fraction decomposed) for the different heating rates ($0.5\,^{\circ}C\ min^{-1} < \beta < 5\,^{\circ}C\ min^{-1}$). The activation energy value (E_a) and the pre-exponential factor values are determined at different α-values without knowledge of the reaction model that describes the reaction by using the following equation:

$$\ln \beta = \ln (AE_a/R) - \ln g(\alpha) - 5.3305 + 1.052E_a/RT$$

The method forms part of the kinetic analysis program [10]. The graph of $\ln \beta_x = f\,(1/T_x)$ will be a straight line with a slope $m = -1.052E_a/R$, during a series of measurements at different heating rates at a fixed degree of conversion. The temperature T_x is the temperature at which the conversion α_x is obtained at a heating rate β_y. The slope of the straight line is directly proportional to the activation energy, E_a. If the determined activation energy is the same for various values of α, then a single-step reaction is present. If E_a changes with an increasing degree of conversion, a complex reaction mechanism is indicated.

The activation energy versus alpha graphs and the Netzsch Thermokinetic Analysis Program [10] are used, and the different solid state decomposition kinetic models [13, page 57] are fitted to the experimental data in the observed fraction reaction ranges. The activation energy versus alpha graphs are kinetic model dependent. The kinetic model that appears to fit the reaction is taken as a good fit if there is a correlation between the activation energy obtained from the model-free isoconversional method and the activation energy value obtained from the fitted kinetic model, and if the fitted kinetic model has a correlation coefficient greater than 0.9.

CHAPTER EIGHT

RESULTS AND DISCUSSION

8.1 GYPSUM

8.1.1 Pure calcium sulphate dihydrate

The thermal decomposition of pure calcium sulphate dihydrate in an air-atmosphere using a heating rate of 5 °C min^{-1} is shown in figure 8.1.1(a). The following table shows the thermal decomposition in different atmospheres.

Table 8.1.1 (a): The thermal decomposition of pure calcium sulphate dihydrate with different sample masses in different atmospheres using a heating rate of 5 °C min^{-1}

Sample Mass(mg)	Atmos-phere	Temperature Range (°C)	Mass Loss (%)	Mass Gain (%)	ΔH in kJ g^{-1}
5	N_2	80 - 150	19	-	5 x 10^{-1}
10	N_2	83 - 144	19	-	5 x 10^{-1}
15	N_2	77 - 148	19	-	5 x 10^{-1}
10	Air	78 - 140	19	-	4 x 10^{-1}
10	Air/H_2O	39 - 77 77 - 88 88 - 133 133 - 234 234 - 373	2 - 20 2 -	- 4 - - 3	- - 3 x 10^{-1} - -

The thermal decomposition of calcium sulphate dihydrate via the hemihydrate to the anhydrite starts at ≈ 60 °C, using a heating rate of 5 °C min^{-1} and is completed at ≈ 240 °C. The total percentage mass losses observed for the 5 and 15 mg samples, are the same as that observed for

10 mg. For this reason, a sample mass of 10 mg or less is used throughout this study for continuity in order to compare results obtained for the kinetics. The theoretical mass loss of 20.9 % calculated compares well with the experimental value of 19 % obtained in an air-atmosphere. The thermograms obtained in air- and in nitrogen-atmospheres, are the same for calcium sulphate dihydrate. (Compare figure 8.1.1 (a) and figure 8.1.1 (b)).

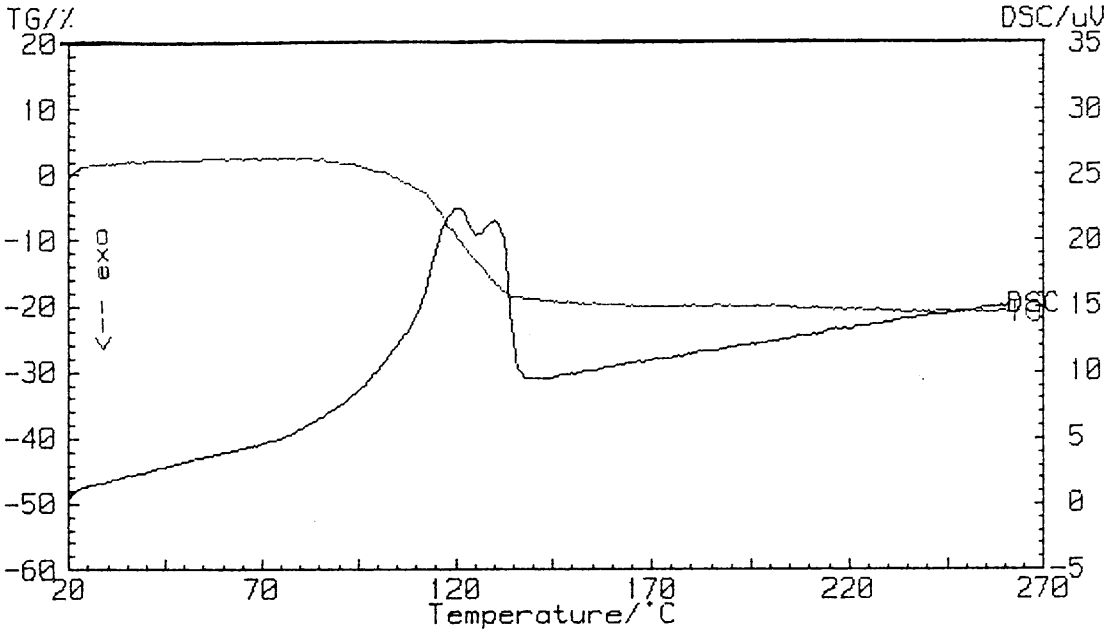

Figure 8.1.1 (a): TG and DSC curves for the decomposition of calcium sulphate dihydrate to anhydrite in an air-atmosphere using a heating rate of 5 °C min^{-1}

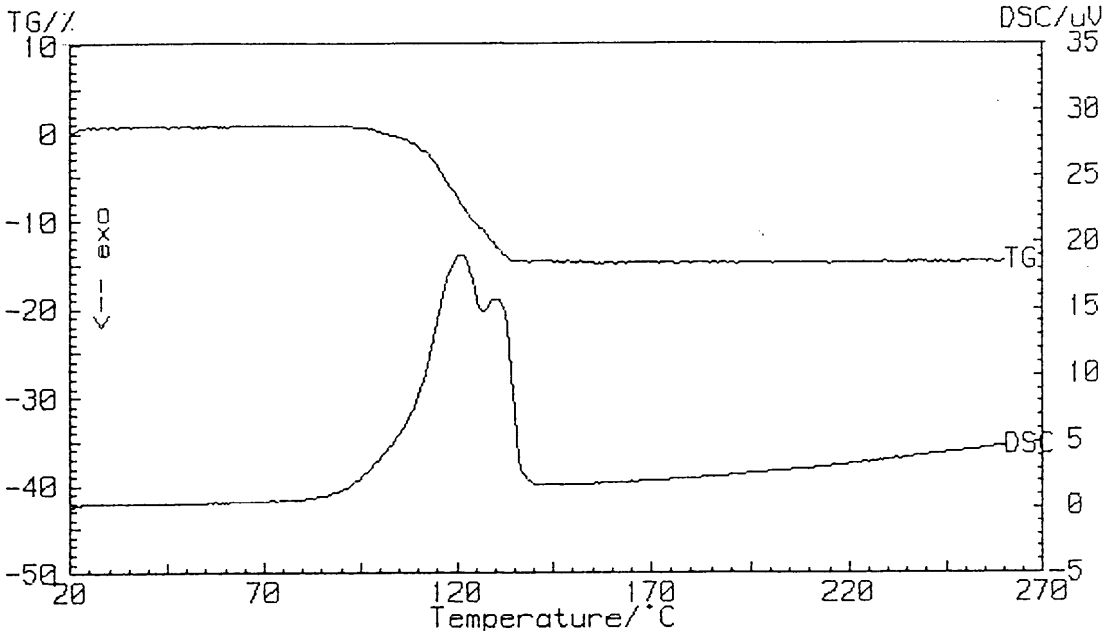

Figure 8.1.1 (b): TG and DSC curves for the decomposition of calcium sulphate dihydrate to anhydrite in a nitrogen-atmosphere using a heating rate of 5 °C min^{-1}

The total mass loss of calcium sulphate dihydrate in an air/water-atmosphere shows a mass loss of 21 % which is the same as the expected theoretical value of 20.9 %. See figure 8.1.1 (c).

There is a very slight mass gain from ≈ 77 °C and ≈ 88 °C. This mass gain could be due to exothermic adsorption of water vapour taking place. In the air/water-atmosphere, the heat of dehydration is found to be less than in air- or nitrogen-atmosphere, namely 3 x 10^{-1} kJ g^{-1}, in comparison to 5 x 10^{-1} kJ g^{-1}.

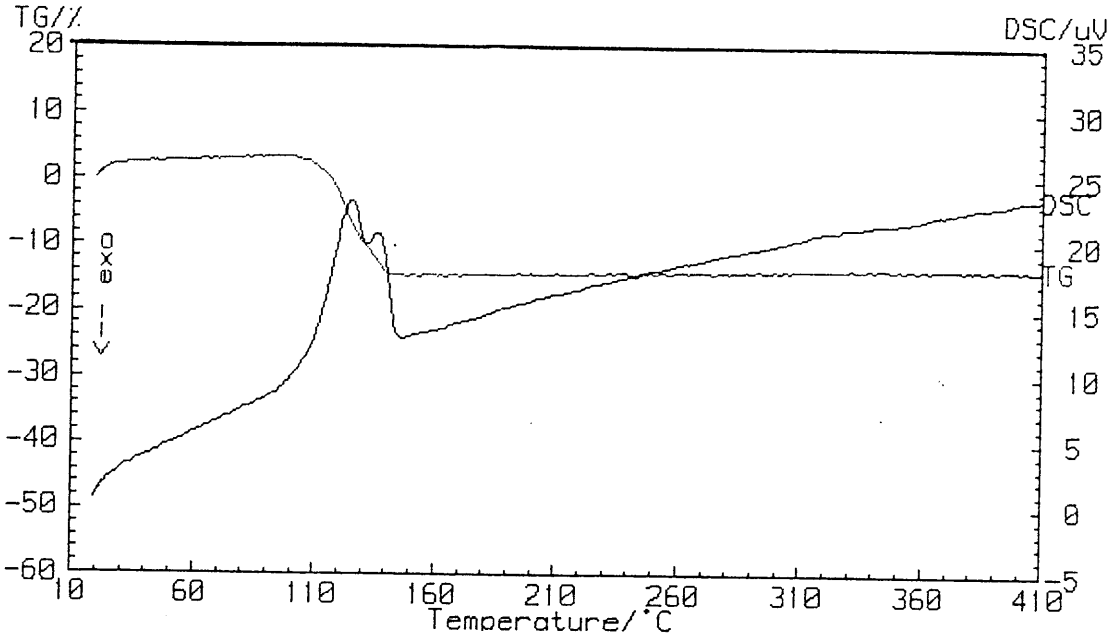

Figure 8.1.1 (c): TG and DSC curves of the decomposition of calcium sulphate dihydrate to anhydrite in air/water-atmosphere using a heating rate of 5 °C min^{-1}

The following is observed when calcium sulphate dihydrate samples are decomposed in air-atmosphere using a heating rate of 5 °C min^{-1} (see figure 8.1.1 (d) for the electron micrographs of the decomposed samples at the various temperatures): The unheated calcium sulphate dihydrate has some calcium sulphate anhydrite impurity present. At ≈ 60 °C, a very small amount of hemihydrate has formed (see table 8.1.1 (b) for the XRD results). At ≈ 170 °C, some hemihydrate and anhydrite have formed and indications of $CaSO_4 \bullet 0.62\ H_2O$ are found. Some $CaSO_4 \bullet 0.15\ H_2O$ also appears to be present. At ≈ 240 °C, only anhydrite is present. The thermogravimetric analysis of pure calcium sulphate dihydrate in figure 8.1.1 (a) shows a very low mass loss (± 1 %) from ambient temperature to 95 °C. The mean mass loss for calcium sulphate dihydrate is 19 % (which corresponds to the loss of 1.8 water molecules from the reactant) but is somewhat less than the 20.9 % calculated for the formation of the anhydrite. The calcium sulphate dihydrate, on calculation, is only ~ 91 % pure. The heat of dehydration is found to be between 0.4 - 0.5 kJ g^{-1}.

Table 8.1.1 (b): XRD results of the thermal decomposition of calcium sulphate dihydrate

SAMPLE $CaSO_4 \bullet 2H_2O$	VALUES OF DATABASE STANDARDS Å Relative Intensity			
Decomposition Temperature- Å Relative Intensity	CALCIUM SULPHATE DIHYDRATE	CALCIUM SULPHATE HEMI-HYDRATE	CALCIUM SULPHATE ANHYDRITE	$CaSO_4 \bullet 0.62H_2O$
	7.630_{100}	6.013_{80}	3.499_{100}	6.001_{80}
	4.283_{100}	3.467_{50}	2.849_{29}	3.467_{40}
	3.065_{75}	3.006_{100}	2.328_{20}	3.003_{80}
	2.873_{45}	2.803_{90}	2.209_{20}	2.812_{100}
	2.685_{35}	1.849_{20}	1.869_{16}	2.137_{20}
	2.685_{35}	1.845_{30}	1.648_{15}	1.848_{30}
	2.086_{25}	1.693_{20}		1.694_{20}
		1.665_{20}		
unheated				
7.588_{100}	✓			
4.286_{65}	✓			
3.055_{65}	✓			
2.868_{31}	✓		✓	
2.684_{18}	✓			
2.212_{17}			✓	
2.043_{5}	✓			
1.869_{12}			✓	
1.646_{8}			✓	
≈ 60 °C				
7.588_{100}	✓			
4.266_{79}	✓			
3.489_{54}		✓	✓	
2.873_{44}	✓	✓		

2.680_{28}	✓			
2.333_{10}			✓	
2.212_{23}			✓	
2.078_{26}	✓			
1.864_{15}			✓	
1.849_{18}		✓		
≈ 170 °C				
5.979_{53}				
3.496_{100}			✓	✓
3.005_{75}				✓
2.855_{25}			✓	
2.327_{22}			✓	
2.209_{19}			✓	
2.139_{19}				✓
1.846_{44}			✓	✓
1.693_{19}				✓
≈ 240 °C				
3.476_{73}			✓	
2.842_{35}			✓	
2.330_{19}			✓	
2.204_{19}			✓	
1.866_{22}			✓	
1.646_{16}			✓	

Figure 8.1.1 (d): Electron micrographs of calcium sulphate dihydrate at various decomposition temperatures

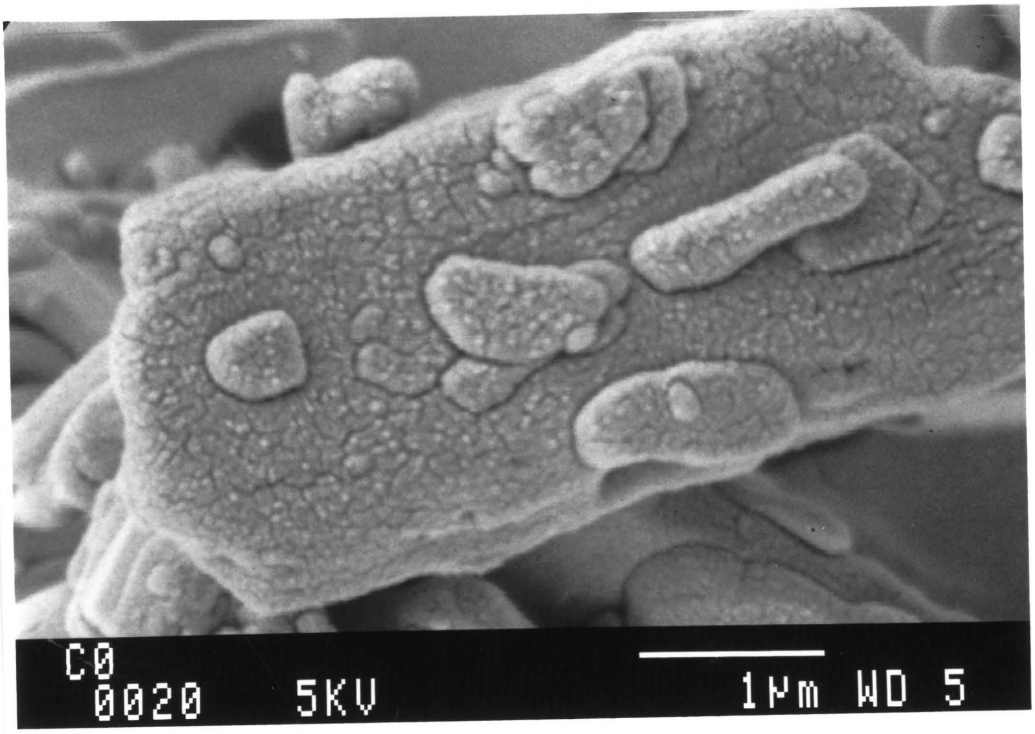

(i) unheated

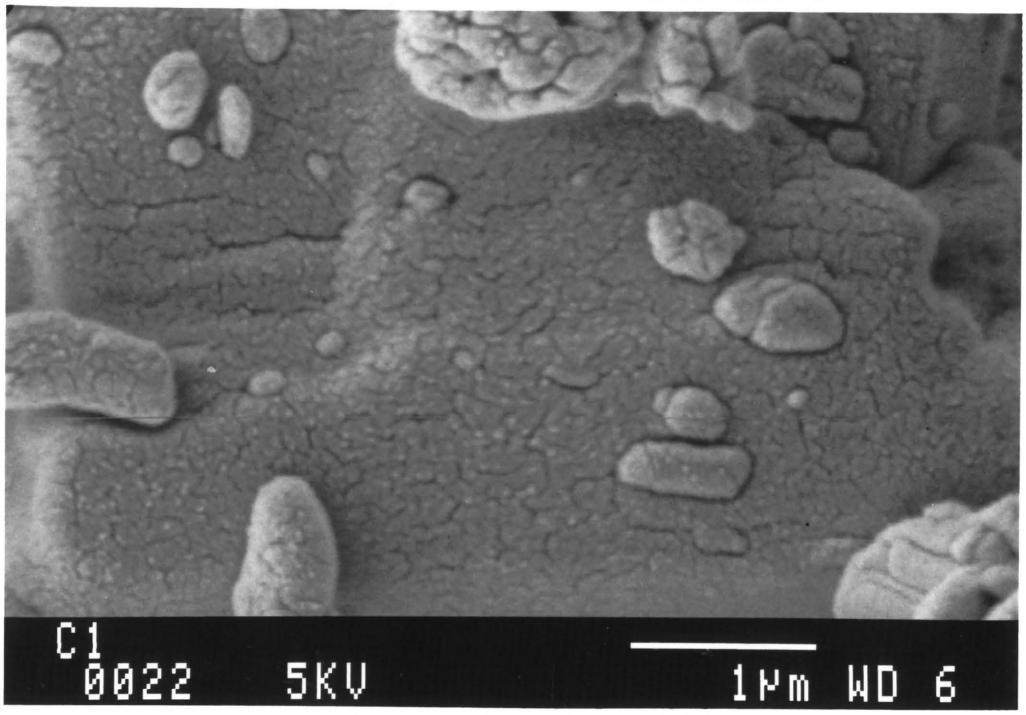

(ii) ≈ 60 °C

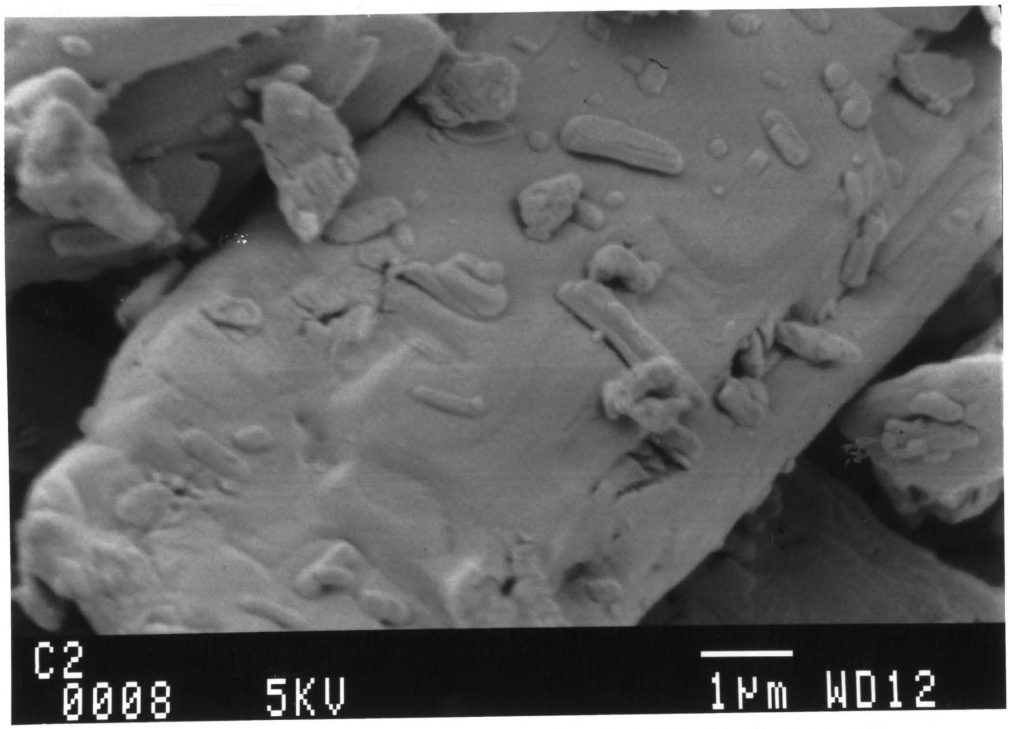

(iii) ≈ 170 °C

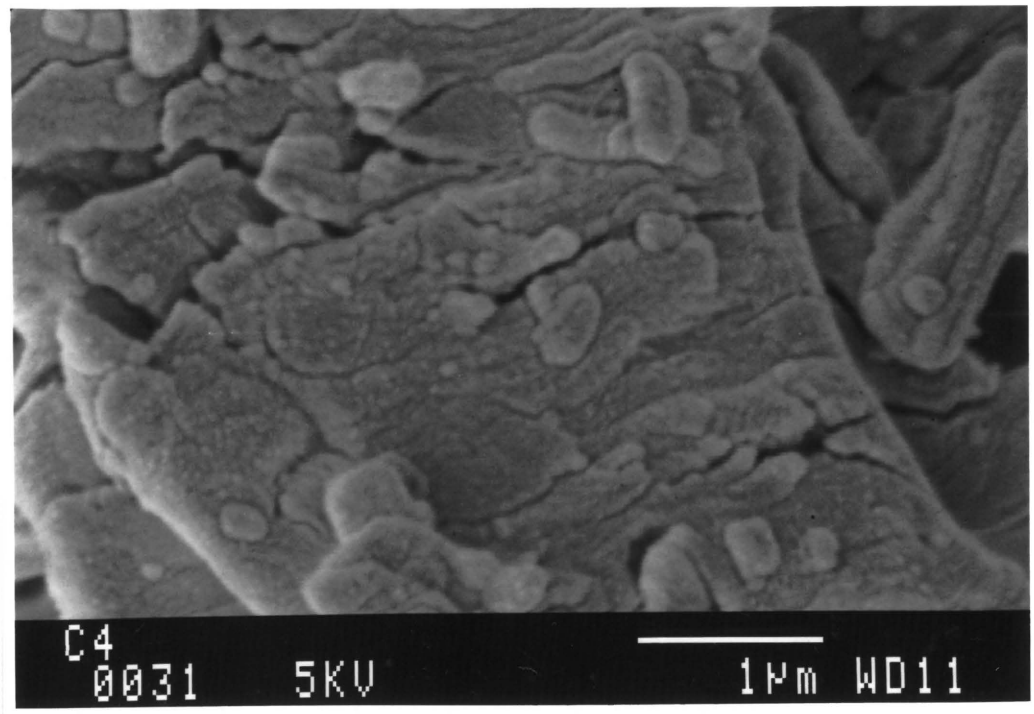

(iv) ≈ 240 °C

8.1.1.1 Kinetics of the dehydration of calcium sulphate dihydrate to calcium sulphate anhydrite in nitrogen-atmosphere

Figure 8.1.1.1 (a) shows a plot of activation energy, E_a, versus α (fraction decomposed) for the dehydration reactions up to 240 °C. It is clear that the dehydration reaction does not occur in a single step. There are at least three stages in the dehydration reaction of calcium sulphate dihydrate (figure 8.1.1.1 (a)).

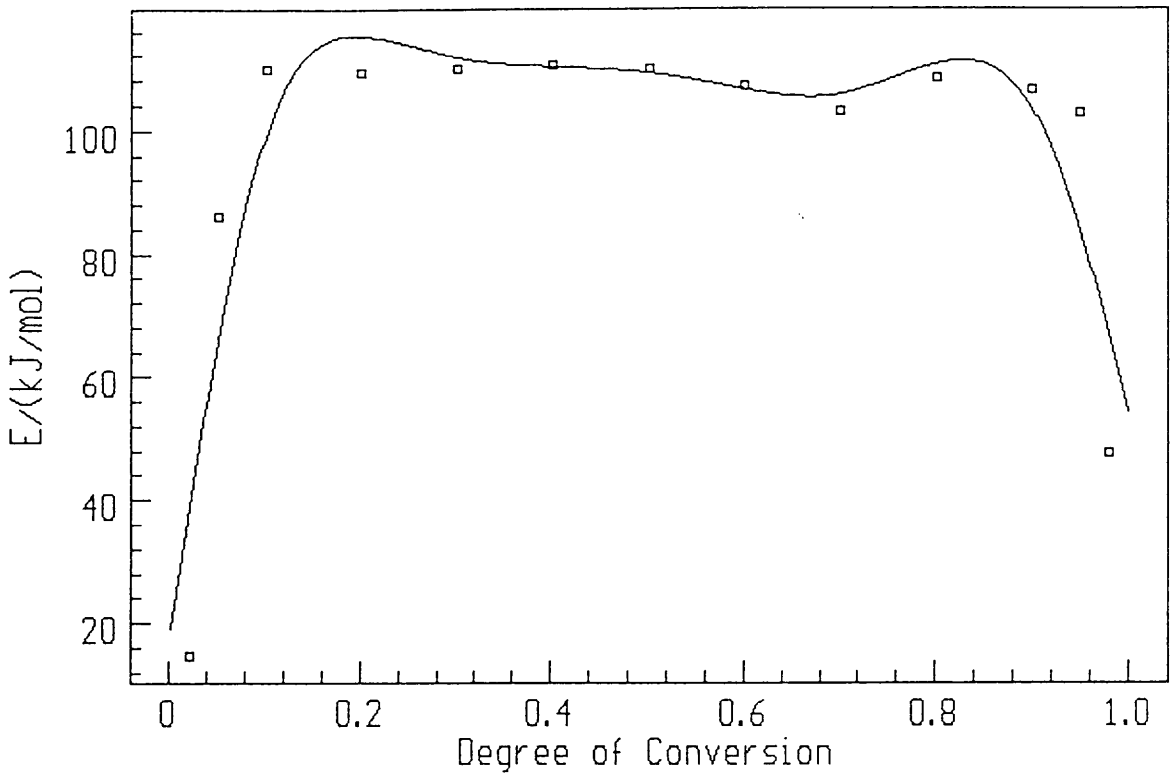

Figure 8.1.1.1 (a): Plot of activation energy, E_a, vs α for the dehydration of calcium sulphate dihydrate to calcium sulphate anhydrite in a nitrogen-atmosphere

The activation energy increases between 0 and 0.1 degree of conversion (from ≈ 10 to ≈ 110 kJ mol^{-1}) which implies that the reaction with the higher activation energy contributes to the heat absorbed [85]. The activation energy remains constant at a value of ≈ 109 kJ mol^{-1} until α = 0.8. Thus, it can be assumed that the temperature dependence of the overall process rate is governed by one activation energy [85]. The average

activation energy is a good approximation for the activation energy of the limiting reaction [85]. The ln A value is ≈ 6 for $0.1 < \alpha < 0.8$. For $0.8 < \alpha < 1$, the activation energy decreases sharply implying that the contribution of the reaction with the higher activation energy, is decreasing [85]. The maximum activation energy is ≈ 110 kJ mol^{-1} and the minimum is ≈ 50 kJ mol^{-1}.

Using the Netzsch Thermokinetic Analysis Program [10], it appears that calcium sulphate dihydrate could dehydrate according to the three-dimensional diffusion equation of Jander for $0 < \alpha < 0.1$. The correlation coefficient is 0.634, ln A = 14 and the Durbin-Watson value is 0.082. The average activation energy recorded is 137 kJ mol^{-1}. It is clear that this mechanism does not describe the decomposition reaction taking place for $0 < \alpha < 0.1$; as the corrrelation coefficient indicates that the experimental and theoretical results do not correlate.

For $0.1 < \alpha < 0.8$, the dehydration reaction can be described by the first order, the n-th order or the d-dimensional Avrami-Erofe'ev. The d-dimensional Avrami-Erofe'ev equation does appear, however, to give the best fit with a correlation coefficient of 0.992 and an average activation energy of 107 kJ mol^{-1}; a Durbin-Watson value of 0.041 and a ln A of 12. The activation energy value corresponds very well with that of ≈ 109 kJ mol^{-1} obtained using the isoconversional method. This decomposition reaction is controlled by the growth of the calcium sulphate hemihydrate and the anhydrite nuclei and their reaction interface.

Figure 8.1.1.1 (b) is the fit of the d-dimensional Avrami-Erofe'ev equation. The experimental data points for $0.1 < \alpha < 0.8$, is represented by the symbols and the various symbols indicate different heating rates. The crosses on the graph represent the degrees of conversion that fall outside the $0.1 < \alpha < 0.8$ region. The solid line is the fitting of the theoretical model for the reaction. There is a poor fit at the start and end of the dehydration process but a good fit for $0.1 < \alpha < 0.8$.

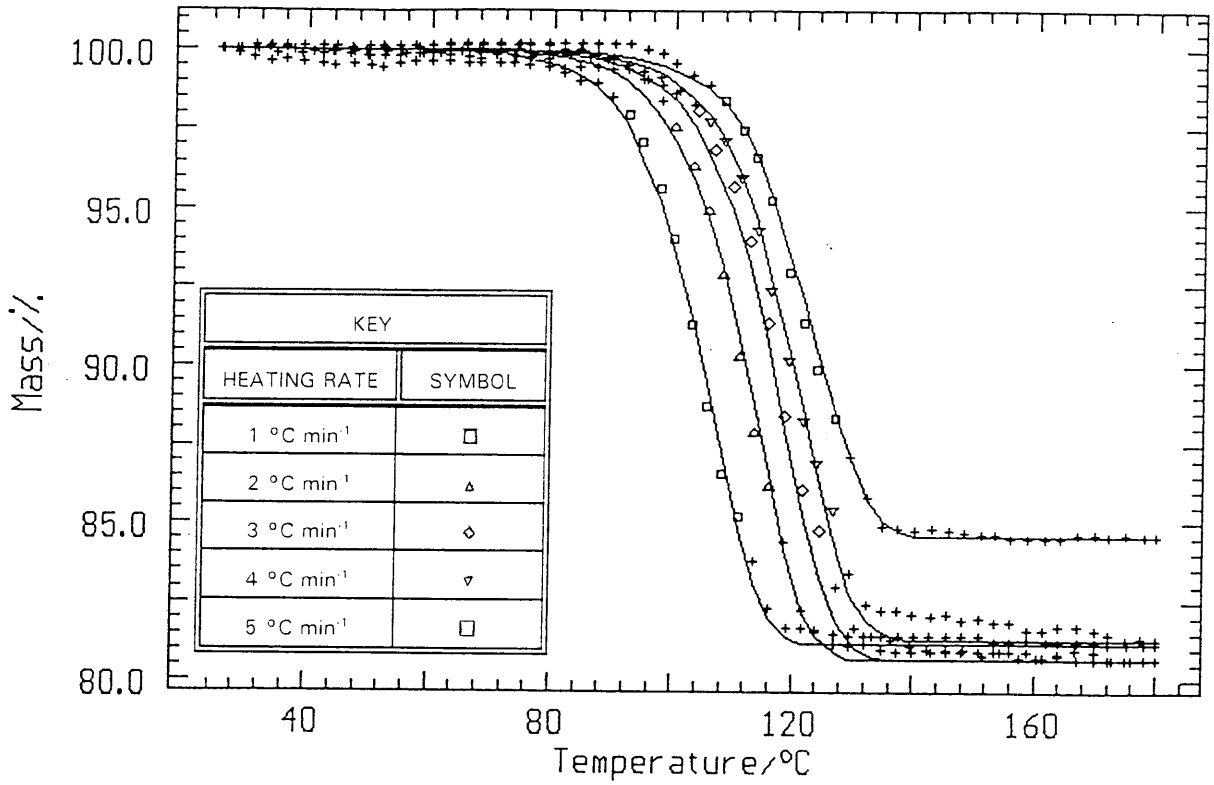

Figure 8.1.1.1 (b): Fitting of experimental data of the decomposition of calcium sulphate dihydrate with the kinetic model for a d-dimensional Avrami-Erofe'ev decomposition reaction in a nitrogen-atmosphere

The last stage of dehydration for $0.8 < \alpha < 1$ appears to be best described by the first order decomposition reaction, $1 - \alpha = e^{-kt}$, with a correlation coefficient of 0.982, a Durbin-Watson value of 0.112 and ln A of 12, and an average activation energy value of 107 kJ mol^{-1}. This is a conclusive fit when comparing the activation energy (107 kJ mol^{-1}) to that obtained from the isoconversional method ($\approx$ 110 kJ mol^{-1}) and the correlation coefficient is 0.982. Generally, the first order kinetic expression holds at the end of the decomposition reaction. The particles are relatively small and it is based on the nucleation of particles by an exponential law followed by rapid two-dimensional growth [14, page 64]. The activation energy values do differ with α-values indicating a complex reaction.

8.1.1.2 Kinetics of the dehydration of calcium sulphate dihydrate to calcium sulphate anhydrite in an air/water-atmosphere

Figure 8.1.1.2 (a) shows a plot of activation energy, E_a, versus α for the dehydration reactions up to 180 °C in the air/water-atmosphere.

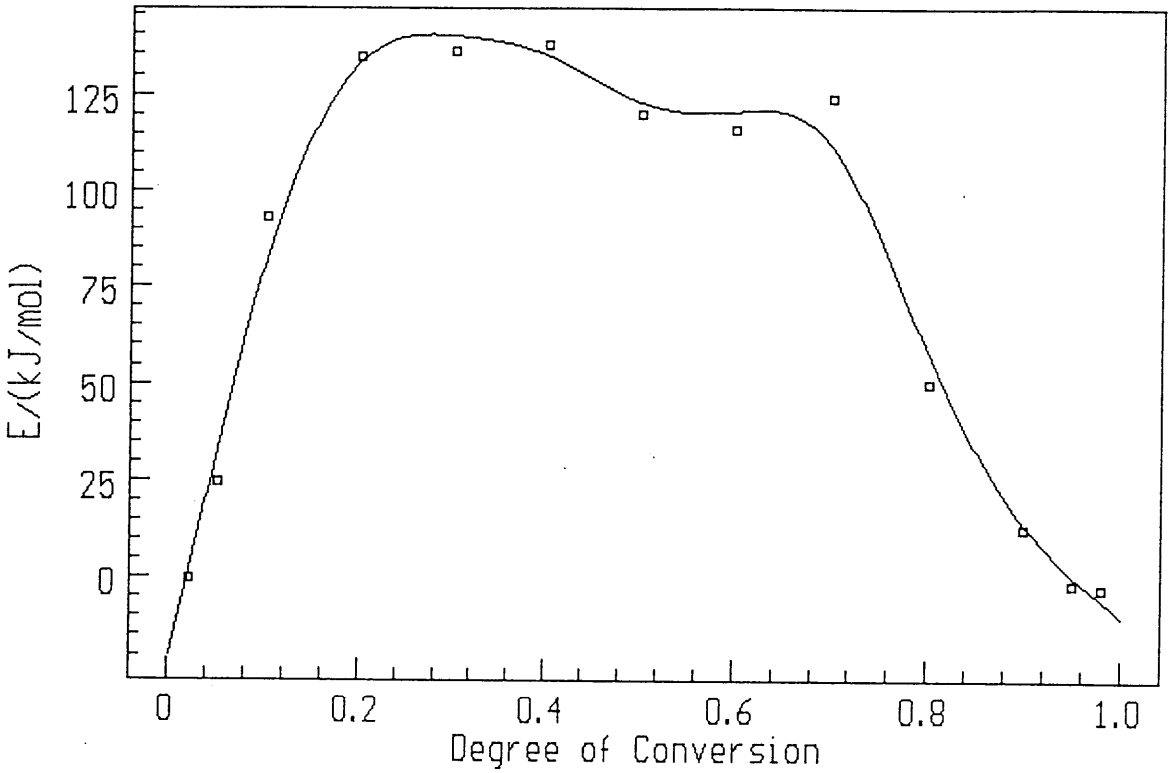

Figure 8.1.1.2 (a): Plot of activation energy, E_a, vs α for calcium sulphate dihydrate in an air/water-atmosphere

There are at least three stages of the dehydration reaction of calcium sulphate dihydrate to the anhydrite in the air/water-atmosphere. The activation energy increases between 0 to 0.2 (from ≈ 0 to ≈ 128 kJ mol^{-1}) which implies that the reaction with the higher activation energy contributes to the heat absorbed [85]. The ascending part of the plot indicates that the reaction with the higher activation energy makes a significant contribution to the heat being absorbed. Once the contribution of the reaction with the higher activation energy reaches its maximum, the activation energy remains constant. The activation energy remains approximately constant at a value of ≈ 128 kJ mol^{-1} until α = 0.7. The ln A value is ≈ 15. Thus, it can be

assumed that between $0.2 < \alpha < 0.7$, the temperature dependence of the overall process rate is governed by one activation energy [85]. The average activation energy is a good approximation for the activation energy of the limiting reaction [85]. For $0.7 < \alpha < 1$, there is a sharply decreasing activation energy value. The maximum activation energy is $\approx$ 128 kJ mol^{-1} and the minimum is $\approx$ 0 kJ mol^{-1}.

Using the Netzsch Thermokinetic Analysis Program [10], no kinetic model appears to fit the experimental results for the $0 < \alpha < 0.2$ range.

For $0.2 < \alpha < 0.7$, the dehydration reaction can be described by the second order or the 3-dimensional diffusion equation of Jander (correlation coefficient = 0.899; Durbin-Watson value = 0.434; activation energy = 174 kJ mol^{-1} and a ln A value = 20). The second order equation does appear, however, to give the best fit with a correlation coefficient of 0.940 and an average activation energy of 156 kJ mol^{-1} and ln A of 19. The activation energy value does not compare well with that of $\approx$ 128 kJ mol^{-1} obtained using the isoconversional method. The order of the reaction is defined in terms of reactant concentration [13, page 377]. The concentration must have constant values throughout the reacting material. They may change with time but not with position.

Figure 8.1.1.2 (b) is the second order fit. It is a reasonable fit for $0.2 < \alpha < 0.7$ but a poor fit at the start and at the end of the dehydration process.

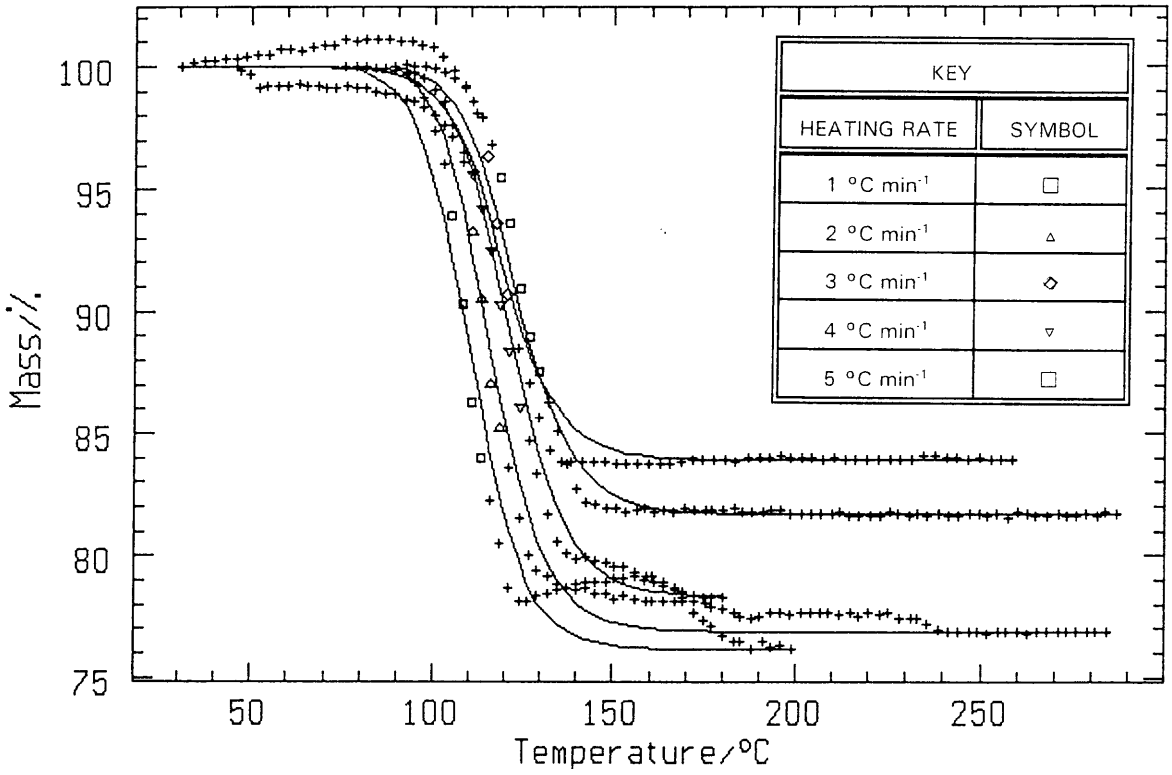

Figure 8.1.1.2 (b): Fitting of experimental data of calcium sulphate dihydrate with the kinetic model for a second order decomposition reaction in an air/water-atmosphere

The last stage of dehydration for $0.7 < \alpha < 1$, appears to be best described by the second order decomposition reaction with a correlation coefficient of 0.952 and ln A of 15, and an average activation energy value of 129 kJ mol^{-1}. There is good correlation between the experimental and the theoretical results but it appears that because the activation energy values decrease with increasing α-values, that the reaction is more complex. The dehydration of the calcium sulphate hemihydrate in an air/water-atmosphere proceeds without an incubation period and the second order reaction appears to be the most suitable description. It would appear that the water molecules in the atmosphere adhere to the nascent anhydrite interface and may prevent the dehydration of the water molecules from the hemihydrate.

Thus, the rate controlling step is likely to be random nucleation.

A summary of the kinetic data for the decomposition of pure calcium sulphate dihydrate in nitrogen- and air/water-atmospheres up to 180 °C is given in table 8.1.1 (c):

Table 8.1.1 (c): Summary of the kinetic data obtained for calcium sulphate dihydrate

Atmosphere	α-Range	Kinetic Data from the Isoconversional Method		Kinetic Data from the Kinetic Models			
				Kinetic Model			
		E_a (kJ mol^{-1})	ln A	E_a (kJ mol^{-1})	ln A	D-W	Corr.Coeff
Nitrogen	$0 < \alpha < 0.1$	10 - 115	-	No fit			
	$0.1 < \alpha < 0.8$	109	6	d-dimensional Avrami-Erovfe'ev equation 107	12	0.041	0.992
	$0.8 < \alpha < 1$	110 - 50	-	first order 107	12	0.112	0.982
Air/water	$0 < \alpha < 0.2$	0 - 128	-	No fit			
	$0.2 < \alpha < 0.7$	128	15	second order 156	19	0.424	0.940
	$0.7 < \alpha < 1$	128 - 0	-	second order 129	15	0.076	0.952

Key of abbreviations in table: E_a = activation energy; D-W = Durbin-Watson value and Corr. Coeff. = correlation coefficient.

8.1.2 Synthetic gypsum

Figure 8.1.2 (a) shows the thermal decomposition of synthetic gypsum in an air-atmosphere using a heating rate of 5 °C min^{-1}. The following table shows the thermal decomposition of synthetic gypsum in different atmospheres.

Table 8.1.2 (a): The thermal decomposition of synthetic gypsum with different sample masses in different atmospheres using a heating rate of 5 °C min^{-1}

Sample mass(mg)	Atmos-phere	Temperature Range (°C)	Mass Loss (%)	Mass Gain (%)	ΔH in kJ g^{-1}
5	N_2	90 - 130	15	-	3×10^{-1}
10	N_2	93 - 146	15	-	3×10^{-1}
15	N_2	100 - 146	15	-	3×10^{-1}
10	Air	98 - 140	15	-	3×10^{-1}
10	Air/H_2O	29 - 106 106 - 135 136 - 300 300 - 348	3 13 - 2	- - 2 -	- 2×10^{-1} - -

The total percentage mass loss for various sample sizes namely 5, 10 and 15 mg, remain constant irrespective of the sample size. Thus, a 10 mg sample mass is used in order to do the kinetic model comparison. The thermograms and the total mass losses are the same for a 10 mg sample using a heating rate of 5 °C min^{-1} in an air-atmosphere and in a nitrogen-atmosphere. Compare figure 8.1.2 (a) and 8.1.2 (b). Thus, nitrogen-atmosphere is used for the kinetic study.

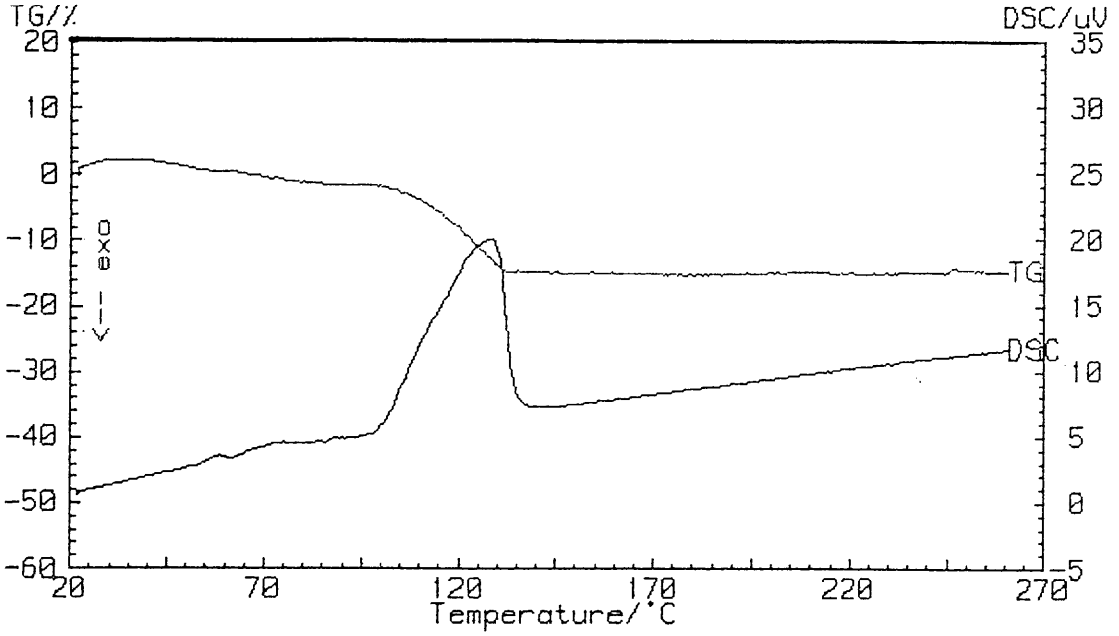

Figure 8.1.2 (a): **TG and DSC curves of the dehydration of synthetic gypsum in an air-atmosphere using a heating rate of 5 °C min^{-1}**

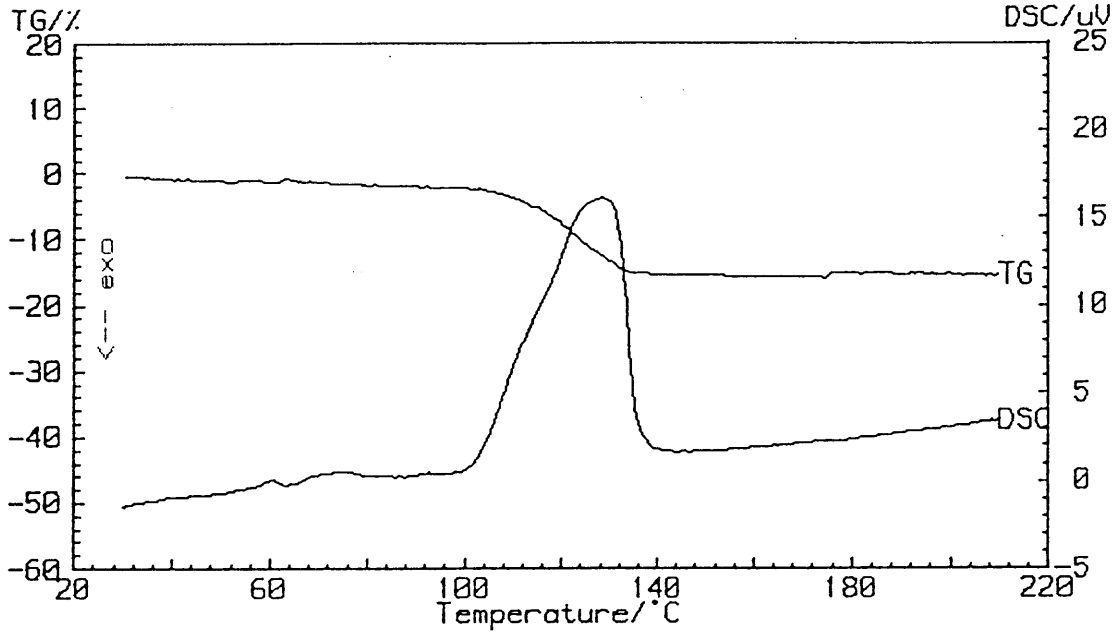

Figure 8.1.2 (b): **TG and DSC curves of the dehydration of synthetic gypsum in a nitrogen-atmosphere using a heating rate of 5 °C min^{-1}**

The thermal decomposition of synthetic gypsum in an air/water-atmosphere gives a mass loss of 16 % (figure 8.1.2 (c)). This is due to the hemihydrate

and anhydrite present as impurities, reacting with the water vapour in the surrounding atmosphere. The heat of dehydration is also less than in air- or nitrogen-atmosphere, possibly due to exothermic adsorption of water vapour occurring. Synthetic gypsum starts to decompose at a lower temperature, namely 29 °C in an air/water-atmosphere than in a nitrogen- or an air-atmosphere. The water vapour present in the air/water-atmosphere, reacts with the hemihydrate and anhydrite present and this adsorbed water is released at low temperatures.

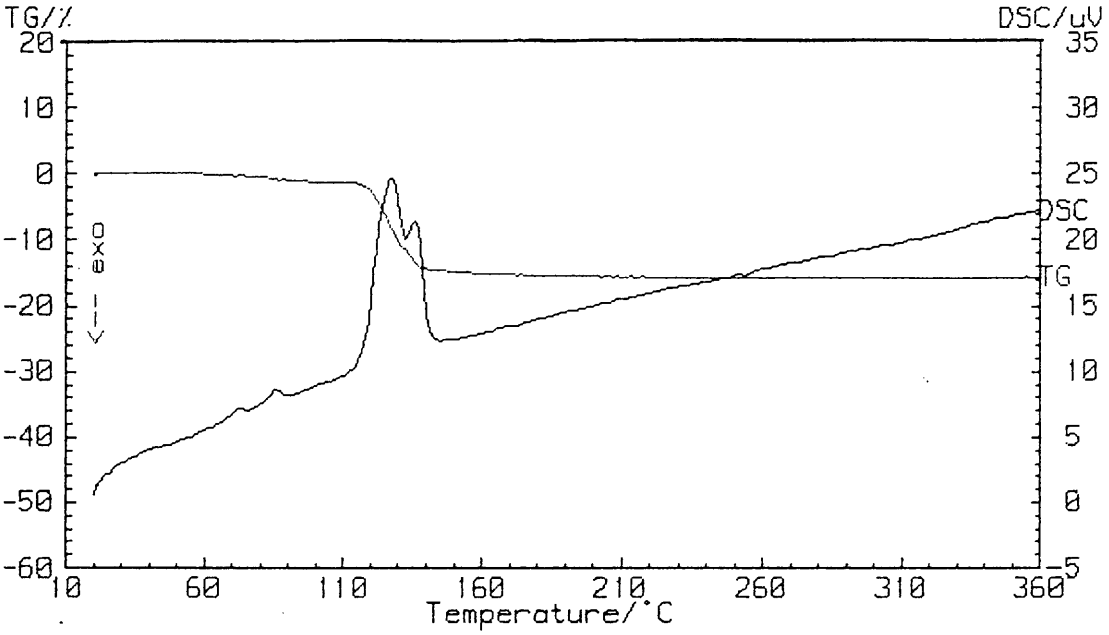

Figure 8.1.2 (c): The TG and DSC curves of the dehydration of synthetic gypsum in an air/water-atmosphere using a heating rate of 5 °C min^{-1}

The following products are obtained on the thermal decomposition of the synthetic gypsum in an air-atmosphere using a heating rate of 5 °C min^{-1}: The XRD results (see table 8.1.2 (b)) indicate that the starting compound of synthetic gypsum consists of the dihydrate and the anhydrite. No hemihydrate is observed. Figure 8.1.2 (d) shows the electron micrographs taken at various decomposition temperatures. No melting is observed from the micrographs. At ≈ 60 °C, a very small amount of the hemihydrate, indicating the very slow dehydration of the dihydrate, is present at the temperatures below 95 °C. At ≈ 165 °C, the main product is anhydrite

but there is still some hemihydrate present. At 250 °C, the reaction mixture consists of $CaSO_4 \bullet 0.15\ H_2O$, calcium sulphite, γ - $CaSO_4$ and possibly some bassinite, $Ca_2(SO_4)_2 \bullet H_2O$. It is also found that even at a temperature of 450 °C, there are small amounts of $CaSO_4 \bullet 0.15\ H_2O$; $Ca_2(SO_4)_2 \bullet H_2O$; $CaSO_3$; γ - $CaSO_4$ and possibly even $Ca_3(SO_3)_2 \bullet SO_4$ present.

Table 8.1.2 (b): XRD results of the thermal decomposition of synthetic gypsum

SAMPLE	VALUES OF DATABASE STANDARDS Å Relative Intensity						
Decomposition Temperature- Å Relative Intensity	CALCIUM SULPHATE DIHYDRATE	CALCIUM SULPHATE HEMI-HYDRATE	CALCIUM SULPHATE ANHYDRITE	$CaSO_4 \bullet 0.62H_2O$	$CaSO_3$	γ - $CaSO_4$	$CaSO_4 \bullet 0.15H_2O$
	7.630_{100}	6.013_{80}	3.499_{100}	6.001_{80}	3.047_{100}	3.498_{100}	6.050_{100}
	4.283_{100}	3.467_{50}	2.849_{29}	3.467_{40}	2.925_{100}	2.854_{80}	3.490_{40}
	3.065_{75}	3.006_{100}	2.328_{20}	3.003_{80}	2.853_{50}	2.332_{50}	3.018_{85}
	2.873_{45}	2.803_{90}	2.209_{20}	2.812_{100}	2.797_{33}	2.211_{50}	2.794_{20}
	2.685_{35}	1.849_{20}	1.869_{16}	2.137_{20}	2.770_{39}	2.110_{50}	1.847_{15}
	2.685_{35}	1.845_{30}	1.648_{15}	1.848_{30}	2.468_{13}	2.088_{20}	1.741_{10}
	2.086_{25}	1.693_{20}		1.694_{20}	2.314_{28}	1.997_{30}	1.694_{10}
		1.665_{20}			2.020_{14}	1.872_{50}	
unheated							
7.588_{53}	✓						
4.286_{93}	✓						
3.489_{61}			✓				
3.055_{100}	✓						
2.868_{61}	✓		✓				
2.684_{53}	✓						
2.212_{20}			✓				
2.043_{53}	✓						

≈ 60 °C							
7.588_{100}	✓						
4.266_{55}	✓						
3.489_{55}			✓				
3.467_{15}		✓					
3.060_{55}	✓						
3.006_{21}		✓					
2.868_{19}			✓				
2.803_{21}		✓					
1.844_{32}		✓					
≈ 165 °C							
6.013_{26}		✓					
4.286_{20}	✓						
3.489_{60}			✓				
3.467_{65}		✓					
3.055_{9}	✓						
3.006_{100}		✓					
2.868_{30}	✓						
2.803_{87}		✓					
2.684_{17}	✓						
1.849_{87}		✓					
≈ 250 °C							
3.498_{80}						✓	✓
3.047_{39}					✓		✓
2.854_{73}						✓	
2.803_{50}		✓					✓
2.468_{25}					✓		
2.332_{45}						✓	
2.211_{45}						✓	
1.997_{49}						✓	
1.845_{100}		✓					✓

Figure 8.1.2 (d): Electron micrographs of synthetic gypsum at various decomposition temperatures

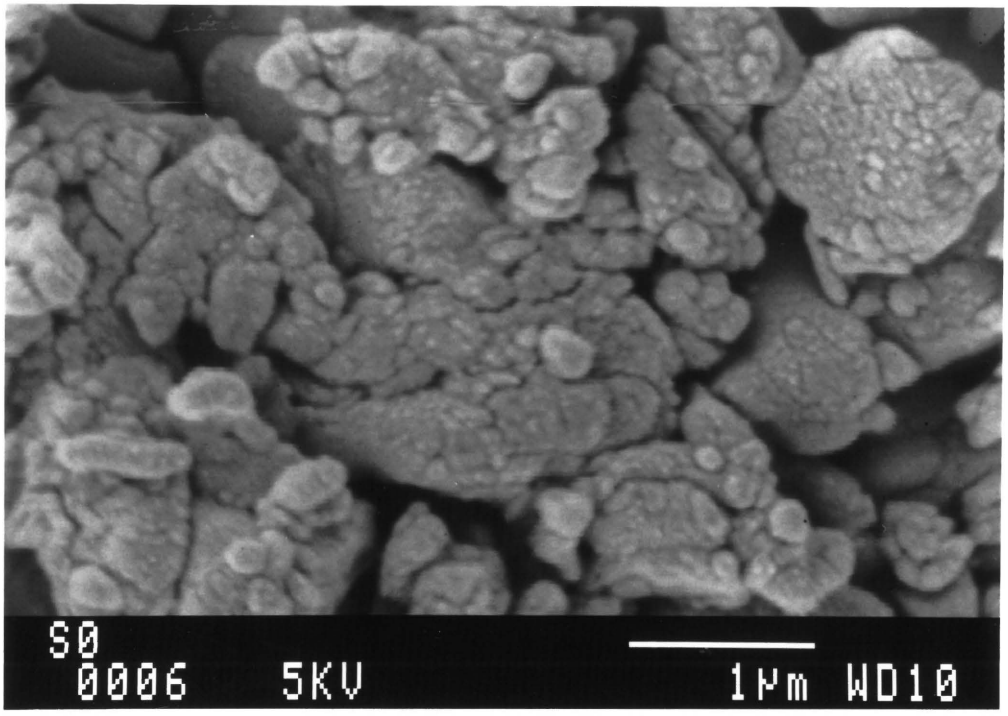

(i) unheated

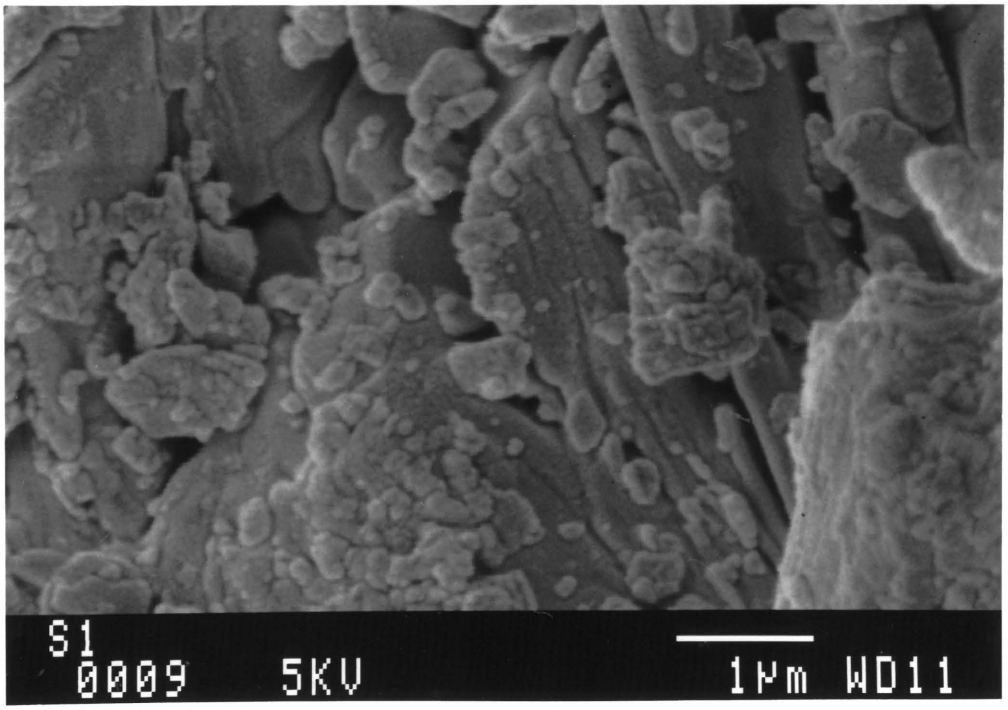

(ii) ≈ 60 °C

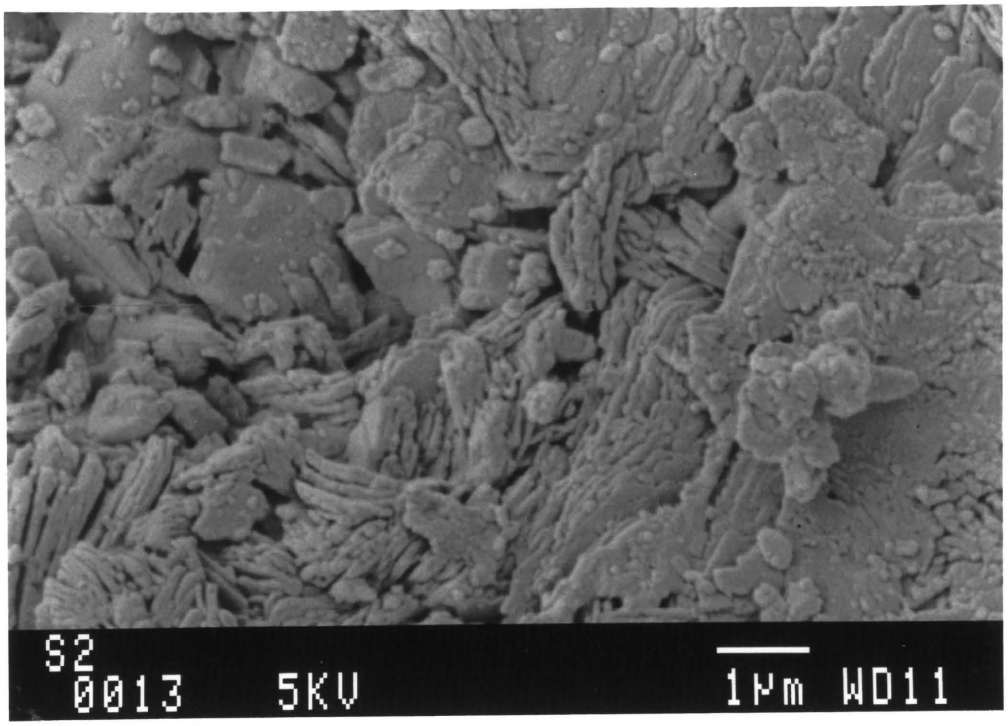

(iii) ≈ 165 °C

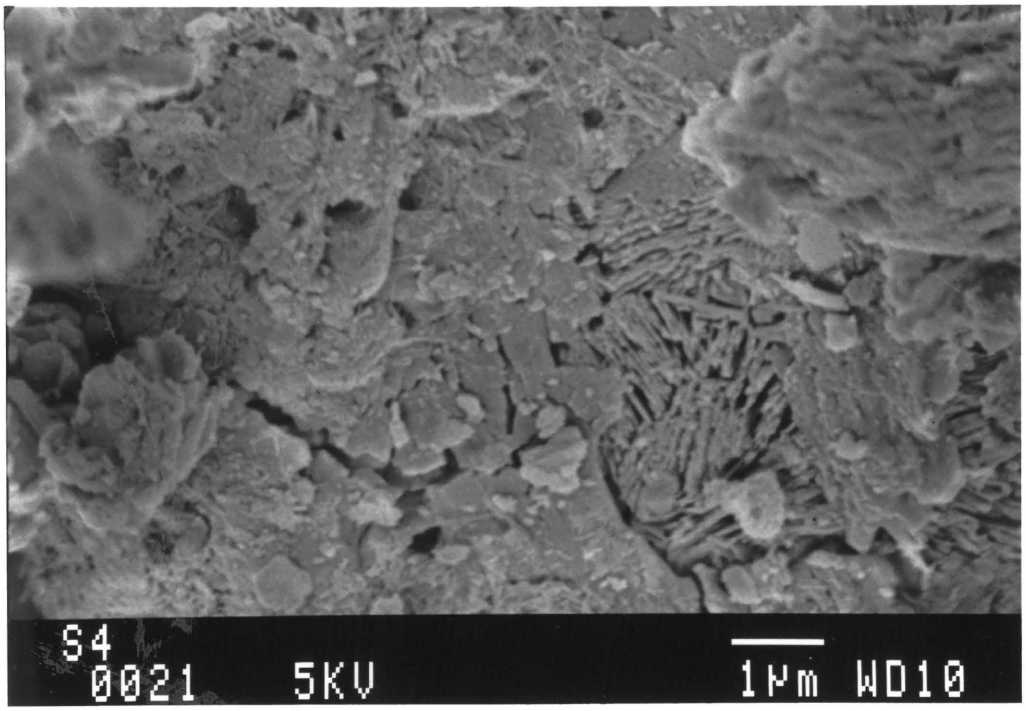

(iv) ≈ 250 °C

Using a heating rate of approximately 5 °C min^{-1}, synthetic gypsum shows firstly a very low mass loss (± 1 %) from ambient temperature to 95 °C in air-atmosphere, as presented in figure 8.1.2 (a). The DSC curve suggested two small reactions between 53 and 63 °C, and between 63 and 84 °C for the first reaction, an enthalpy value of between 2 x 10^{-3} and 3 x 10^{-3} kJ g^{-1} gypsum sample is obtained, and for the second process it is found to be 7 x 10^{-3} kJ g^{-1}. These two processes are observed on all the DSC curves and could be the result of the dehydration reactions of some of the other impurities in the gypsum samples. Since it has proved impossible to obtain 100 % homogeneous gypsum samples, the percentage mass loss and the enthalpy values are found to differ slightly for the various samples. The greatest mass loss (between 14 and 17 % for different samples) occurs between 95 and 170 °C using a heating rate of ≈ 5 °C min^{-1} (figure 8.1.2 (a)). Enthalpy change value for this total reaction is found to be 0.4 kJ g^{-1}.

8.1.2.1 Kinetics of the dehydration of synthetic gypsum to anhydrite in nitrogen-atmosphere

Using the temperature values at different α-values for different heating rates (0.5 °C min^{-1} < β < 5 °C min^{-1}), figure 8.1.2.1 (a) (activation energy E_a vs α) is obtained for the dehydration reactions of gypsum up to 180 °C.

From figure 8.1.2.1 (a), it is clear that the dehydration reactions do not occur in a single step. At least three stages in the dehydration can be observed. The activation energy increases between an α-value of 0 and 0.2 (from ≈ -10 to ≈ 100 kJ mol^{-1}) which implies that the reaction with the higher activation energy contributes to the heat absorbed [85]. The activation energy remains constant at a value of ≈ 100 kJ mol^{-1} until α = 0.8. The ln A value is ≈ 10. Thus, it can be assumed that the temperature dependence of the overall process rate is governed by one activation energy [85]. The average activation energy is a good approximation for the activation energy of the limiting reaction [85]. For 0.8 < α < 1, a sharply decreasing activation energy value with fraction reaction is observed. The

maximum activation energy is ≈ 100 kJ mol^{-1} and the minimum is ≈ 0 kJ mol^{-1}.

For α-values between 0 and 0.2, there is no mathematical fit.

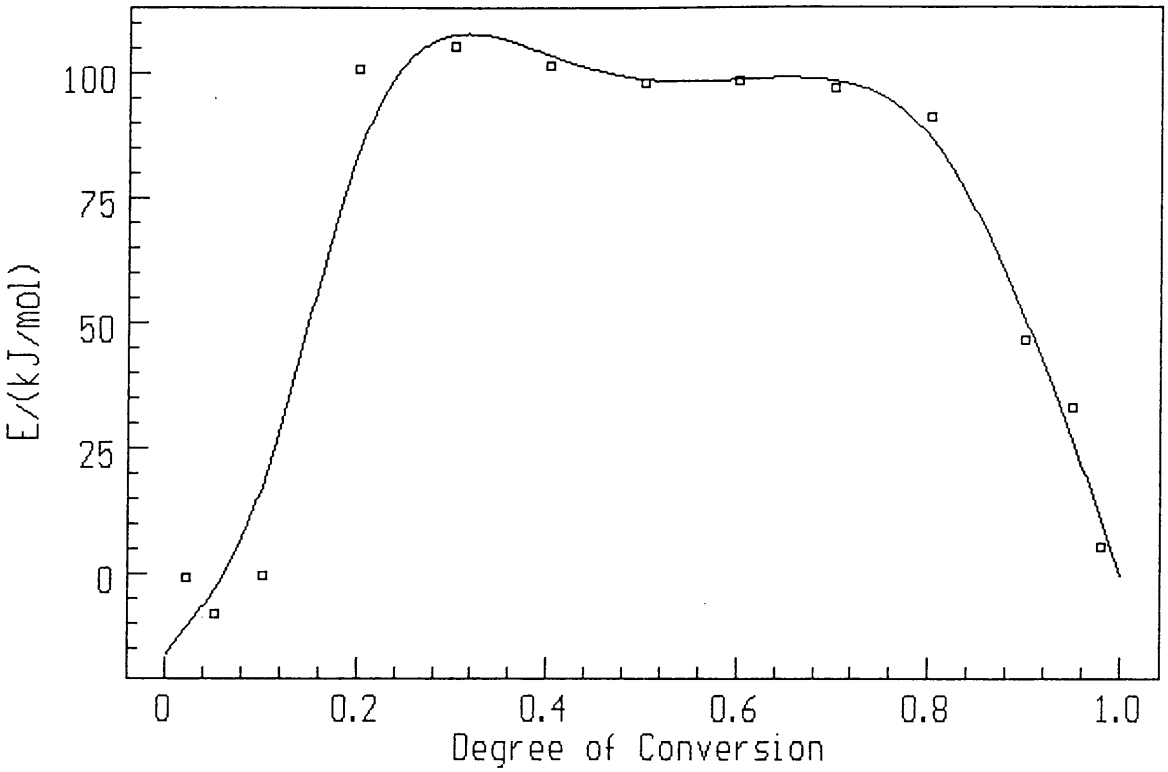

Figure 8.1.2.1 (a): Plot of activation energy, E_a, vs α for the dehydration of synthetic gypsum to the anhydrite in a nitrogen-atmosphere

Between α-values of 0.2 and 0.8, the first order reaction with autocatalytic activation appears to fit the data the best. Fitting of the model to experimental data gives a correlation coefficient value of 0.989 and a Durbin-Watson value of 0.047, both implying a good correlation between the experimental and theoretical data for this model. The activation energy value of 101 kJ mol^{-1} and ln A of 11, also correlate very well with the values obtained using the isoconversional method. As the calcium sulphate dihydrate decomposes, the nuclei of the hemihydrate are forming at the sites

present and by a mechanism referred to as branching. Nucleation might occur along dislocation lines.

Figure 8.1.2.1 (b) gives the fitting of the experimental data ($0.2 < \alpha < 0.8$) to the first order with autocatalytic reaction model.

The Sestak-Berggren equation best describes (correlation coefficient = 0.954, Durbin-Watson value = 0.116) the dehydration during the last stage of the dehydration reactions of gypsum to anhydrite (up to a maximum temperature of 180 °C for $0.8 < \alpha < 1.0$. An activation energy of 96 kJ mol^{-1} and ln A of 10 is calculated using this model.

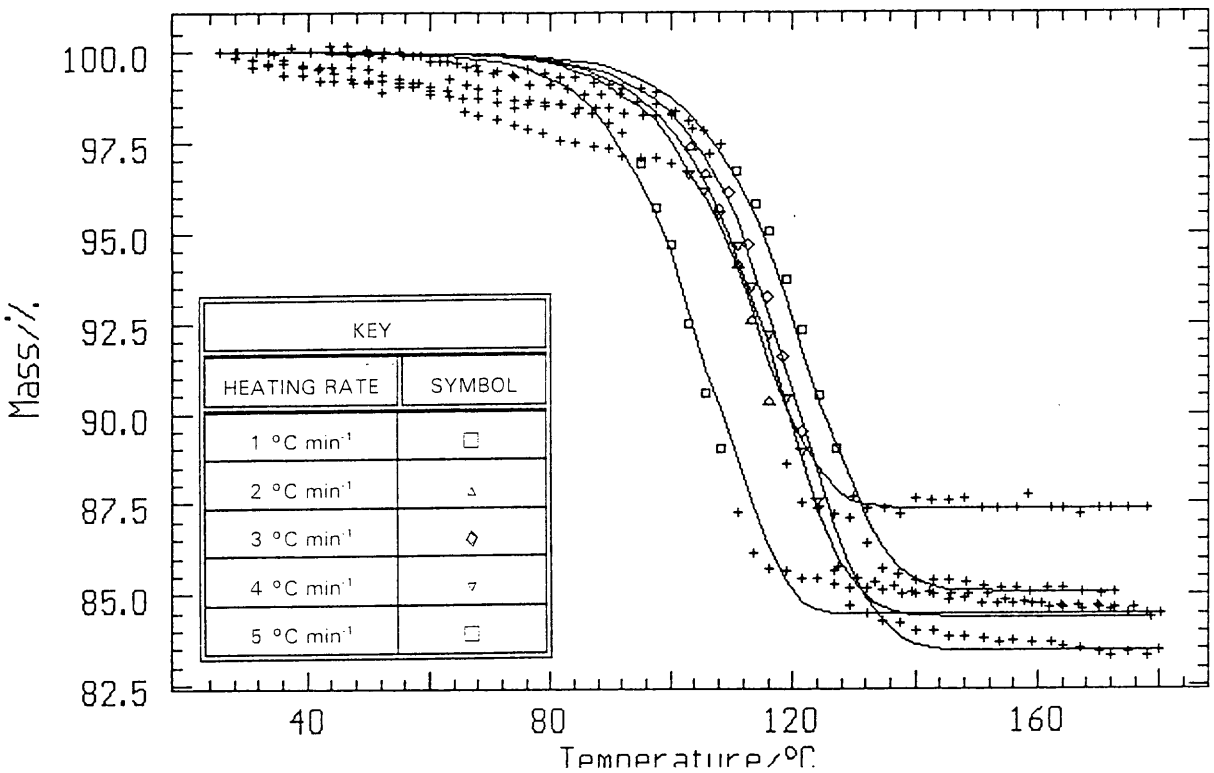

Figure 8.1.2.1 (b): Fitting of experimental mass loss data to the kinetic model for a first-order decomposition reaction with autocatalytic activation in a nitrogen-atmosphere

It is clear that for α-values between 0.2 and 0.8, a good correlation is obtained, but that during the beginning and end of the reactions combined mechanisms must be dominating.

8.1.2.2 Kinetics of the dehydration of synthetic gypsum to anhydrite in an air/water-atmosphere

Using the temperature values at different α-values for different heating rates ($0.5\ ^{\circ}C\ min^{-1} < \beta < 5\ ^{\circ}C\ min^{-1}$), figure 8.1.2.2 (a) (activation energy, E_a, vs α), is obtained for the dehydration reactions of synthetic gypsum in an air/water-atmosphere up to 180 °C.

From figure 8.1.2.2 (a), it is clear that the dehydration reactions do not occur in a single step. At least four stages can be observed.

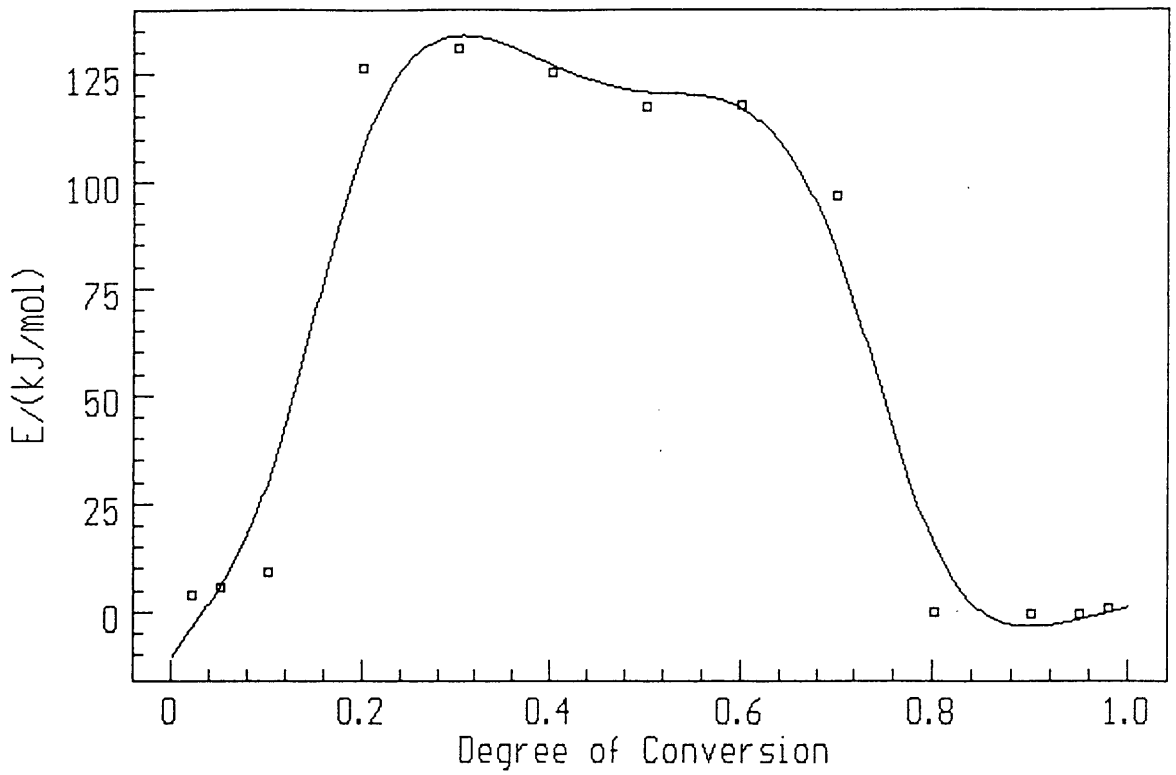

Figure 8.1.2.2 (a): Plot of activation energy, E_a, vs α for the dehydration of synthetic gypsum to anhydrite in an air/water-atmosphere

The activation energy increases between an α-value of 0 and 0.2 (from $\approx$ 0 to $\approx$ 125 kJ mol^{-1}) which implies that the reaction with the higher activation energy contributes to the heat absorbed [85]. The activation energy remains constant at a value of $\approx$ 125 kJ mol^{-1} until α = 0.7. The ln A value is $\approx$ 13. Thus, it can be assumed that the temperature dependence of the overall process rate is governed by one activation energy [85]. The average activation energy is a good approximation for the activation energy of the limiting reaction [85]. For $0.7 < \alpha < 0.8$, a sharply decreasing activation energy value with fraction reaction is observed. The maximum activation energy is $\approx$ 125 kJ mol^{-1} and the minimum is $\approx$ 0 kJ mol^{-1}, where it stays more or less constant until α = 1.0.

For α-values between 0 and 0.2, no kinetic model is found to fit the experimental data.

Between α-values of 0.2 and 0.7, a much better fit of the equations of Sestak-Berggren and a first order reaction with autocatalytic activation, is observed. The Sestak-Berggren equation, however, appears to be the conclusive fit, with a correlation coefficient of 0.968 and a Durbin-Watson value of 0.234. The activation energy value of 114 kJ mol^{-1} and ln A = 13, compares very well to the values of $\approx$ 119 kJ mol^{-1} and ln A of $\approx$ 13 obtained using the isoconversional method.

No fit is obtained for $0.7 < \alpha < 0.8$. The isoconversional method gives an activation energy value of $\approx$ 125 to 0 kJ mol^{-1} and a ln A value of $\approx$ 3.

The first order equation and the first order equation with autocatalytic activation both give a good description for $0.8 < \alpha < 1$ (correlation coefficient is 0.954 for both models but the Durbin-Watson value are 0.433 and 0.372 respectively). The activation energy value for the first order equation is 88 kJ mol^{-1} and ln A = 9; while for the first order reaction with autocatalysis, the activation energy is 89 kJ mol^{-1} and ln A = 9. There is no conclusive fit.

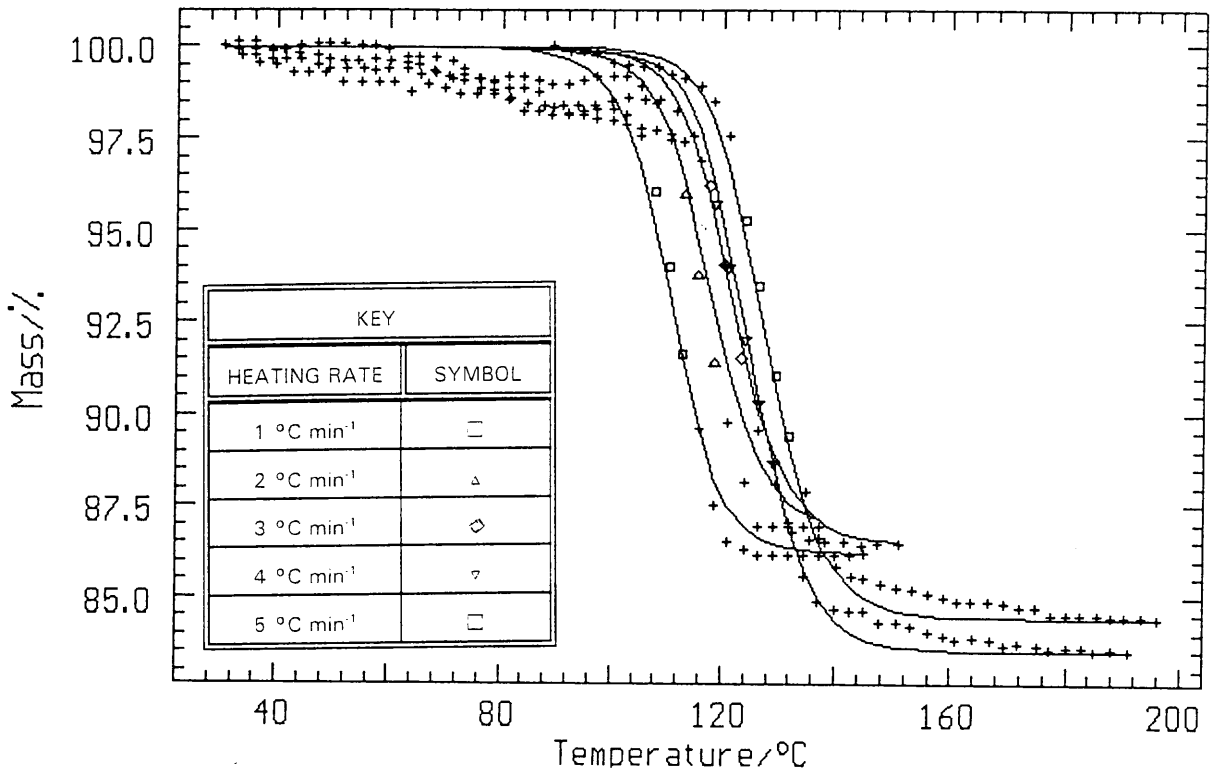

Figure 8.1.2.2 (b): Fitting of the experimental mass loss data to the kinetic model of the Sestak-Berggren in an air/water-atmosphere

Figure 8.1.2.2 (b) gives the fitting of the experimental data ($0 < \alpha < 1$) to the Sestak-Berggren model. A good correlation is obtained for α-values between 0.2 and 0.7, but other mechanisms must be dominating at the start and end of the dehydration reaction.

A summary of the kinetic data for synthetic gypsum in a nitrogen- and an air/water- atmospheres up to 180 °C is given in table 8.1.2 (c):

Table 8.1.2 (c): Summary of kinetic data obtained for synthetic gypsum

Atmosphere	α-Range	Kinetic Data from the Isoconversional Method		Kinetic Data from the Kinetic Models			
				Kinetic Model			
		E_a (kJ mol^{-1})	ln A	E_a (kJ mol^{-1})	ln A	D-W	Corr. Coeff
Nitrogen	$0 < \alpha < 0.2$	(- 10) - 100	-	No fit			
	$0.2 < \alpha < 0.8$	100	10	First order with autocatalytic activation 101	11	0.047	0.989
	$0.8 < \alpha < 1$	100 - 0	-	Sestak-Berggren equation 96	10	0.116	0.954
Air/water	$0 < \alpha < 0.2$	0 - 125	-	No fit			
	$0.2 < \alpha < 0.7$	119	13	Sestak-Berggren equation 114	13	0.234	0.968
	$0.7 < \alpha < 0.8$	125 - 0	-	No fit			
	$0.8 < \alpha < 1$	0	-	first order 88	9	0.433	0.954
				or first order with autocatalysis 89	9	0.372	0.954
				(no conclusive fit)			

Key of abbreviations in table: E_a = activation energy; D-W = Durbin-Watson value and Corr. Coeff. = correlation coefficient.

8.1.3 Natural gypsum

The thermal decomposition of natural gypsum in an air-atmosphere using a heating rate of 5 °C min^{-1} is shown in figure 8.1.3 (a).

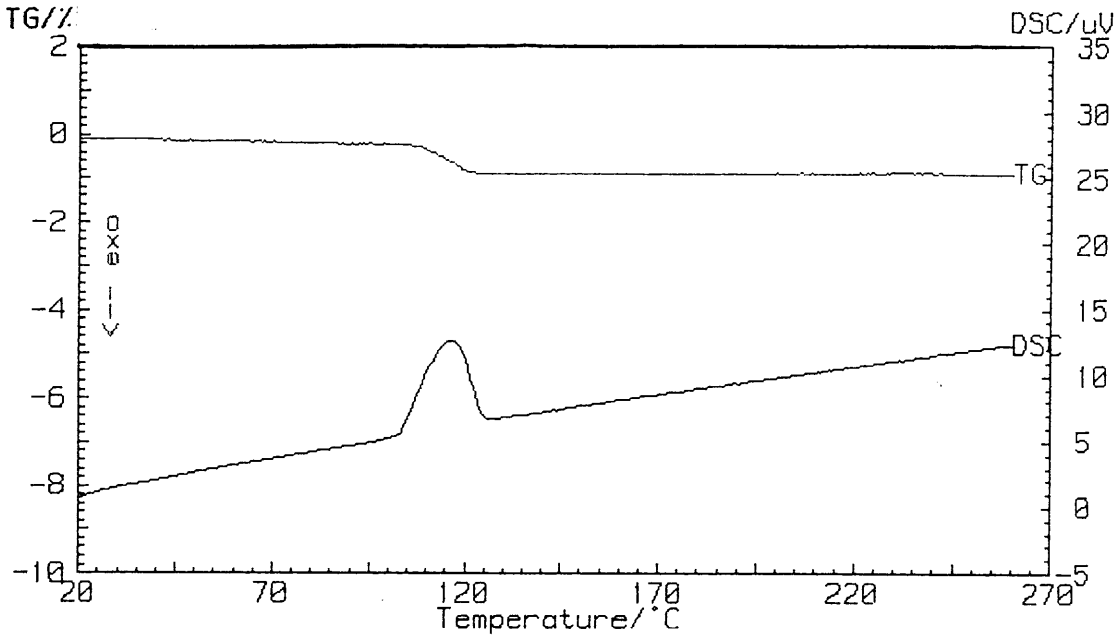

Figure 8.1.3 (a): The TG and DSC curves of the thermal decomposition of natural gypsum in an air-atmosphere using a heating rate of 5 °C min^{-1}

The following table shows the thermal decomposition of natural gypsum in different atmospheres.

Table 8.1.3 (a): The thermal decomposition of natural gypsum with different sample masses in different atmospheres using a heating rate of 5 °C min^{-1}

Sample mass(mg)	Atmos-phere	Temperature Range (°C)	Mass Loss (%)	Mass Gain (%)	ΔH in kJ g^{-1} x 10^{-1}
5	N_2	97 - 127	8	-	2
10	N_2	100 - 134	7	-	2
15	N_2	100 - 134	7	-	2
10	Air	94 - 134	7	-	2
10	Air/H_2O	40 - 53	1	-	-
		53 - 104	-	1	-
		104 - 123	6	-	1
		123 - 198	-	1	-
		198 - 303	1	-	-
		83 - 247	-	-	-

Figure 8.1.3 (b) is a thermogram of the thermal decomposition of natural gypsum in a nitrogen-atmosphere. No notable difference is observed between the thermogram obtained in an air- (figure 8.1.3 (a)) and in a nitrogen-atmosphere (figure 8.1.3 (b)).

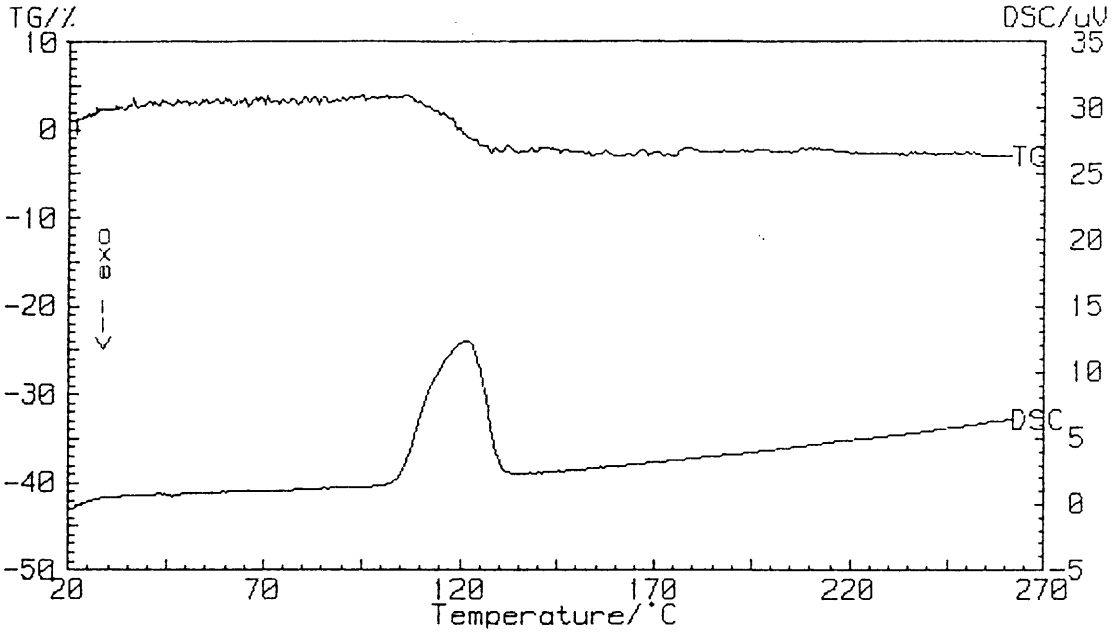

Figure 8.1.3 (b): TG and DSC curves of the dehydration reaction of natural gypsum in a nitrogen-atmosphere using a heating rate of 5 °C min^{-1}

Thus, nitrogen is used as the inert atmosphere for the kinetic comparison with 10 mg samples.

Natural gypsum samples are decomposed in an air-atmosphere using a heating rate of 5 °C min^{-1} and the following is observed (figure 8.1.3 (c) for the electron micrographs and table 8.1.3 (b) for the XRD results):
The unheated samples have calcium sulphate dihydrate and silicon dioxide present. At ≈ 60 °C, calcium sulphate dihydrate, anhydrite, silicon dioxide and a small amount of calcium sulphate hemihydrate are observed. At ≈ 170 °C, the XRD results show that the hemihydrate and anhydrite contents increase and $CaSO_4 \bullet 0.62H_2O$ can possibly also be present. Some $CaSO_4 \bullet 0.15H_2O$ also appears to be present. At ≈ 240 °C, there appears to be more $CaSO_4 \bullet 0.15H_2O$ present than hemihydrate. At ≈ 450 °C, only anhydrite and hemihydrate appear to be present.

Figure 8.1.3 (c): Electron micrographs of natural gypsum at various decomposition temperatures

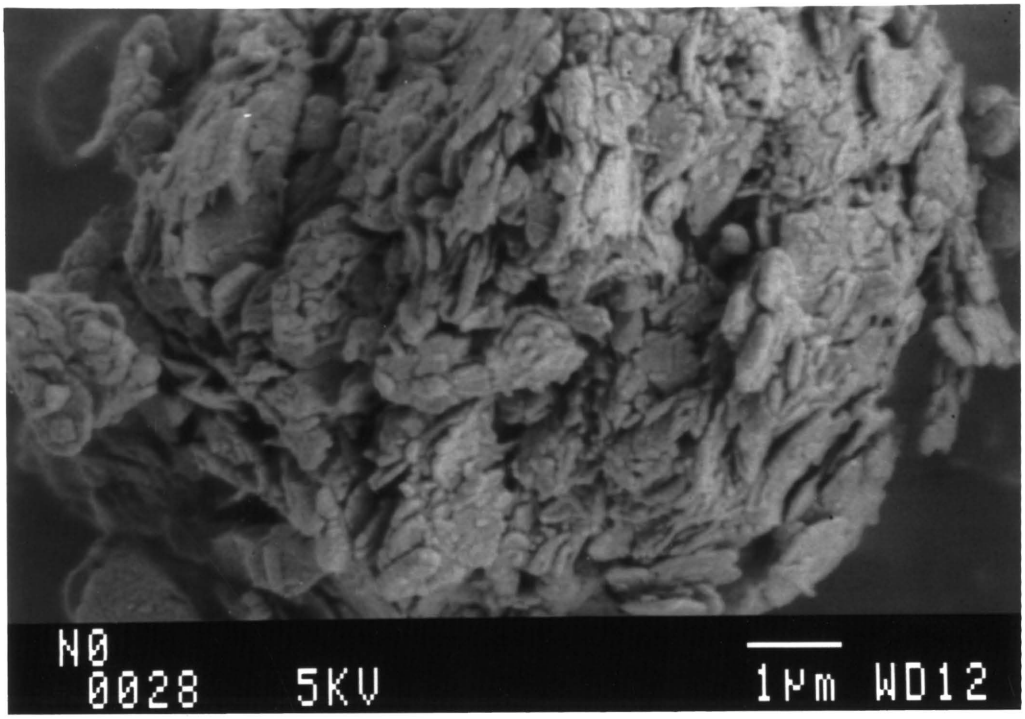

(i) unheated

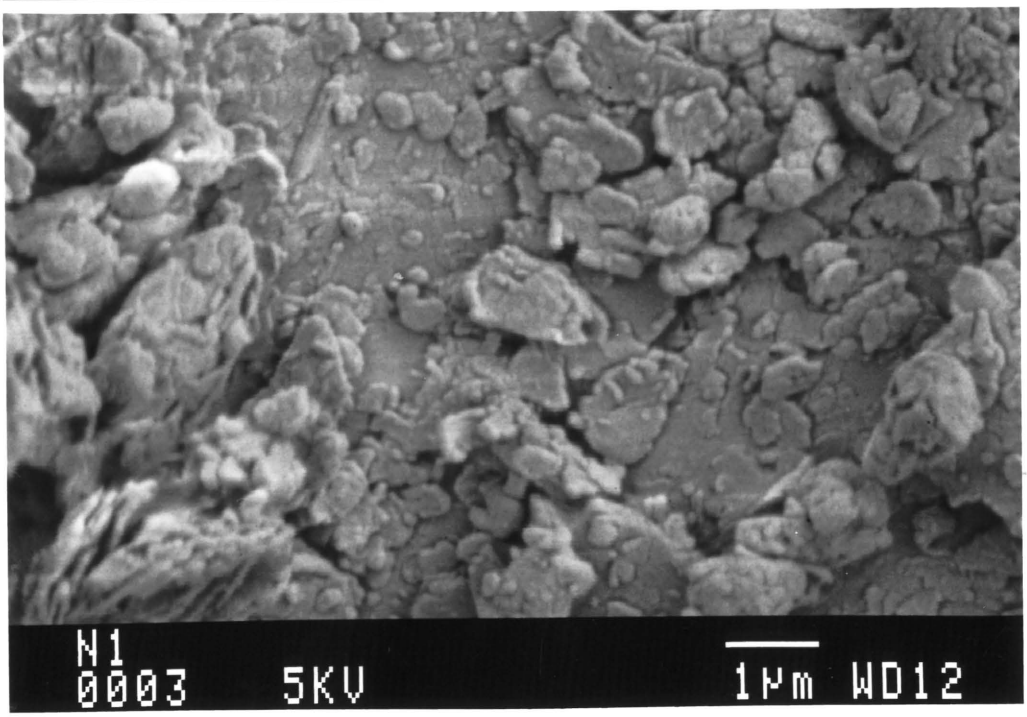

(ii) ≈ 60 °C

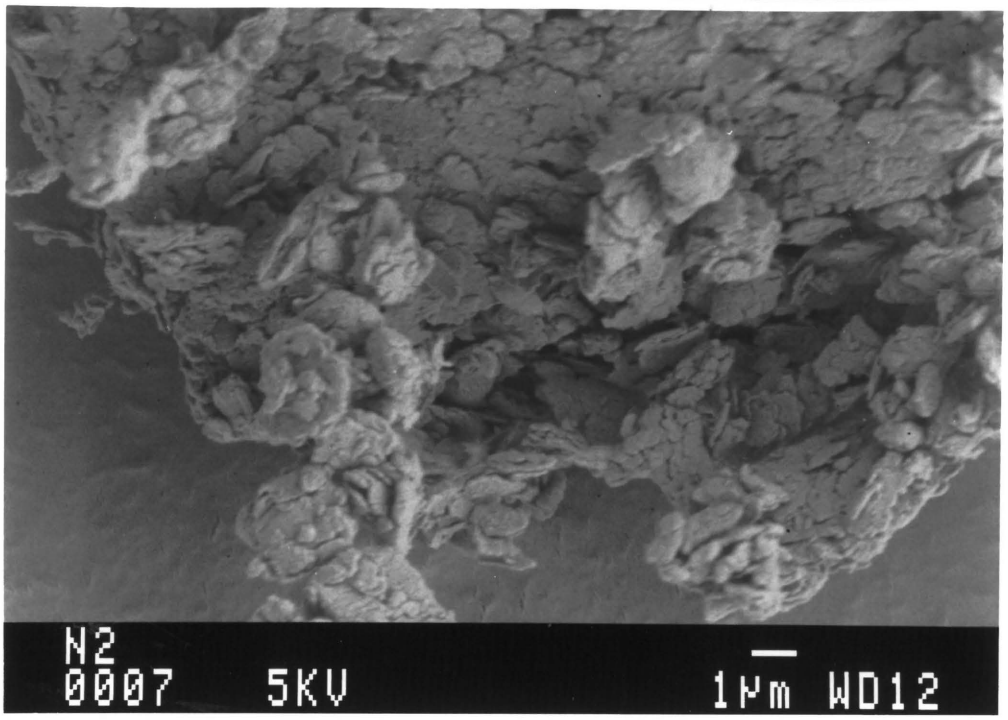

(iii) ≈ 170 °C

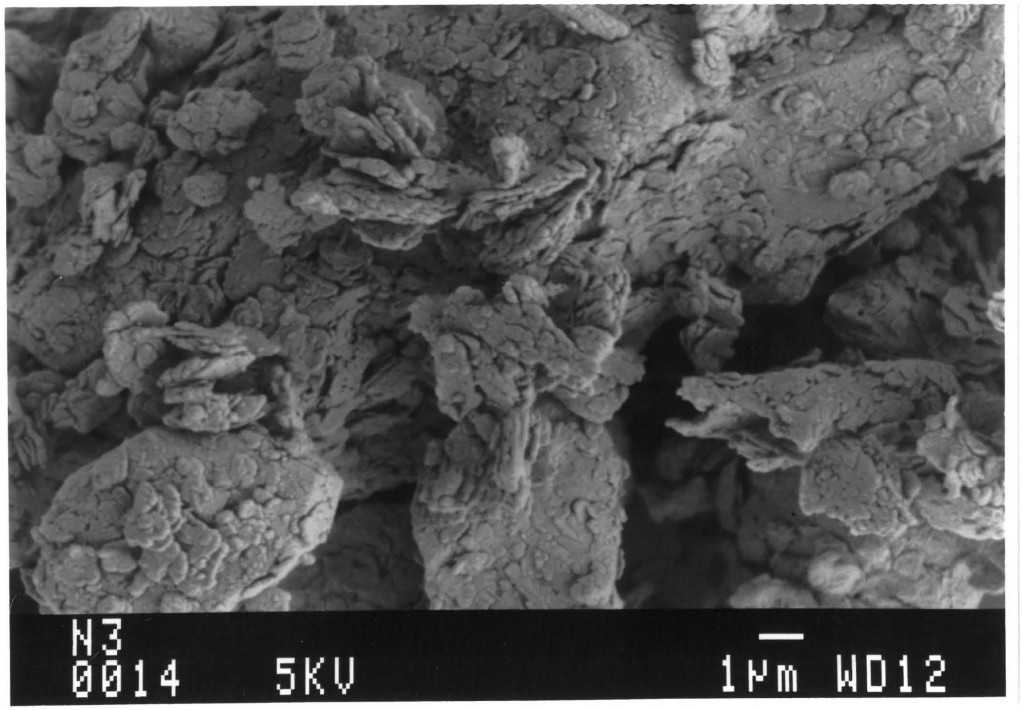

(iv) ≈ 240 °C

Table 8.1.3 (b): XRD results of the thermal decomposition of natural gypsum

SAMPLE	VALUES OF DATABASE STANDARDS Å Relative Intensity					
Decomposition Temperature- Å Relative Intensity	CALCIUM SULPHATE DIHYDRATE	CALCIUM SULPHATE HEMI-HYDRATE	CALCIUM SULPHATE ANHYDRITE	$CaSO_4 \cdot 0.62H_2O$	SiO_2	$CaSO_4 \cdot 0.15H_2O$
	7.630_{100}	6.013_{80}	3.499_{100}	6.001_{80}	4.256_{18}	6.050_{100}
	4.283_{100}	3.467_{50}	2.849_{29}	3.467_{40}	3.335_{45}	3.490_{40}
	3.065_{75}	3.006_{100}	2.328_{20}	3.003_{80}	2.456_{8}	3.018_{85}
	2.873_{45}	2.803_{90}	2.209_{20}	2.812_{100}	2.287_{4}	2.794_{20}
	2.685_{35}	1.849_{20}	1.869_{16}	2.137_{20}	2.122_{5}	1.847_{15}
	2.685_{35}	1.845_{30}	1.648_{15}	1.848_{30}	1.979_{4}	1.741_{10}
	2.086_{25}	1.693_{20}		1.694_{20}	1.817_{10}	1.694_{10}
	1.899_{16}	1.665_{20}			1.539_{7}	
unheated						
7.588_{49}	✓					
4.286_{46}	✓					
3.335_{100}					✓	
2.873_{37}	✓					
2.680_{40}	✓					
1.899_{37}	✓					
1.818_{36}					✓	
≈ 60 °C						
7.588_{18}	✓					
3.335_{27}					✓	
2.466_{27}			✓			
1.899_{46}	✓					
1.873_{55}			✓			
1.812_{100}	✓					

1.779_{46}	✓					
≈ 170 °C						
7.588_{10}	✓					
4.286_{10}	✓					
3.490_{12}						✓
3.467_{12}				✓		
3.018_{100}						✓
3.003_{16}				✓		
2.854_{10}			✓			
2.812_{16}				✓		
2.332_{10}			✓			
2.137_{16}				✓		
2.110_{10}			✓			
1.845_{85}		✓				
≈ 240 °C						
3.490_{12}						✓
3.489_{10}			✓			
3.476_{13}			✓			
3.018_{100}						✓
2.842_{10}			✓			

The mass loss for natural gypsum in air-atmosphere is 7 % of the original reactant. On calculation, it appears that ~ 34 % of the sample is calcium sulphate dihydrate.

The heat of dehydration is obtained from the DSC curve and is found to be between 1 x 10^{-1} and 2 x 10^{-1} kJ g^{-1}. On using an air/water-atmosphere, the total mass loss remains the same (figure 8.1.3 (d)).

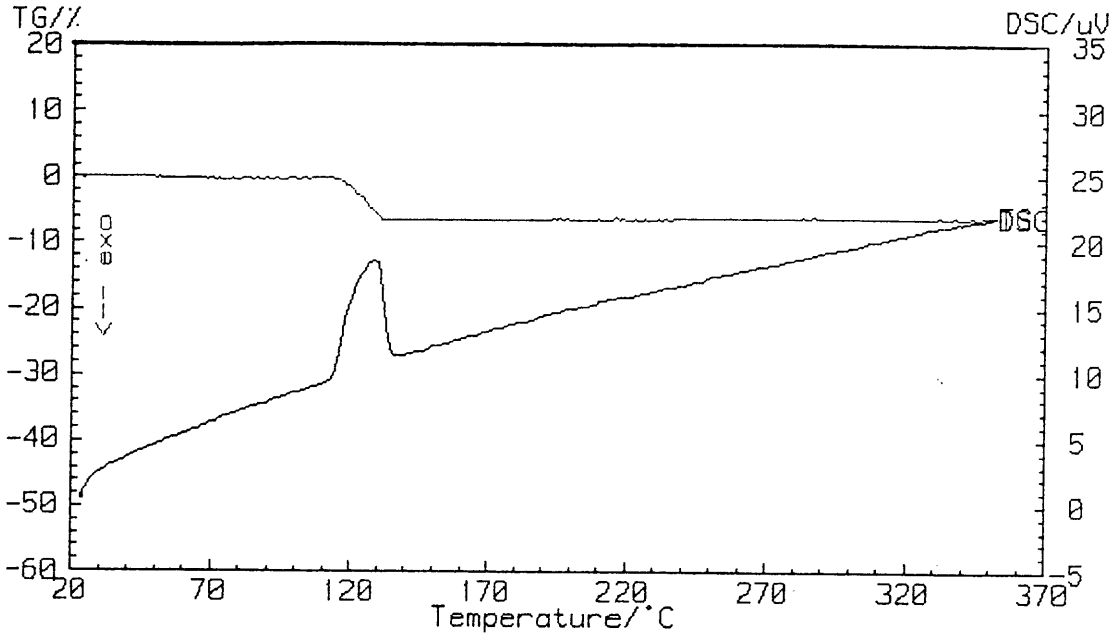

Figure 8.1.3 (d): **TG and DSC curves of the dehydration reaction of natural gypsum in an air/water-atmosphere using a heating rate of 5 °C min^{-1}**

8.1.3.1 Kinetics of the dehydration of natural gypsum to anhydrite in nitrogen-atmosphere

Figure 8.1.3.1 (a) shows a plot of activation energy, E_a, versus fraction decomposed, α, for natural gypsum. The dehydration reaction does not occur in a single step. At least four stages of decomposition can be observed from the plot of activation energy versus fraction decomposed. There is an increasing character of dependence on the degree of transformation until $\alpha = 0.2$ (activation energy varies between 0 to $\approx$ 95 kJ mol^{-1}) where it remains constant at a value of $\approx$ 94 kJ mol^{-1} until $\alpha = 0.5$. The ln A value is $\approx$ 10 for this part. This suggests that the reaction with the higher activation energy makes a growing contribution to the heat that is absorbed [85]. On reaching the maximum, the dependence becomes less due to the lesser contribution being made to the reaction with the higher activation energy as there is a sharply decreasing activation energy value (from $\approx$ 95 to 0 kJ mol^{-1}) for $0.5 < \alpha < 0.6$. The process then appears to be almost completely single-stage from $0.6 < \alpha < 1.0$ with an

average activation energy of ≈ 0 kJ mol^{-1}.

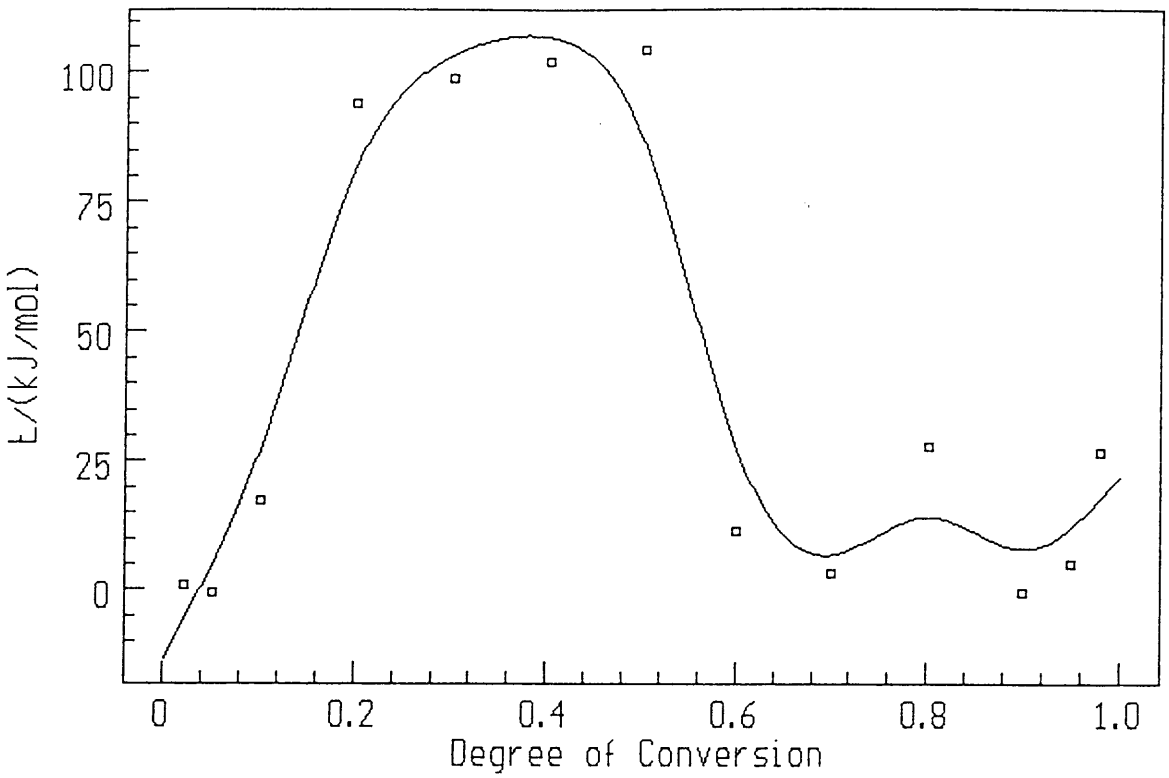

Figure 8.1.3.1 (a): Plot of activation energy versus α for the dehydration of natural gypsum to anhydrite in a nitrogen-atmosphere

For the α-values of natural gypsum in the range 0 and 0.2, no kinetic model appears to fit the experimental data conclusively. For α-values between 0.2 and 0.5, the first order with autocatalytic activation is obtained. The correlation coefficient is 0.974. The average activation energy value of 98 kJ mol^{-1} and ln A of 10 correlates very well with the average values for activation energy ≈ 95 kJ mol^{-1} and ln A ≈ 10 obtained, using the isoconversional method. From figure 8.1.3.1 (b), it can be seen that the fit is good between 0.2 and 0.5, but that at the start and end of the dehydration process other mechanisms could be dominating. For $0.5 < \alpha < 0.6$, quite a few models appear to fit the data well, namely the d-

dimensional Avrami-Erofe'ev equation, or the second order equation, or the first order with autocatalytic activation or even the first order on two-dimensional phase boundary model. The best fit however, is the d-dimensional Avrami-Erofe'ev equation with a correlation coefficient of 0.989 and Durbin-Watson value of 0.049. An average activation energy value of 97 kJ mol^{-1} is obtained and a ln A value of 11. Thus, as the temperature increases the reaction may be expressed as a d-dimensional Avrami-Erofe'ev equation. There is growth of the hemihydrate intermediate nuclei.

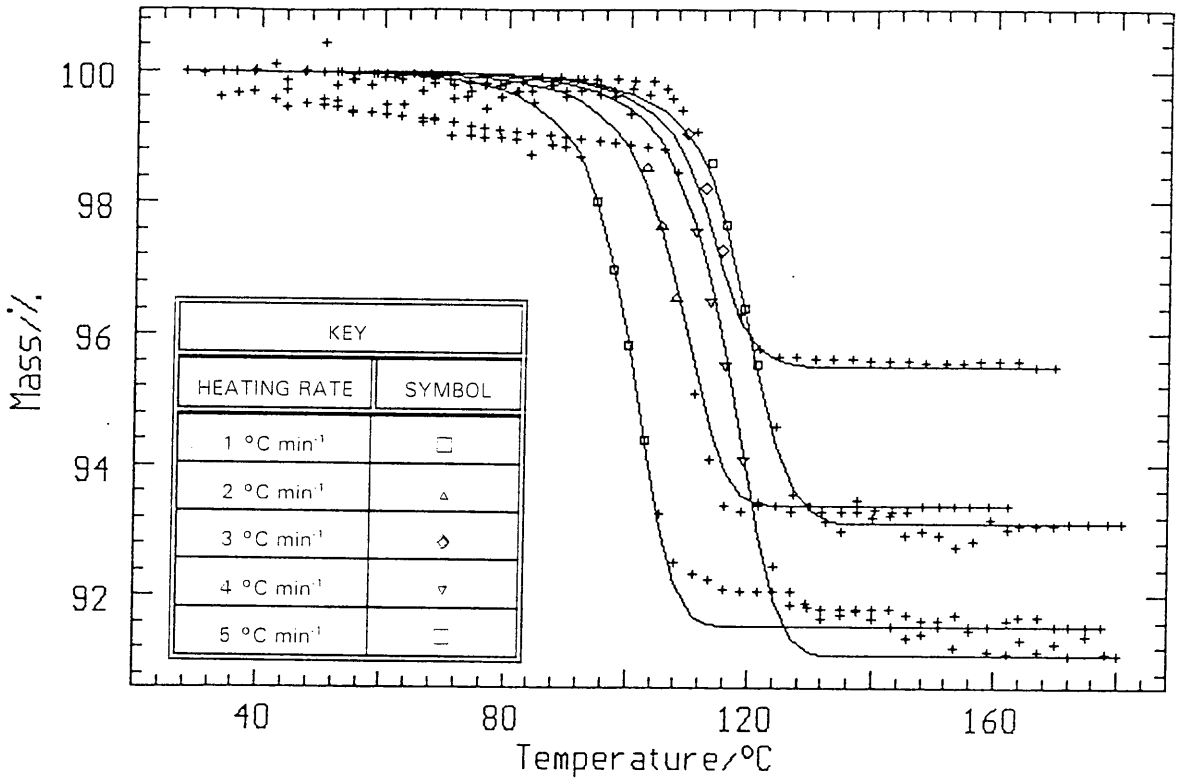

Figure 8.1.3.1 (b): Fitting of experimental data of natural gypsum with theoretical data of the first order reaction with autocatalytic activation for $0.2 < \alpha < 0.5$ in a nitrogen-atmosphere

The two-dimensional Avrami-Erofe'ev equation appears to fit the data the best for $0.6 < \alpha < 1$ with a correlation coefficient of 0.982 and Durbin-Watson value of 0.248. An average activation energy value of 94 kJ mol^{-1} was obtained and ln A of 10. This kinetic model implies that there is two-

dimensional growth of the anhydrite nuclei. Some of the nuclei will start to touch each other and growth will cease at the areas of contact in the later stages of the growth of the reaction interface. The second order, first order with autocatalytic activation and even first order kinetic models are also found to be reasonable descriptions of the dehydration in this stage of the dehydration reaction from the electron micrographs (figure 8.1.3 (c)), no evidence of melting is found since no rounded textures are found in the decomposed material. Dehydration of natural gypsum results in minor changes to the surface texture. Partial decomposition ($\alpha < 0.1$) ($\sim$ 60 °C) results in no marked textural change, for $0.1 < \alpha < 1.0$ (figure 8.1.3 (c)), the texture appears to be more spongy and the reaction interface appears to grow three-dimensionally.

8.1.3.2 Kinetics of the dehydration of natural gypsum to anhydrite in an air/water-atmosphere

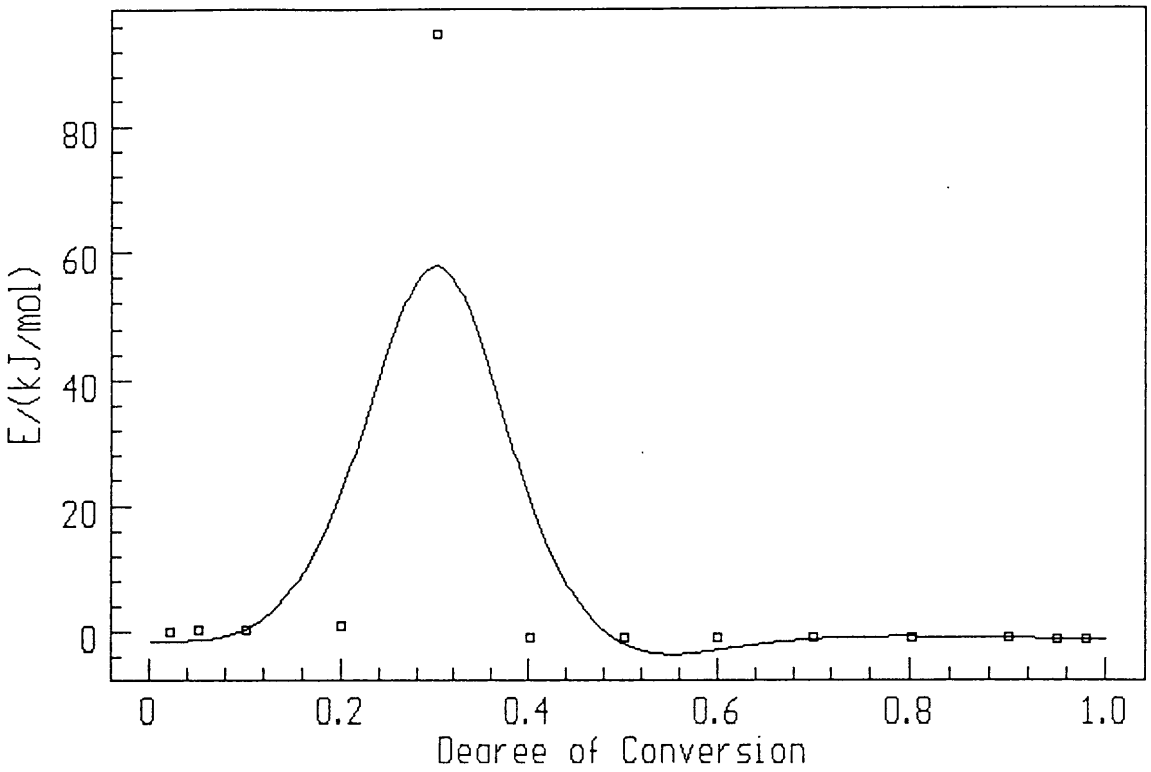

Figure 8.1.3.2 (a): Plot of activation energy, E_a, vs α for the dehydration of natural gypsum to anhydrite in an air/water-atmosphere

Figure 8.1.3.2 (a) shows a plot of activation energy, E_a, versus fraction decomposed, α, for natural gypsum in an air/water-atmosphere. It is clear that the dehydration reaction does not occur in a single step. There are at least three stages. The activation energy remains constant at $\approx$ 0 kJ mol^{-1} for $0 < \alpha < 0.2$; after which it increases (from $\approx$ 0 to $\approx$ 60 kJ mol^{-1}) and with a ln A $\approx$ 5 for $0 < \alpha < 0.2$. This means that at the very beginning of the process, the activation energy does not appear to depend on the conversion [85]. Thus, the process rate at the beginning is determined by a single-step reaction. As the activation energy increases from $\approx$ 0 to $\approx$ 60 kJ mol^{-1} for $0.2 < \alpha < 0.3$, it implies that the reaction with the higher activation energy contributes to the heat absorbed [85]. The activation energy then decreases from $\approx$ 60 kJ mol^{-1} to 0 kJ mol^{-1} for $0.3 < \alpha < 0.4$. For $0.4 < \alpha < 1.0$, the average activation energy remains constant at $\approx$ 0 kJ mol^{-1}. Thus, it can be assumed that the temperature dependence of the overall process rate is governed by one activation energy [85].

No kinetic models fit the experimental data from $0 < \alpha < 0.2$, $0.2 < \alpha < 0.3$ and $0.3 < \alpha < 0.4$.

The activation energy remains more or less constant from $0.4 < \alpha < 1.0$. The n-th order and Sestak-Berggren equations appear to fit but on comparing the average activation energy obtained from the isoconversional method with these two models, it is clear that there is no fit. The n-th order equation has an average activation energy of 387 kJ mol^{-1} and ln A = 53 with a correlation coefficient of 0.982 and a Durbin-Watson value = 0.164. The average activation energy from the Sestak-Berggren kinetic model is 53 kJ mol^{-1} and ln A = 4 with a correlation coefficient of 0.922 and a Durbin-Watson value = 0.038. The isoconversional method gives an average activation energy of $\approx$ 0 kJ mol^{-1} and ln A $\approx$ - 4 (refer to Chapter 9.1). The dehydration reactions of natural gypsum in air/water-atmosphere is obviously a complex reaction consisting of multi-step reactions.

A summary of the kinetic data for natural gypsum in a nitrogen- and an

air/water-atmospheres up to 180 °C is given in table 8.1.3 (c):

Table 8.1.3 (c): Summary of the kinetic data obtained for natural gypsum

Atmosphere	α-Range	Kinetic Data from the Isoconversional Method		Kinetic Data from the Kinetic Models			
				Kinetic Model			
		E_a (kJ mol^{-1})	ln A	E_a (kJ mol^{-1})	ln A	D-W	Corr. Coeff
Nitrogen	$0 < \alpha < 0.2$	0 - 95	-	No fit			
	$0.2 < \alpha < 0.5$	95	10	First order with autocatalytic activation			
				98	10	0.064	0.974
	$0.5 < \alpha < 0.6$	95 - 0	-	d-dimensional Avrami-Erofe'ev			
				97	11	0.049	0.989
	$0.6 < \alpha < 1.0$	0	-	two-dimensional Avrami-Erofe'ev			
				94	10	0.248	0.982
Air/water	$0 < \alpha < 0.2$	0	5	No fit			
	$0.2 < \alpha < 0.3$	0 - 60	-	No fit			
	$0.3 < \alpha < 0.4$	60 - 0	-	No fit			
	$0.4 < \alpha < 1.0$	0	-4	n-th order			
				387	53	0.164	0.982
				or Sestak-Berggren equation			
				53	4	0.038	0.922

Key of abbreviations in table: E_a = activation energy; D-W = Durbin-Watson value and Corr. Coeff. = correlation coefficient.

8.2 CALCIUM CARBONATE (LIMESTONE)

8.2.1 Pure calcium carbonate

The thermal decomposition of pure calcium carbonate in an air-atmosphere using a heating rate of 5 °C min^{-1} is shown in figure 8.2.1(a).

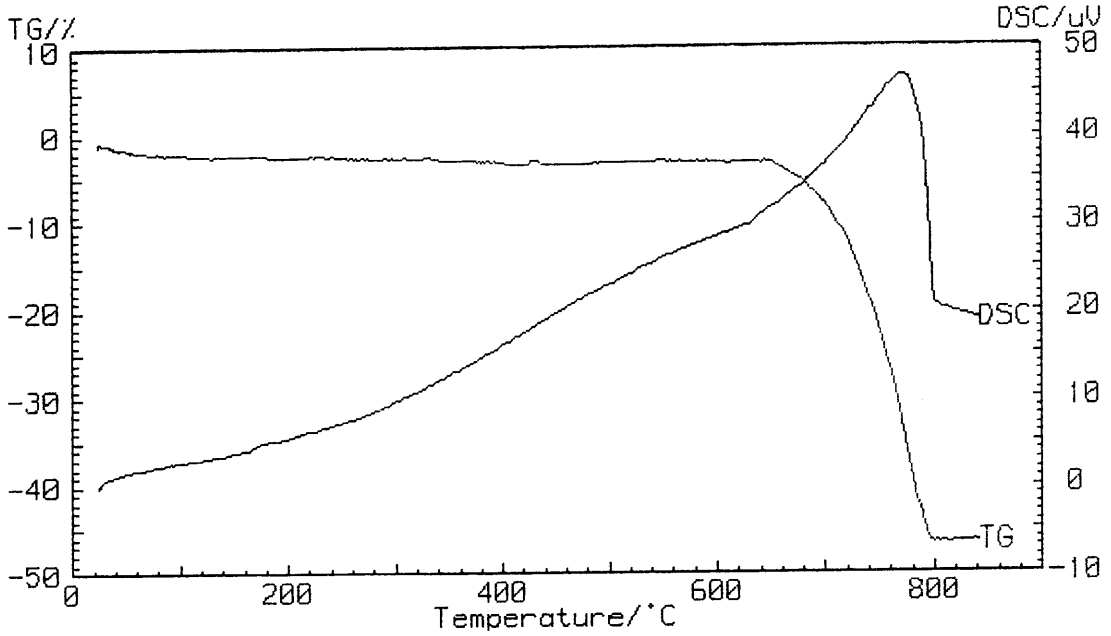

Figure 8.2.1(a): TG and DSC curves for the decomposition of pure calcium carbonate to calcium oxide in an air-atmosphere using a heating rate of 5 °C min^{-1}

The calcium carbonate starts to decompose at 655 °C in an air-atmosphere when using a heating rate of 5 °C min^{-1} and the decarbonation is completed at 808 °C. The following table shows the thermal decomposition of calcium carbonate in different atmospheres.

Table 8.2.1 The thermal decomposition of calcium carbonate in different atmospheres using a heating rate of 5 °C min^{-1} and sample mass between 5 - 15 mg

Atmosphere	Temperature Range (°C)	Mass Loss (%)	Mass Gain (%)	ΔH (kJ g^{-1})
Air	655 - 808	44	-	2
Air/H_2O	70 - 587	-	2	-
	588 - 778	43	-	-
	70 - 778	-	-	-
CO_2	57 - 904	3	-	-
	904 - 987	44	-	2
	57 - 987	-	-	-
CO_2/Air	40 - 864	3	-	-
	864 - 952	44	-	1
	40 - 952	-	-	-
CO_2/H_2O	130 - 187	-	5	-
	265 - 452	-	-	-
	452 - 738	-	-	-
	738 - 854	-	-	-
	854 - 920	44	-	1

The thermal decomposition of calcium carbonate in a CO_2-atmosphere shows a mass loss over a small temperature range (figure 8.2.1(b)). The percentage mass loss of the calcium carbonate decomposing in air is 44 % (theoretical value is 43.97 %). This indicates that the calcium carbonate used is pure and corresponds with the XRD results (Chapter 7.2) where only calcium carbonate is detected.

The heat of decomposition determined from the thermochemical data available at 298 K is 178.5 kJ mol^{-1} [71] while the heat of decomposition obtained in the air-atmosphere at the decomposition temperature of 655 °C, is 204 kJ mol^{-1}. The heat of decomposition is 172 kJ mol^{-1} in CO_2-atmosphere, 115 kJ mol^{-1} in CO_2/air-atmosphere and 117 kJ mol^{-1} in CO_2/water-atmosphere. A possible explanation for this is that the decomposition of calcium carbonate is controlled by the transfer of heat to the reaction boundary and by the transfer of CO_2 away from the surface of

the sample. If the CO_2 is not removed, the decomposition reaction will be hindered and the heat of decomposition will be affected.

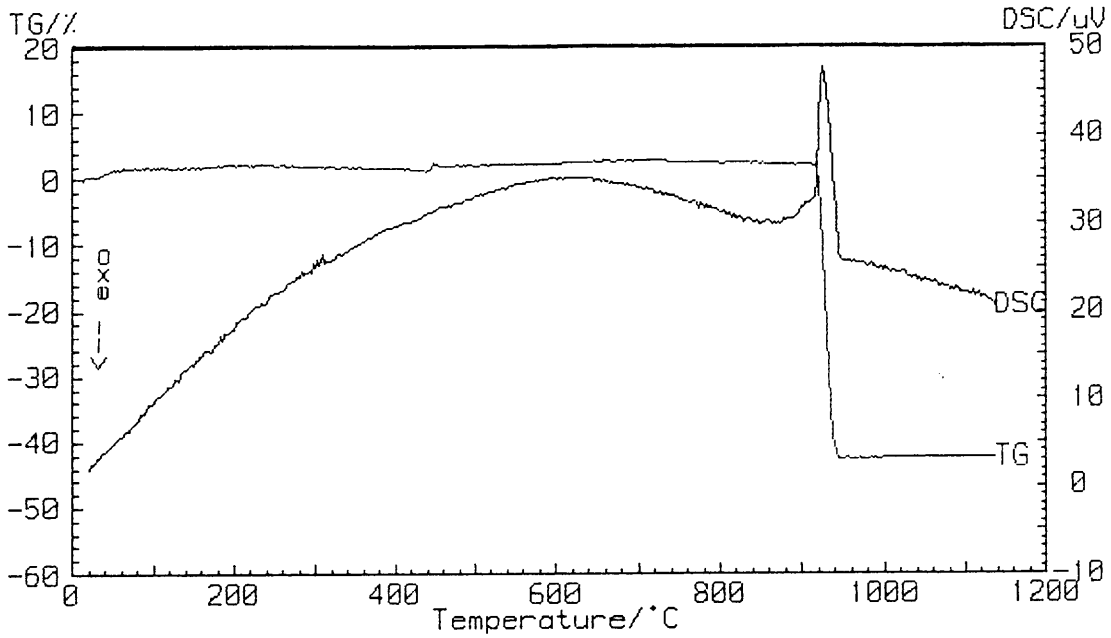

Figure 8.2.1(b): TG and DSC curves for the decomposition of $CaCO_3$ to CaO in a CO_2-atmosphere using a heating rate of 5 °C min^{-1}

The mass loss obtained in the CO_2-rich-atmospheres is the same as obtained in an air-atmosphere, namely 44 %. Due to the partial pressure of CO_2, the start of the decomposition of calcium carbonate is shifted to a higher temperature of 850 °C. In the air-atmosphere, the start of the decomposition is observed at 655 °C. From the TG curve for the decomposition of calcium carbonate in an air/water-atmosphere (figure 8.2.1(c)), a slower rate of decomposition is observed in the air/water-atmosphere, in comparison to the decomposition of calcium carbonate in an air-atmosphere. Figure 8.2.1(c) is a thermogram of calcium carbonate decomposing in an air/water-atmosphere using a heating rate of 5 °C min^{-1}. The decarbonation reaction starts at 588 °C and ends at 778 °C. The decarbonation reaction in the air/water-atmosphere starts at a lower temperature (588 °C) than in air-atmosphere (655 °C).

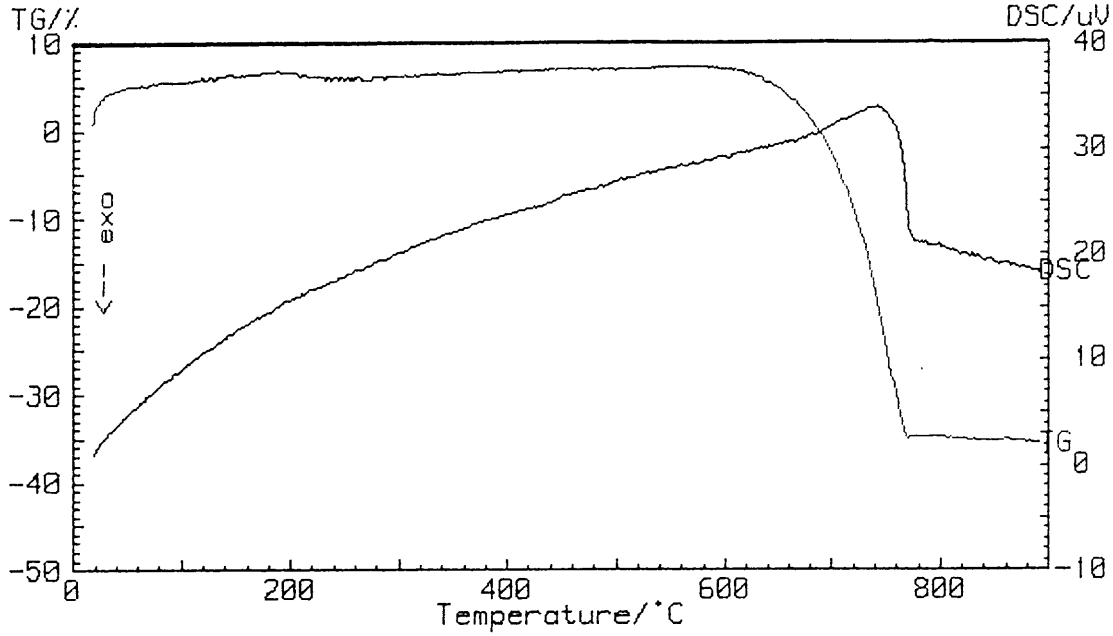

Figure 8.2.1 (c): **TG and DSC curves for the decomposition of $CaCO_3$ to CaO in an air/water-atmosphere using a heating rate of 5 °C min^{-1}**

Figure 8.2.1 (d) and figure 8.2.1 (e) are the thermograms for calcium carbonate decomposing in a CO_2/air- and a CO_2/water-atmospheres

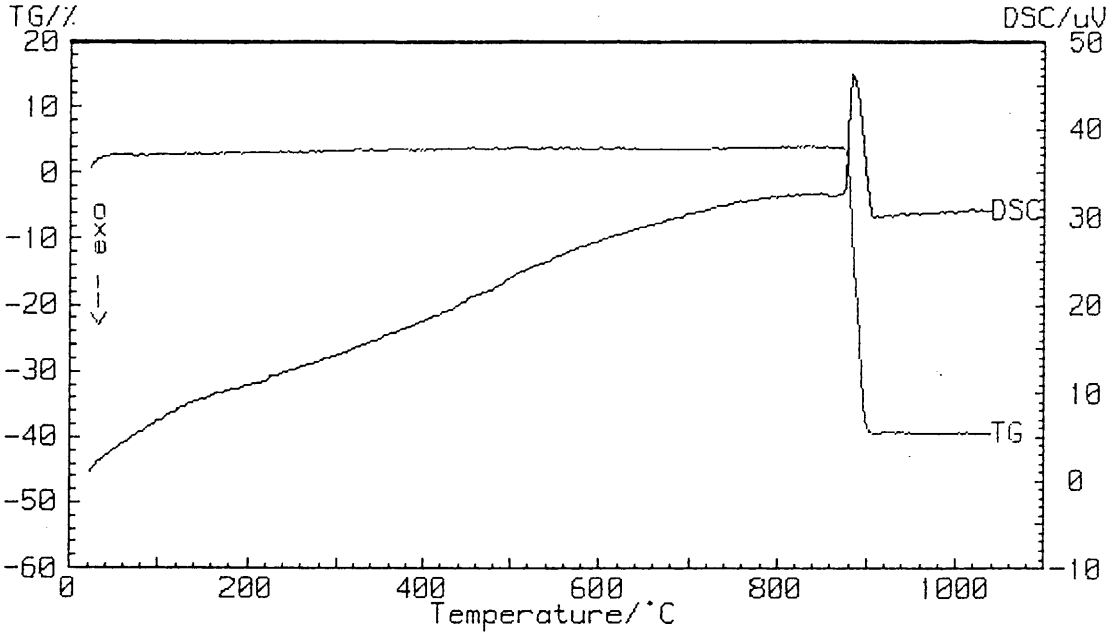

Figure 8.2.1 (d): **TG and DSC curves of calcium carbonate decomposing in a CO_2/air- atmosphere using a heating rate of 5 °C min^{-1}**

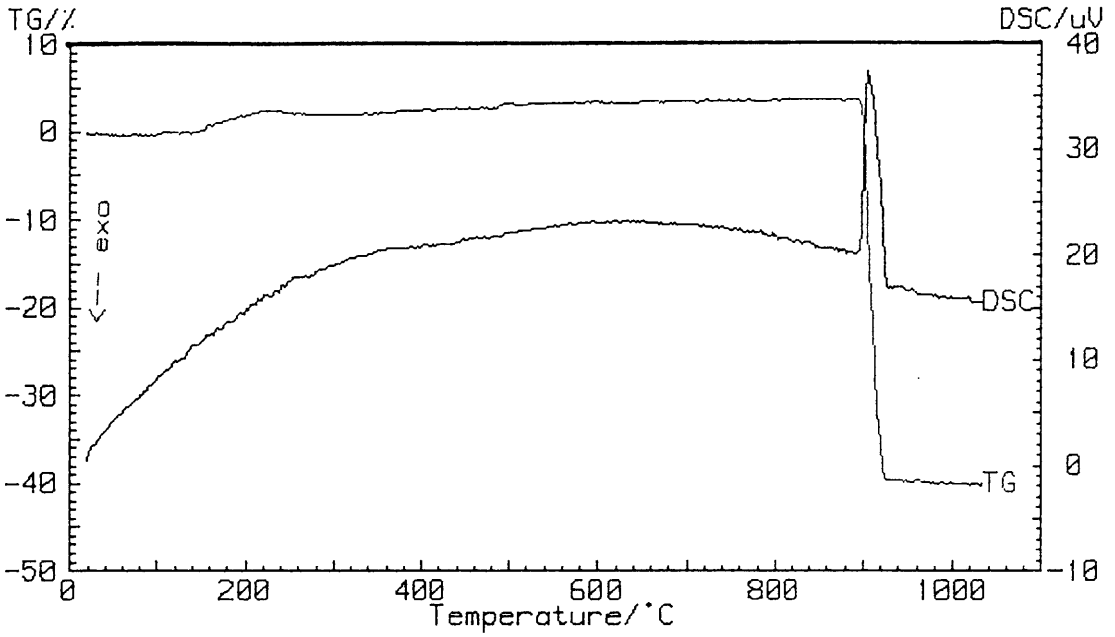

Figure 8.2.1 (e): TG and DSC curves of calcium carbonate decomposing in a CO_2/water-atmosphere using a heating rate of 5 °C min^{-1}

The thermal decomposition of calcium carbonate in a CO_2/air-atmosphere starts at 864 °C and ends at 952 °C. There is an initial mass loss of adsorbed water from the sample before the thermal decomposition of the calcium carbonate to calcium oxide. The thermal decomposition starts at a higher temperature than in an air-atmosphere (655 °C) but at a lower temperature than observed in the CO_2-atmosphere (904 °C).

The thermal decomposition of calcium carbonate in a CO_2/water-atmosphere shows an initial loss of mass due to adsorbed water and then a gain in mass from 130 °C until 210 °C whereafter the mass remains constant until the decomposition commences at around 854 °C. The theoretical mass loss value of calcium carbonate decomposing to calcium oxide is 43.97 %. A mass loss value of 44 % is obtained. The gain in mass is probably due to the adsorption of water.

8.2.1.1 Kinetics of the decomposition of calcium carbonate to calcium oxide in an air-atmosphere

Figure 8.2.1.1(a) shows a plot of activation energy, E_a, versus α (fraction decomposed) for the decomposition reactions up to 808 °C in air. The form of this plot of activation energy versus fraction decomposed shows the conversion dependence of the activation energy [85]. The ascending part of the plot indicates that the reaction with the higher activation energy makes a significant contribution to the heat being absorbed. Once the contribution of the reaction with the higher activation energy reaches its maximum, the activation energy remains constant.

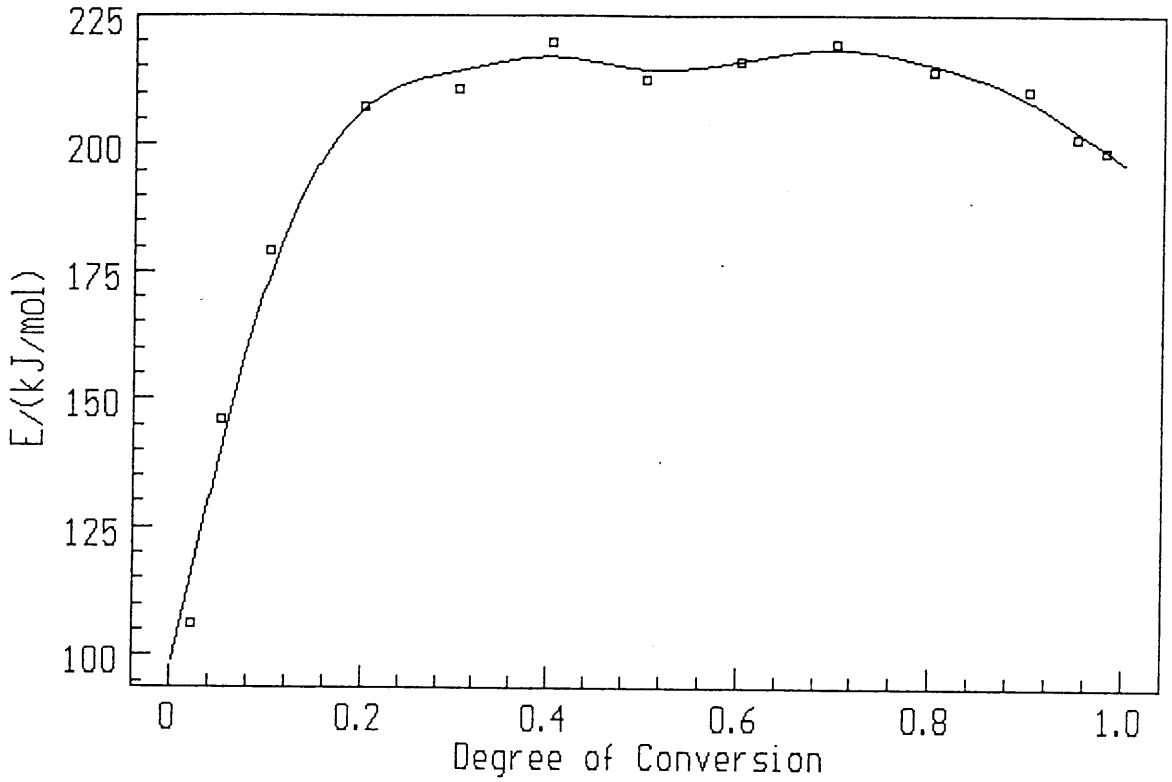

Figure 8.2.1.1 (a): Plot of activation energy, E_a, vs α for calcium carbonate decomposing to calcium oxide in air-atmosphere

It is clear that the decarbonation reaction does not occur in single steps. The activation energy increases between α-values of 0 to 0.2, from ± 100 to 200 kJ mol^{-1}. It then remains constant at a value of ≈ 211 kJ mol^{-1} until

$\alpha = 1.0$. The ln A value for $0.2 < \alpha < 1.0$, is ≈ 8.

It appears that calcium carbonate decarbonates according to the one-dimensional diffusion equation for $0 < \alpha < 0.1$. The average activation energy is calculated as being 443 kJ mol^{-1}; ln A = 20; correlation coefficient = 0.9088 and the Durbin-Watson value = 0.031. The isoconversional method obtains an average activation energy of $\approx$ 144 kJ mol^{-1} and a ln A of $\approx$ 4. When comparing the activation energies obtained from the two different methods, the one-dimensional diffusion equation is found not to be a description of the mechanism of the decomposition reaction between $0 < \alpha < 0.1$, as there is no correlation between the average activation energies obtained from the kinetic model and the isoconversional method.

The average activation energy recorded for $0.2 < \alpha < 1.0$, is 212 kJ mol^{-1} and a ln A value of 8, using the n-th order equation with a correlation coefficient of 0.99996 and a Durbin-Watson value of 0.223. The Sestak-Berggren equation gives an activation energy of 213 kJ mol^{-1} and a ln A value of 8, with a correlation coefficient of 0.99996 and a Durbin-Watson value of 0.226. These activation energy values compare very well with that of $\approx$ 211 kJ mol^{-1} obtained using the isoconversional method and a ln A of $\approx$ 8. Figure 8.2.1.1 (b) is the n-th order fit and Figure 8.2.1.1 (c) is the Sestak-Berggren fit. There is no conclusive fit for $0.2 < \alpha < 1.0$.

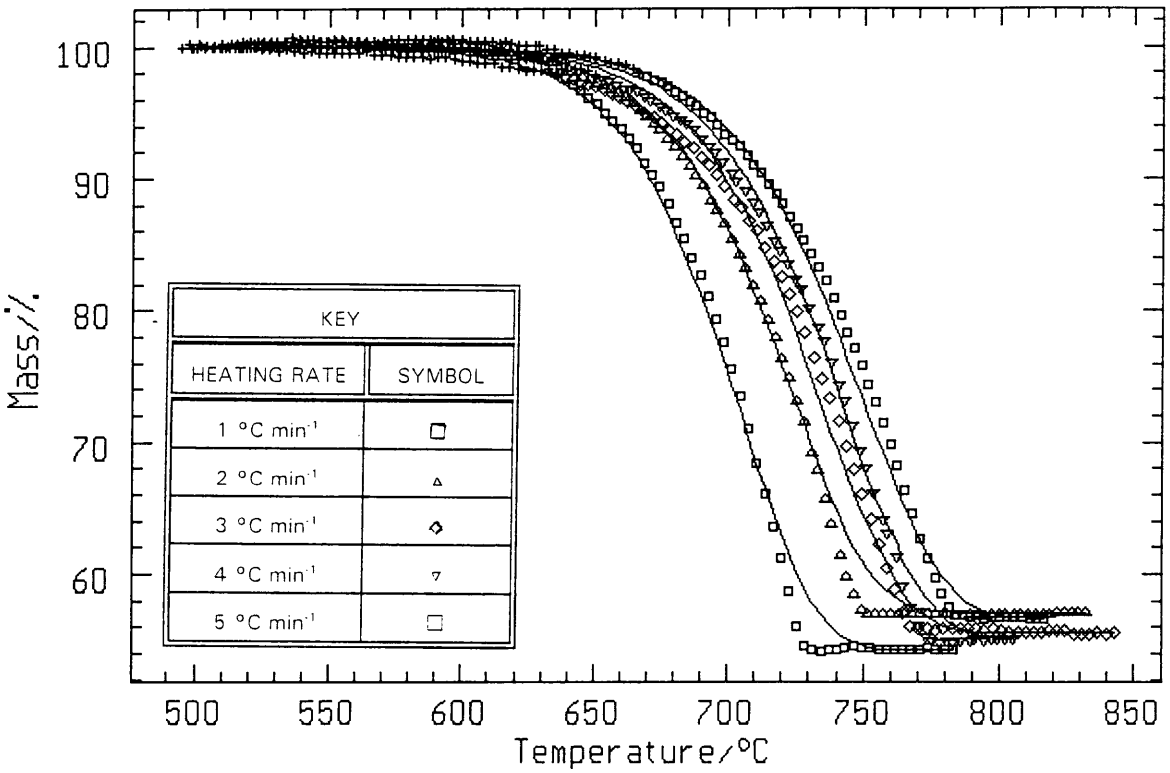

Figure 8.2.1.1 (b): Fitting of experimental data of calcium carbonate with the kinetic model for a n-th order decomposition reaction in an air-atmosphere

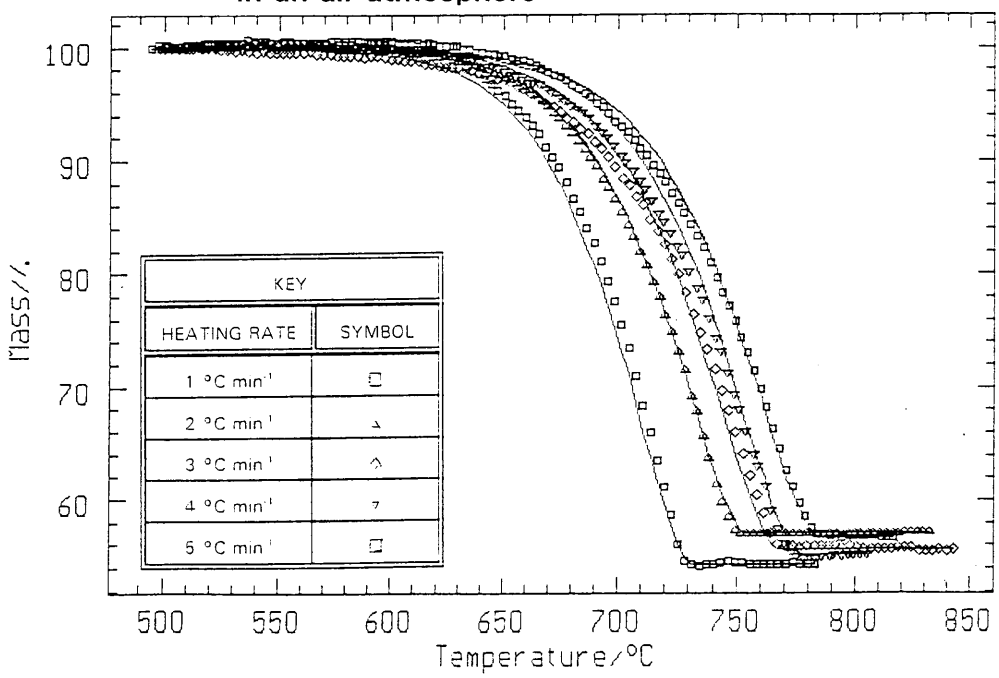

Figure 8.2.1.1 (c): Fitting of experimental data of calcium carbonate with the kinetic model for a Sestak-Berggren type of decomposition reaction in an air-atmosphere

8.2.1.2 Kinetics of the decomposition of calcium carbonate to calcium oxide in an air/water-atmosphere

Figure 8.2.1.2 (a) shows a plot of activation energy, E_a, versus the fraction decomposed for the decomposition reaction up to 778 °C. From the shape of this plot, it is clear that the reaction is complex because the activation parameters depend on the fraction decomposed [86]. The plot indicates that the reaction with the smaller activation energy has a constantly increasing contribution to the total heat that is absorbed [85]. The low activation energy at the large fraction decomposed value, is characteristic of the diffusion of a gas. The kinetic models are fitted over the $0 < \alpha < 1.0$ range. The models which give the best correlations between the theoretical and experimental data, are the n-th order and the two-dimensional phase boundary equations. These models are only mathematical descriptions of the kinetics of the overall reaction.

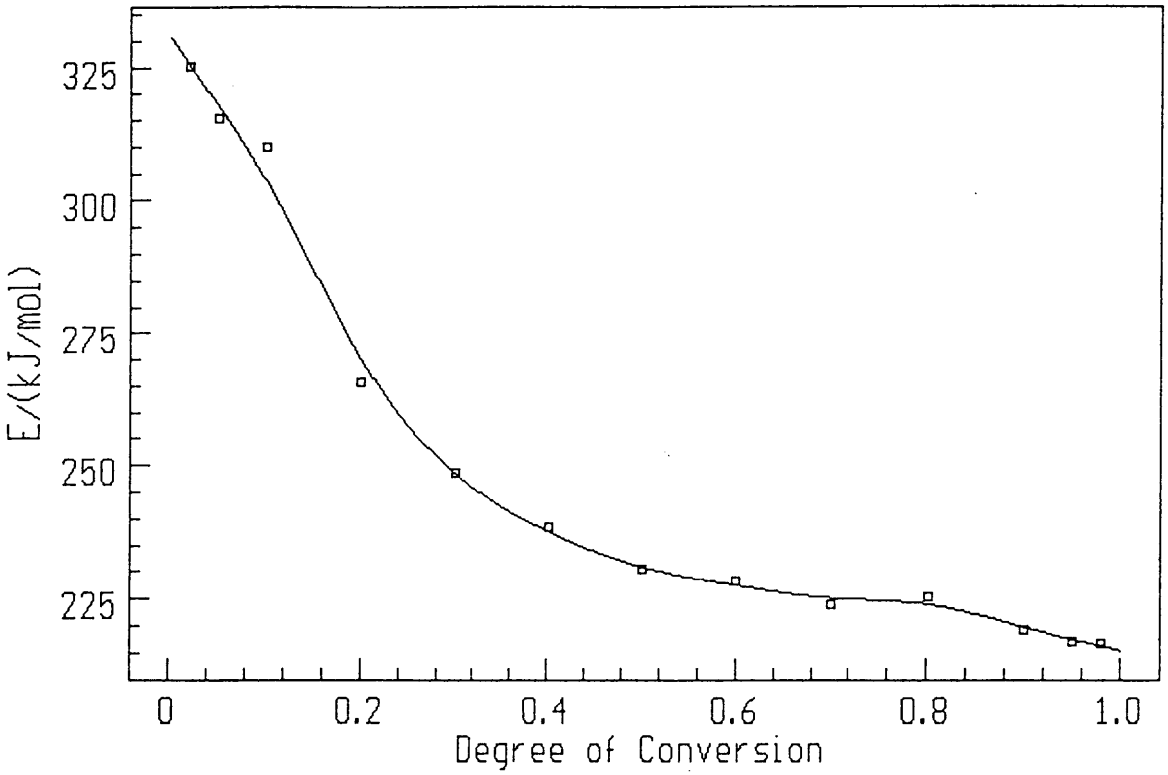

Figure 8.2.1.2 (a): Plot of activation energy, E_a, vs α for calcium carbonate in an air/water-atmosphere

The isoconversional method obtains an average activation energy of ≈ 251 kJ mol $^{-1}$ and an average ln A value of ≈ 11. Figure 8.2.1.2 (b) shows the kinetic model fit of the two-dimensional phase boundary which gives an average activation energy of 228 kJ mol^{-1} and a ln A of 9. (The correlation coefficient is 0.9993 and the Durbin-Watson value is 0.047). An activation energy of 226 kJ mol^{-1} and a ln A of 9, is obtained for the n-th order equation (figure 8.2.1.2 (c)). (The correlation coefficient is 0.9993 and the Durbin-Watson value is 0.042). Both kinetic models appear to fit the experimental data and the activation energy values compare well with the isoconversional method values. Thus, there is no conclusive fit.

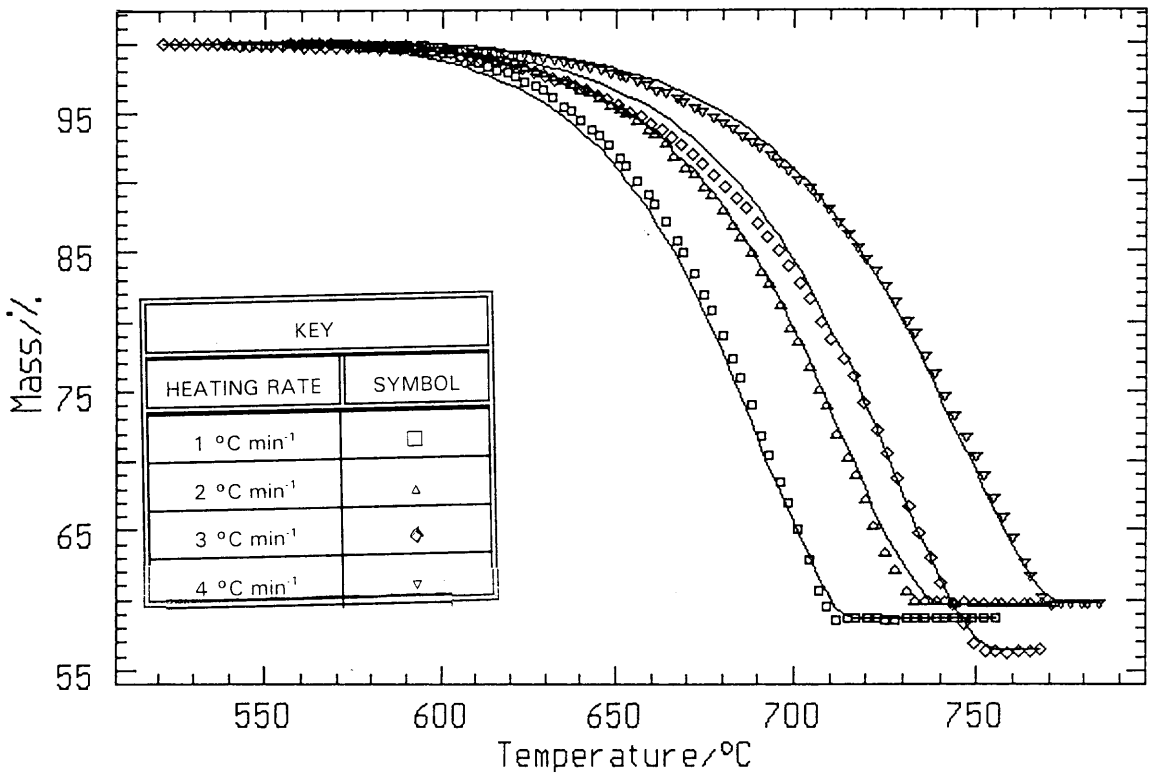

Figure 8.2.1.2 (b): The two-dimensional phase boundary kinetic model fitted to the experimental data of calcium carbonate decomposing in an air/water-atmosphere

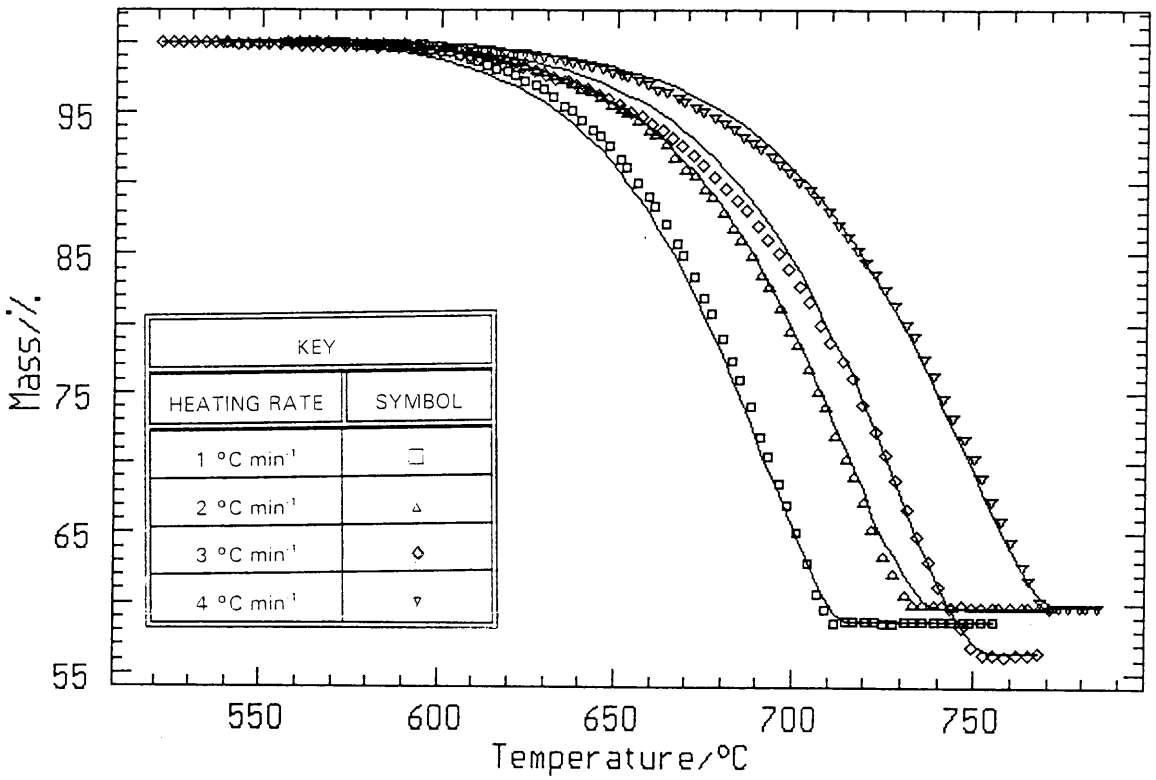

Figure 8.2.1.2 (c): The n-th order kinetic model fitted to the experimental data of calcium carbonate decomposing in an air/water-atmosphere

8.2.1.3 Kinetics of the decomposition of calcium carbonate to calcium oxide in a CO_2-atmosphere

The kinetics of the decomposition of calcium carbonate is studied from 590 to 980 °C. Figure 8.2.1.3 (a) shows a plot of activation energy versus fraction decomposed for calcium carbonate in CO_2-atmosphere.

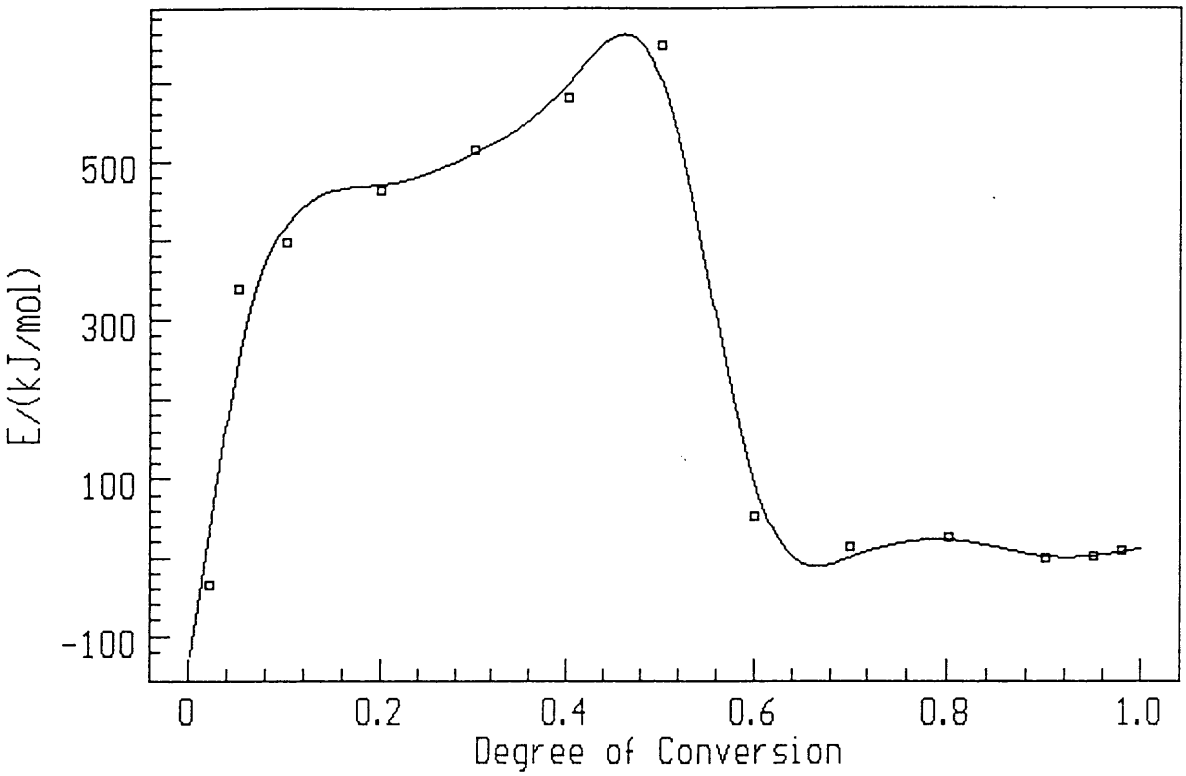

Figure 8.2.1.3 (a): The plot of activation energy, E_a, versus α, fraction decomposed, for calcium carbonate decomposing in CO_2-atmosphere

The shape of this plot is an indication of possible parallel reactions as there is an increasing dependency on the degree of transformation from $0 < \alpha < 0.5$ [87]. There is a decreasing dependency on the degree of transformation from 0.5 to 0.6, from where it remains constant until 1.0. For $0.05 < \alpha < 0.2$, none of the kinetic models fitted the experimental data mathematically. This is also an indication of the complex decomposition reaction which is occurring. The average activation energy values for $0 < \alpha < 0.2$, varied between 0 and approximately 490 kJ mol^{-1} using the isoconversional method.

The kinetic models are fitted for $0.2 < \alpha < 0.5$, and there are no models which appear to fit the experimental data. The isoconversional method

gives an average activation energy of ≈ 520 kJ mol^{-1} and a ln A of ≈ 18. The average activation energy obtained from the isoconversional method for $0.5 < \alpha < 0.6$, varies from ≈ 613 to 0 kJ mol^{-1}.

No kinetic models were found to fit for $0.6 < \alpha < 1.0$. The isoconversional method gives an average activation energy ≈ 18 kJ mol^{-1} and average ln A ≈ -3 (see Chapter 9.2).

8.2.1.4 Kinetics of the decomposition of calcium carbonate to calcium oxide in a CO_2/air-atmosphere

The kinetic data obtained for calcium carbonate decomposing in a CO_2/air-atmosphere (from 500 to 970 °C) shows an increase in activation energy from $0 < \alpha < 0.1$, then a decrease from $0.1 < \alpha < 0.4$, from where it remains constant at an average activation energy value of ≈ -1 kJ mol^{-1} and an average ln A value of ≈ - 4 (figure 8.2.1.4 (a)) - refer to Chapter 9.2. The activation energy is dependent on the degree of conversion. The increasing character of dependence on the degree of transformation until $\alpha = 0.2$ suggests that the reaction with the higher activation energy makes a growing contribution to the heat that is absorbed [85]. On reaching the maximum, the dependence becomes less due to the lesser contribution being made by the reaction with the higher activation energy.

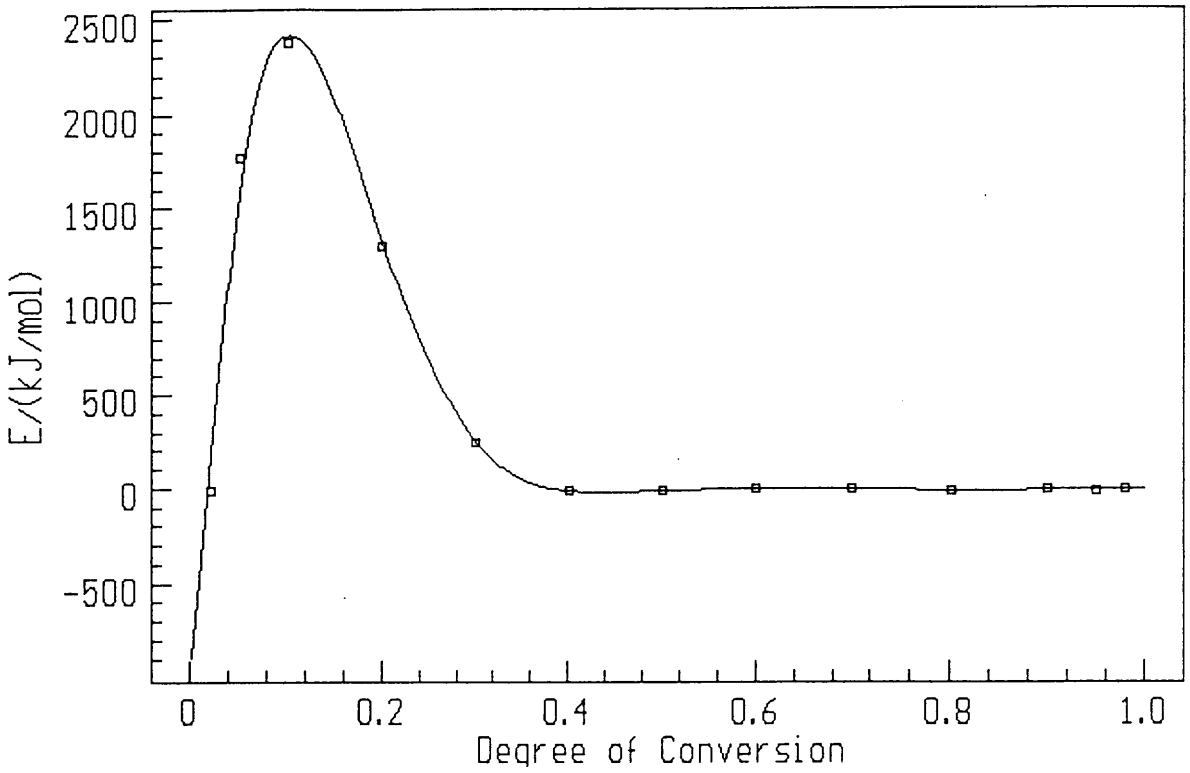

Figure 8.2.1.4 (a): Plot of E_a vs α for $CaCO_3$ decomposing in a CO_2/air-atmosphere

For $0.1 < \alpha < 0.4$, the best kinetic model fit was the first order with autocatalysis (figure 8.2.1.4 (b)) giving an activation energy value of 1816 kJ mol^{-1} and a ln A of 80 (refer to Chapter 9.2). The correlation coefficient is 0.9773 and the Durbin-Watson value 0.988. The isoconversional method obtains an average activation energy value of $\approx$ 1312 kJ mol^{-1} and an average ln A value of $\approx$ 56.

The kinetics of the decomposition reaction for $0.4 < \alpha < 1.0$ can be best described by the three-dimensional diffusion equation of Jander (activation energy = 2083 kJ mol^{-1}; ln A = 91 ; correlation coefficient = 0.9821 and a Durbin-Watson value = 0.549), the first order with autocatalysis equation (activation energy = 1585 kJ mol^{-1}; ln A = 69; correlation coefficient = 0.9895 and Durbin-Watson value = 0.404) and the first order equation. The first order equation (figure 8.2.1.4 (c)), however, gives the best fit with

a correlation coefficient of 0.9903, a Durbin-Watson value of 0.411, an activation energy value of 1641 kJ mol $^{-1}$ and ln A of 72. This does not compare with the average activation energy value of ≈ -1 kJ mol^{-1} and ln A value of ≈ -4 (refer to Chapter 9.2) obtained from the isoconversional method. The first order kinetic expression normally holds at the end of the decomposition reaction i.e. at higher temperatures. It is based on nucleation and rapid two-dimensional growth [14, page 64].

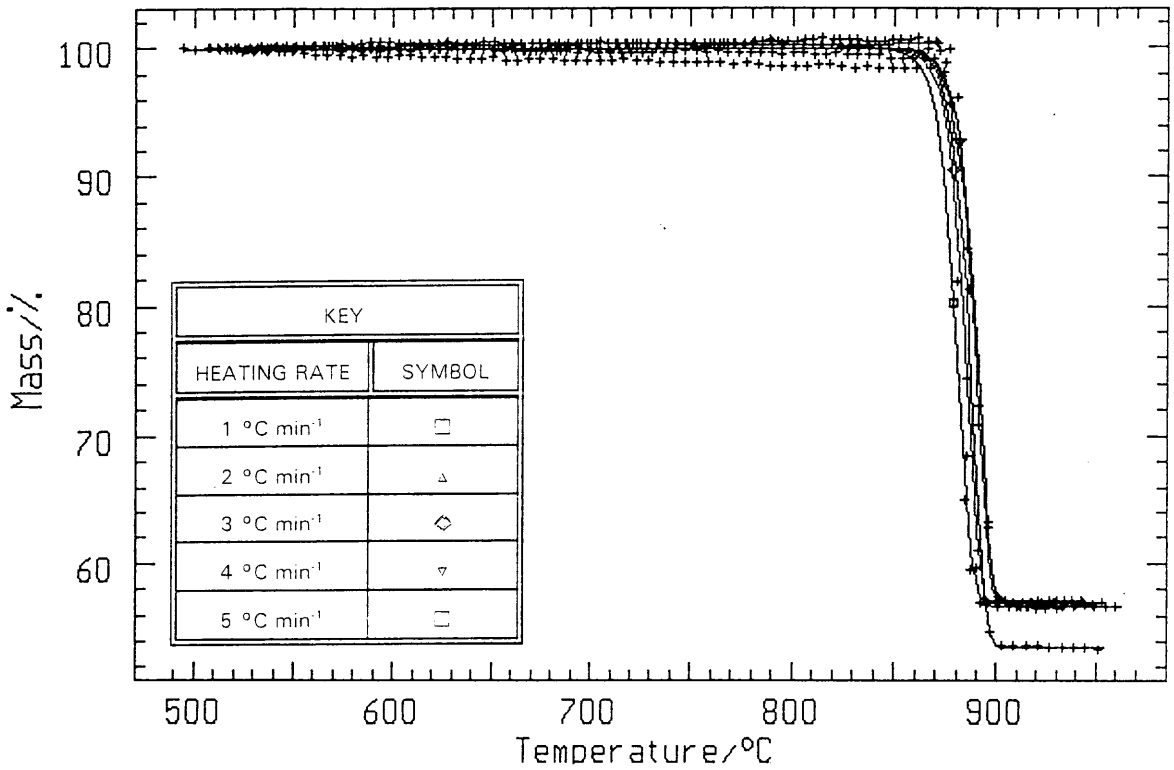

Figure 8.2.1.4 (b): Fitting of the first order with autocatalysis kinetic model for $CaCO_3$ decomposing in a CO_2/air-atmosphere for 0.1 < α < 0.4

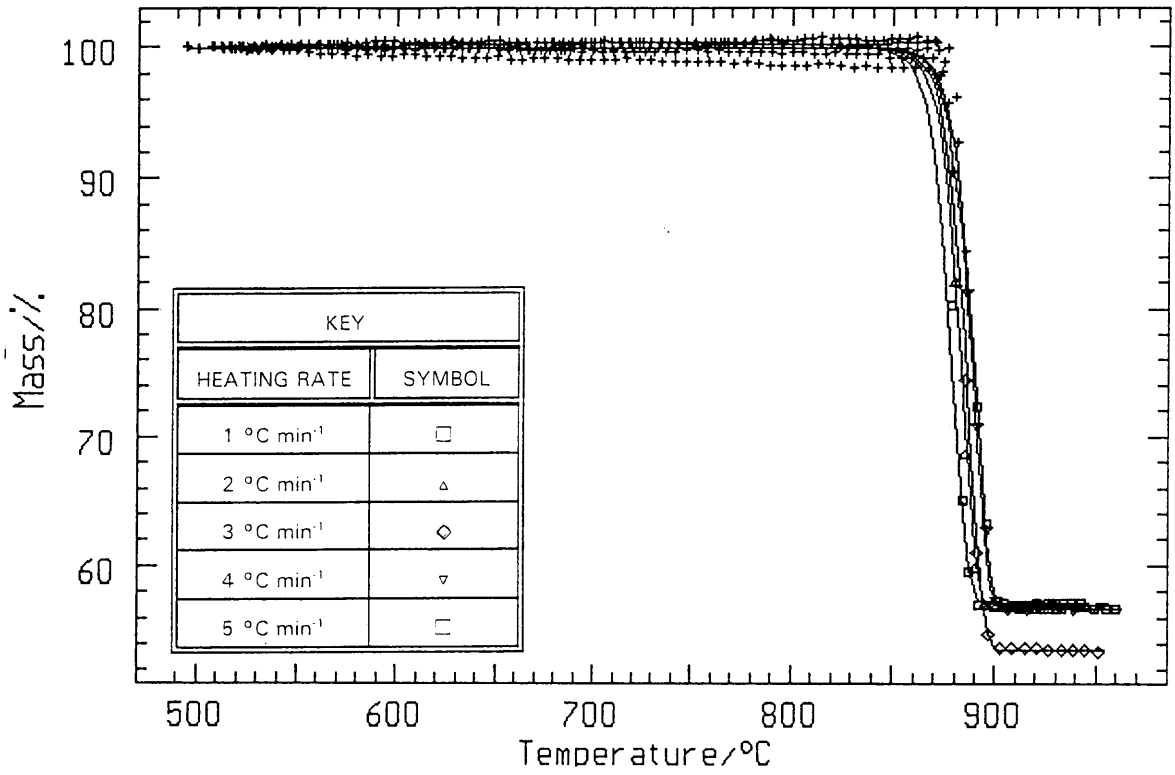

Figure 8.2.1.4 (c): Fitting of the first order kinetic model for $CaCO_3$ decomposing in a CO_2/air-atmosphere for $0.4 < \alpha < 1.0$

8.2.1.5 Kinetics of the decomposition of calcium carbonate to calcium oxide in a CO_2/water-atmosphere

The kinetic models were fitted for calcium carbonate decomposing in a CO_2/water- atmosphere from 515 °C to 1016 °C. From figure 8.2.1.5 (a), it is clear that the decomposition reaction does not occur in a single step. There are at least three steps. The increasing character of dependence on the degree of transformation until $\alpha = 0.2$ suggests that the reaction with the higher activation energy makes a growing contribution to the heat that is absorbed [85]. On reaching the maximum, the dependence becomes less due to the lesser contribution being made to the reaction with the higher

activation energy. The process then appears to be single-stage from 0.5 < α < 1.0.

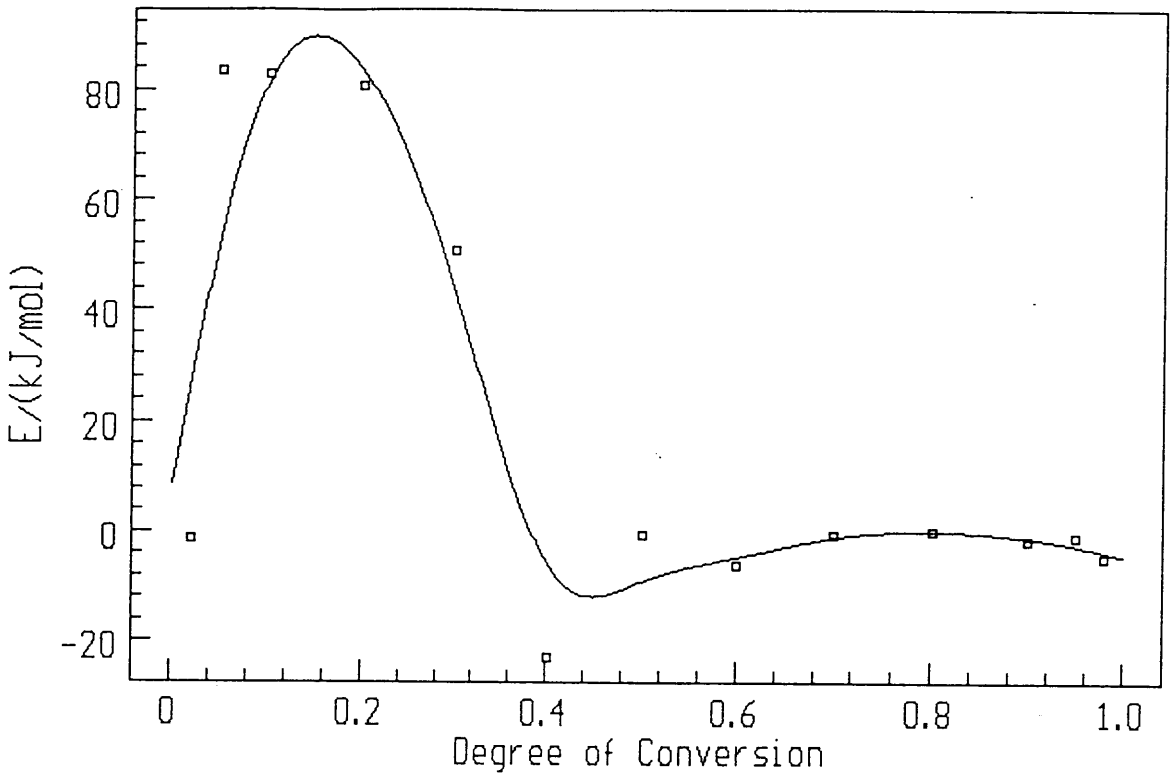

Figure 8.2.1.5 (a): Plot of activation energy versus fraction decomposed for calcium carbonate decomposing to calcium oxide in a CO_2/water-atmosphere

For 0 < α < 0.2, no kinetic models can be fitted conclusively. The isoconversional method gives an activation energy from ≈ 10 to 90 kJ mol^{-1} and ln A of ≈ -1 (refer to Chapter 9.2). It is not possible to obtain a negative pre-exponential factor as it reflects the collisions that occur during the reaction [88]. For 0.2 < α < 0.4, no kinetic models are found to fit conclusively. The isoconversional method gives an activation energy that starts at ≈ 90 kJ mol^{-1} and ends at ≈ -23 kJ mol^{-1}; and an average ln A of ≈ -2 (refer to Chapter 9.2). For 0.5 < α < 1.0, the Prout-Tompkins equation appears to fit. This equation proposed by Prout and Tompkins did not depend on an assumed mechanism but on an assumed linear relationship

between the degree of conversion and a termination constant for chain-branching. Once all the initial sites are exhausted, the carrier of the chain-branching process can react by either migrating to an unreacted site and thereby giving rise to a new nucleus or it can interact with a site that has already reacted and thereby destroying the carrier without producing a new nucleus. Prout-Tompkins kinetic model seems to fit with a correlation coefficient of 0.8533 and Durbin-Watson value of 0.265. The activation energy calculated is 179 kJ mol^{-1} and the ln A value is 6. The isoconversional method gives an average activation energy of ≈ -5 kJ mol^{-1} and ln A of ≈ -4 (refer to Chapter 9.2). The Prout-Tompkins model is thus not a conclusive fit when the activation energy value is compared with that obtained from the isoconversional method - figure 8.2.1.5 (b). It can be used, however, to describe the kinetic path of the reaction, but it is not a description of the mechanism of the reaction.

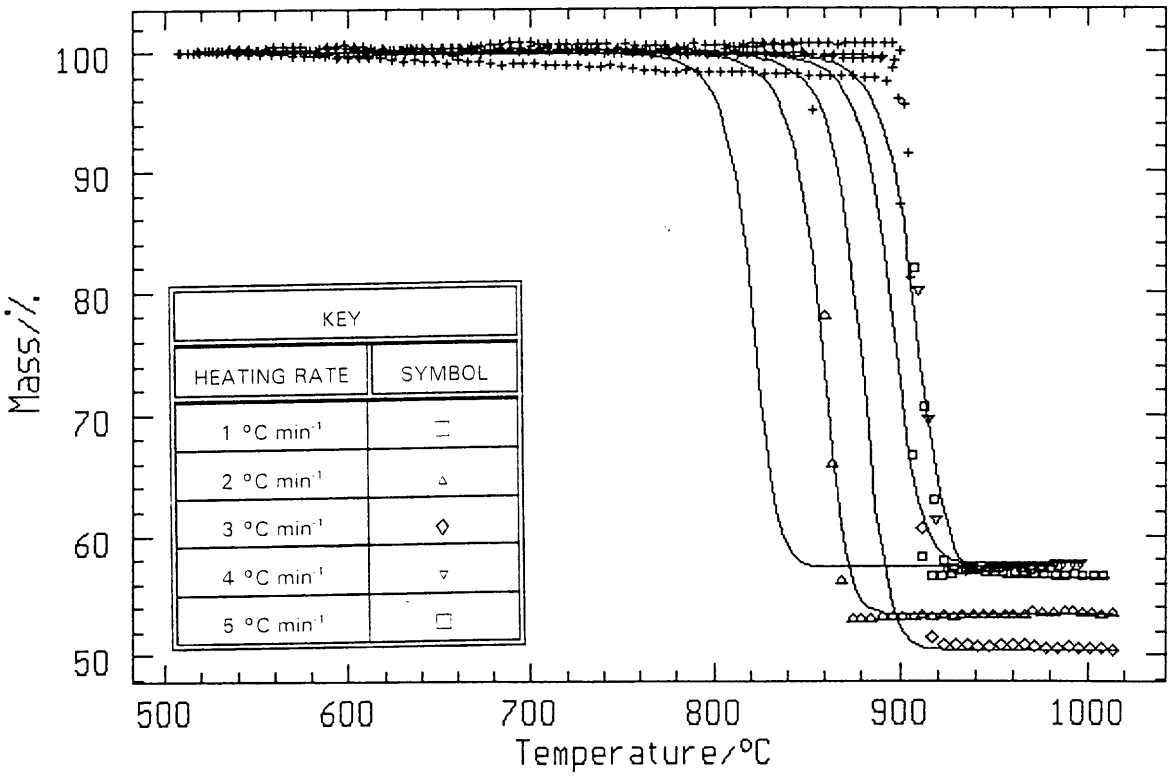

Figure 8.2.1.5 (b): Fitting of the Prout-Tompkins kinetic model to the experimental data for 0.4 < α < 1.0 of $CaCO_3$ decomposing in a CO_2/water-atmosphere

Table 8.2.2 is a summary of all the kinetic data for the decomposition of calcium carbonate in the different atmospheres used.

Table 8.2.2 Summary of the kinetic data of the thermal decomposition of calcium carbonate in different atmospheres

Atmosphere	Temperature Range (°C)	Fraction Decomposed	Kinetic Data from the Isocon. Method		Kinetic Data from the Kinetic Models			
			Average E_a (kJ mol^{-1})	ln A	Kinetic Model E_a (kJ mol^{-1})	ln A	D-W	Corr. Coeff.
Air	430 - 808	$0 < \alpha < 0.1$	144	4	no fit			
		$0.2 < \alpha < 1.0$	211	8	no conclusive fit			
Air/water	420 - 778	$0 < \alpha < 1.0$	251	11	two-dimensional phase boundary 228	9	0.047	0.9993
					or n-th order 226	9	0.042	0.9993 (no conclusive fit)
CO_2	590 - 980	$0 < \alpha < 0.2$	-	-	no fit			
		$0.2 < \alpha < 0.5$	520	18	no fit			
		$0.5 < \alpha < 0.6$	613 - 0	-	no fit			
		$0.6 < \alpha < 1.0$	18	3	no fit			
CO_2/air	500 - 970	$0 < \alpha < 0.1$	-	-	no fit			
		$0.1 < \alpha < 0.4$	1312	56	first order with autocatalysis 1816	80	0.988	0.9773
		$0.4 < \alpha < 1.0$	-1	-4	first order 1641	72	0.411	0.9903 (not a conclusive fit because the activation energies do not compare but the correlation coefficient is a good fit)
CO_2/water	515 - 1016	$0 < \alpha < 0.2$	10 - 90	-1	no fit			
		$0.2 < \alpha < 0.4$	90 - (- 10)	-2	no fit			
		$0.5 < \alpha < 1.0$	-5	-4	no fit			

Key of abbreviations in table: Isocon. = isoconversional method; E_a = activation energy; D-W = Durbin-Watson value and Corr. Coeff. = correlation coefficient.

8.2.1.6 Kinetics of the decarbonation of recarbonated calcium oxide in a CO_2-atmosphere

Table 8.2.3 The thermal decomposition of recarbonated calcium oxide in a CO_2-atmosphere using different heating rates from 1 to 5 °C min^{-1}

Heating Rate (°C min^{-1})	Temperature Range (°C)	Mass Loss (%)	Mass Gain (%)	ΔH (kJ g^{-1})
1	150 - 897 897 - 949	- 63	38 -	- 3 x 10^3
2	150 - 896 898 - 936	- 54	51 -	- 3 x 10^3
3	140 - 881 882 - 957	- 44	61 -	- 3 x 10^3
4	130 - 840 842 - 942	- 43	60 -	- 3 x 10^3
5	100 - 851 852 - 1018	- 50	53 -	- 3 x 10^3

A study was done on the decarbonation of $CaCO_3$ to calcium oxide in an air-atmosphere; and then recarbonating it to $CaCO_3$ by heating in a CO_2-atmosphere. A 15 mg sample of $CaCO_3$ was decomposed in an air-atmosphere to 900 °C using a heating rate of 10 °C min^{-1}. The product, CaO, was cooled down to room temperature and then heated again in a CO_2-atmosphere to 1100 °C using a heating rate from 1 to 5 °C min^{-1} on different samples. Figure 8.2.1.6 (a) is the thermogram for the decomposition reaction of the recarbonated calcium oxide. The percentage recarbonation using a heating rate of 5 °C min^{-1}, is > 100 % (the theoretical mass gain is 43.97 %).

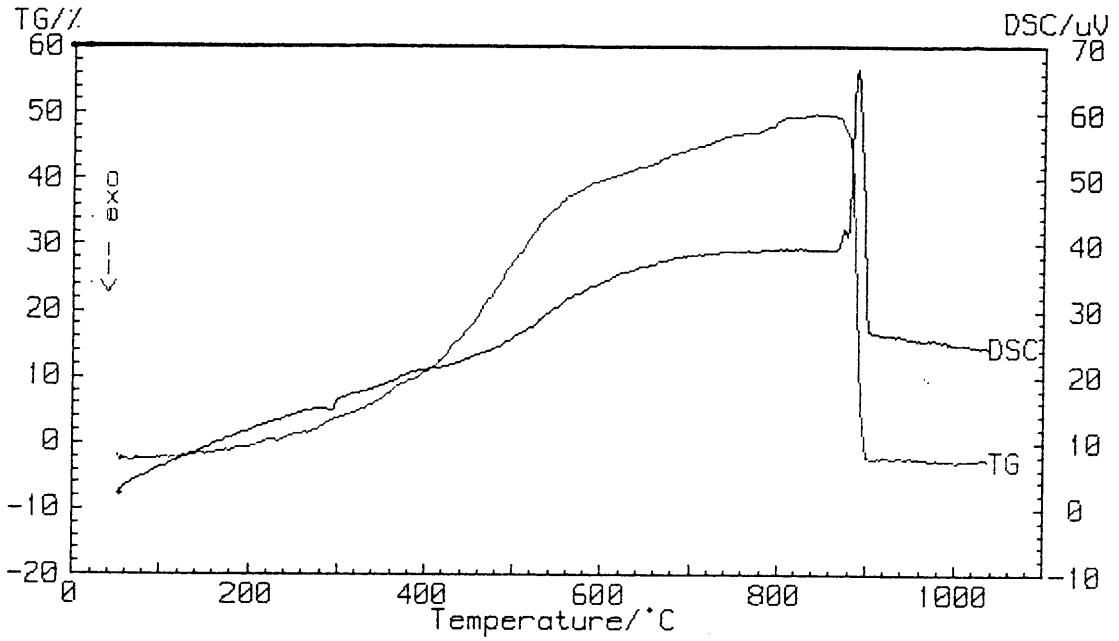

Figure 8.2.1.6 (a): TG and DSC curves of recarbonated and decarbonated CaO compound decomposing in a CO_2-atmosphere using a heating rate of 5 °C min^{-1}

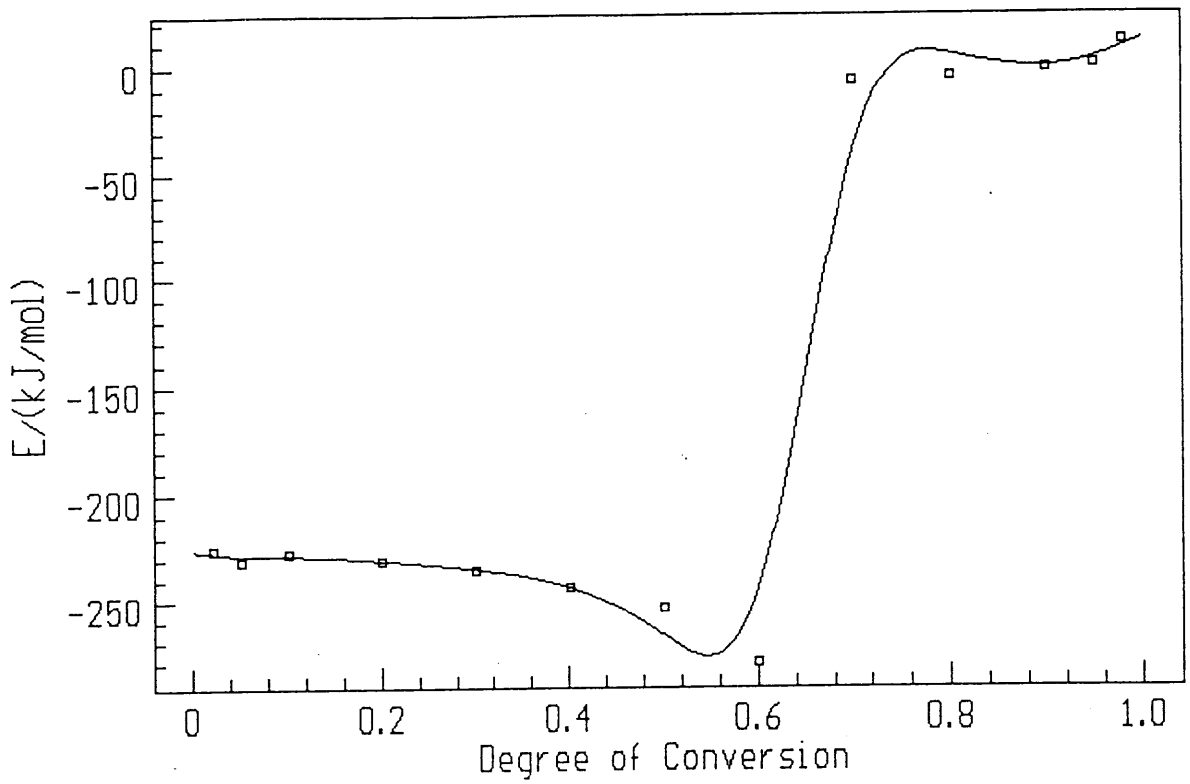

Figure 8.2.1.6 (b): Plot of E_a vs α for recarbonated and decarbonated CaO compound decomposing in a CO_2-atmosphere

The plot of activation energy versus fraction decomposed (figure 8.2.1.6 (b)) shows that a multi-step reaction is occurring. The activation energy does not appear to depend on the conversion at the onset of the decomposition reaction for $0 < \alpha < 0.6$. Thus, the rate appears to be determined by a single-step reaction [89] with an average activation energy of $\approx$ - 240 kJ mol^{-1} (refer to Chapter 9.2) and a ln A value of $\approx$ 7. None of the kinetic models conclusively fit the experimental data between $0 < \alpha < 0.6$. For $0.6 < \alpha < 0.7$, none of the kinetic models appear to fit. The minimum activation energy is $\approx$ - 280 kJ mol^{-1} and the maximum $\approx$ 10 kJ mol^{-1} for $0.6 < \alpha < 0.7$. For $0.7 < \alpha < 0.9$, the isoconversional method gave an average activation energy of $\approx$ - 4 kJ mol^{-1} and ln A value of $\approx$ - 4 (refer to Chapter 9.2). No kinetic models are found to fit. The kinetic data obtained from the decarbonation of calcium carbonate in a CO_2-atmosphere, shows that the pure calcium carbonate appears to decompose in the CO_2-atmosphere via the first order with autocatalysis model for $0.6 < \alpha < 1.0$. The activation energy obtained for $0.6 < \alpha < 1.0$, is 358 kJ mol^{-1}; ln A = 12; Durbin-Watson value = 0.405 and a correlation coefficient of 0.8722. These values do not correlate at all with the decarbonation of the (CaO + CO_2) compound, indicating a different decomposition mechanism.

8.2.2 Beestekraal Limestone

The thermal decomposition of Beestekraal limestone in an air-atmosphere using a heating rate of 5 °C min^{-1} is shown in figure 8.2.2(a).

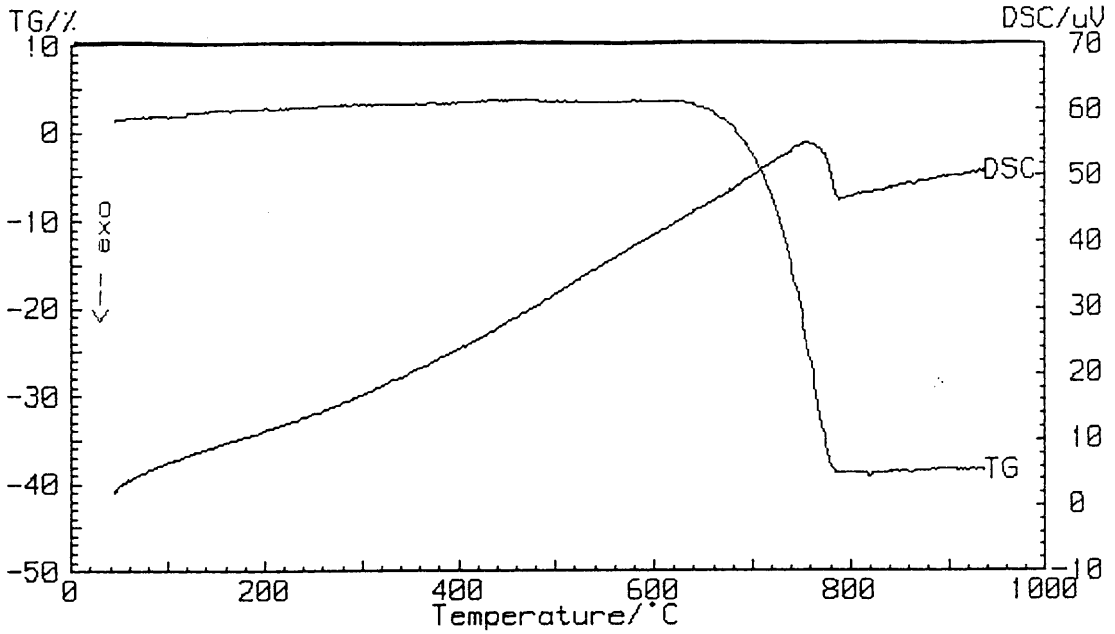

Figure 8.2.2(a): TG and DSC curves of the thermal decomposition of Beestekraal limestone decomposing in an air-atmosphere using a heating rate of 5°C min^{-1}

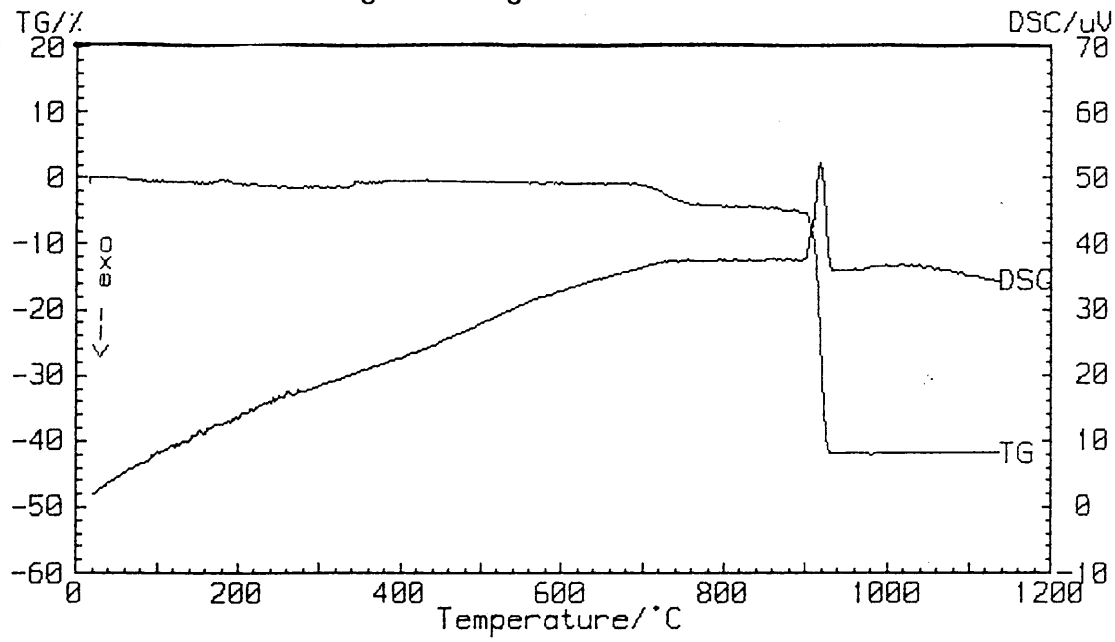

Figure 8.2.2(b): TG and DSC curves of the thermal decomposition of Beestekraal limestone decomposing in a CO_2-atmosphere using a heating rate of 5 °C min^{-1}

The decarbonation mass loss starts at 590 °C in an air-atmosphere, but at 883 °C in a CO_2-atmosphere (figure 8.2.2(b)). The partial pressure of CO_2 influences the decomposition of the calcium carbonate.

The following table shows the thermal decomposition of Beestekraal limestone in different atmospheres.

Table 8.2.2 The thermal decomposition of Beestekraal limestone in different atmospheres using a heating rate of 5 °C min^{-1} with sample masses between 5 - 15 mg

Atmosphere	Temperature Range (°C)	Mass Loss (%)	ΔH (kJ g^{-1})
Air	590 - 889 50 - 889	41 -	2 -
Air/H_2O	569 - 834 50 - 834	42 -	- -
CO_2	890 - 1011 45 - 1011	36 -	8 x 10^{-1} -
CO_2/Air	861 - 953 100 - 953	37 -	8 x 10^{-1} -
CO_2/H_2O	883 - 942 112 - 942	37 -	8 x 10^{-1} -

A faster rate of mass loss (at a higher decarbonation temperature) is observed for the CO_2-atmosphere than in the air-atmosphere. The percentage mass loss of the decomposition of $CaCO_3$ in an air-atmosphere using a heating rate of 5 °C min^{-1}, is 41 % for the Beestekraal limestone. This is in accordance with the XRD results (Chapter 7.2) which indicates that the Beestekraal limestone is not pure (approximately 94 % pure). The heat of decomposition is 2 kJ g^{-1} and for pure calcium carbonate it is also found to be 2 kJ g^{-1}. The heat of decomposition for the Beestekraal limestone in the CO_2- and CO_2-rich atmospheres is less (0.8 kJ g^{-1}) than that obtained in an air-atmosphere (2 kJ g^{-1}). Figures 8.2.2 (c); 8.2.2 (d) and 8.2.2 (e) are thermograms of Beestekraal limestone decomposing in

air/water-; CO_2/air- and CO_2/water-atmospheres respectively.

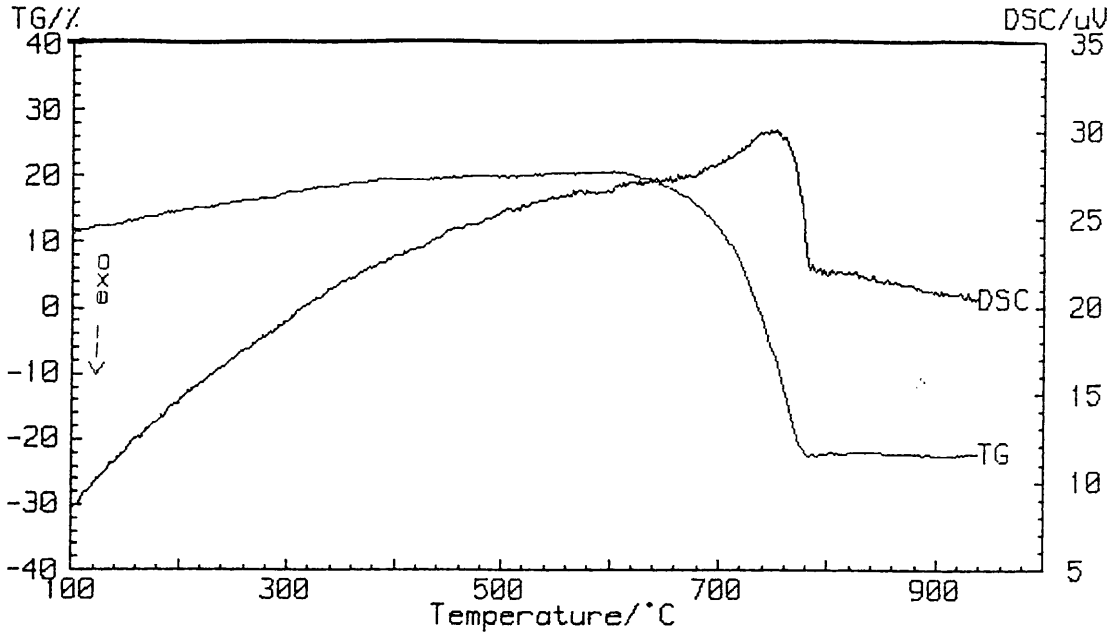

Figure 8.2.2 (c): TG and DSC curves of the thermal decomposition of Beestekraal limestone decomposing in an air/water-atmosphere using a heating rate of 5 °C min^{-1}

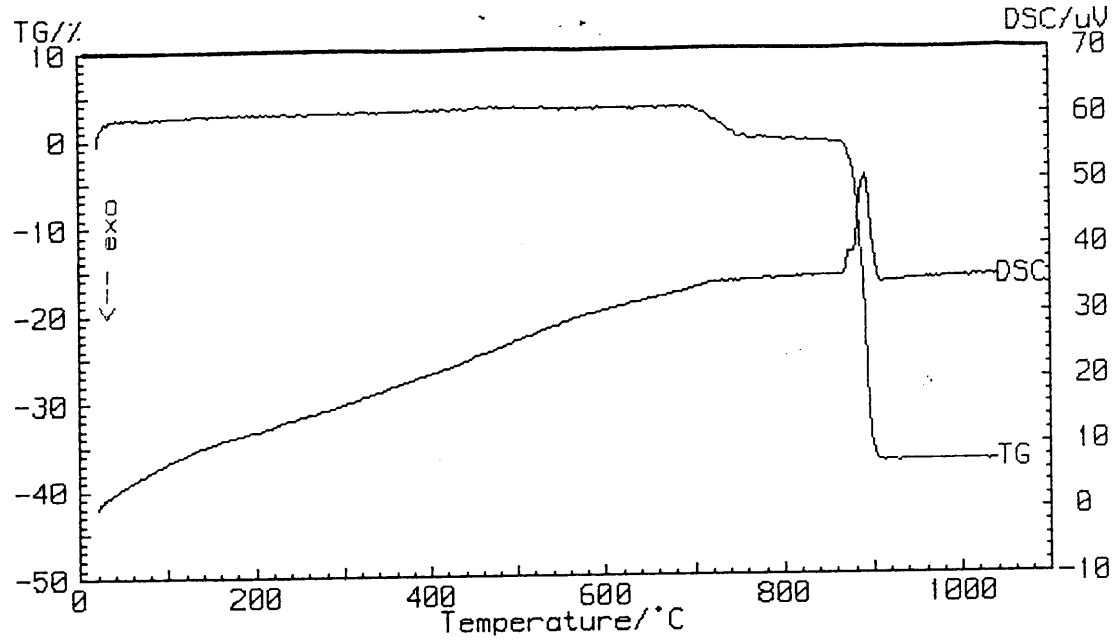

Figure 8.2.2 (d): TG and DSC curves of the thermal decomposition of Beestekraal limestone decomposing in a CO_2/air-atmosphere using a heating rate of 5 °C min^{-1}

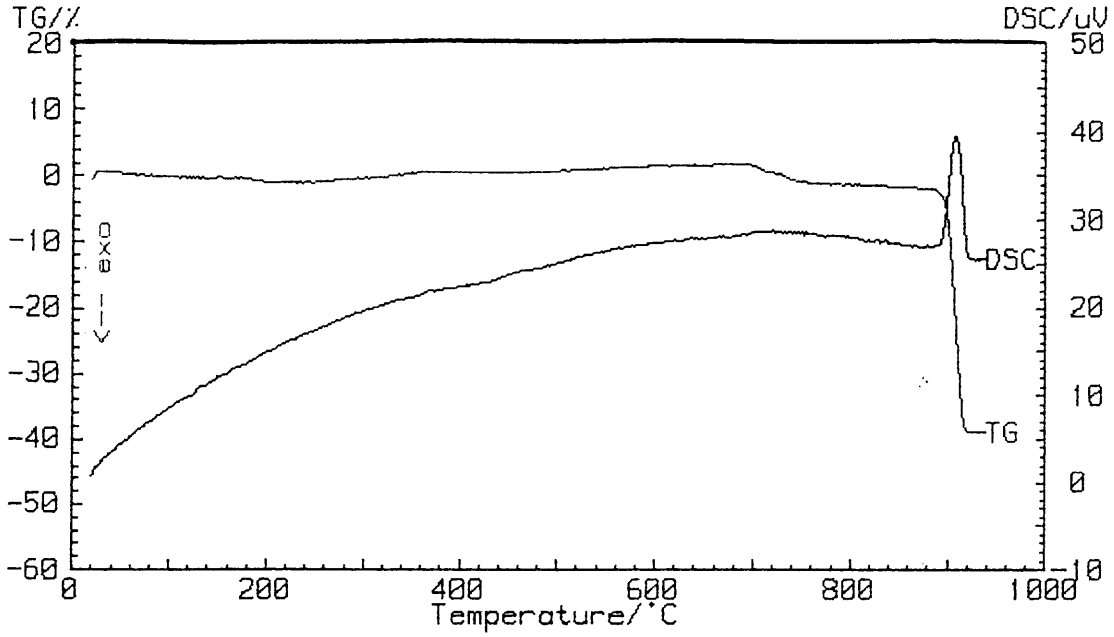

Figure 8.2.2 (e): TG and DSC curves of the thermal decomposition of Beestekraal limestone decomposing in a CO_2/water-atmosphere using a heating rate of 5 °C min^{-1}

8.2.2.1 Kinetics of the thermal decomposition of Beestekraal limestone to calcium oxide in an air-atmosphere

The kinetics of the decomposition of Beestekraal limestone was followed from 490 °C to 850 °C. From figure 8.2.2.1 (a), it appears that the decomposition reaction did not take place via a single-step reaction. The ascending part of the graph indicates that the reaction with the higher activation energy makes a continually increasing contribution to the heat being absorbed. On reaching the maximum activation energy, the dependence becomes descending because of the decreasing contribution by the reaction with the higher activation energy [85].

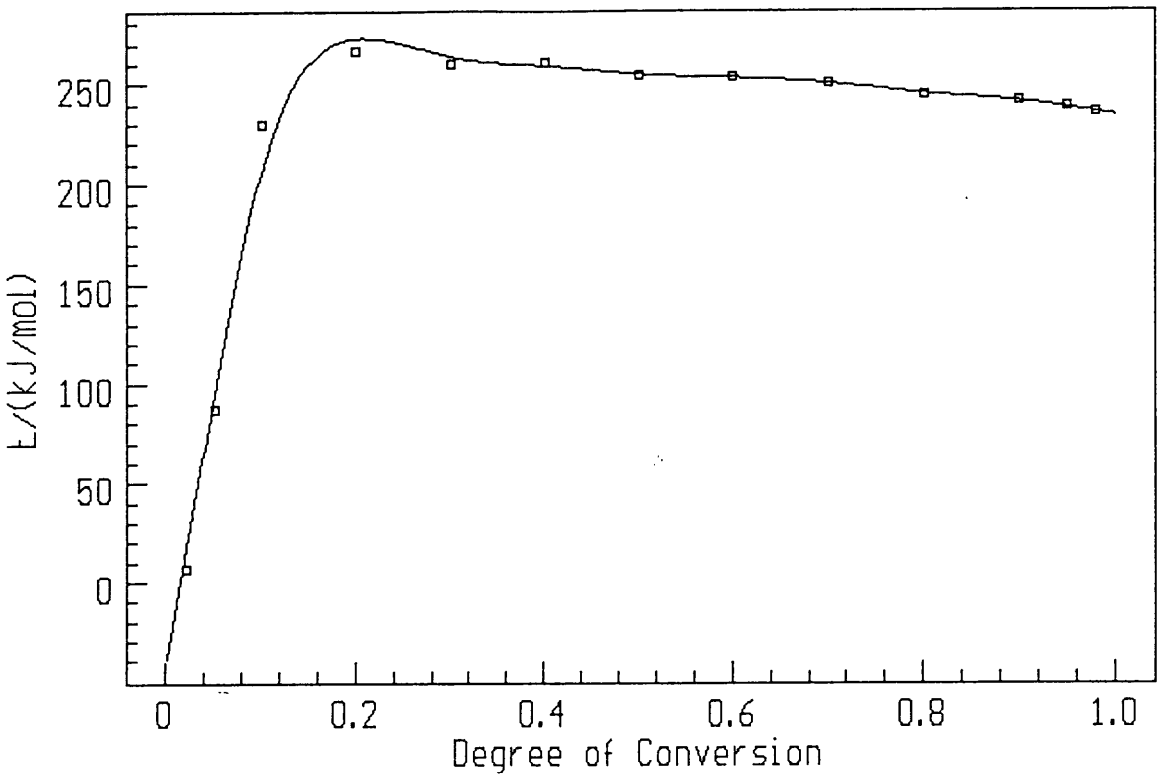

Figure 8.2.2.1 (a): Plot of activation energy versus fraction decomposed for the thermal decomposition reaction of Beestekraal limestone to calcium oxide in an air-atmosphere

No kinetic model was found to fit the range $0 < \alpha < 0.1$. The isoconversional method gave an activation energy varying from ≈ 0 to $\approx$ 249 kJ mol^{-1}. The kinetic models are fitted for $0.1 < \alpha < 1.0$. The best fit for this range is the n-th order equation. The activation energy obtained is 250 kJ mol^{-1} with a ln A value of 10. (The correlation coefficient is 0.9993 and the Durbin-Watson value is 0.018). The isoconversional method gives an average activation energy of $\approx$ 249 kJ mol^{-1} and a ln A of $\approx$ 10. This is an excellent correlation as can be seen from the theoretical fit of the experimental data in figure 8.2.2.1 (b).

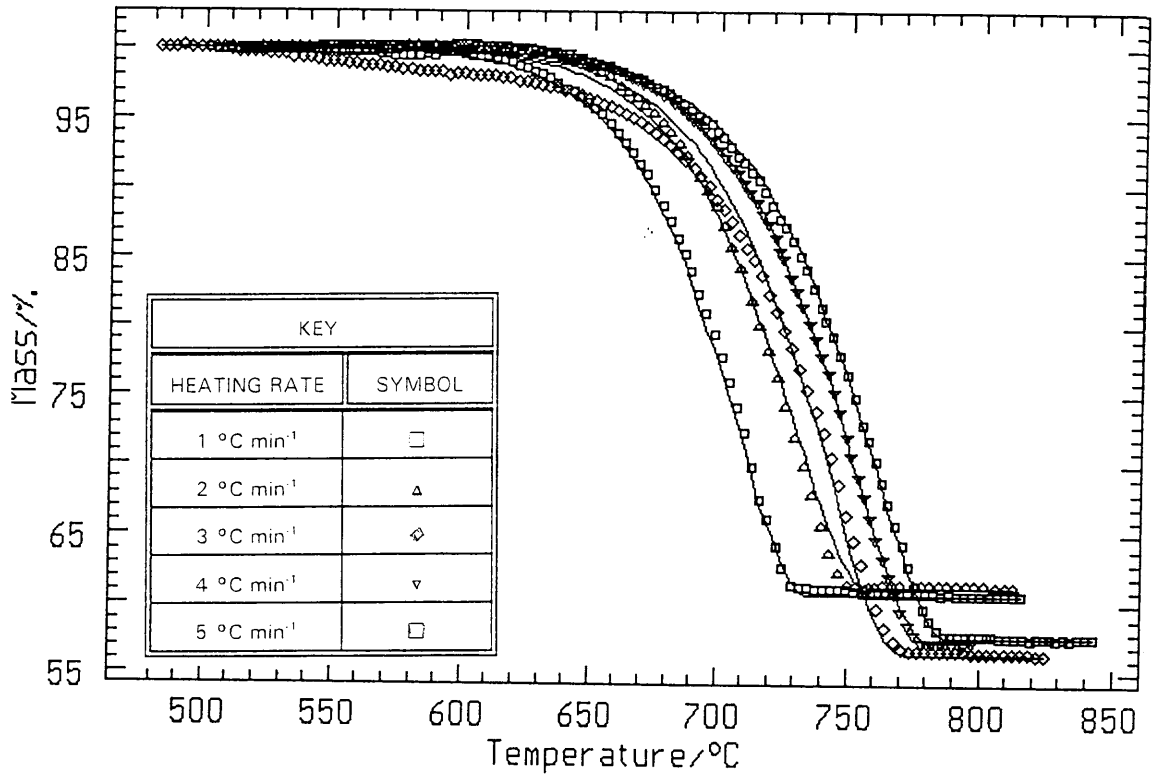

Figure 8.2.2.1 (b): Fitting of the n-th order kinetic model for the decomposition reaction of Beestekraal limestone in an air-atmosphere

8.2.2.2 Kinetics of the thermal decomposition of Beestekraal limestone to calcium oxide in an air/water-atmosphere

The thermal decomposition reaction of Beestekraal limestone in an air/water-atmosphere is followed from 497 °C to 810 °C. Figure 8.2.2.2 (a) shows a plot of activation energy versus the fraction decomposed for Beestekraal limestone. From figure 8.2.2.2(a), the activation energy increases from ≈ 210 kJ mol^{-1} to ≈ 266 kJ mol^{-1} for $0 < \alpha < 0.1$. The activation energy then decreases until $\alpha = 0.2$, where it remains more or less constant at ≈ 242 kJ mol^{-1} and ln A = 10. The reaction with the higher activation energy

makes a growing contribution to the heat absorbed initially for $0 < \alpha < 0.2$. The kinetic models are fitted over the $0.2 < \alpha < 1.0$ range. The isoconversional method gives an average activation energy value of $\approx$ 242 kJ mol^{-1} and a ln A value of $\approx$ 10 for $0.2 < \alpha < 1.0$.

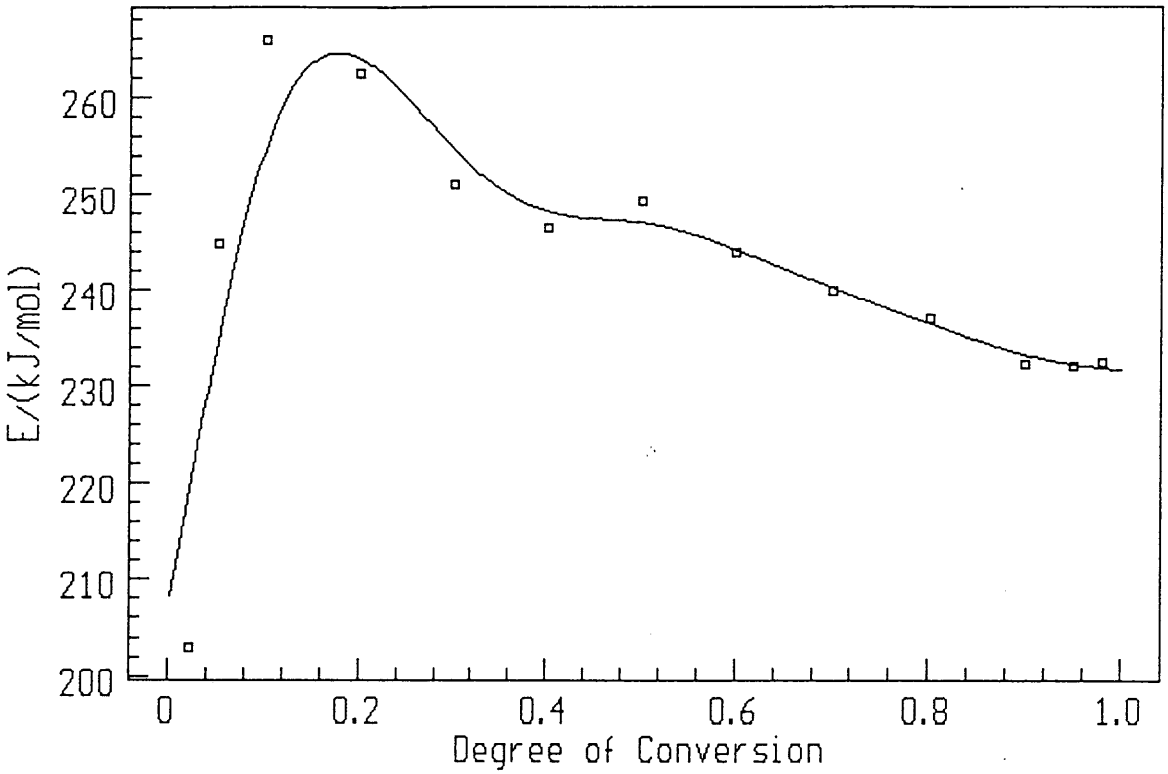

Figure 8.2.2.2 (a): Plot of activation energy vs fraction decomposed for Beestekraal limestone decomposing in an air/water-atmosphere

The kinetic models that appear to fit are: the two-dimensional phase boundary (activation energy = 233 kJ mol^{-1}; ln A = 9; correlation coefficient = 0.9996 and a Durbin-Watson value of 0.046), the n-th order (activation energy = 236 kJ mol^{-1}; ln A = 9; correlation coefficient = 0.9997 and a Durbin-Watson value of 0.060) and the first order with autocatalysis (activation energy = 241 kJ mol^{-1}; ln A = 10; correlation coefficient = 0.9992 and a Durbin-Watson value of 0.061). The best fit is the Sestak-Berggren with an activation energy of 243 kJ mol^{-1} and a ln A of

10. (The correlation coefficient = 0.9998 and the Durbin-Watson value = 0.080). Figure 8.2.2.2 (b) shows the kinetic model fit of the Sestak-Berggren equation to the experimental data. Thus, from the activation energy values the Sestak-Berggren model is the best fit and its correlation coefficient value is the best.

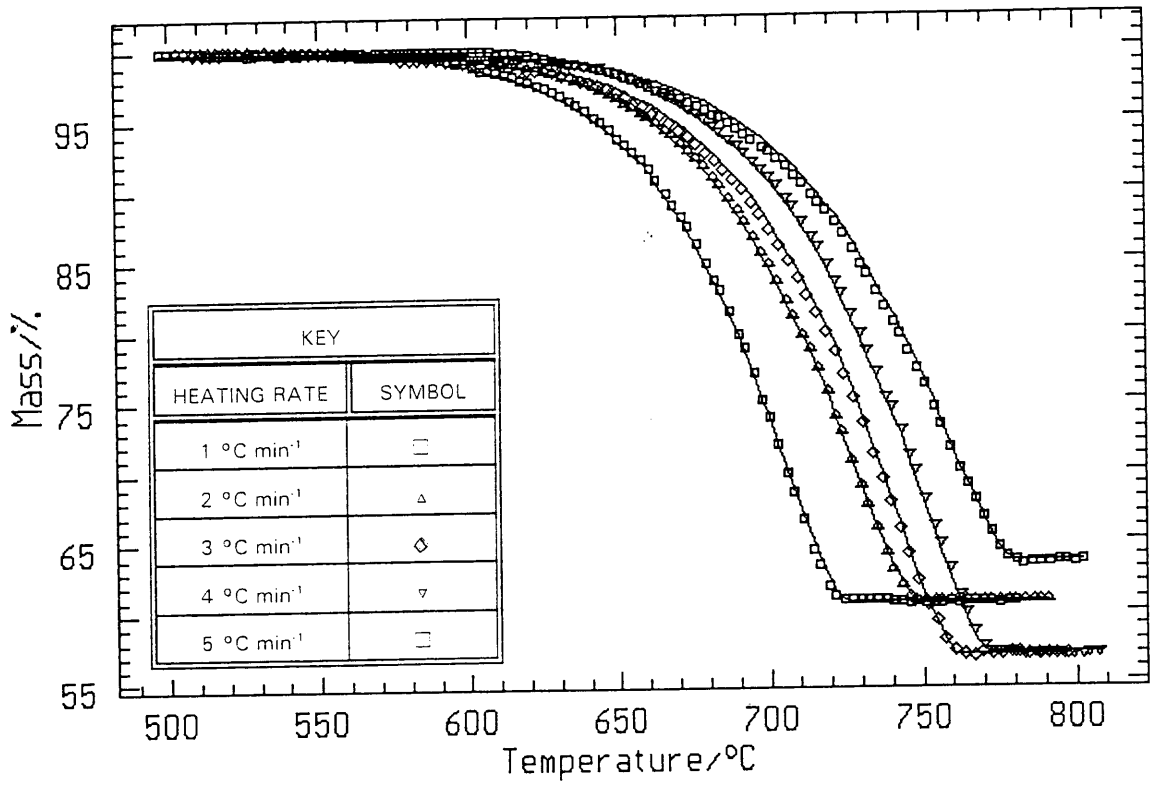

Figure 8.2.2.2 (b): The Sestak-Berggren kinetic model fitted to the experimental data of Beestekraal limestone decomposing in an air/water-atmosphere

8.2.2.3 Kinetics of the thermal decomposition of Beestekraal limestone to calcium oxide in a CO_2-atmosphere

The thermal decomposition reaction of Beestekraal limestone in CO_2-atmosphere gives two mass loss curves between 605 °C and 780 °C and

between 785 °C and 995 °C. Figure 8.2.2.3 (a) shows a plot of activation energy versus fraction decomposed for Beestekraal limestone in a CO_2-atmosphere between 605 °C and 780 °C. From figure 8.2.2.3 (a), it is clear that the average activation energy increases gradually until α = 0.95, after which it decreases sharply. From the isoconversional method, the average activation energy increases gradually from ≈ 30 kJ mol^{-1} at α = 0 to ≈ 350 kJ mol^{-1} at α = 0.95. The average activation energy then decreases from ≈ 350 to 0 kJ mol^{-1} at α = 1.0.

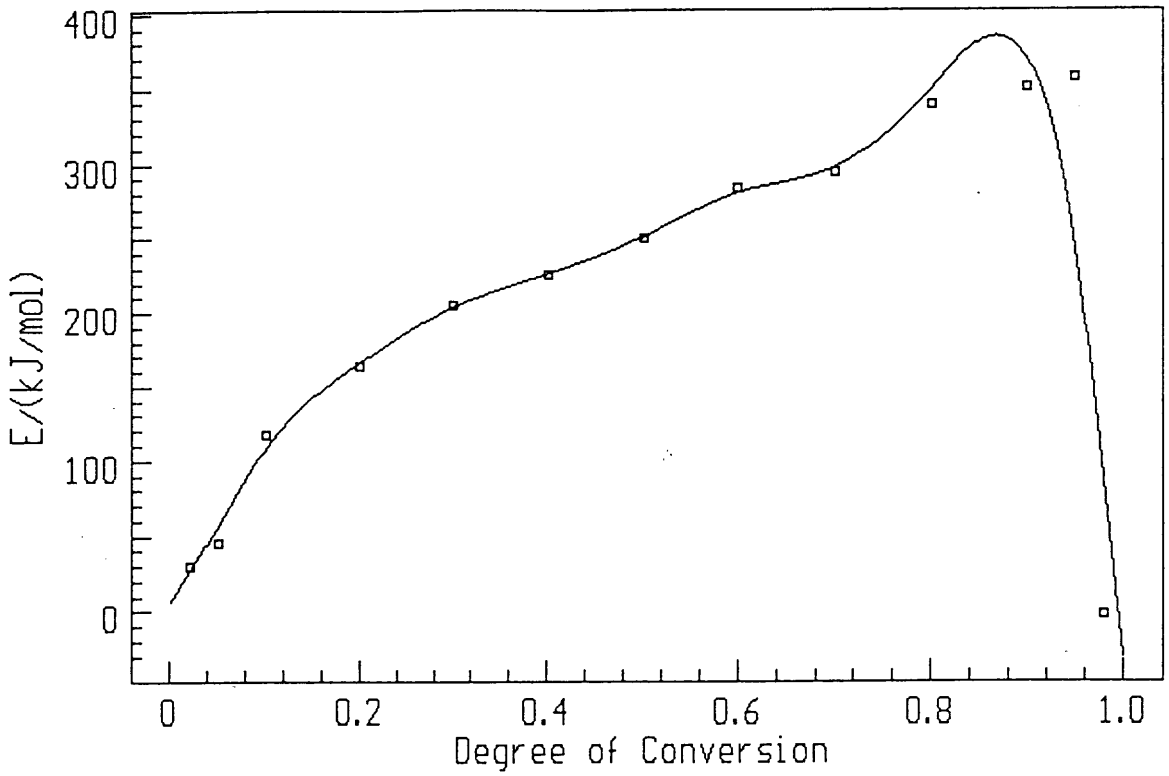

Figure 8.2.2.3 (a): Plot of E_a vs α for Beestekraal limestone decomposing to calcium oxide in a CO_2-atmosphere between 605 °C and 780 °C

The dependence of activation energy on the degree of conversion ascends gradually indicating that the reaction with the higher activation energy

makes a growing contribution to the heat absorbed. On reaching the maximum activation energy at ≈ 350 kJ mol^{-1} at α = 0.95, the average activation energy decreases sharply as the contribution by the reaction with the higher activation energy decreases sharply until α = 1.0. The average activation energy value is ≈ 240 kJ mol^{-1} (which is only an estimate activation energy [85]) and a ln A value of ≈ 10. Thus, all the kinetic models which appear to fit are: the d-dimensional Avrami-Erofe'ev equation (activation energy = 273 kJ mol^{-1}; ln A = 12; correlation coefficient = 0.9948 and a Durbin-Watson value of 0.348), the Sestak-Berggren equation (activation energy = 269 kJ mol^{-1}; ln A = 12; correlation coefficient = 0.9949 and a Durbin-Watson value of 0.355), first order with autocatalysis (activation energy = 269 kJ mol^{-1}; ln A = 11; correlation coefficient = 0.9945 and a Durbin-Watson value of 0.334), first order (activation energy = 300 kJ mol^{-1}; ln A = 13; correlation coefficient = 0.9941 and a Durbin-Watson value of 0.309) and the n-th order equation (activation energy = 286 kJ mol^{-1}; ln A = 12; correlation coefficient = 0.9944 and a Durbin-Watson value of 0.325). The best fit according to the Durbin-Watson value and also activation energy (comparing with that obtained from the isoconversional method which is clearly not a good estimate), is the two-dimensional phase boundary equation. The activation energy is 255 kJ mol^{-1}, with a ln A value of 10, a correlation coefficient of 0.9920 and a Durbin-Watson value of 0.247. The phase boundary is present and it makes limitations on the rate, but the rate of diffusion of CO_2 through the reacted material (CaO), also makes a contribution to the overall rate. The two-dimensional diffusion controlled reaction into a cylinder of radius follows the equation:

$$(1 - \alpha)\ln(1 - \alpha) + \alpha = kt/r^2$$

where α is the fraction decomposed

k is the rate constant

t is the time

r is the radius of the particles [14].

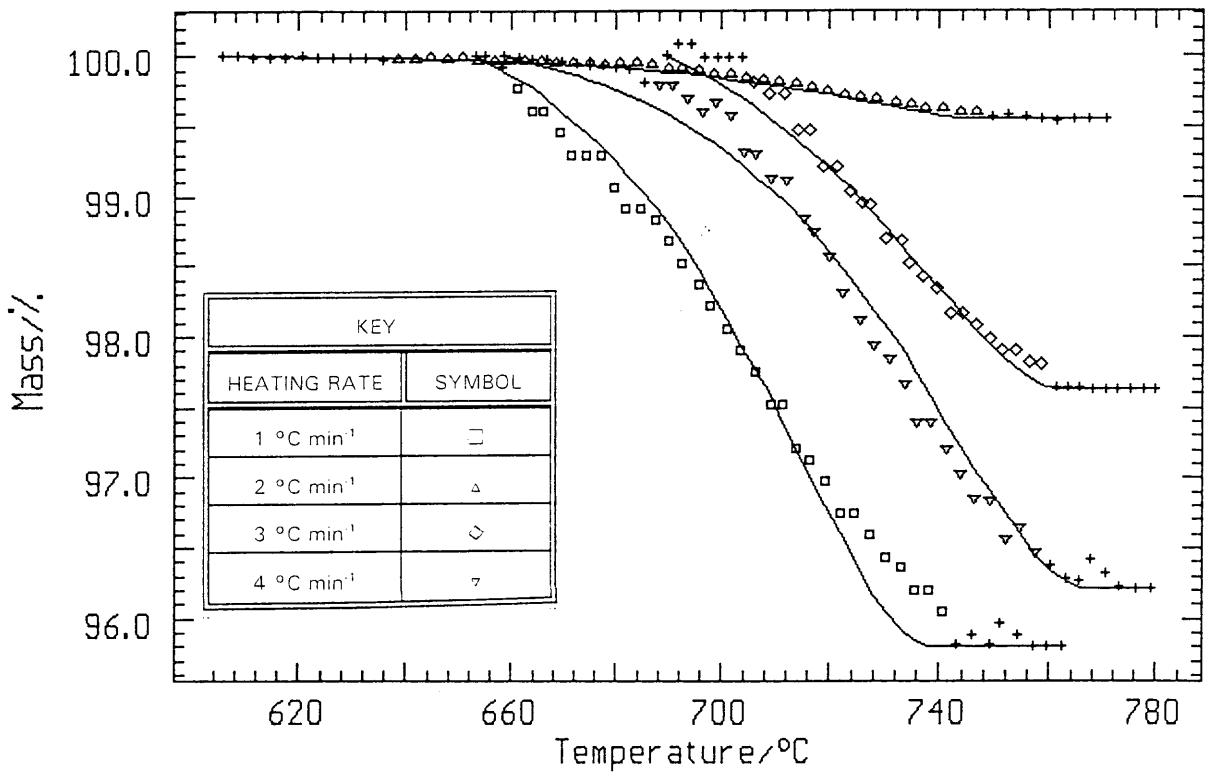

Figure 8.2.2.3 (b): Fitting of experimental data of the decomposition of Beestekraal limestone in a CO_2-atmosphere with the kinetic model of the two-dimensional phase boundary

The kinetics of the second mass loss curve is followed between 785 °C and 995 °C. From figure 8.2.2.3 (c), the activation energy changes with the

fraction decomposed, thus the decomposition reaction is clearly a complex reaction. The average activation energy increases sharply from ≈ 0 to ≈ 2600 kJ mol^{-1} from $0 < \alpha < 0.2$. The average activation energy remains constant for $0.2 < \alpha < 0.5$ at ≈ 2300 kJ mol^{-1}. The average activation energy decreases rapidly to ≈ 0 kJ mol^{-1} where it remains constant for $0.6 < \alpha < 1.0$. The ascending part of the dependence indicates that the reaction with the higher activation energy makes an increasing contribution to the heat absorbed from 0 to 0.1. The kinetic models are fitted for $0.2 < \alpha < 0.5$ and $0.6 < \alpha < 1.0$ which are the stages that are indicative of single-stage processes [88].

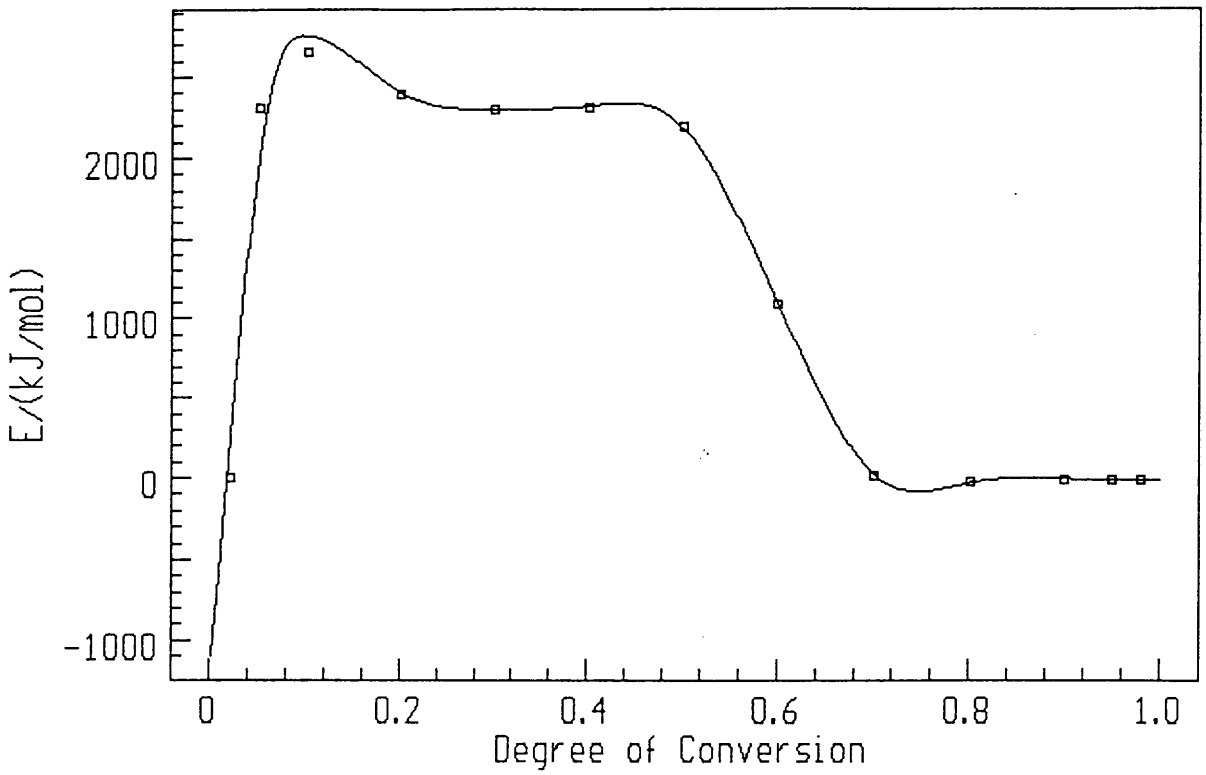

Figure 8.2.2.3 (c): Plot of activation energy vs fraction decomposed for Beestekraal limestone decomposing in a CO_2-atmosphere between 785 °C and 995 °C

The isoconversional method gives an average activation energy value of ≈ 1913 kJ mol^{-1} and a ln A value of ≈ 81 for $0.2 < \alpha < 0.5$. The kinetic

models which appear to fit are the following: the three-dimensional diffusion equation of Ginstling-Brounshtein (activation energy = 3309 kJ mol^{-1}; ln A = 142; correlation coefficient = 0.9689 and a Durbin-Watson value of 0.294), the two-dimensional diffusion equation (activation energy = 3216 kJ mol^{-1}; ln A = 139; correlation coefficient = 0.9685 and a Durbin-Watson value of 0.287), the three-dimensional diffusion equation of Jander (activation energy = 3500 kJ mol^{-1}; ln A = 150; correlation coefficient = 0.9694 and a Durbin-Watson value of 0.301) and the one-dimensional diffusion equation (activation energy = 2934 kJ mol^{-1}; ln A = 126; correlation coefficient = 0.9662 and a Durbin-Watson value of 0.270). The best fit is the second order equation which gives an activation energy value of 2679 kJ mol^{-1}; a ln A value of 116; a correlation coefficient of 0.9731 and a Durbin-Watson value of 0.202 (figure 8.2.2.3.(d)).

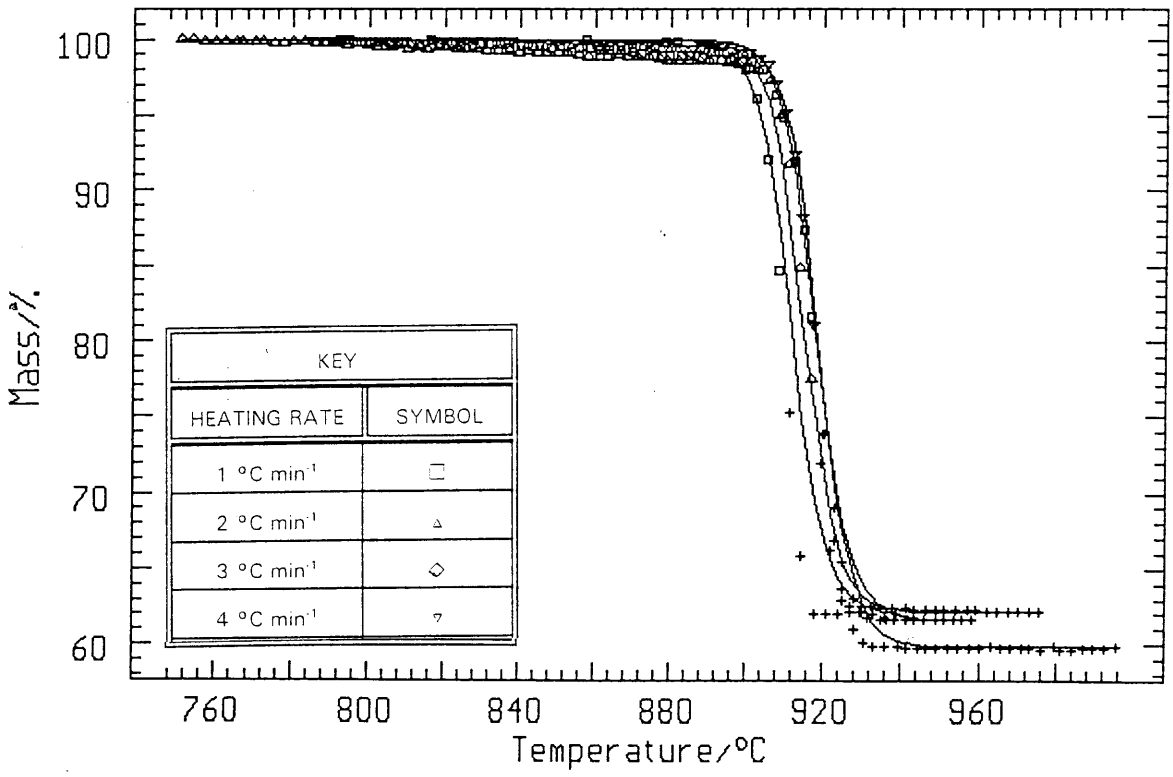

Figure 8.2.2.3 (d): Fitting of the experimental data of the decomposition reaction of Beestekraal limestone decomposing in a CO_2-atmosphere between 785 °C and 995 °C

However, if the plot of activation energy versus fraction decomposed is considered for $0.2 < \alpha < 1.0$, it appears to fit the shape expected for diffusion reactions but the activation energy is too high. Generally, a low value of the activation energy at a high degree of transformation is characteristic of the diffusion of a gas [89]. As the activation energy is too high this cannot be the case for this complex reaction.

No fit is found for $0.6 < \alpha < 1.0$.

8.2.2.4 Kinetics of the thermal decomposition of Beestekraal limestone to calcium oxide in a CO_2/air-atmosphere

There are two mass loss curves which have to be fitted to the kinetic models i.e. between 640 and 755 °C, and between 760 and 960 °C. The kinetic data obtained for Beestekraal limestone decomposing in CO_2/air-atmosphere shows an increase in activation energy from $0 < \alpha < 0.2$, where it remains constant at an activation energy value of $\approx$ 379 kJ mol^{-1} from $0.2 < \alpha < 0.8$, after which it decreases (figure 8.2.2.4 (a)). It is clear that the decomposition reaction does not occur in a single step. There are at least three stages in the decomposition reaction of Beestekraal limestone (figure 8.2.2.4 (a)). The increase in the activation energy for $0 < \alpha < 0.2$ (from $\approx$ 140 to $\approx$ 390 kJ mol^{-1}) implies that the reaction with the higher activation energy contributes to the heat absorbed [85]. The average activation energy remains constant at a value of $\approx$ 379 kJ mol^{-1} until $\alpha =$ 0.8. Thus, it can be assumed that the temperature dependence of the overall process rate is governed by one activation energy [85]. The average activation energy is a good approximation for the activation energy of the limiting reaction [85].

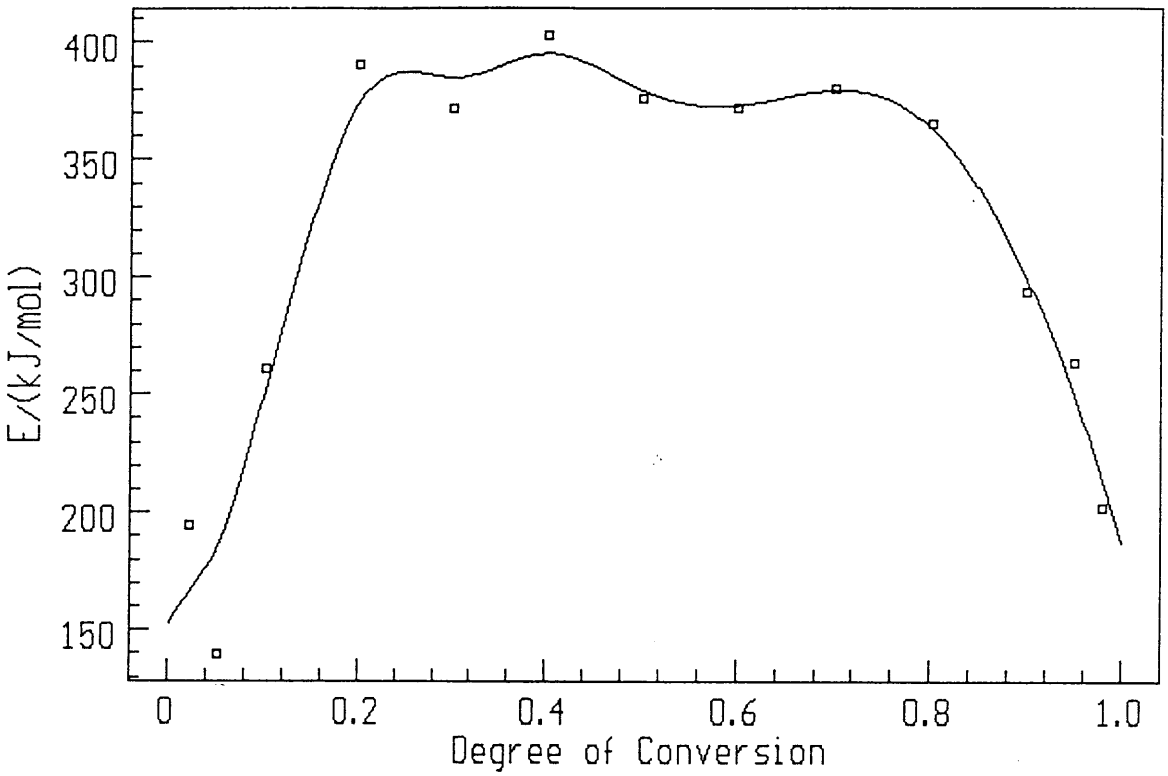

Figure 8.2.2.4 (a): Plot of E_a vs α for Beestekraal limestone decomposing to calcium oxide in a CO_2/air-atmosphere between 640 °C and 755 °C

The ln A value is ≈ 17 for $0.2 < \alpha < 0.8$. For $0.8 < \alpha < 1$, the activation energy decreases sharply implying that the dependence of the activation energy on the degree of conversion becomes descending because of the decreasing contribution of the reaction with the higher activation energy [85]. The maximum activation energy is ≈ 379 kJ mol^{-1} and the minimum is ≈ 200 kJ mol^{-1}.

For $0.2 < \alpha < 0.8$, the d-dimensional Avrami-Erofe'ev equation appears to fit, giving an activation energy value of 375 kJ mol^{-1} and a ln A of 17. The correlation coefficient is 0.9934 and the Durbin-Watson value is 0.812. The first order kinetic model (figure 8.2.2.4 (b)) also appears to fit the

experimental data with an activation energy of 380 kJ mol^{-1}, a ln A value of 17, a correlation coefficient of 0.9933 and a Durbin-Watson value of 0.795.

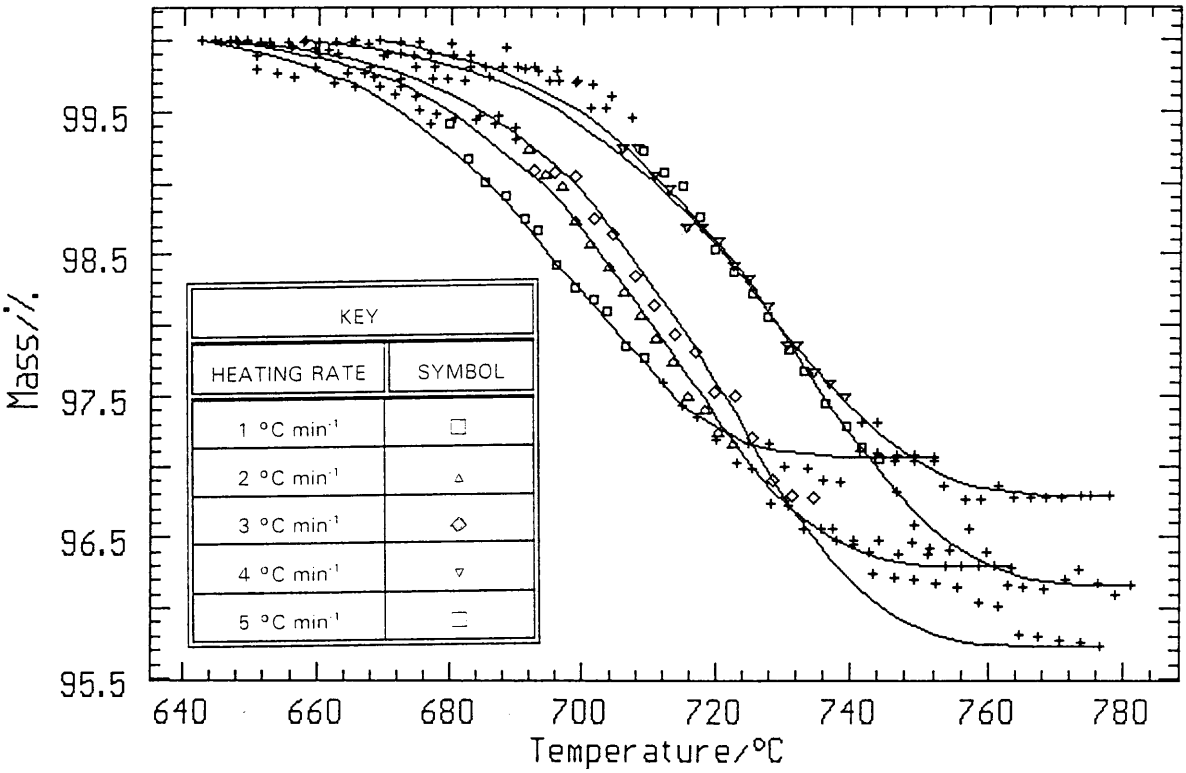

Figure 8.2.2.4 (b): Fitting of the first order kinetic model for Beestekraal limestone decomposing to calcium oxide in a CO_2/air-atmosphere for $0.2 < \alpha < 0.8$

The isoconversional method obtains an average activation energy value of ≈ 379 kJ mol^{-1} and a ln A value of ≈ 17. The n-th order kinetic model (figure 8.2.2.4. (c) - correlation coefficient = 0.9933) gives an activation energy value of 380 kJ mol^{-1} and a ln A value of 17. The Durbin-Watson value is 0.796. On comparing the activation energy values, the n-th order and the first order kinetic models fit. No single conclusive fit can be found.

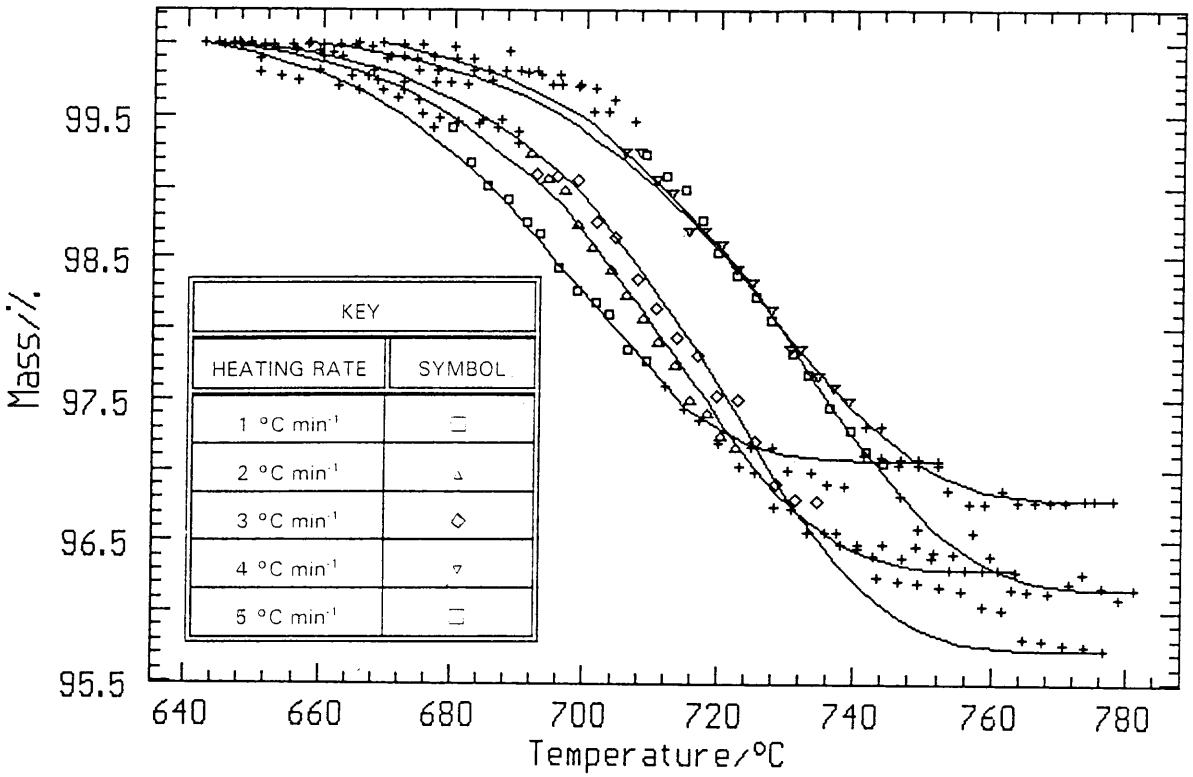

Figure 8.2.2.4 (c): Fitting of the n-th order equation for Beestekraal limestone decomposing to calcium oxide in a CO_2/air-atmosphere for $0.2 < \alpha < 0.8$

The decomposition reaction for $0 < \alpha < 0.2$ has an activation energy varying from $\approx$ 140 to 390 kJ mol^{-1} and a ln A value of $\approx$ 7. No fit is obtained for this range. No conclusive kinetic model fit can be found for the decomposition reaction range of $0.9 < \alpha < 1.0$. The isoconversional method gives an average activation energy varying from $\approx$ 379 to 200 kJ mol^{-1} and a ln A value of $\approx$ 11.

The kinetic models are fitted to the decomposition reaction occurring between 760 °C and 960 °C (the second mass loss curve). From figure 8.2.2.4 (d), it can be seen that this decomposition reaction does not occur

in a single-step.

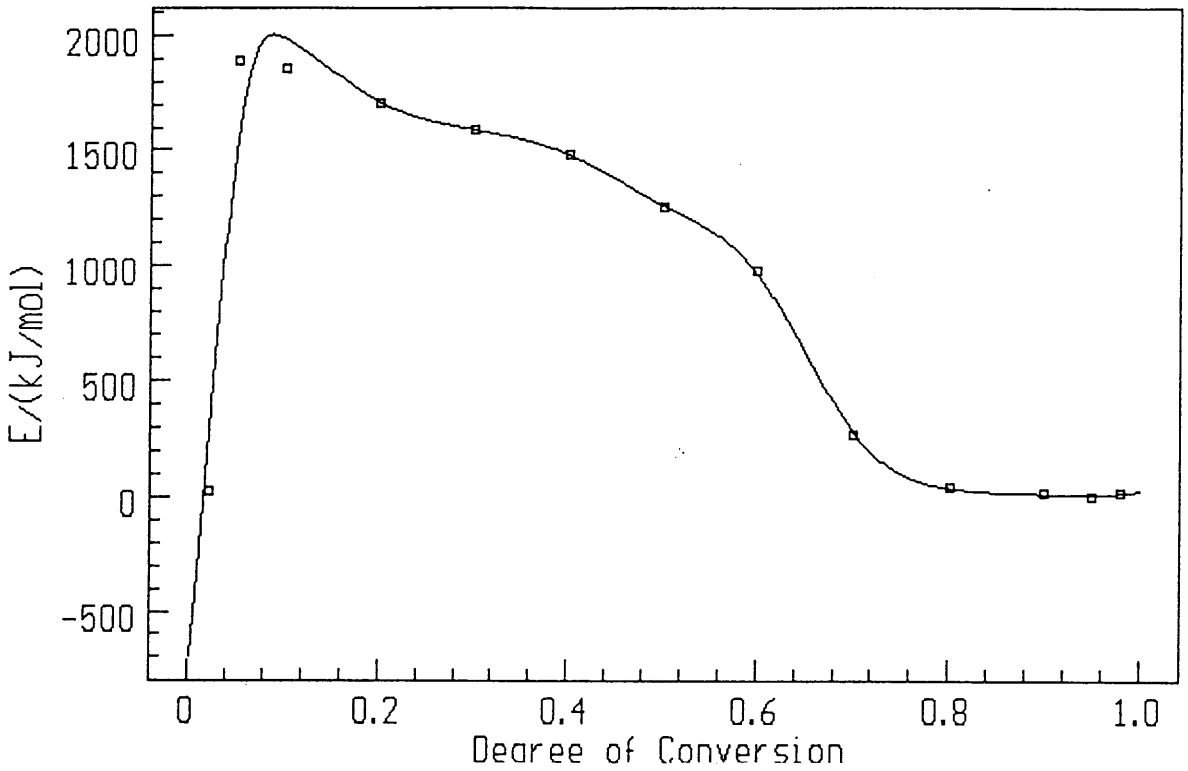

Figure 8.2.2.4 (d): Plot of activation energy vs fraction decomposed for Beestekraal limestone in a CO_2/air-atmosphere between 760 °C and 960 °C

The ascending part of the dependence of the activation energy on the degree of conversion indicates that the reaction with the higher activation energy makes an increasing contribution to the heat absorbed. On reaching the maximum of ≈ 1900 kJ mol^{-1}, the activation energy decreases, indicating that the dependence is descending as there is a decreasing contribution by the reaction with the higher activation energy [85]. The kinetic models are fitted from $0.05 < \alpha < 0.6$ and then from $0.7 < \alpha < 1.0$. The isoconversional method gives an average activation energy value of ≈ 1539 kJ mol^{-1} and a ln A value of ≈ 67. There are two models that appear to fit for $0.05 < \alpha < 0.6$. They are the first order equation and the

first order with autocatalysis. The first order gives an activation energy value of 1759 kJ mol^{-1}, a ln A value 77, a correlation coefficient of 0.9550 and a Durbin-Watson value of 0.297. The first order with autocatalysis (figure 8.2.2.4 (e)) model gives the best correlation, with the average activation energy obtained from the isoconversional method and the values of the correlation coefficient and Durbin-Watson the best. The activation energy obtained for this model is 1616 kJ mol^{-1}, a ln A value of 70, a correlation coefficient of 0.9562 and a Durbin-Watson value of 0.183. As the calcium carbonate decomposes, the nuclei of the calcium oxide are forming at the sites present and by a mechanism referred to as branching. Nucleation might occur along dislocation lines.

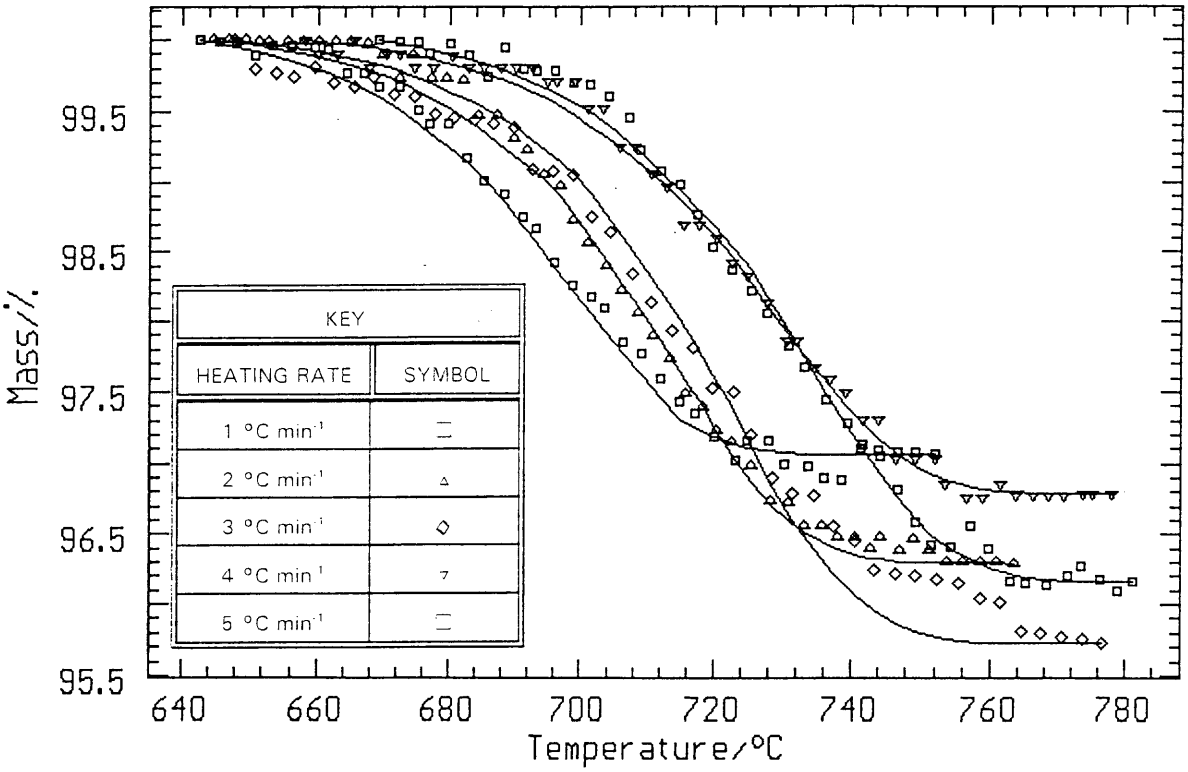

Figure 8.2.2.4 (e): Fitting of the first order with autocatalysis kinetic model for Beestekraal limestone decomposing in a CO_2/air-atmosphere between 760 °C and 960 °C for $0.05 < \alpha < 0.6$

The kinetic models which appear to describe the kinetics of the decomposition reactions occurring for $0.7 < \alpha < 1.0$, are the first order kinetic model (activation energy = 1323 kJ mol^{-1}; ln A = 57; correlation coefficient = 0.9610 and a Durbin-Watson value of 0.409), the d-dimensional Avrami-Erofe'ev model (activation energy = 1275 kJ mol^{-1}; ln A = 55; correlation coefficient = 0.9638 and a Durbin-Watson value of 0.311) and the three-dimensional diffusion equation of Jander (activation energy = 1396 kJ mol^{-1}; ln A = 60; correlation coefficient = 0.9471 and a Durbin-Watson value of 0.624). There is no conclusive fit on comparing the data from these kinetic models and that obtained from the isoconversional method (average activation energy = $\approx$ 70 kJ mol^{-1} and the ln A value = $\approx$ - 0.1 (see Chapter 9.2)). These models can be used to describe the kinetic path of the reaction but they are not a description of the mechanism of the reaction.

8.2.2.5 Kinetics of the decomposition of Beestekraal limestone to calcium oxide in a CO_2/water-atmosphere

The kinetics of the decomposition of Beestekraal limestone in a CO_2/water-atmosphere is followed between 590 °C and 785 °C and between 820 °C and 970 °C. For the first mass loss curve, the plot of activation energy versus fraction decomposed (figure 8.2.2.5(a)), shows that there are at least three steps in the decomposition reaction between 590 °C and 785 °C.

The average activation energy increases between 0 and 0.4 (from $\approx$ 45 to $\approx$ 200 kJ mol^{-1}) which implies that the reaction with the higher activation energy contributes to the heat absorbed [85]. The average activation energy remains constant at a value of $\approx$ 175 kJ mol^{-1} until α = 0.9. Thus, it can be assumed that the temperature dependence of the overall process rate is governed by one activation energy [85]. The average activation energy is a good approximation for the activation energy of the limiting reaction [85]. The ln A value is $\approx$ 6 for $0.4 < \alpha < 0.9$. For $0.9 < \alpha <$

1.0, the activation energy decreases sharply implying that the contribution made to the heat absorbed, is decreasing [85]. The maximum average activation energy was ≈175 kJ mol^{-1} and the minimum was ≈115 kJ mol^{-1}.

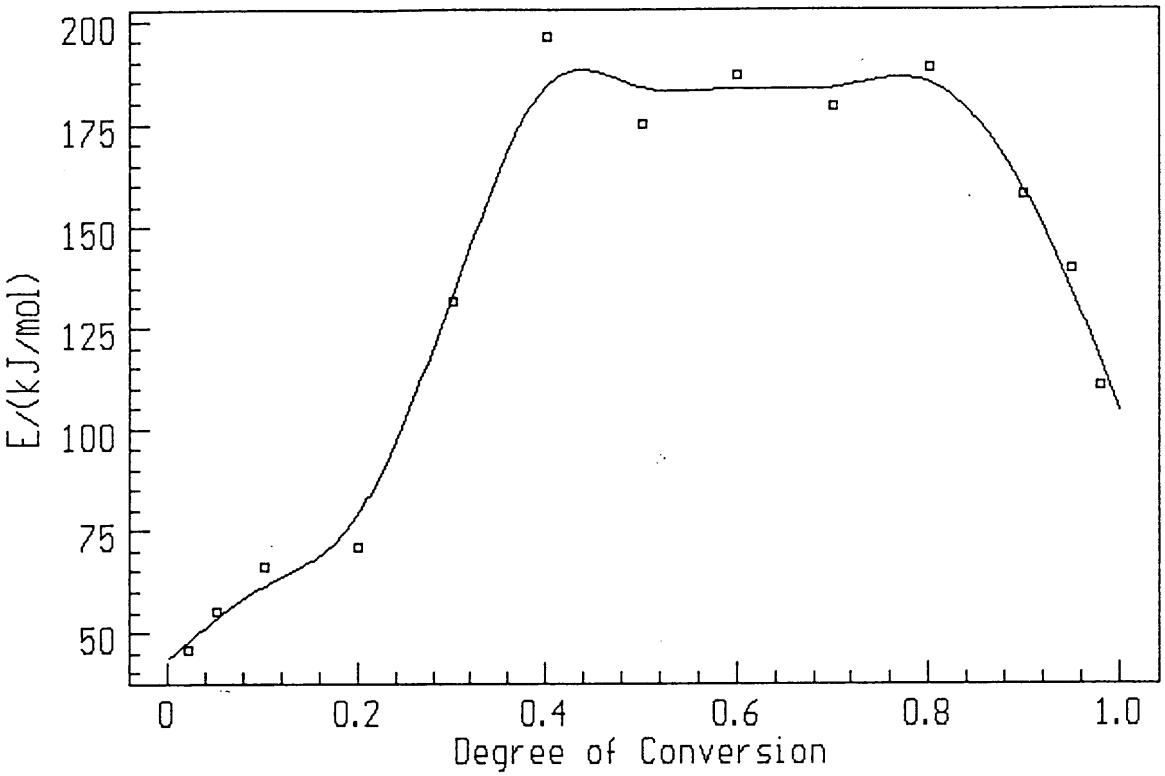

Figure 8.2.2.5 (a): Plot of activation energy vs fraction decomposed for Beestekraal limestone decomposing in a CO_2/water-atmosphere between 590 °C and 785 °C

For $0 < \alpha < 0.4$, none of the kinetic models fitted appear to fit the experimental data. The isoconversional method gave an average activation energy from ≈ 45 to ≈ 200 kJ mol^{-1} and ln A of ≈ -1 (Chapter 9.2).

The kinetic models which appear to fit for $0.4 < \alpha < 0.9$, are the second order and the first order with autocatalysis kinetic models. The isoconversional method gives an average activation energy value of ≈ 175 kJ mol^{-1} and a ln A value of ≈ 6. The second order equation has a correlation coefficient of 0.9564, a Durbin-Watson value of 0.104, an

activation energy value of 381 kJ mol^{-1} and a ln A value of 18. This is not a good fit as the activation energy and ln A values do not correspond with that obtained from the isoconversional method. The first order with autocatalysis kinetic model (figure 8.2.2.5 (b)) appears to fit the best, with an activation energy value of 211 kJ mol^{-1}, a ln A value of 8, a correlation coefficient of 0.9867 and a Durbin-Watson value of 0.278.

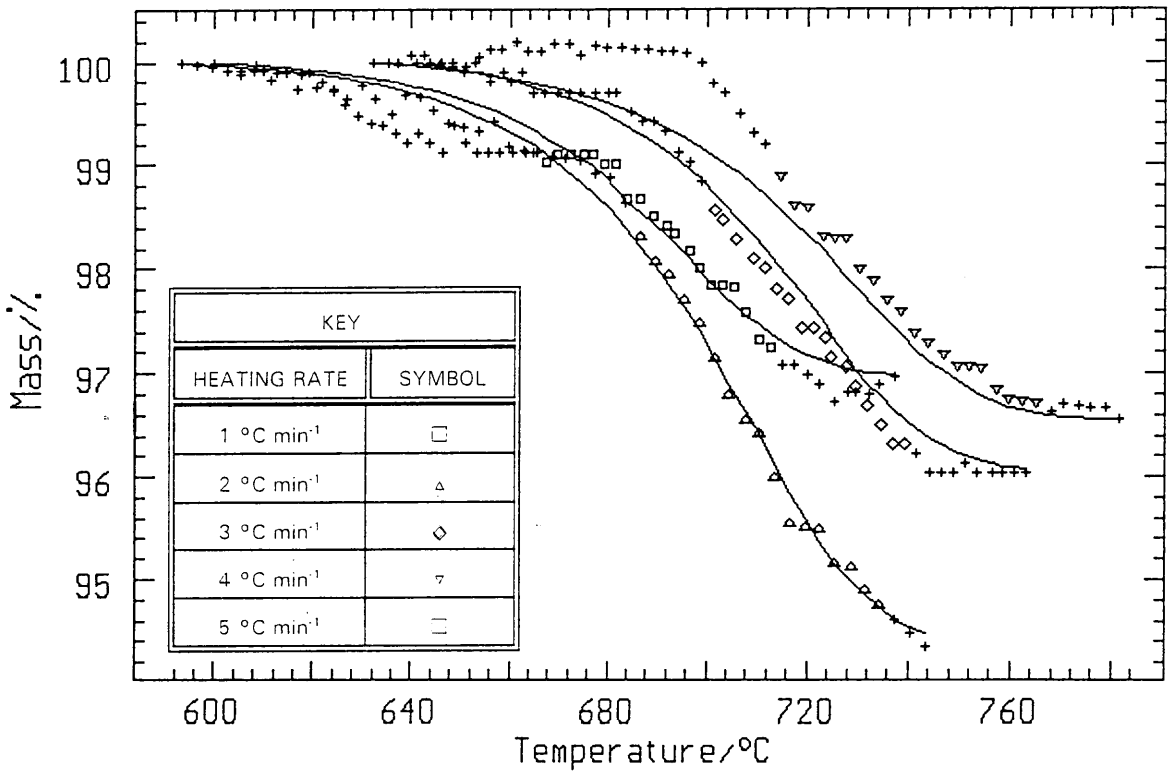

Figure 8.2.2.5 (b): Fitting of the first order with autocatalysis kinetic model for Beestekraal limestone decomposing in a CO_2/water-atmosphere between 590 °C and 785 °C for 0.4 < α < 0.9

The kinetic models are fitted for the second mass loss curve between 820 °C and 970 °C. From the graph of fraction decomposed versus activation energy, figure 8.2.2.5 (c), it is clear that it is not a single-step decomposition reaction.

The kinetic models are fitted from $0 < \alpha < 0.2$, $0.2 < \alpha < 0.6$ and $0.7 < \alpha < 1.0$. None of the kinetic models fitted satisfy the experimental data for these ranges. The data obtained from the isoconversional method gives an average activation energy of $\approx$ - 390 kJ mol^{-1} (see Chapter 9.2) and a ln A value of $\approx$ 14 for $0.2 < \alpha < 0.6$.

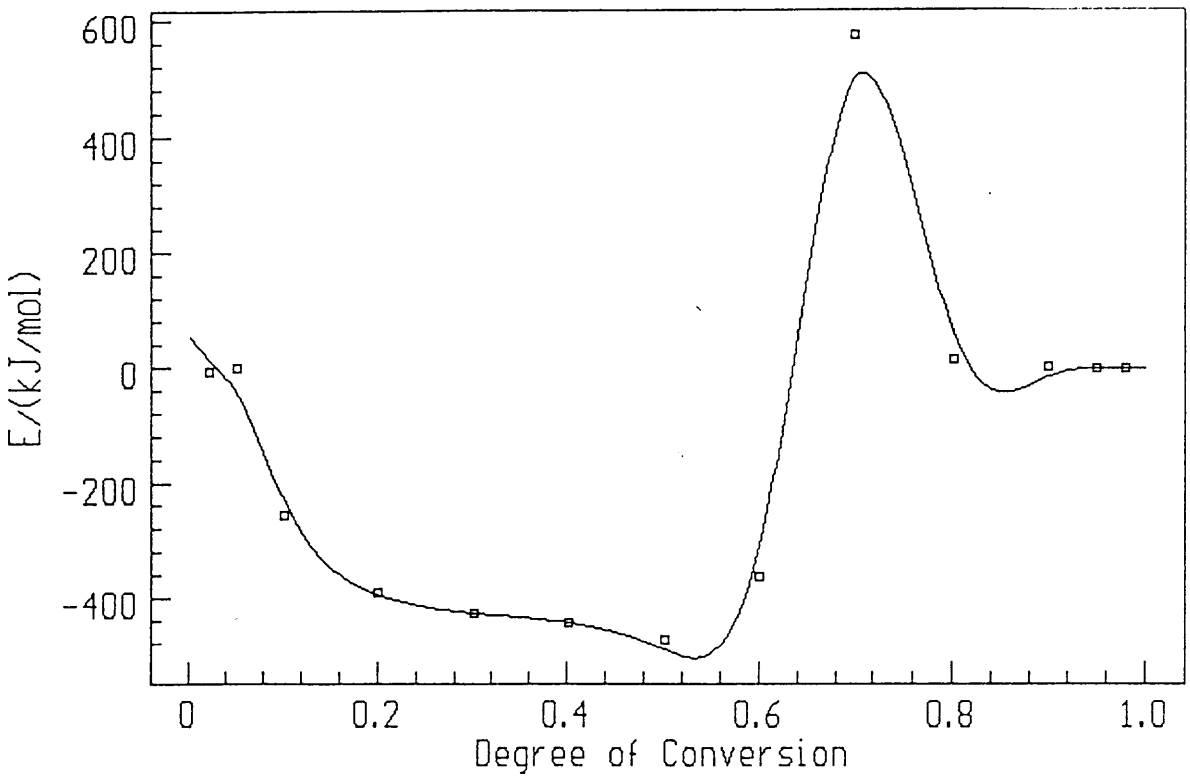

Figure 8.2.2.5 (c): Plot of activation energy vs fraction decomposed for Beestekraal limestone decomposing in a CO_2/water-atmosphere between 820 °C and 970 °C

The isoconversional method obtained an average activation energy of $\approx$ 116 kJ mol^{-1} and a ln A value of $\approx$ - 2 (see Chapter 9.2) for $0.7 < \alpha < 1.0$. Table 8.2.2.1 is a summary of all the kinetic data for the decomposition of Beestekraal limestone to calcium oxide in the different atmospheres used.

Table 8.2.2.1 **Summary of the kinetic data of the thermal decomposition of Beestekraal limestone in different atmospheres**

Atmosphere	Temperature Range (°C)	Fraction Decomposed	Kinetic Data from the Isoconversional Method		Kinetic Data from the Kinetic Models			
			E_a (kJ mol^{-1})	ln A	Kinetic Model E_a (kJ mol^{-1})	ln A	D-W	Corr. Coeff.
Air	490 - 850	$0 < \alpha < 0.1$	0 - 249	-	no fit			
		$0.1 < \alpha < 1.0$	249	10	n-th order 250	10	0.018	0.9993
Air/water	497 - 810	$0 < \alpha < 0.1$	210 - 266	-	no fit			
		$0.1 < \alpha < 0.2$	266 - 242	-	no fit			
		$0.2 < \alpha < 1.0$	242	10	Sestak-Berggren 243	10	0.080	0.9998
CO_2	605 - 780				two-dimensional phase boundary			
		$0 < \alpha < 0.95$	30 - 350	10	255	10	0.247	0.9920
	785 - 995	$0 < \alpha < 0.2$	0 - 2600	-	no fit			
		$0.2 < \alpha < 0.5$	2300	81	second order 2679	116	0.202	0.9731
		$0.6 < \alpha < 1.0$	0	0	no fit			
CO_2/air	640 - 755	$0 < \alpha < 0.2$	140 - 390	7	no fit			
		$0.2 < \alpha < 0.8$	379	17	n-th order 380	17	0.796	0.9933
					first order 380	17	0.795	0.9933
		$0.9 < \alpha < 1.0$	379 - 200	11	no fit			
	760 - 960				first order with autocatalysis			
		$0.05 < \alpha < 0.6$	1539	67	1616	70	0.183	0.9562
		$0.7 < \alpha < 1.0$	70	-0.1	no fit			
CO_2/water	590 - 785	$0 < \alpha < 0.4$	45 - 200	-1	no fit			
		$0.4 < \alpha < 0.9$	175	6	first order with autocatalysis 211	8	0.278	0.9867
		$0.9 < \alpha < 1.0$	175 - 115	6	no fit			
	820 - 970	$0 < \alpha < 0.2$	0 - (-390)	-	no fit			
		$0.2 < \alpha < 0.6$	-390	14	no fit			
		$0.7 < \alpha < 1.0$	116	-2	no fit			

Key of abbreviations used in the table: E_a = activation energy; D-W = Durbin-Watson value and Corr. Coeff. = correlation coefficient.

8.2.3 Pienaars River Limestone

A faster rate of mass loss is also observed for Pienaars River limestone in the CO_2-atmosphere than in the air-atmosphere. The decomposition in an air-atmosphere (figure 8.2.3 (a)) shows two mass losses, the first mass loss starts at 52 °C and the second mass loss starts at 624 °C.

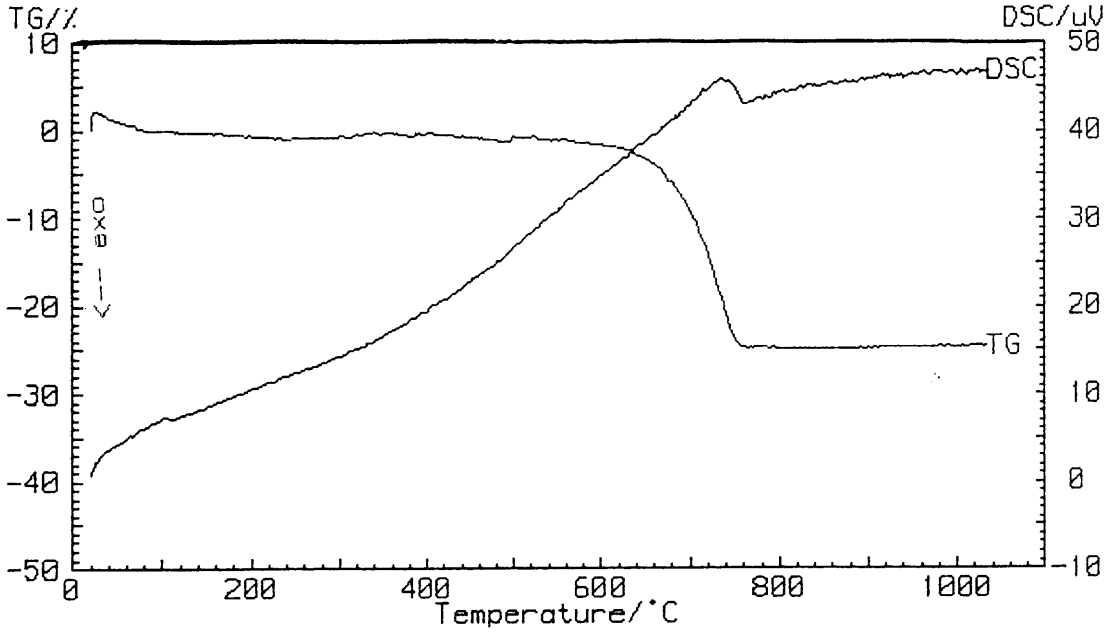

Figure 8.2.3(a): TG and DSC curves for the decomposition of Pienaars River limestone decomposing in an air-atmosphere using a heating rate of 5 °C min^{-1}

The first mass loss is due to the dehydration of adsorbed water. The second mass loss between 624 °C and 810 °C, is due to the decomposition of the calcium carbonate. The 23 % mass loss obtained for Pienaars River limestone in an air-atmosphere between 624 °C and 810 °C, indicates that approximately 53 % of the sample is calcium carbonate. This percentage mass loss is much lower than obtained for the pure calcium carbonate (44 %) and for the Beestekraal limestone samples (41 %).

In the CO_2-atmosphere, the Pienaars River limestone has three mass losses. The first mass loss between 72 °C and 338 °C, is due to the dehydration of adsorbed water. The second mass loss curve between 642 and 840 °C (10 %), can be due to the decomposition of the dolomite (calcium

magnesium carbonate), present as an impurity (Chapter 7.2), to its oxides. The theoretical percentage mass loss of dolomite decomposing to magnesium oxide and calcium oxide is 44.81 %. The experimental mass loss value obtained of 10 % indicates that approximately 22 % of the sample is dolomite. The third mass loss between 840 °C and 1056 °C, can be attributed to the decomposition of calcium carbonate to calcium oxide. The percentage mass loss of approximately 20 % in CO_2-atmosphere between 840 °C and 1056 °C is a better reflection of the decomposition reaction taking place as the reactions tend to overlap in an air-atmosphere and were not separated as is the case in the CO_2-atmosphere. The calculated percentage calcium carbonate present in Pienaars River limestone using the third mass loss of 20 % obtained in the CO_2-atmosphere, is ≈ 46 %. Figure 8.2.3(b) is the TG of Pienaars River limestone decomposing in the CO_2-atmosphere. There is also a gain in mass at approximately 540 °C to 640 °C of ≈ 2 %. This could possibly be due to CaO present as an impurity, reacting with the CO_2 present, to form calcium carbonate. However, no CaO was found to be present in the XRD analyses. The XRD analyses could, however, be relatively insensitive to trace quantities of impurity present.

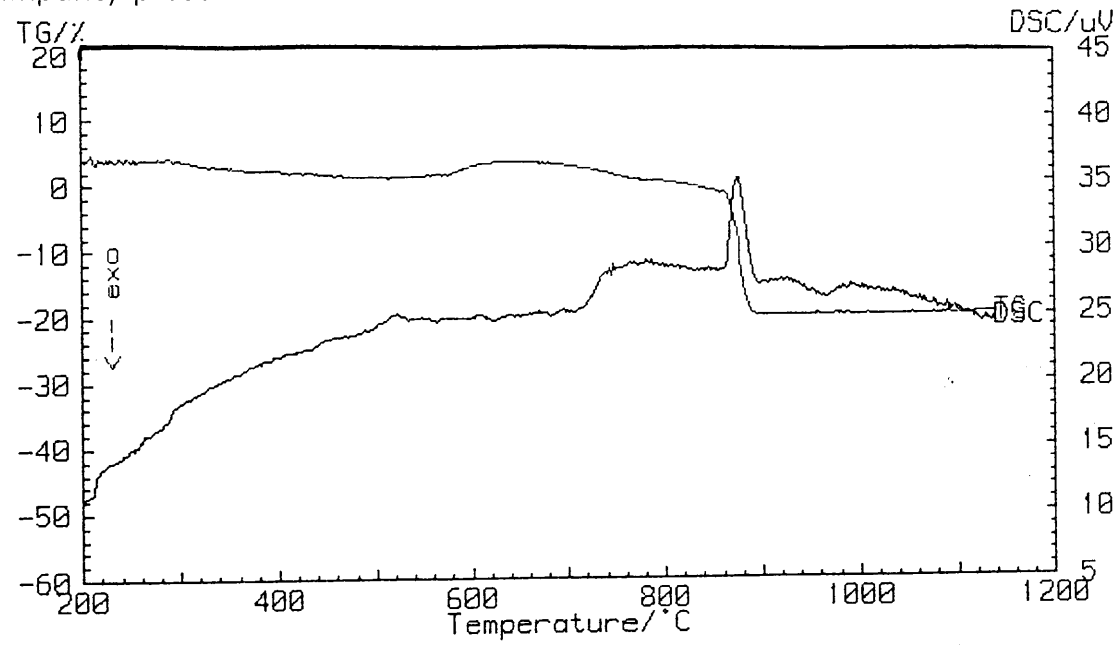

Figure 8.2.3(b): TG and DSC curves of the decomposition of Pienaars River limestone decomposing in a CO_2-atmosphere using a heating rate of 5 °C min^{-1}

In CO_2/water- and CO_2/air-atmospheres, there are only two mass loss curves observed (figure 8.2.3 (c) and (d) respectively). The first mass loss curve is due to the loss of adsorbed water. The second mass loss curve is due to the calcium carbonate decomposing to calcium oxide.

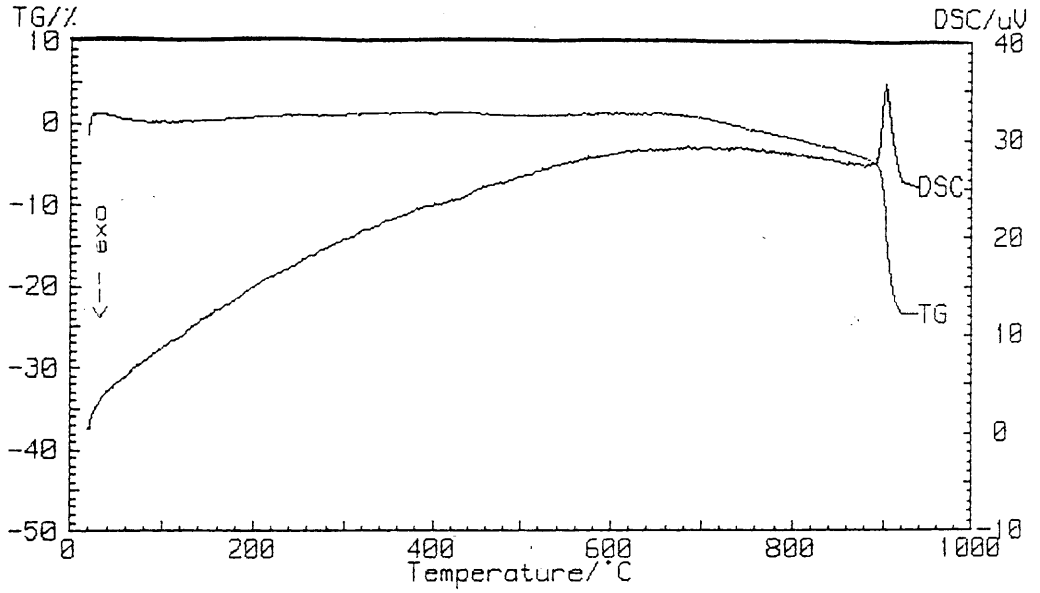

Figure 8.2.3 (c): **TG and DSC curves of the decomposition of Pienaars River limestone decomposing in a CO_2/water-atmosphere using a heating rate of 5 °C min^{-1}**

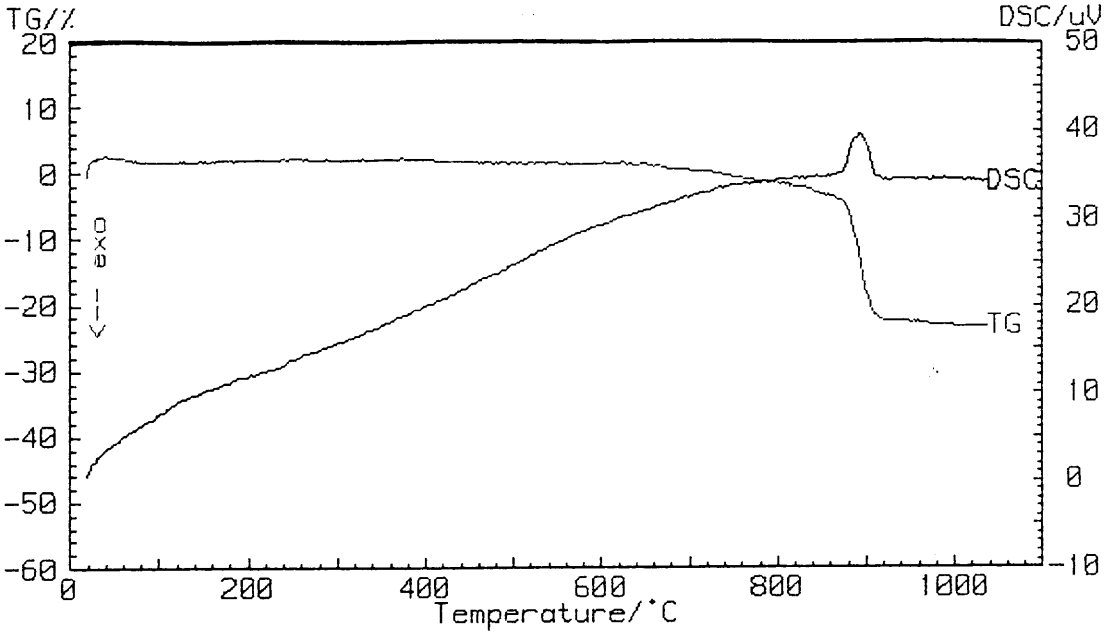

Figure 8.2.3 (d): **TG and DSC curves of the decomposition of Pienaars River limestone decomposing in a CO_2/air-atmosphere using a heating rate of 5 °C min^{-1}**

In the CO_2/water-atmosphere, there is a slight mass gain between 67 °C and 398 °C of 1%. This can possibly be due to CaO present as an impurity reacting with the water present to form calcium hydroxide. But this mass gain is not observed in the air/water-atmosphere. Also, no calcium oxide was observed in the XRD analysis of the sample. This could be due to the relative insensitivity of the XRD analysis on trace quantities of impurity present. Figure 8.2.3 (e) is the thermogram of Pienaars River limestone decomposing in an air/water-atmosphere.

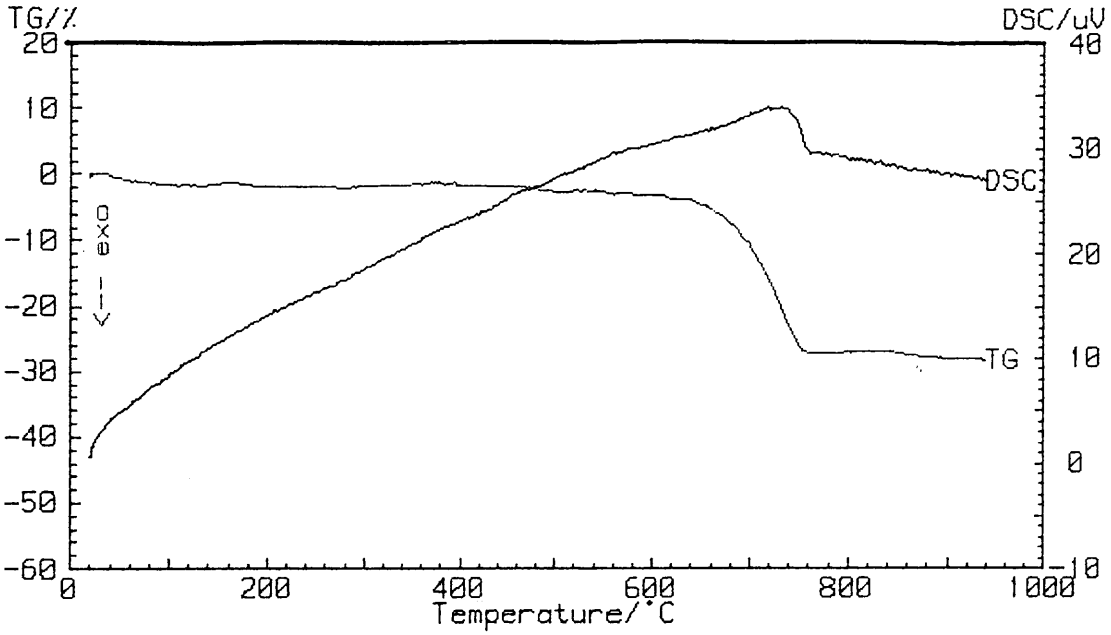

Figure 8.2.3 (e): TG and DSC curves of the decomposition of Pienaars River limestone decomposing in air/water-atmosphere using a heating rate of 5 °C min^{-1}

Table 8.2.3 shows the thermal decomposition of Pienaars River limestone in different atmospheres.

Table 8.2.3 The thermal decomposition of Pienaars River limestone in different atmospheres using a heating rate of 5 °C min^{-1} with sample masses between 5 - 15 mg

Atmosphere	Temperature Range (°C)	Mass Loss (%)	Mass Gain (%)	ΔH (kJ g^{-1}) x 10^{-1}
Air	51 - 623 623 - 830	5 23	- -	- 3
Air/H_2O	25 - 570 570 - 836	7 25	- -	- -
CO_2	72 - 338 540 - 640 642 - 840 840 - 1056	1 2 10 20	- - - -	- - 4 -
CO_2/Air	658 - 836 836 - 960	8 19	- -	- 4
CO_2/H_2O	67 - 398 400 - 885 886 - 936	- 9 18	1 - -	- - 3

The heat of decomposition for the Pienaars River limestone (3.0 x 10^{-1} kJ g^{-1}) in an air-atmosphere is lower than the heat of decomposition obtained for the pure calcium carbonate (2.0 kJ g^{-1}) sample. The reason being that the presence of the impurities, influences the value obtained for Pienaars River limestone and the sample is only about 50 % calcium carbonate. The heat of decomposition obtained in the CO_2- and the CO_2/air-atmosphere, is slightly higher (0.4 kJ g^{-1}) than that obtained in an air- and a CO_2/water-atmosphere (0.3 kJ g^{-1}).

8.2.3.1 Kinetics of the decomposition of Pienaars River limestone to calcium oxide in an air-atmosphere

Figure 8.2.3.1 (a) shows a plot of activation energy versus α (fraction decomposed) for the decomposition reactions between 624 °C and 810 °C in an air-atmosphere.

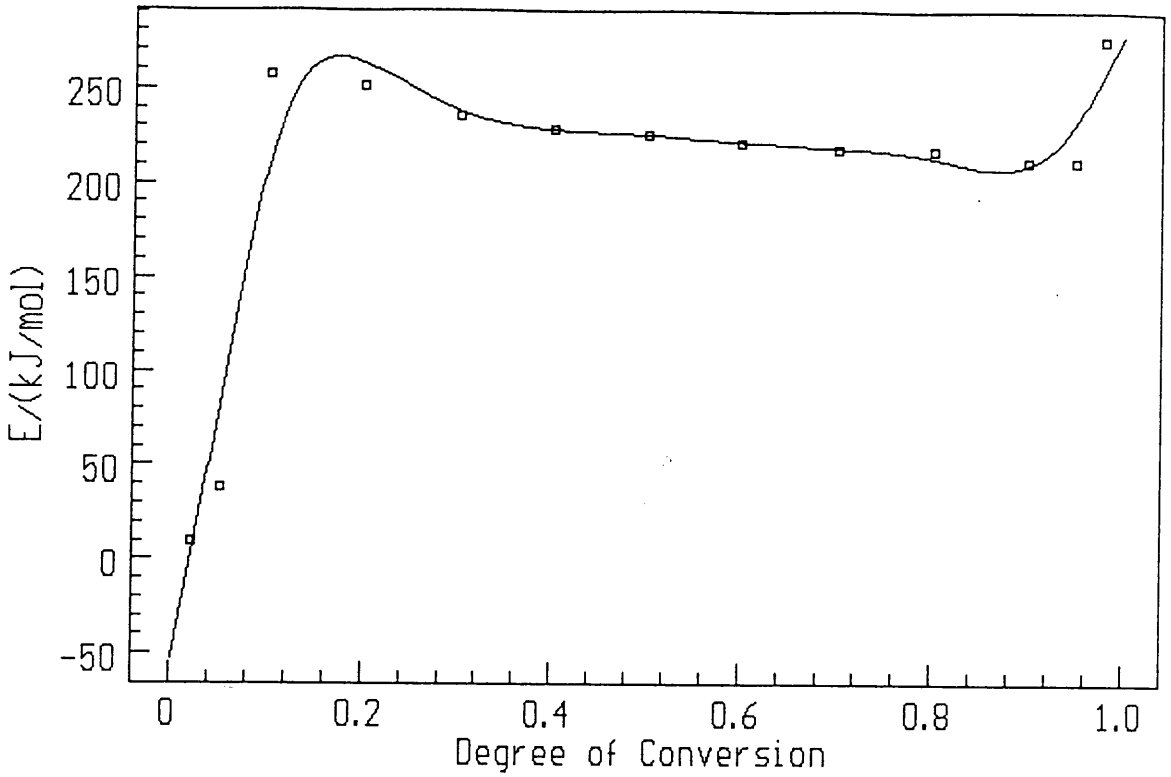

Figure 8.2.3.1 (a): Plot of activation energy vs α for Pienaars River limestone decomposing to calcium oxide in an air-atmosphere

It is clear that the decarbonation reaction does not occur in a single step. The activation energy increases sharply from $0 < \alpha < 0.2$, from $\approx$ 10 to $\approx$ 250 kJ mol^{-1} (ln A = $\approx$ - 4 (see Chapter 9.2)), indicating that the reaction with the higher activation energy makes an increasing contribution to the heat absorbed. The activation energy remains constant at a value of $\approx$ 233 kJ mol^{-1} until α = 0.95. No kinetic models appear to fit the range $0 < \alpha < 0.2$.

For the range, $0.2 < \alpha < 0.95$, there are four kinetic models which appear to fit. The n-th order kinetic model gives an activation energy of 226 kJ mol^{-1}, a ln A value of 9, a correlation coefficient of 0.9973 and a Durbin-Watson value of 0.028. The two-dimensional phase boundary equation

gives an activation energy of 227 kJ mol^{-1}, a ln A value of 9, a correlation coefficient of 0.9973 and a Durbin-Watson value of 0.019. The Sestak-Berggren equation gives an activation energy of 228 kJ mol^{-1}, a ln A value of 9, a correlation coefficient of 0.9974 and a Durbin-Watson value of 0.030. The first order with autocatalysis equation gives an activation energy of 228 kJ mol^{-1}, a ln A value of 9, a correlation coefficient of 0.9965 and a Durbin-Watson value of 0.034. The Sestak-Berggren and the first order with autocatalysis kinetic models appear to give the best mathematical description of the experimental data. The values obtained from these two models compare well with the average activation energy value of ≈ 233 kJ mol^{-1} obtained using the isoconversional method and the ln A value of ≈ 10. Figure 8.2.3.1 (b) is the first order with autocatalysis kinetic model fit and Figure 8.2.3.1 (c) is the Sestak-Berggren kinetic model fit. Thus, there is no conclusive fit.

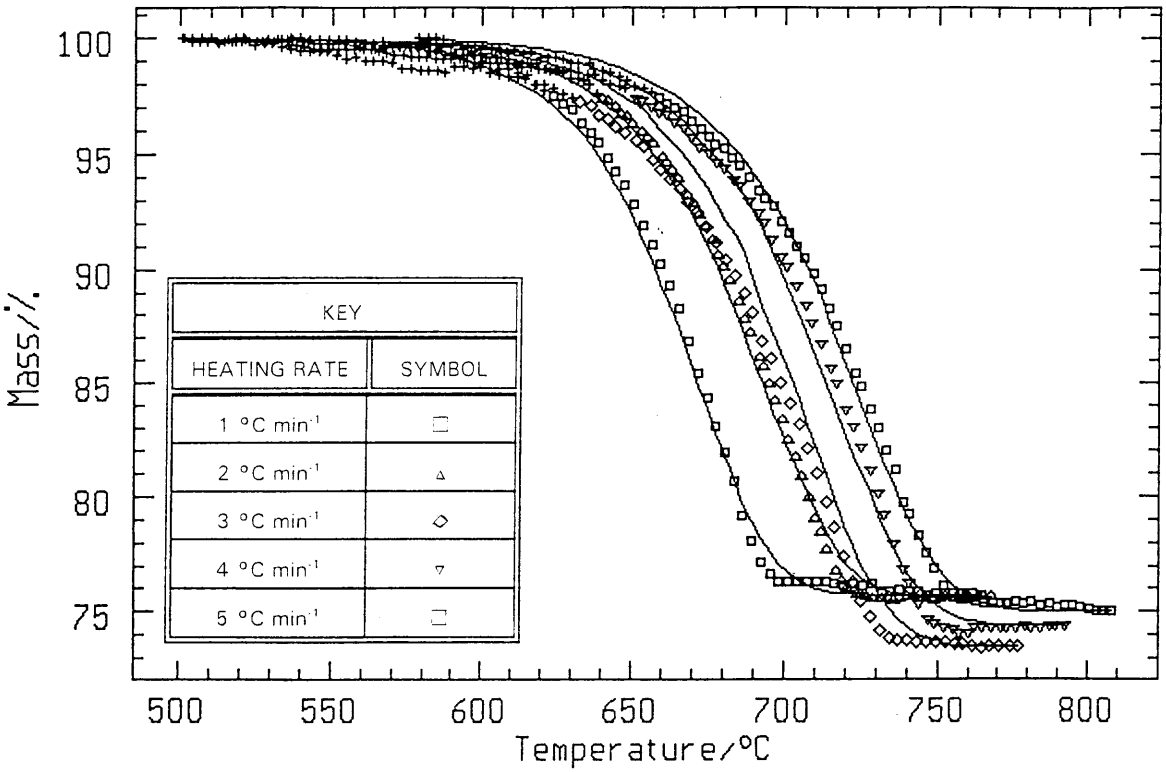

Figure 8.2.3.1 (b): Fitting of experimental data of Pienaars River limestone with the kinetic model for the first order with autocatalysis decomposition reaction in an air-atmosphere

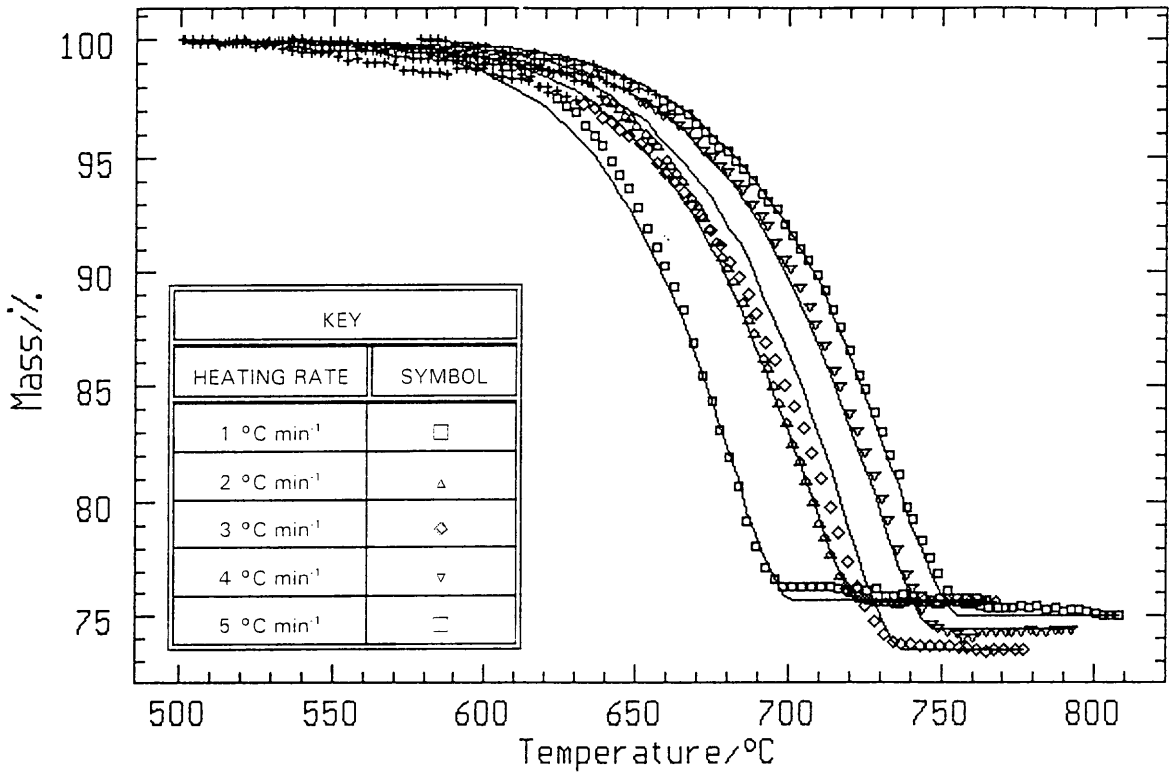

Figure 8.2.3.1 (c): Fitting of experimental data of Pienaars River limestone with the kinetic model for a Sestak-Berggren decomposition reaction in an air-atmosphere

8.2.3.2 Kinetics of the decomposition of Pienaars River limestone to calcium oxide in an air/water-atmosphere

Figure 8.2.3.2 (a) shows a plot of activation energy, E_a, versus the fraction decomposed between 400 °C and 790 °C. The kinetic models are fitted over the range, $0 < \alpha < 0.2$, $0.2 < \alpha < 0.3$ and $0.3 < \alpha < 0.95$. The isoconversional method gives an average activation energy value of $\approx$ 45 kJ mol^{-1} and a ln A value of $\approx$ 2 for the range $0 < \alpha < 0.2$. No kinetic model is found to fit the experimental data conclusively for this range.

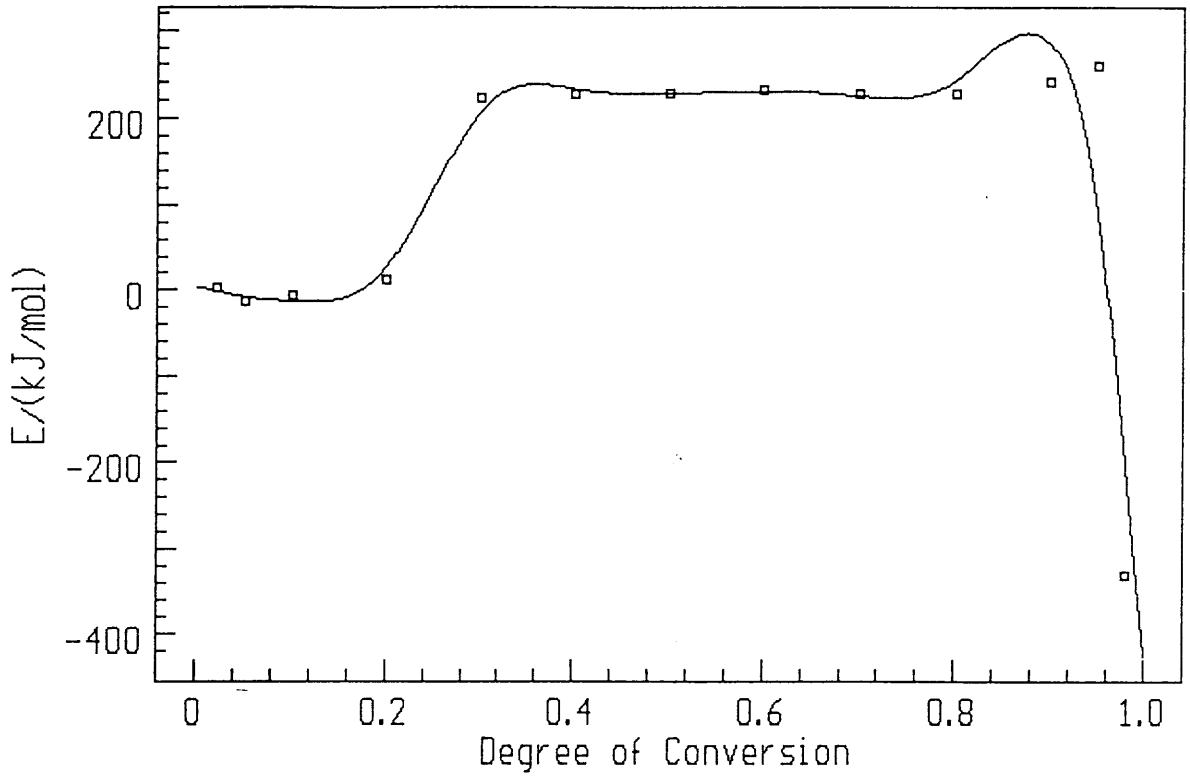

Figure 8.2.3.2 (a): Plot of activation energy, E_a, vs α for Pienaars River limestone decomposing in an air/water-atmosphere

The activation energy does not appear to depend on the degree of conversion up to $\alpha = 0.2$. Thus, the rate can be described by a single-step reaction [88]. The activation energy then increases from $\approx$ 45 to $\approx$ 236 kJ mol^{-1} between $0.2 < \alpha < 0.3$. No kinetic models appear to fit the experimental data conclusively for this range.

For the range $0.3 < \alpha < 0.95$, the isoconversional method obtained an average activation energy of $\approx$ 236 kJ mol^{-1} and a ln A value of $\approx$ 10. The one-dimensional diffusion equation (figure 8.2.3.2 (b)) gives an activation energy of 246 kJ mol^{-1} and a ln A of 10. (The correlation coefficient is 0.9763 and the Durbin-Watson value is 0.044). An activation energy of 320 kJ mol^{-1} and a ln A of 13 is obtained for the three-dimensional diffusion equation of Jander - figure 8.2.3.2 (c). The correlation coefficient is 0.9801 and the Durbin-Watson value is 0.126.

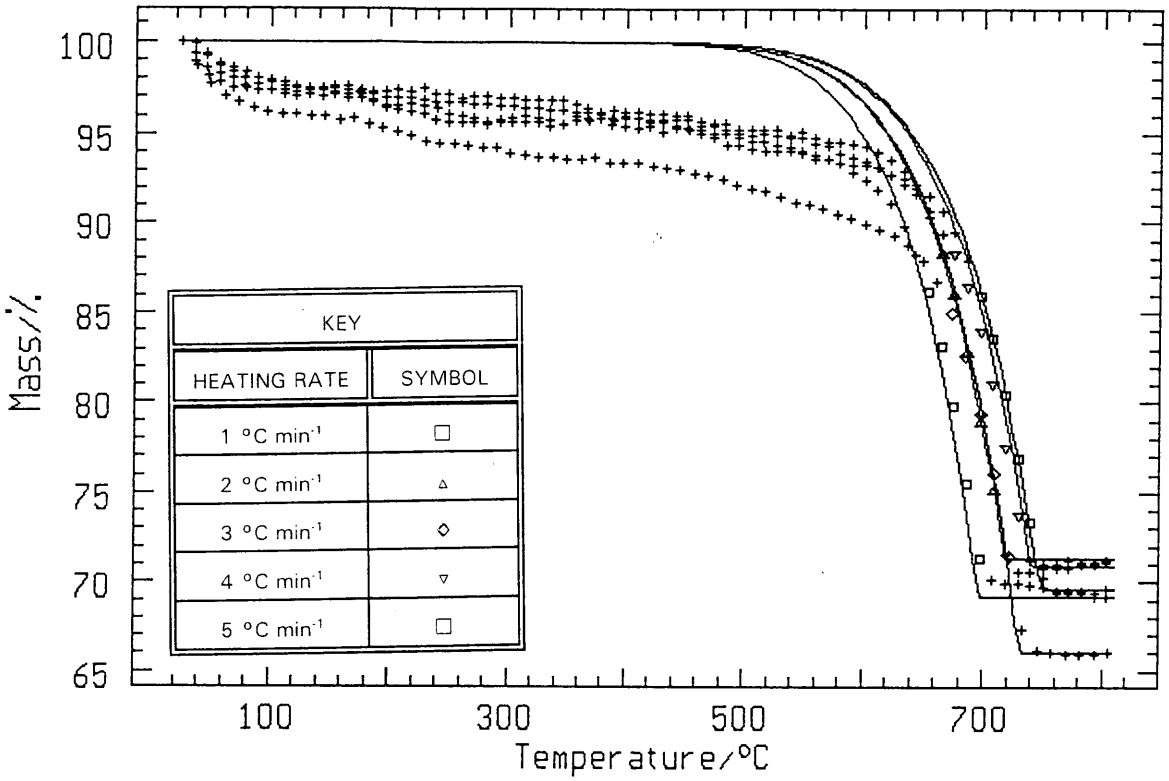

Figure 8.2.3.2 (b): The one-dimensional diffusion kinetic model fitted to the experimental data of Pienaars River limestone decomposing in an air/water-atmosphere

The three-dimensional diffusion equation of Jander appears to have the better correlation coefficient but the one-dimensional diffusion equation appears to be a more conclusive fit when comparing the activation energy values obtained from the isoconversional method (which is not kinetic model dependent) and that obtained from the one-dimensional diffusion equation. One-dimensional diffusion describes the decomposition reaction in terms of mass transfer and diffusion in the calcium carbonate, as well as the diffusion through the CaO layer.

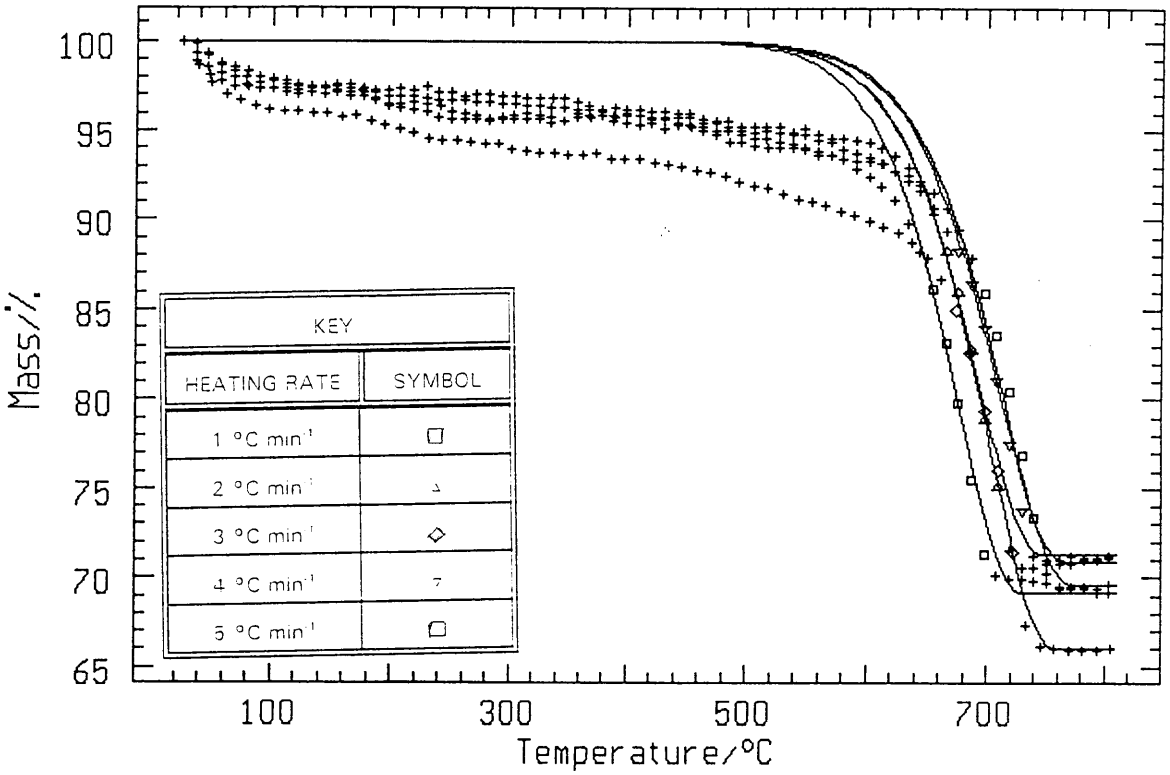

Figure 8.2.3.2 (c): The three-dimensional diffusion equation of Jander fitted to the experimental data of Pienaars River limestone decomposing in an air/water-atmosphere

8.2.3.3 Kinetics of the decomposition of Pienaars River limestone to calcium oxide in a CO_2-atmosphere

Figure 8.2.3.3 (a) is a plot of activation energy versus fraction for Pienaars River limestone decomposing between 680 °C and 960 °C in CO_2-atmosphere. From figure 8.2.3.3 (a), the kinetic models are fitted for the ranges: 0 to 0.2, 0.3 to 0.8, 0.8 to 0.9 and then for 0.9 to 1.0. The activation energy does not appear to be dependent on the degree of conversion initially up to $\alpha = 0.2$. The activation energy then increases gradually up to $\approx$ 260 kJ mol^{-1} for $\alpha = 0.8$. The activation energy increases from $\approx$ 260 to 700 kJ mol^{-1} for $0.8 < \alpha < 0.9$ after which the activation energy decreases from $\approx$ 700 to 20 kJ mol^{-1} for $0.9 < \alpha < 1.0$.

For the range $0 < \alpha < 0.2$, no kinetic models were found to fit. The isoconversional method obtained an average activation energy value of $\approx$ - 23 kJ mol^{-1} (see Chapter 9.2) and a ln A value of $\approx$ 4. For $0.3 < \alpha < 0.8$, no kinetic models were found to fit. The isoconversional method gives an average activation energy value of $\approx$ 163 kJ mol^{-1} and a ln A of $\approx$ 4.

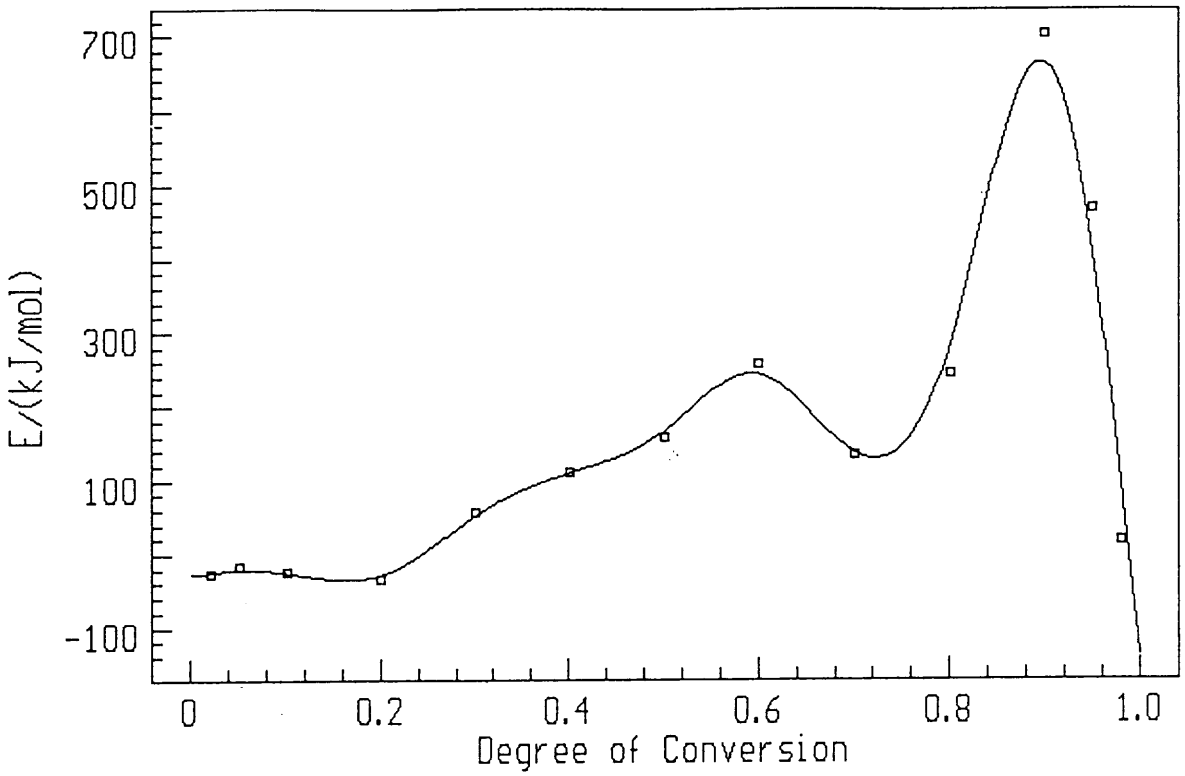

Figure 8.2.3.3 (a): Plot of activation energy vs fraction decomposed for Pienaars River limestone decomposing in a CO_2-atmosphere

For $0.9 < \alpha < 1.0$, no kinetic model was found to fit. The isoconversional method gives an average activation energy from $\approx$ 700 to 20 kJ mol^{-1}. The reaction is far more complex and can not be described by consecutive reactions.

8.2.3.4 Kinetics of the decomposition of Pienaars River limestone to calcium oxide in a CO_2/air-atmosphere

The kinetic models are fitted to the kinetic data obtained for Pienaars River limestone decomposing between 590 °C and 950 °C in a CO_2/air-atmosphere for the ranges, $0 < \alpha < 0.2$, $0.2 < \alpha < 0.4$ and $0.4 < \alpha < 1.0$. The plot of activation energy versus fraction decomposed can be followed in figure 8.2.3.4 (a).

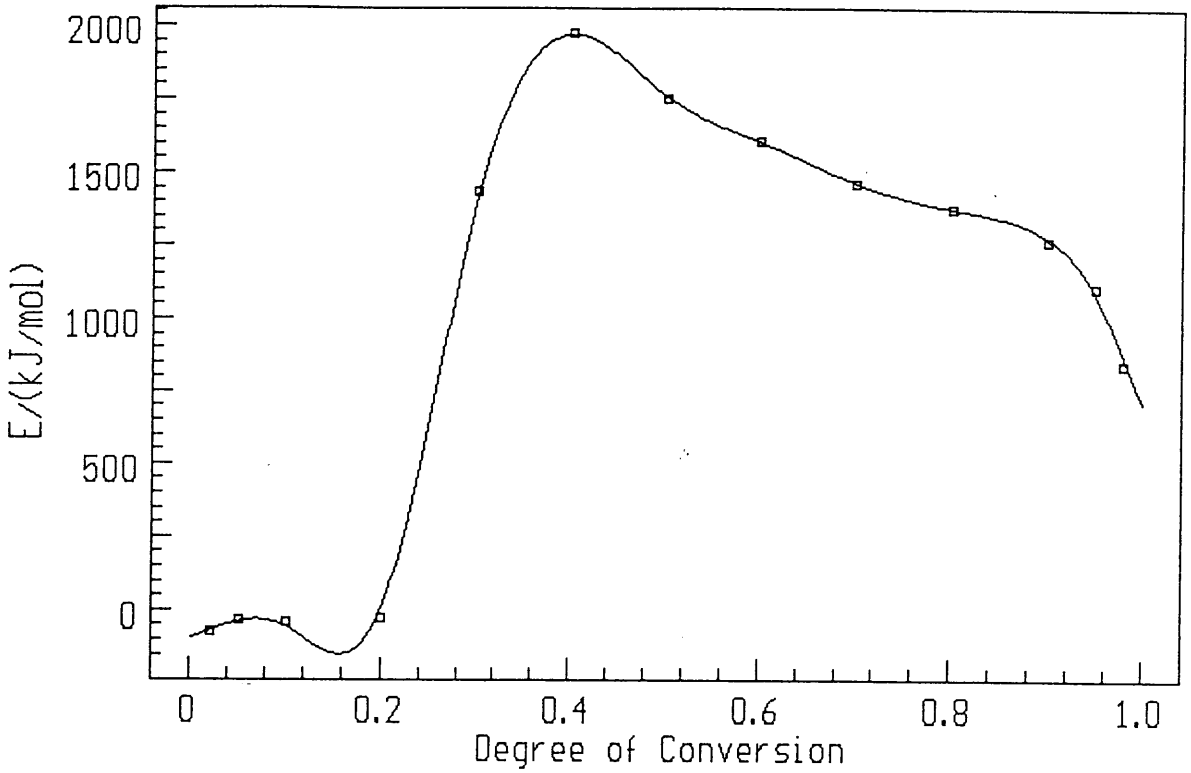

Figure 8.2.3.4 (a): Plot of E_a vs α for Pienaars River limestone decomposing in a CO_2/air-atmosphere

For $0 < \alpha < 0.2$, the activation energy does not appear to depend on the degree of conversion. The kinetic models which appear to fit the experimental data are the Sestak-Berggren equation (activation energy = 1458 kJ mol^{-1}; ln A = 72; correlation coefficient = 0.9628 and a Durbin-Watson value of 0.032) and the n-th order equation (activation energy = 1106 kJ mol^{-1}; ln A = 57; correlation coefficient = 0.9598 and a Durbin-Watson value of 0.031). These fits are non-conclusive as the average activation energy is ≈ - 40 kJ mol^{-1} and ln A value is ≈ -3 (see Chapter 9.2)

as obtained from the isoconversional method.

The activation energy increases sharply from ≈ - 40 to ≈ 2000 kJ mol^{-1} for $0.2 < \alpha < 0.4$. The reaction with the higher activation energy makes a significant increasing contribution to the heat absorbed [85]. No kinetic models appear to fit the experimental data for this range.

The decomposition reaction for $0.4 < \alpha < 1.0$ can be best described by the three-dimensional diffusion equation of Jander and the three-dimensional diffusion equation of Ginstling-Brounshtein. The three-dimensional diffusion equation of Jander (figure 8.2.3.4 (b)) gives a correlation coefficient of 0.9940, a Durbin-Watson value of 0.132 and an activation energy value of 1704 kJ mol^{-1} and ln A of 73.

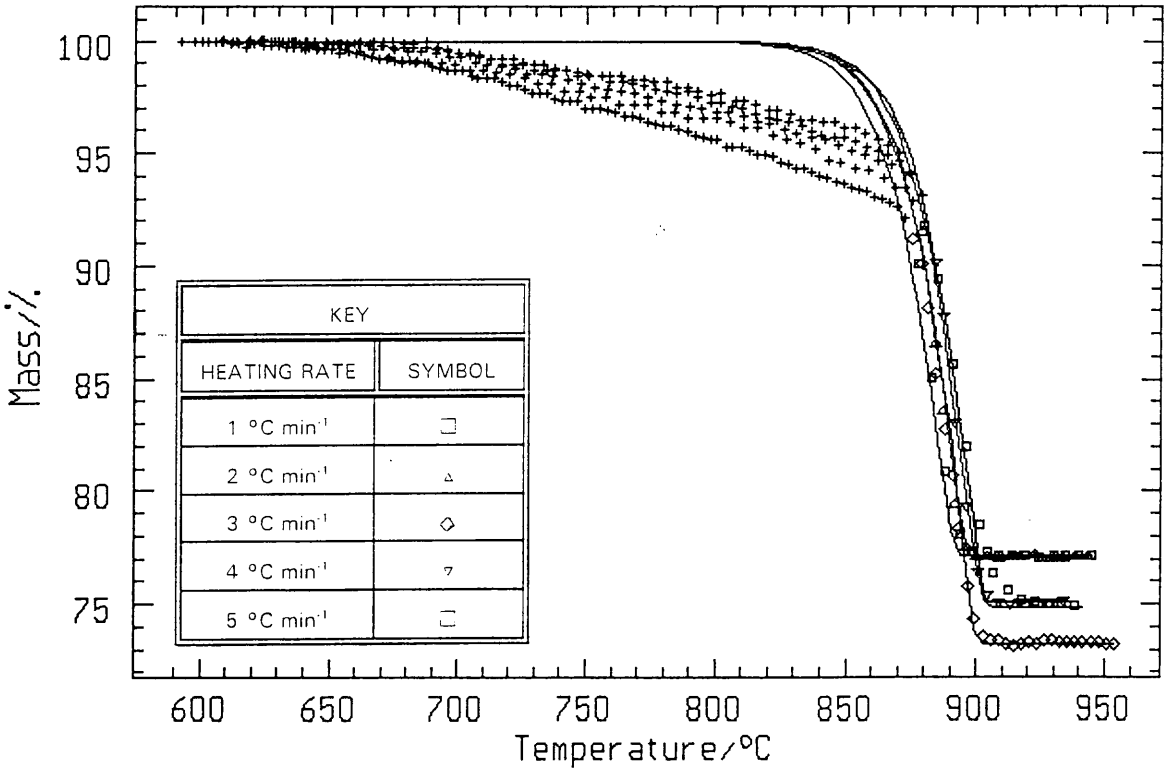

Figure 8.2.3.4 (b): Fitting of the kinetic data of Pienaars River limestone decomposing in a CO_2/air-atmosphere with the three-dimensional diffusion equation of Jander for $0.4 < \alpha < 1.0$

This does not compare well with the average activation energy value of ≈ 1426 kJ mol^{-1} and ln A value of ≈ 62, obtained from the isoconversional method. This model describes the kinetic path but not the mechanism.

The activation energy obtained from the three-dimensional diffusion equation of Ginstling-Brounshtein (figure 8.2.3.4 (c)), is 1520 kJ mol^{-1} with a ln A of 65, a correlation coefficient of 0.9934 and a Durbin-Watson value of 0.167.

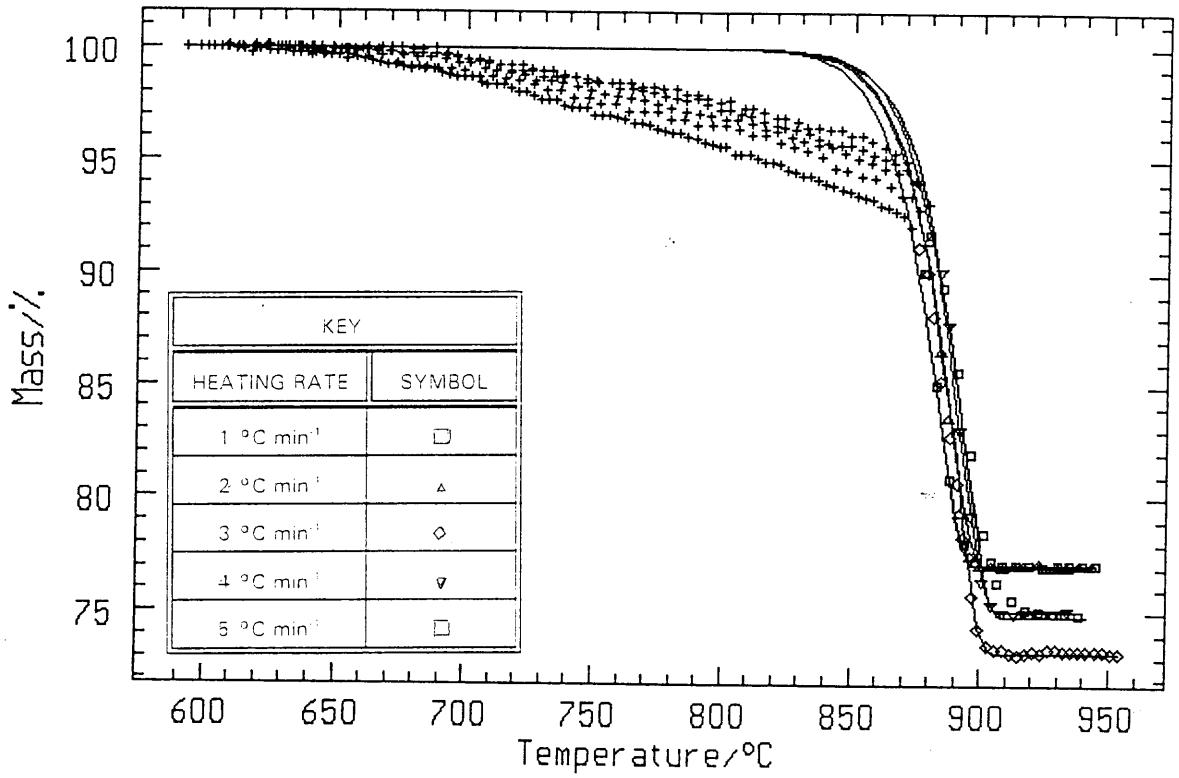

Figure 8.2.3.4 (c): Fitting of the three-dimensional diffusion equation of Ginstling-Brounshtein for Pienaars River limestone decomposing in a CO_2/air-atmosphere for 0.3 < α < 1.0

The activation energy values obtained from the three-dimensional diffusion equation of Ginstling-Brounshtein also did not compare well to those obtained from the isoconversional method. The three-dimensional diffusion equation of Jander, however, has the better correlation coefficient and Durbin-Watson value. The plot of the activation energy versus fraction decomposed for 0.4 < α < 1.0, appears to have the form expected for

diffusion reactions but the activation energy values are too large to suggest such diffusion reactions [89]. There is no conclusive fit.

8.2.3.5 Kinetics of the decomposition of Pienaars River limestone to calcium oxide in a CO_2/water-atmosphere

The kinetic models were applied for Pienaars River limestone decomposing in a CO_2/water-atmosphere between 680 °C and 950 °C. From figure 8.2.3.5 (a), it is clear that the decomposition reaction does not occur in a single step. The activation energy does not appear to be dependent on the degree of conversion initially but from $0.3 < \alpha < 0.9$, the activation energy increases showing an increased contribution to the reaction of the process with the higher activation energy [85]. The activation energy then decreases from $\approx$ 1000 kJ mol^{-1} to $\approx$ 50 kJ mol^{-1}.

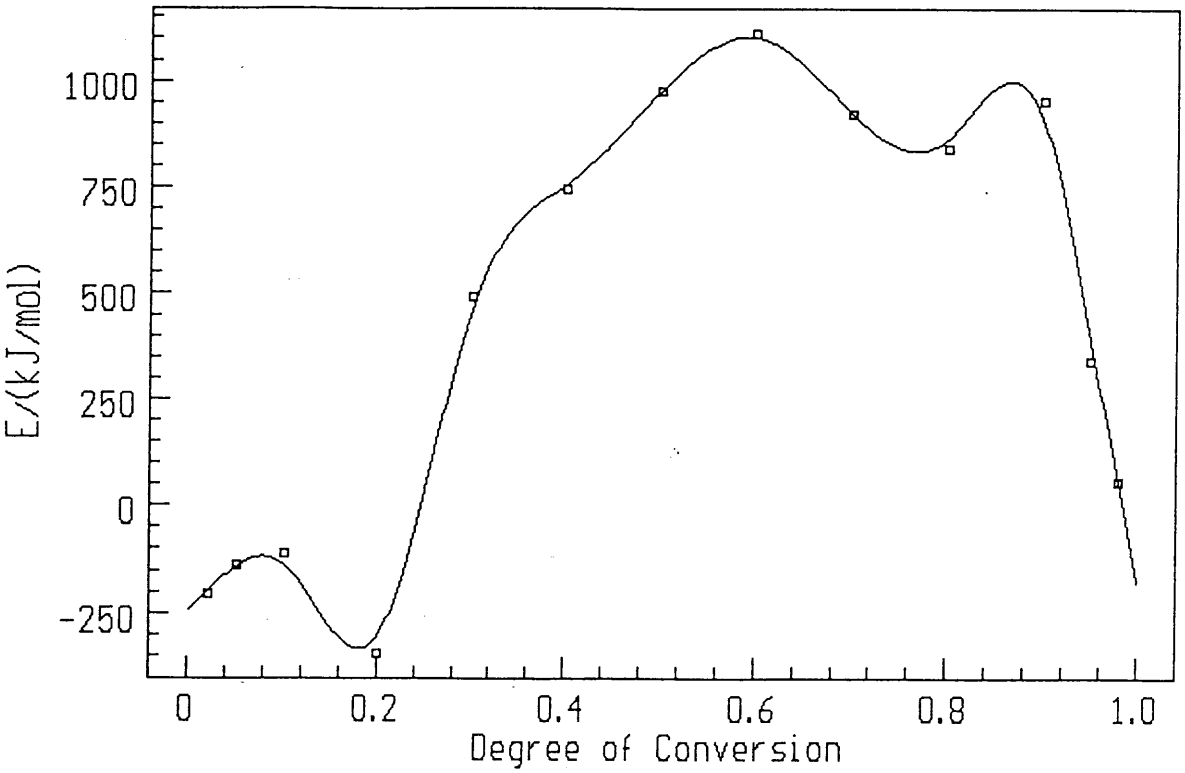

Figure 8.2.3.5 (a): Plot of activation energy vs fraction decomposed for Pienaars River limestone decomposing in a CO_2/water-atmosphere

For $0 < \alpha < 0.2$, no kinetic model fits the experimental data. The isoconversional method gives an average activation energy of $\approx$ -199 kJ mol^{-1} (see Chapter 9.2) and ln A of $\approx$ 5.

For $0.2 < \alpha < 0.9$, no kinetic model is found to fit the experimental data. The isoconversional method gives an average activation energy of $\approx$ 800 kJ mol^{-1} and ln A of $\approx$ 33.

Table 8.2.3.1 is a summary of all the kinetic data for the decomposition of Pienaars River limestone to calcium oxide in the different atmospheres used.

Table 8.2.3.1 **Summary of the kinetic data of the thermal decomposition of Pienaars River limestone to calcium oxide in different atmospheres**

Atmosphere	Temperature Range (°C)	Fraction Decomposed	Kinetic Data from the Isoconversional Method		Kinetic Data from the Kinetic Models			
					Kinetic Model			
			E_a (kJ mol^{-1})	ln A	E_a (kJ mol^{-1})	ln A	D-W	Corr. Coeff.
Air	624 - 810	$0 < \alpha < 0.2$	10 -250	-4	no fit			
		$0.2 < \alpha < 0.95$	233	10	first order with autocatalysis 228	9	0.034	0.9965
					Sestak-Berggren equation 228	9	0.030	0.9974
Air/water	400 - 790	$0 < \alpha < 0.2$	45	2	no fit			
		$0.2 < \alpha < 0.3$	45 - 236	-	no fit			
		$0.3 < \alpha < 0.95$	236	10	one-dimensional diffusion 246	10	0.044	0.9763
CO_2	680 - 960	$0 < \alpha < 0.2$	-23	4	no fit			
		$0.3 < \alpha < 0.8$	163	4	no fit			
		$0.8 < \alpha < 0.9$	260 - 700	6	no fit			
		$0.9 < \alpha < 1.0$	700 - 20	15	no fit			
CO_2/air	590 - 950	$0 < \alpha < 0.2$	-40	-3	no fit			
		$0.2 < \alpha < 0.4$	-40 - 2000	59	no fit			
		$0.4 < \alpha < 1.0$	1426	62	no conclusive fit			
CO_2/water	680 - 950	$0 < \alpha < 0.2$	-199	5	no conclusive fit			
		$0.3 < \alpha < 0.9$	800	33	no conclusive fit			
		$0.9 < \alpha < 1.0$	1000 - 50	17	no conclusive fit			

Key of abbreviations used in the table: E_a = activation energy; D-W = Durbin-Watson value; Corr. Coeff. = correlation coefficient.

8.2.4 Lime Acres Limestone

Table 8.2.4 The thermal decomposition of Lime Acres Limestone in different atmospheres using a heating rate of 5 °C min^{-1} with sample masses between 5 - 15 mg

Atmosphere	Temperature Range (°C)	Mass Loss (%)	Mass Gain (%)	ΔH (kJ g^{-1})
Air	49 - 271	-	-	-
	271 - 540	2	-	-
	593 - 794	44	-	2
Air/H_2O	65 - 326	-	3	-
	601 - 808	43	-	-
CO_2	32 - 117	-	2	-
	117 - 190	1	-	-
	190 - 615	-	2	-
	688 -893	44	-	1
CO_2/Air	100 - 411	-	1	-
	411 - 852	3	-	-
	858 - 950	43	-	9×10^{-1}
CO_2/Water	226 - 658	-	3	-
	658 - 844	4	-	-
	844 - 910	44	-	1

The TG curves for Lime Acres limestone show a mass gain in all the atmospheres. The thermal decomposition of this limestone in an air-atmosphere shows a slower rate of mass loss (see figure 8.2.4(a)) at 5 °C min^{-1} in comparison to that of pure calcium carbonate in figure 8.2.1(a). The total mass loss in air is 46 % which is higher than the theoretical mass loss of 43.97% expected for calcium carbonate decomposing to calcium oxide. There are possibly two reactions occurring. The first mass loss between 271 °C and 540 °C, is possibly due to the loss of adsorbed water. The main mass loss is the decomposition reaction of calcium carbonate to calcium oxide.

The slight mass gain of from 2 to 3 %, from an air- to an air/H_2O-atmosphere is due to the increased partial pressure of water vapour.

The heats of decomposition (refer to table 8.2.4) of Lime Acres limestone obtained in the different atmospheres are slightly less than those obtained for the pure calcium carbonate (table 8.2.1) except for the heat of decomposition obtained in the air-atmosphere (which is the same). The heats of decomposition of the Lime Acres limestone in the different atmospheres, are higher than the values obtained for the other carbonate samples (tables 8.2.2 and 8.2.3).

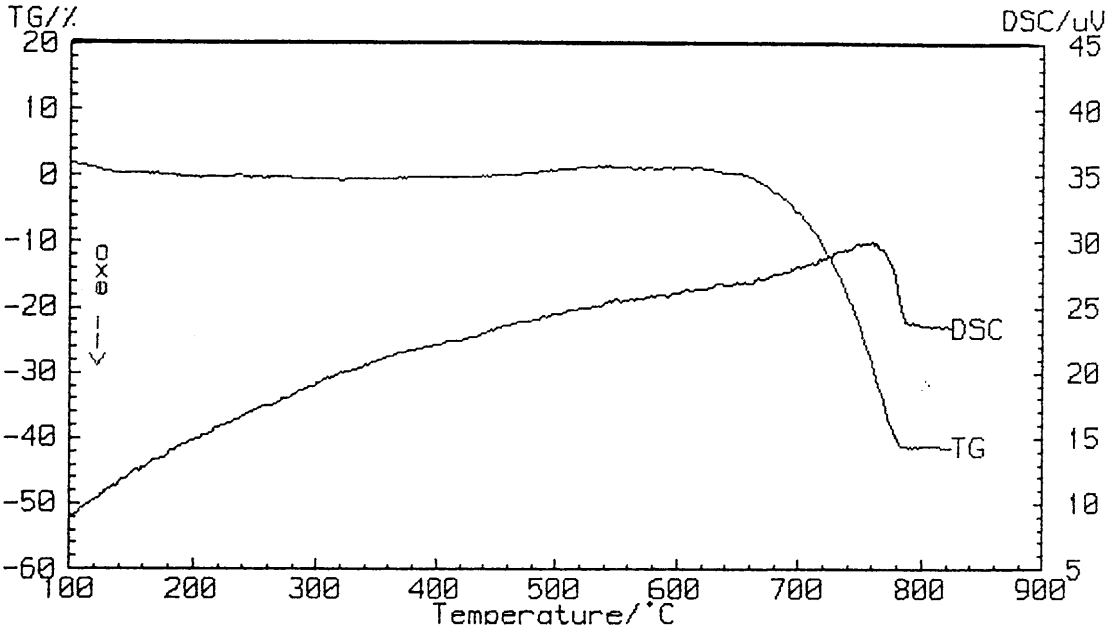

Figure 8.2.4(a): TG and DSC curves of the thermal decomposition of Lime Acres limestone decomposing in an air-atmosphere using a heating rate of 5 °C min^{-1}

In the CO_2-atmosphere, the starting temperatures of the decomposition mass loss curves shift to higher temperatures and the decomposition reaction is completed over a smaller temperature range (figure 8.2.4(b)). The onset of decomposition in the CO_2-atmospheres, is inhibited by the partial pressure of the CO_2, which delays the limestone decomposition to the oxide. The total mass loss is 45 % while there is a mass gain of 4 %. The actual mass loss corresponding to the percentage calcium carbonate present decomposing in the sample, is 41 %. The limestone sample appears to be ≈ 93 % calcium carbonate with a small amount of calcium oxide and dolomite (refer to Chapter 7.2) as impurities. The mass gain is slightly

higher in the CO_2/H_2O-atmosphere indicating that the partial pressure of the water vapour enhances recarbonation of the calcium oxide impurity. The main mass loss is the same in the CO_2-atmosphere as in the CO_2/H_2O-atmosphere. This mass loss is a good indication of the calcium carbonate content of the limestone sample.

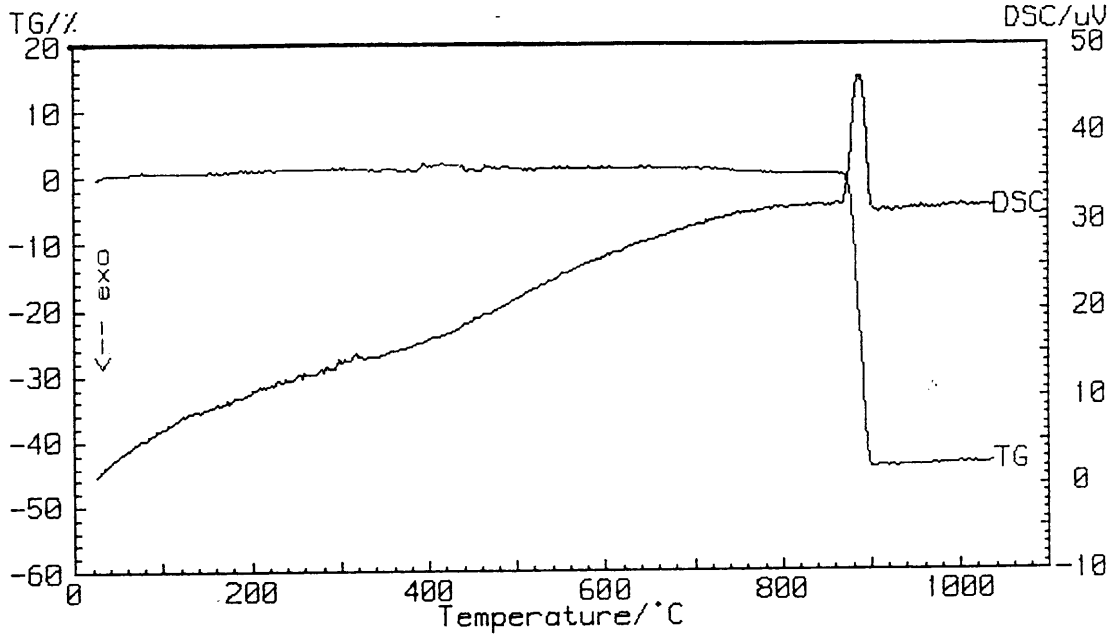

Figure 8.2.4 (b): TG and DSC curves of the thermal decomposition of Lime Acres limestone decomposing in a CO_2-atmosphere using a heating rate of 5 °C min^{-1}

Figures 8.2.4 (c), (d) and (e) are thermograms of Lime Acres limestone decomposing in an air/water-; CO_2/air- and CO_2/water-atmospheres respectively.

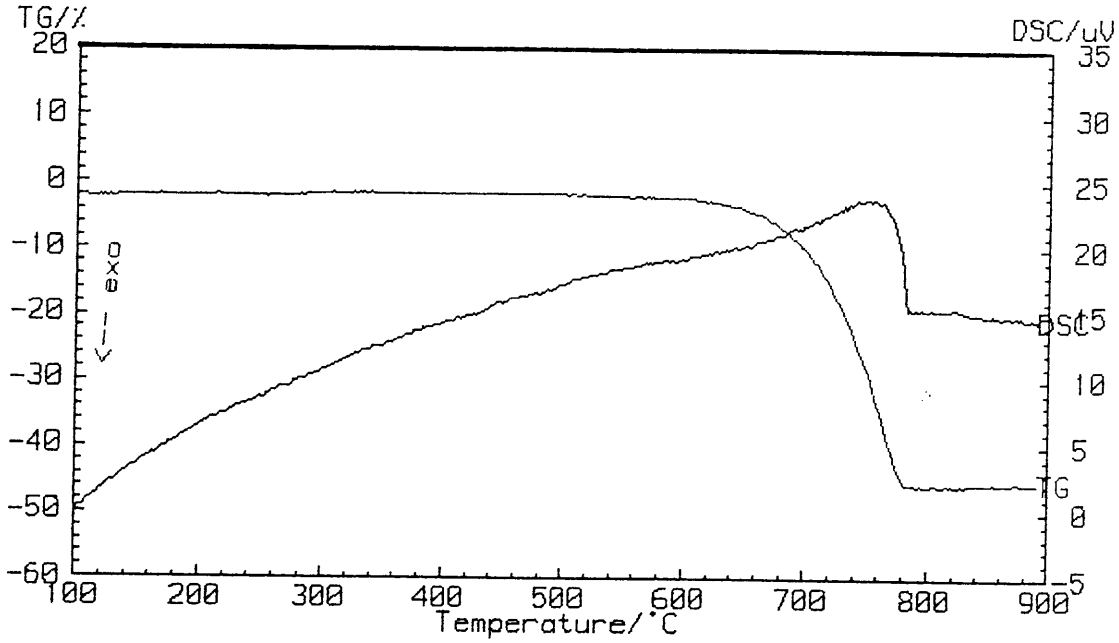

Figure 8.2.4 (c): TG and DSC curves of the thermal decomposition of Lime Acres limestone decomposing in an air/water-atmosphere using a heating rate of 5 °C min^{-1}

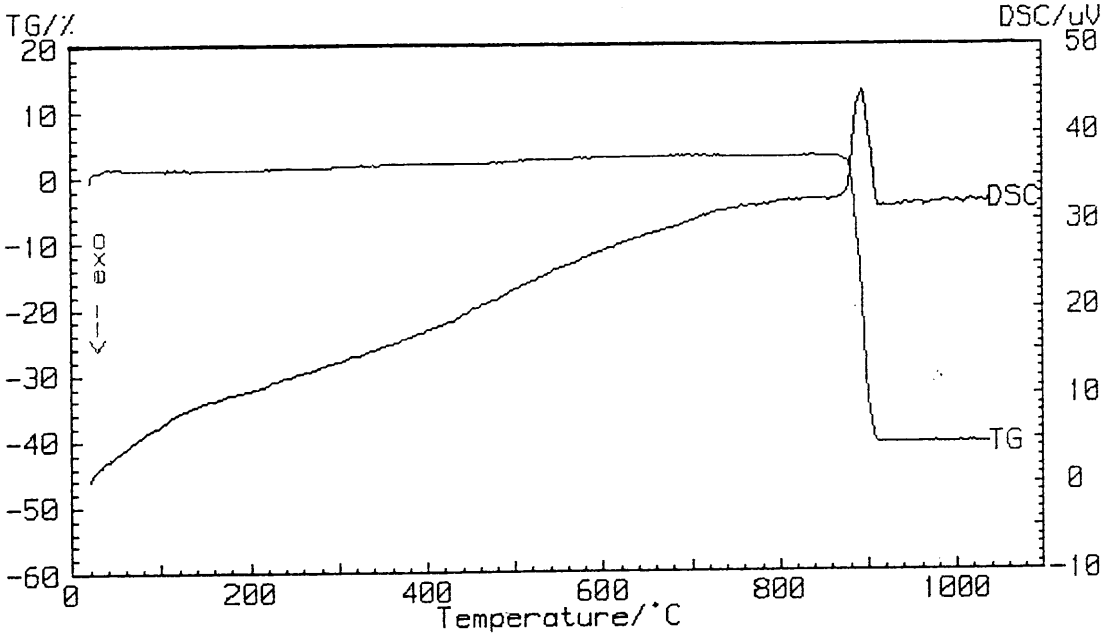

Figure 8.2.4 (d): TG and DSC curves of the thermal decomposition of Lime Acres limestone decomposing in a CO_2/air-atmosphere using a heating rate of 5 °C min^{-1}

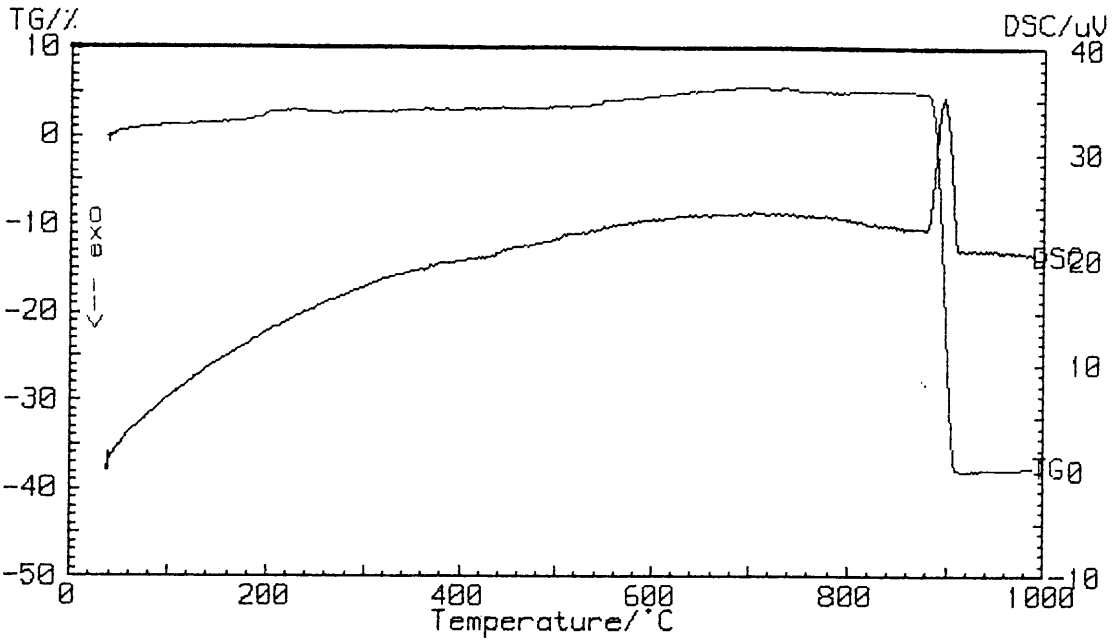

Figure 8.2.4 (e): **TG and DSC curves of the thermal decomposition of Lime Acres limestone decomposing in a CO_2/water-atmosphere using a heating rate of 5 °C min^{-1}**

8.2.4.1 Kinetics of the decomposition reaction of Lime Acres limestone in an air-atmosphere

Figure 8.2.4.1 (a) shows a plot of activation energy, E_a, versus the fraction decomposed for the reactions between 490 °C and 800 °C.

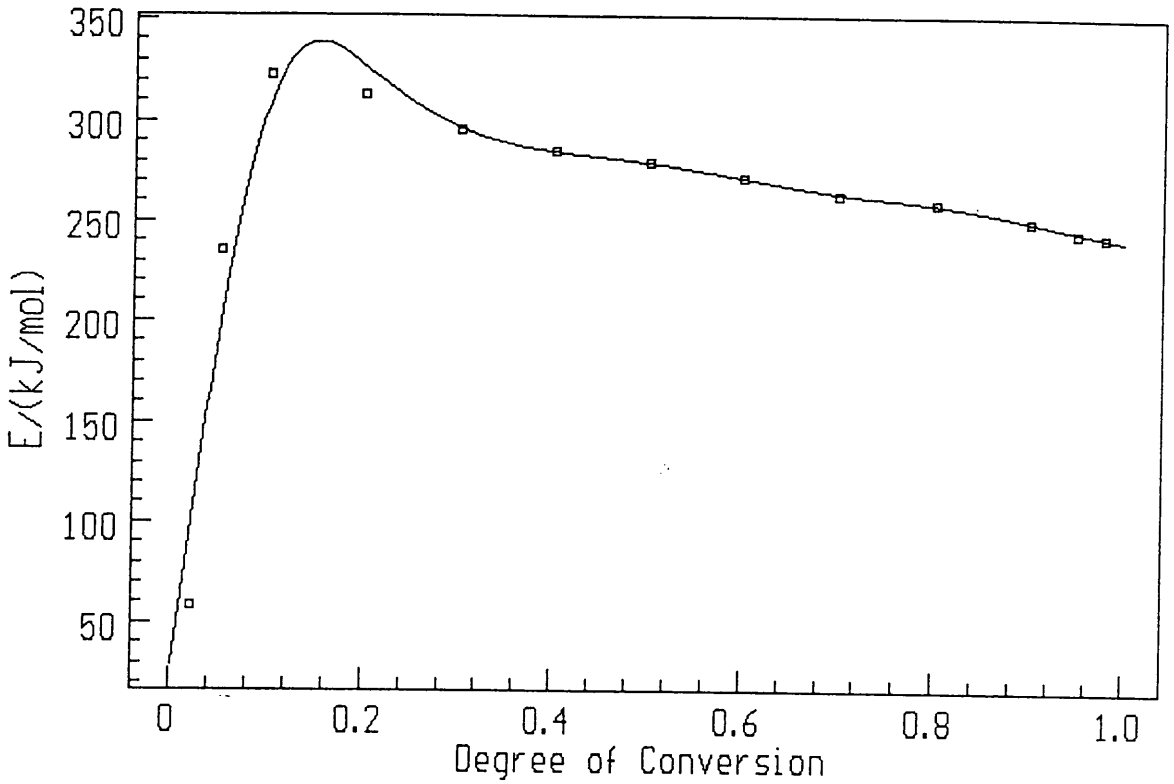

Figure 8.2.4.1 (a): Plot of activation energy, E_a, vs α for Lime Acres limestone in an air-atmosphere

The ascending part of the dependence of the activation energy on the fraction decomposed, $0 < \alpha < 0.2$, indicates that the reaction with the higher activation energy makes a significant increasing contribution to the heat absorbed [85]. The average activation energy increases from $\approx$ 50 kJ mol^{-1} to $\approx$ 330 kJ mol^{-1} for $0 < \alpha < 0.2$ after which it decreases slightly showing a decreasing contribution of the reaction with the higher activation energy to the total heat absorbed [85]. The overall process is considered to be governed by one activation energy for $0.2 < \alpha < 1.0$ [85]. The effective activation energy is thus considered to be a good approximation for the average activation energy of the limiting reaction for $0.2 < \alpha < 1.0$. The average activation energy is $\approx$ 273 kJ mol^{-1}. The kinetic models are fitted over the $0 < \alpha < 0.2$ and $0.2 < \alpha < 1.0$ ranges. No kinetic model appears to fit the $0 < \alpha < 0.2$ range. The following kinetic models appear to fit the experimental data of the range $0.2 < \alpha < 1.0$: the n-th order,

two-dimensional phase boundary equation, first order, the two-dimensional diffusion equation and the three-dimensional diffusion equation of Ginstling-Brounshtein.

The isoconversional method obtained an average activation energy of ≈ 273 kJ mol $^{-1}$ and a ln A value of ≈ 11. Figure 8.2.4.1 (b) shows the kinetic model of the n-th order equation with an activation energy of 262 kJ mol^{-1} and a ln A of 11. (The correlation coefficient is 0.9985 and the Durbin-Watson value is 0.042). An activation energy of 252 kJ mol^{-1} and a ln A of 10 is obtained for the two-dimensional phase boundary equation (figure 8.2.4.1 (c)). The correlation coefficient is 0.9982 and the Durbin-Watson value is 0.022.

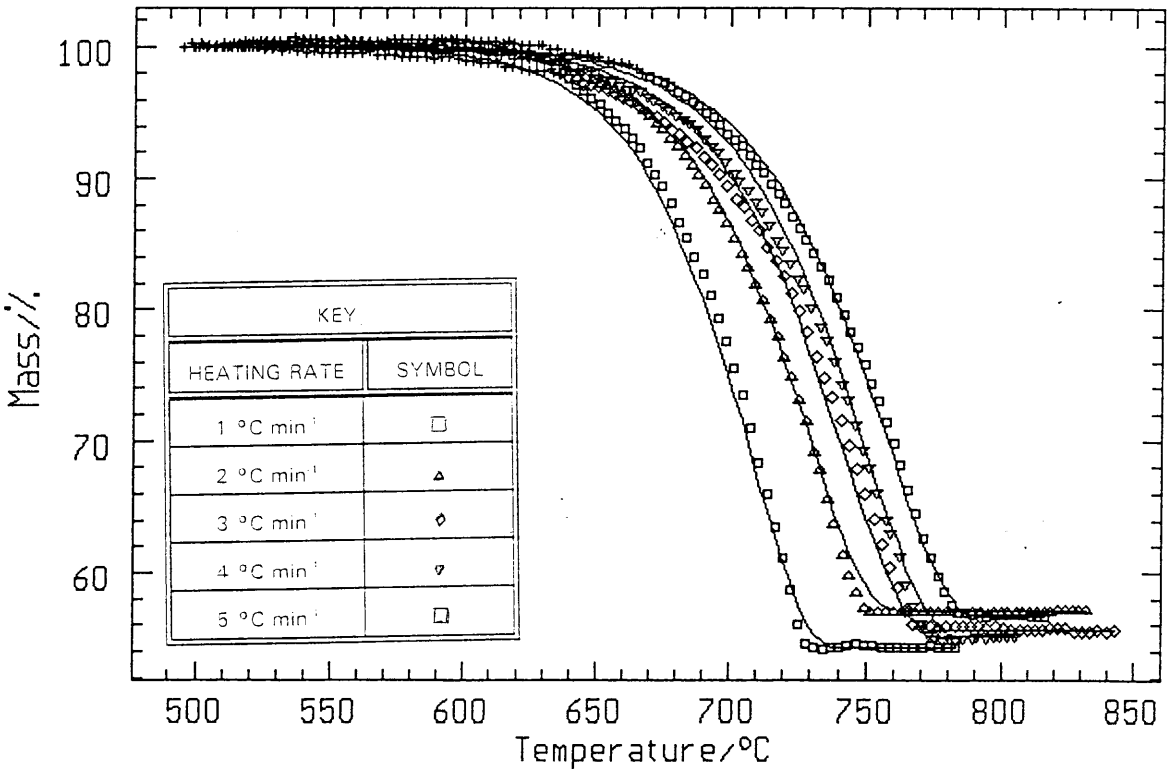

Figure 8.2.4.1 (b): The n-th order kinetic model fitted to the experimental data of Lime Acres limestone decomposing in an air-atmosphere.

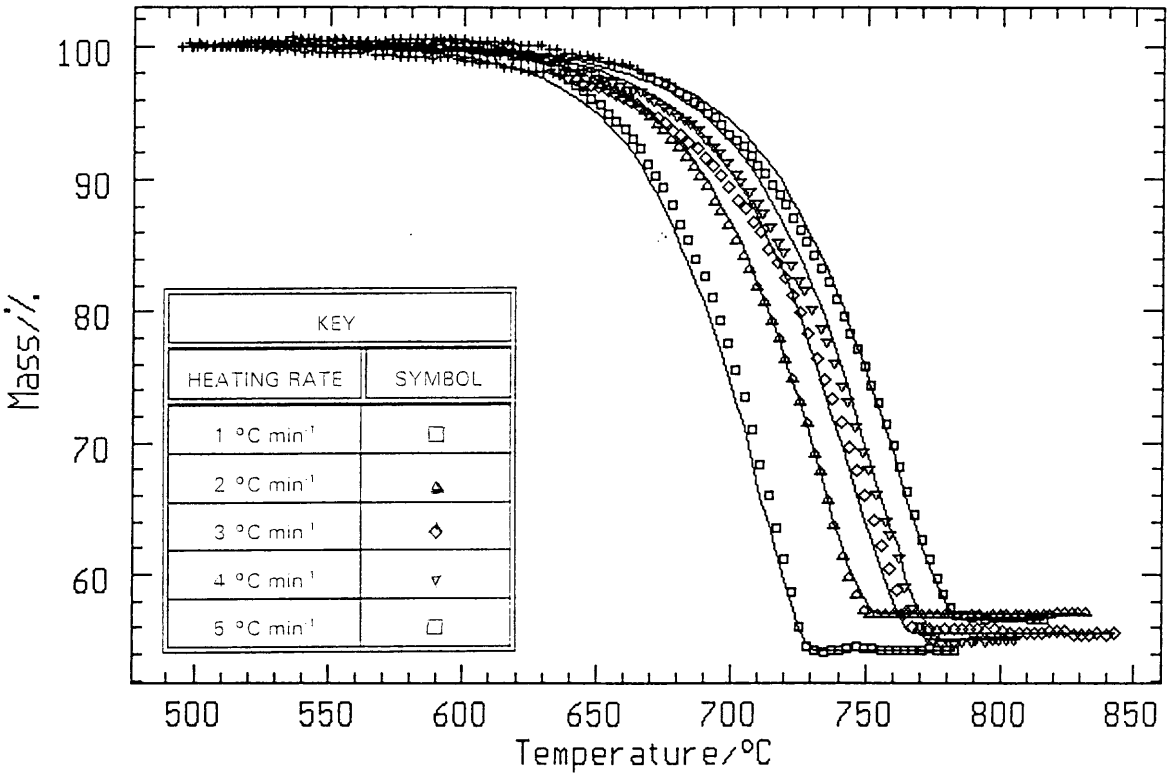

Figure 8.2.4.1 (c): The two-dimensional phase boundary kinetic model fitted to the experimental data of Lime Acres limestone decomposing in an air-atmosphere.

The first order kinetic model gives an activation energy of 288 kJ mol^{-1} and a ln A value of 12 (figure 8.2.4.1 (d)). The correlation coefficient is 0.9974 and the Durbin-Watson value is 0.052.

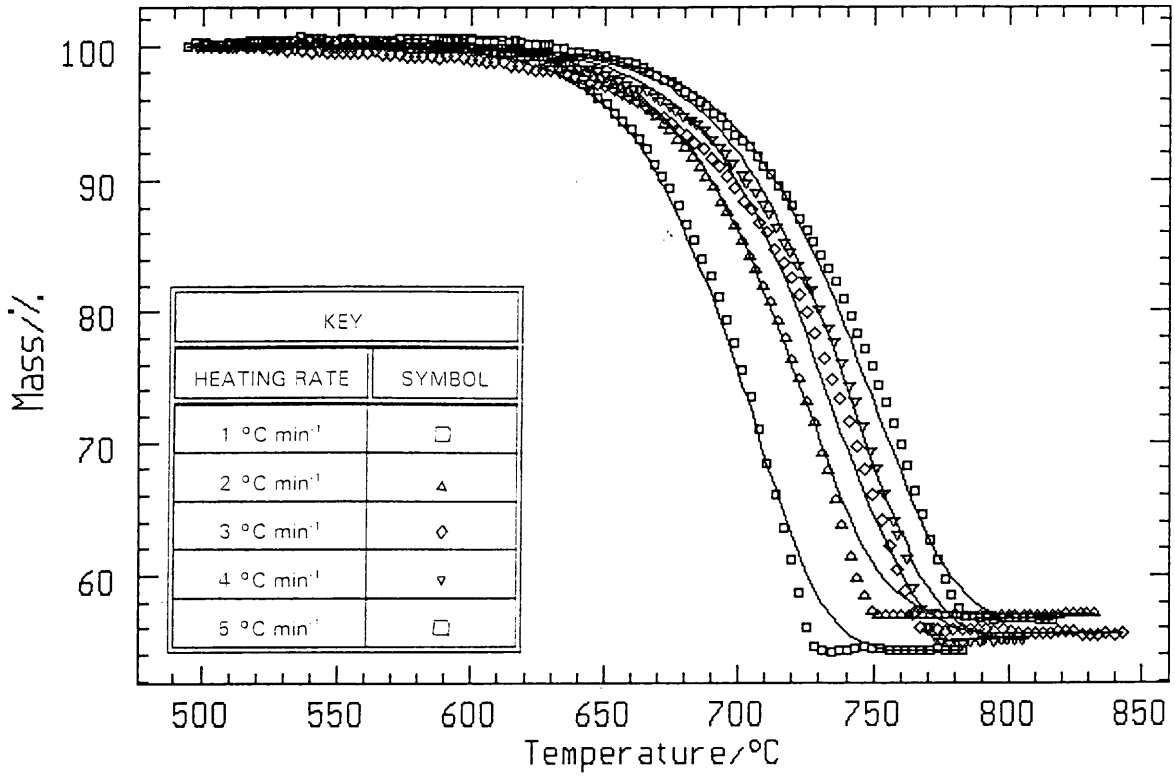

Figure 8.2.4.1 (d): The first order kinetic model fitted to the experimental data of Lime Acres limestone decomposing in an air-atmosphere

The activation energy obtained for the two-dimensional diffusion equation is 387 kJ mol^{-1} with a ln A of 17. The correlation coefficient is 0.9933 and the Durbin-Watson value is 0.026. The activation energy obtained is 406 kJ mol^{-1} for the three-dimensional Ginstling-Brounshtein equation with a ln A of 17. The correlation coefficient is 0.9922 with a Durbin-Watson value of 0.023). Thus, the n-th order kinetic model (with an activation energy 262 kJ mol^{-1}) appears to be the best fit, on comparing the activation energy obtained with that of the isoconversional method (273 kJ mol^{-1}) and on comparing the correlation coefficients of all the kinetic models. However, the two-dimensional phase boundary equation has the best Durbin-Watson value, namely 0.022.

8.2.4.2 Kinetics of the decomposition of Lime Acres limestone in an air/water-atmosphere

Figure 8.2.4.2 (a) shows a plot of activation energy, E_a, versus the fraction decomposed for the reactions from 500 °C to 820 °C. The kinetic models are fitted over the $0 < \alpha < 0.2$ and $0.2 < \alpha < 1.0$ ranges. The plot of activation energy versus fraction decomposed has the same shape as the plot obtained in an air-atmosphere (section 8.2.4.1). There is an ascending dependence of the activation energy on the degree of conversion from ≈ 40 to 300 kJ mol^{-1} for $0 < \alpha < 0.2$, after which it decreases slightly. For $0.2 < \alpha < 1.0$, the activation energy is considered to be governed by a single-step reaction with an average activation energy of ≈ 246 kJ mol^{-1}. No kinetic models fit the experimental data for $0 < \alpha < 0.2$. The kinetic models which appear to fit the range $0.2 < \alpha < 1.0$, are the n-th order equation, the two-dimensional phase boundary equation and the first order equation.

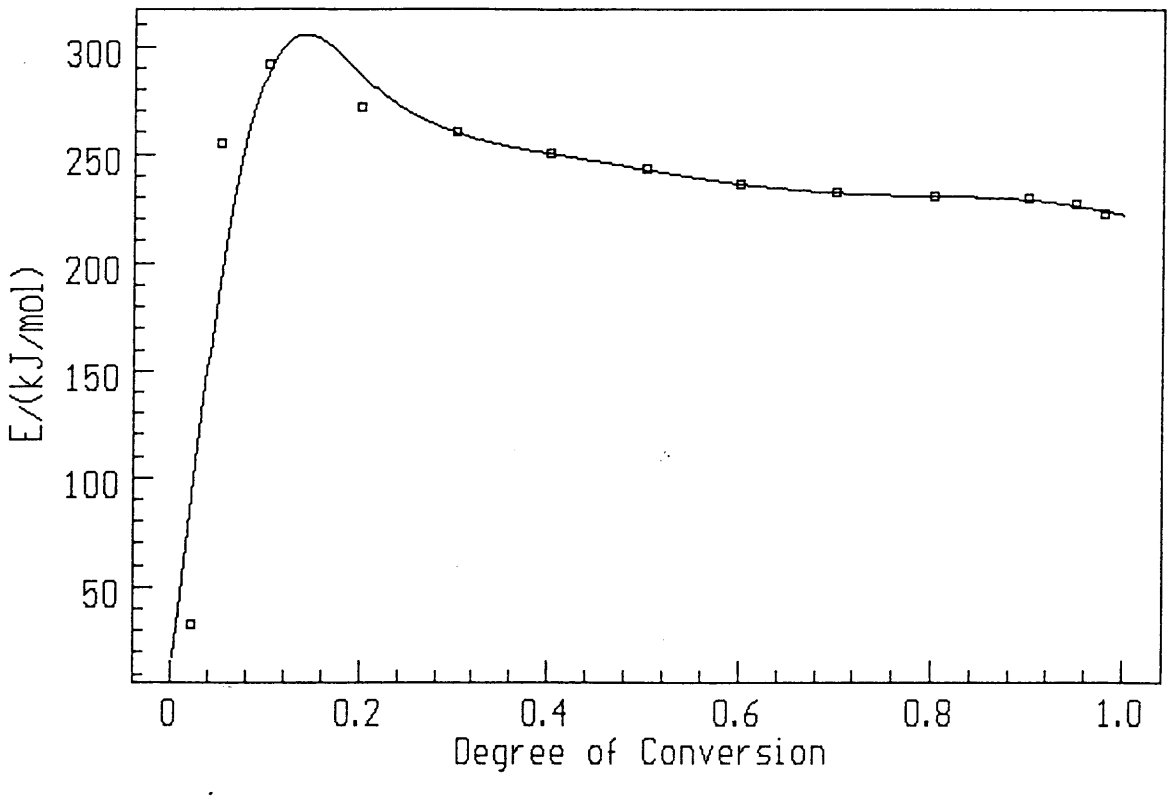

Figure 8.2.4.2 (a): Plot of activation energy, E_a, vs α for Lime Acres limestone in an air/water-atmosphere

The isoconversional method obtained an average activation energy of ≈ 246 kJ mol $^{-1}$ and a ln A value of ≈ 10. Figure 8.2.4.2 (b) shows the kinetic model of the n-th order fit, with an activation energy of 237 kJ mol^{-1} and a ln A of 9. The correlation coefficient is 0.9977 and the Durbin-Watson value is 0.026.

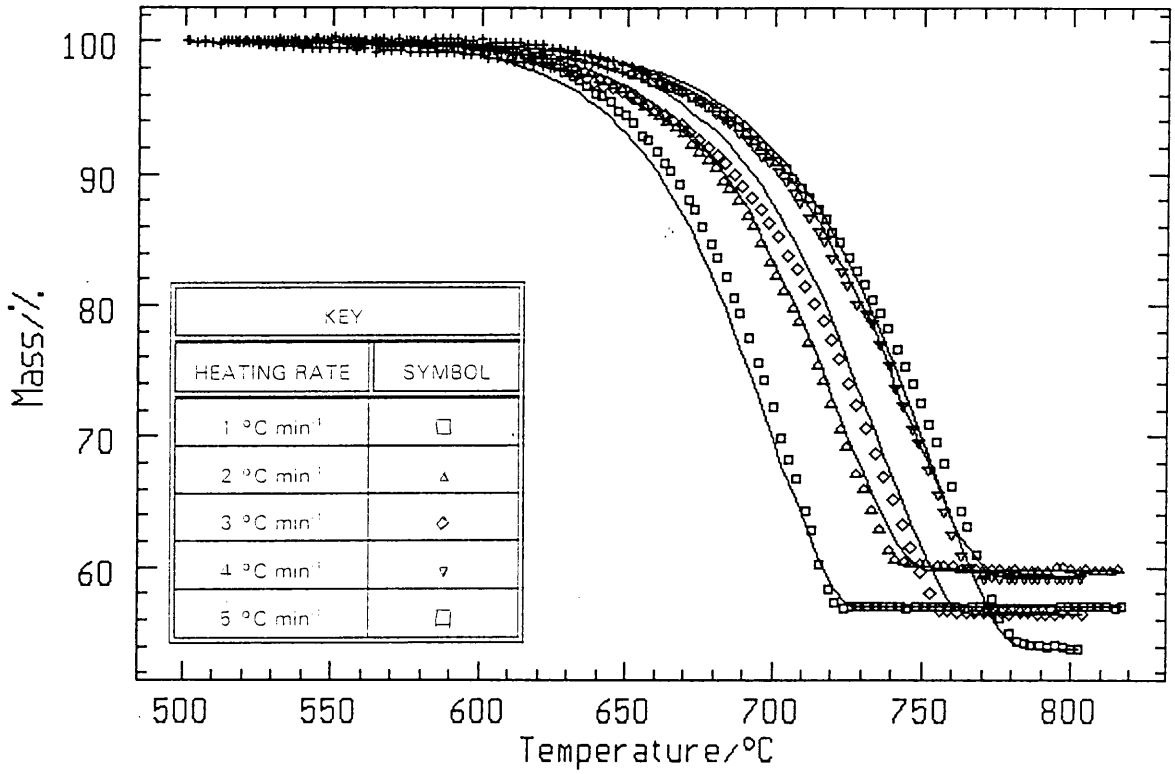

Figure 8.2.4.2 (b): The n-th order kinetic model fitted to the experimental data of Lime Acres limestone decomposing in an air/water-atmosphere

An activation energy of 233 kJ mol^{-1} and a ln A of 9 is obtained for the two-dimensional phase boundary equation (figure 8.2.4.2 (c)). The correlation coefficient is 0.9976 and the Durbin-Watson value is 0.021.

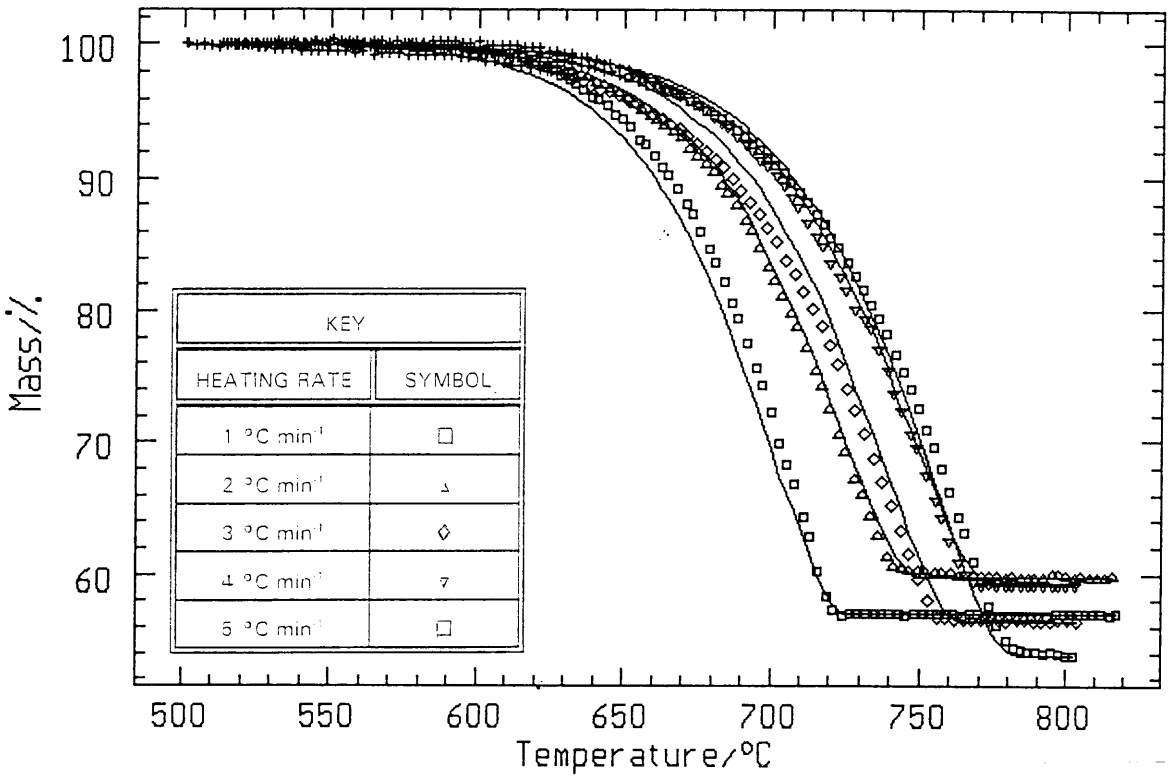

Figure 8.2.4.2 (c): The two-dimensional phase boundary model fitted to the experimental data of Lime Acres limestone decomposing in an air/water-atmosphere

The activation energy obtained using the first order equation is 266 kJ mol^{-1} with a ln A value of 11. The correlation coefficient is 0.9959 and the Durbin-Watson value is 0.035. The n-th order equation appears to fit the experimental data the best when comparing the activation energies. The n-th order kinetic model has an activation energy of 237 kJ mol^{-1} and the average activation energy obtained from the isoconversional method (which is not reaction model dependent), is 246 kJ mol^{-1}. However, the two-dimensional phase boundary equation has a good correlation coefficient and its Durbin-Watson value is the best. Thus, both the n-th order equation and the two-dimensional phase boundary equation fit the experimental data well. Thus, there is no single conclusive fit.

8.2.4.3 Kinetics of the decomposition of Lime Acres limestone in a CO_2-atmosphere

Figure 8.2.4.3 (a) shows a plot of activation energy versus fraction decomposed for Lime Acres limestone in a CO_2-atmosphere from 490 °C to 970 °C.

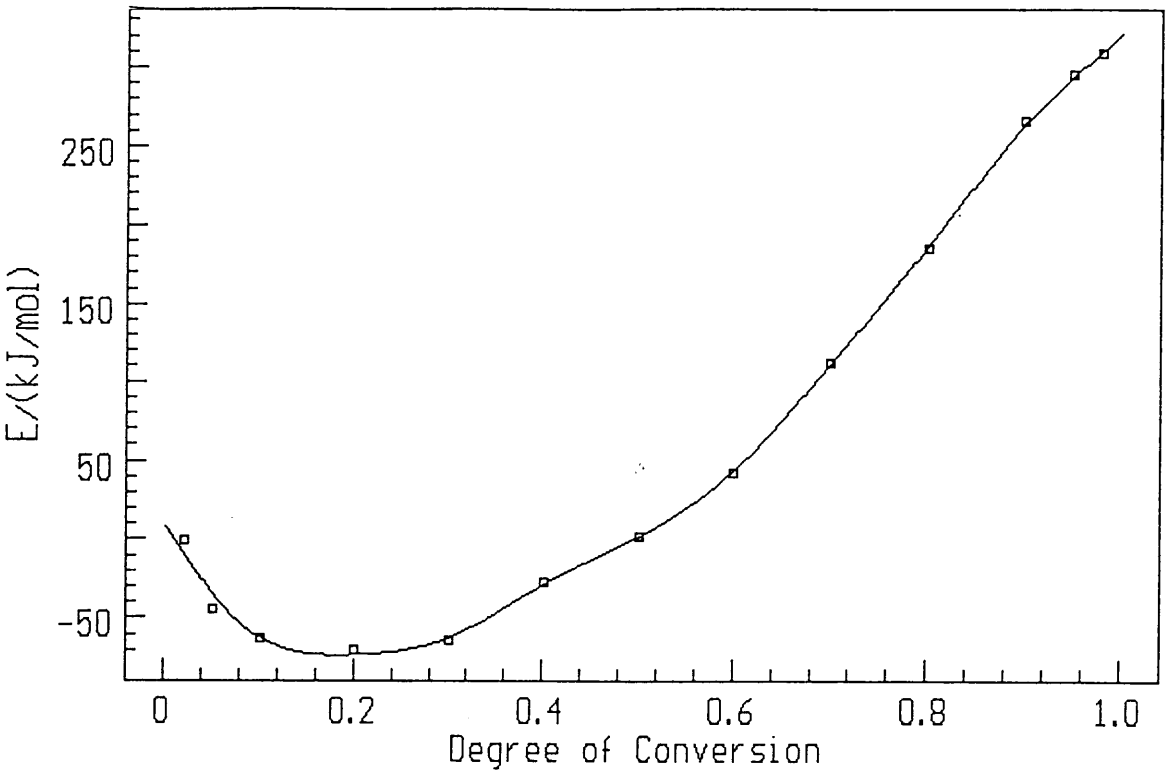

Figure 8.2.4.3 (a): Plot of E_a vs α for Lime Acres limestone in a CO_2-atmosphere

From figure 8.2.4.3 (a), the activation energy decreases from 0 to 0.2 ($\approx$ 0 to - 50 kJ mol^{-1}) and then increases from 0.2 to 1.0 ($\approx$ - 50 to 320 kJ mol^{-1}). The plot goes through a minimum near α = 0.2.

No kinetic model fitted the experimental data for $0 < \alpha < 0.2$. For $0.2 < \alpha < 1.0$, the three-dimensional diffusion equation of Jander, the three-dimensional equation of Ginstling-Brounshtein and the second order equation appear to fit. The best fit is obtained with the three-dimensional diffusion equation of Jander on comparing the correlation coefficient and Durbin-

Watson values. This reaction is diffusion controlled and the rate depends on the diffusion of the CO_2 through the product layer, CaO. The activation energy value is 516 kJ mol^{-1} and a ln A value of 23 (figure 8.2.4.3 (b)). The correlation coefficient is 0.9471 and the Durbin-Watson value is 0.011. The average activation energy from the isoconversional method is ≈ 135 kJ mol^{-1}. Thus, on comparing the activation energy values, there is no conclusive fit. The activation energy values obtained from the other two equations are 468 kJ mol^{-1} with a ln A value of 20 for the three-dimensional diffusion equation of Ginstling-Brounshtein (correlation coefficient of 0.9432 and a Durbin-Watson value of 0.012) and 461 kJ mol^{-1} with a ln A value of 21 for the second order equation (correlation coefficient 0.9348 and a Durbin-Watson value of 0.014).

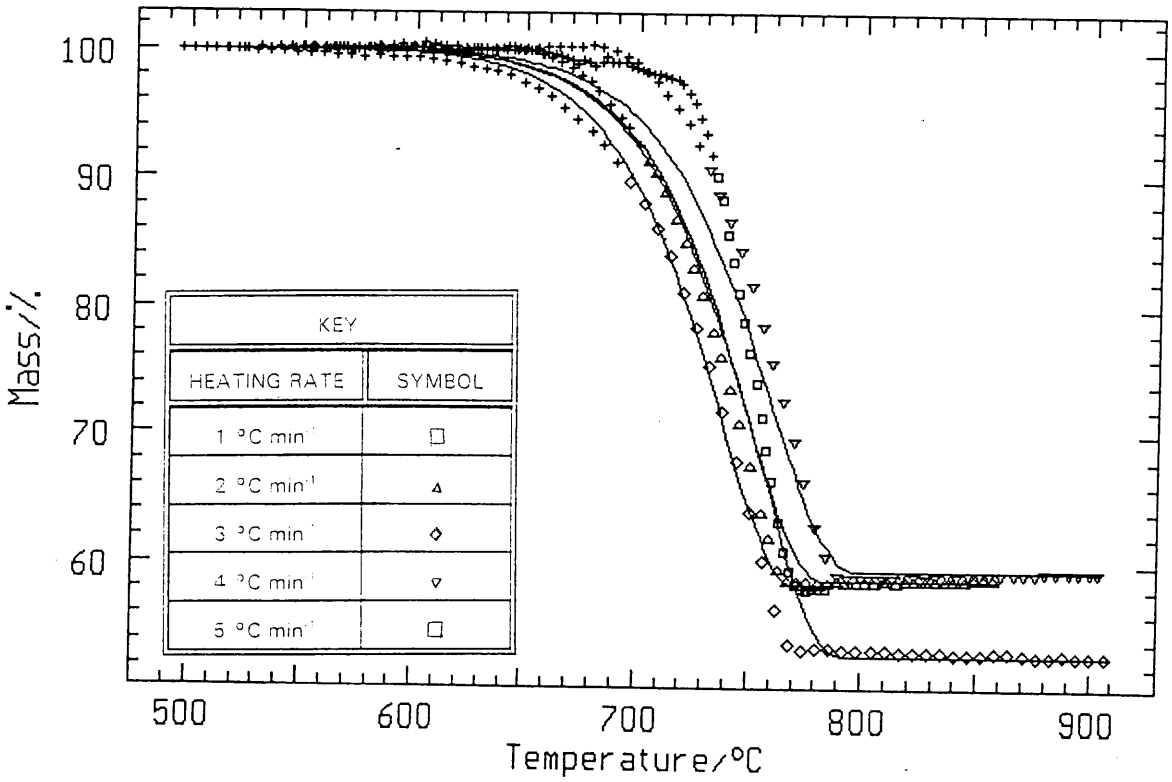

Figure 8.2.4.3 (b): Fitting of experimental data of the decomposition of Lime Acres limestone in a CO_2-atmosphere with the kinetic model of the three-dimensional diffusion equation of Jander

8.2.4.4 Kinetics of the decomposition of Lime Acres limestone in a CO_2/air-atmosphere

The kinetic data obtained for Lime Acres limestone decomposing in CO_2/air-atmosphere from 500 °C to 960 °C, shows an increase in activation energy from $0 < \alpha < 0.2$ ($\approx$ 0 to 2500 kJ mol^{-1}), then a decrease from $0.2 < \alpha < 0.6$ ($\approx$ 2500 to 13 kJ mol^{-1}), where it remains constant at an activation energy value of $\approx$ 13 kJ mol^{-1} and a ln A value of -3 (refer to Chapter 9.2) - figure 8.2.4.4 (a). There is initially an increasing contribution to the heat absorbed by the reaction with the higher activation energy, after which the contribution decreases [85]. The activation energy then remains constant with increasing fraction decomposed, from which is concluded that the overall process rate is governed by a single activation energy namely 13 kJ mol^{-1} [85].

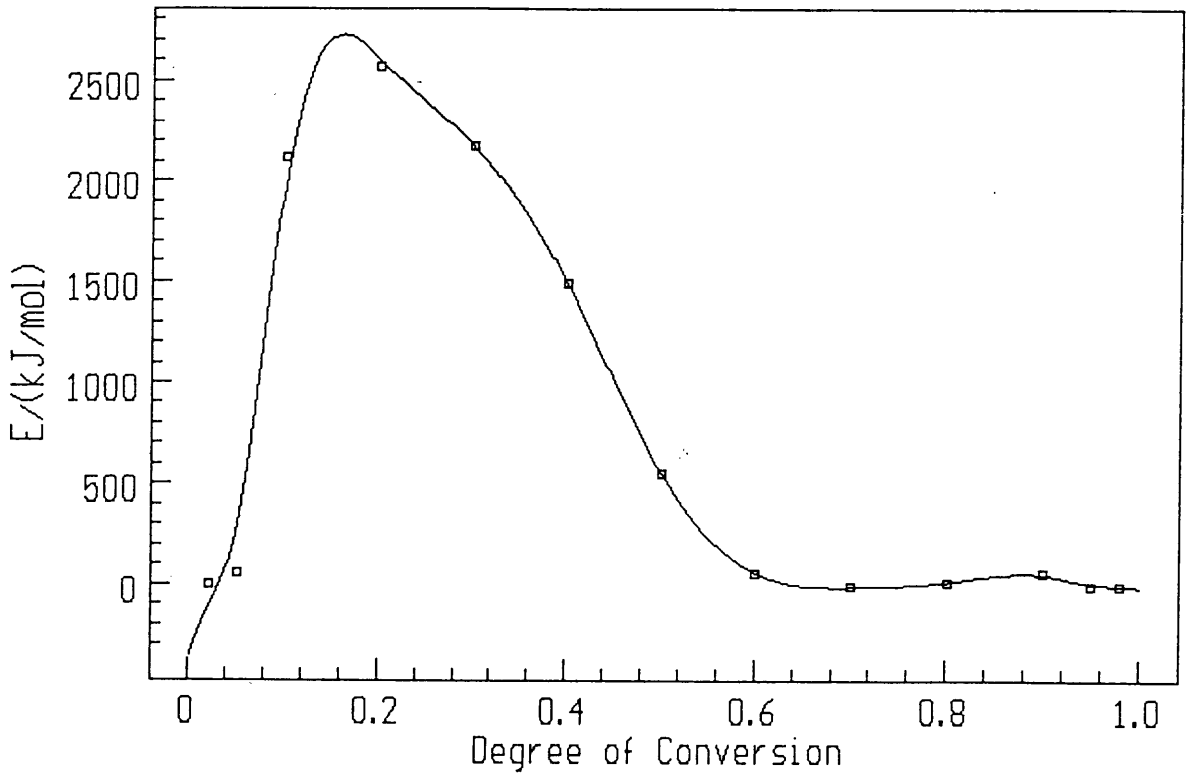

Figure 8.2.4.4 (a): Plot of E_a vs α for Lime Acres limestone in a CO_2/air-atmosphere

For $0.2 < \alpha < 0.6$, the best kinetic model fit is the second order (figure

8.2.4.4 (b)), which gives an activation energy value of 2603 kJ mol^{-1} and a ln A of 115. The correlation coefficient is 0.9865 and the Durbin-Watson value is 0.195. The isoconversional method obtained an average activation energy value from ≈ 2500 to 13 kJ mol^{-1} and a ln A value of ≈ 78.

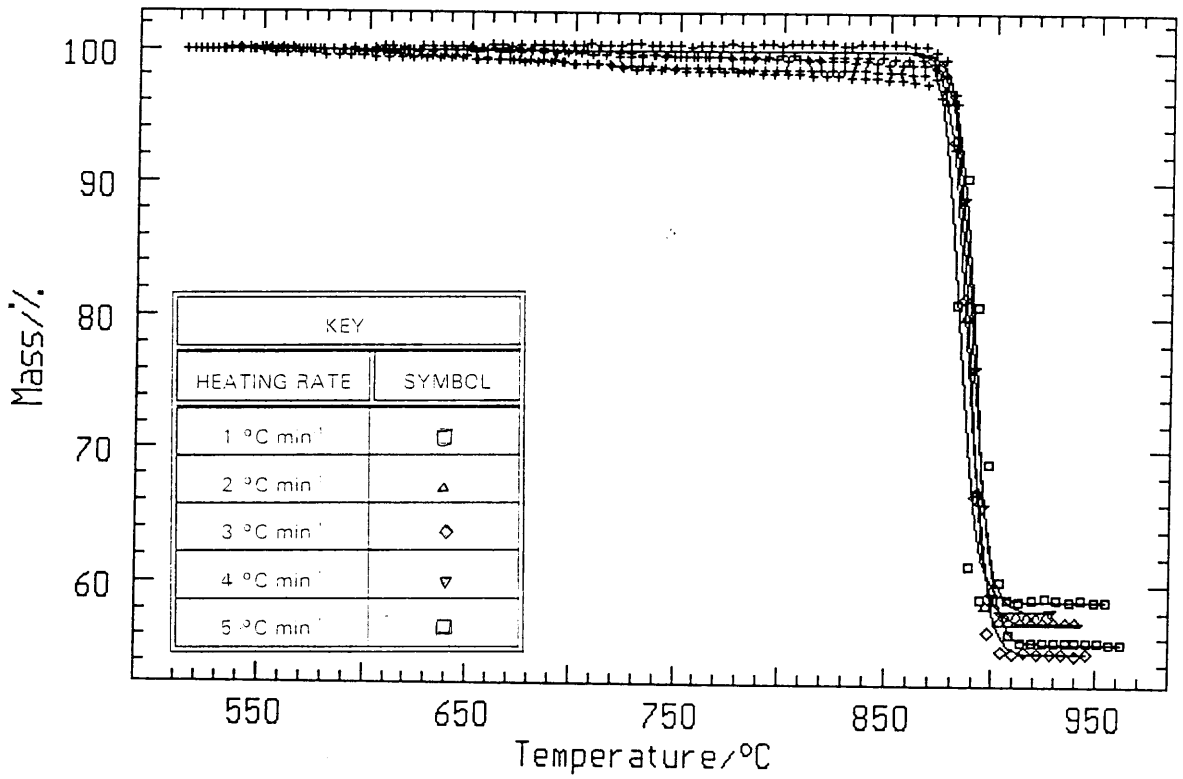

Figure 8.2.4.4 (b): Fitting of the second order equation for Lime Acres limestone decomposing in a CO_2/air-atmosphere for 0.2 < α < 0.6

There are two kinetic models which appear to fit the experimental data of the decomposition reaction for 0.6 < α < 1.0. They are the three-dimensional diffusion equation of Jander and the three-dimensional diffusion equation of Ginstling-Brounshtein. The three-dimensional diffusion equation of Ginstling-Brounshtein (figure 8.2.4.4 (c)), however, gives the best fit with a correlation coefficient of 0.9836 and an activation energy value of 2465 kJ mol^{-1}; ln A of 107 and a Durbin-Watson value of 0.270. This activation energy value does not compare well with the average activation energy obtained of ≈ 13 kJ mol^{-1} and ln A value of ≈ -3 from the isoconversional

method. The Ginstling-Brounshtein equation is diffusion controlled. Nucleation, nucleation growth and the advance of the reaction interface are dominant. The activation energy obtained from the three-dimensional diffusion equation of Jander is 2748 kJ mol^{-1} and a ln A value of 120 and a correlation coefficient of 0.9826 and a Durbin-Watson value of 0.280.

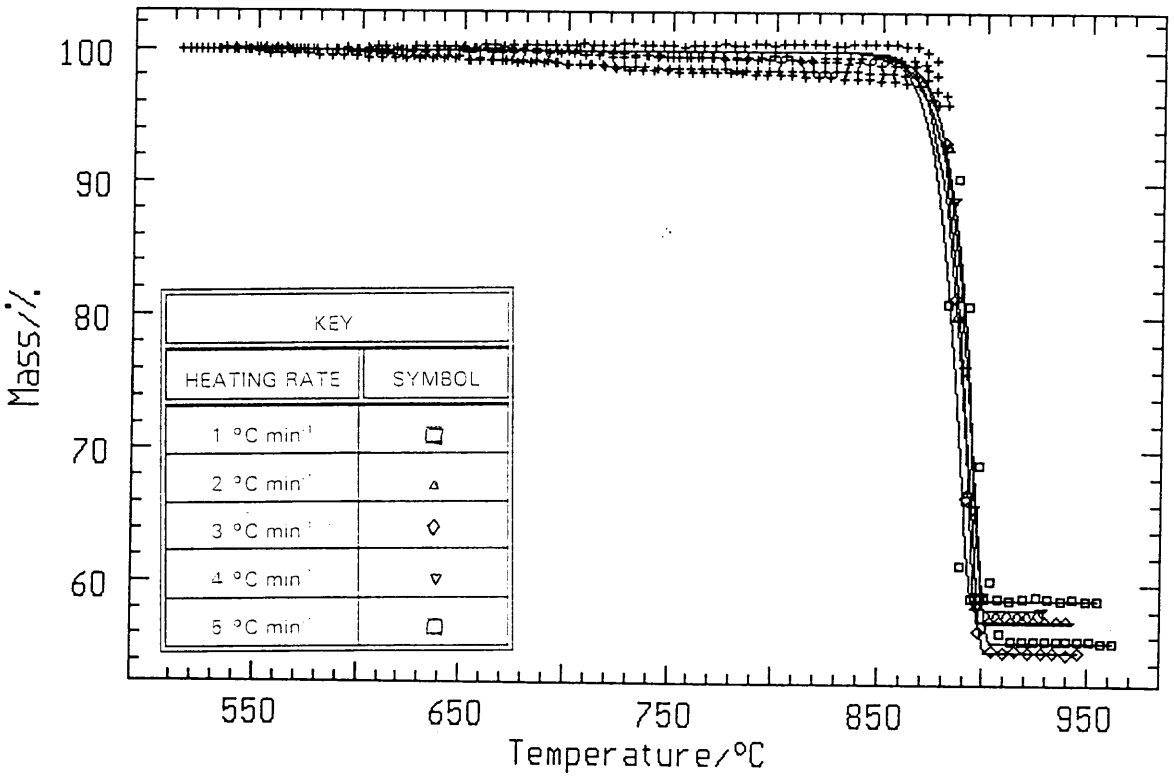

Figure 8.2.4.4 (c): Fitting of the three-dimensional diffusion equation of Ginstling-Brounshtein for Lime Acres limestone decomposing in a CO_2/air-atmosphere for 0.6 < α < 1.0

8.2.4.5 Kinetics of the decomposition of Lime Acres limestone in a CO_2/water-atmosphere

Figure 8.2.4.5 (a) shows a plot of activation energy versus the fraction decomposed for Lime Acres limestone decomposing in a CO_2/water-atmosphere from 840 °C to 940 °C. It is clear that the decomposition reaction does not occur in a single step. There are at least three steps. There is an increasing contribution to the heat absorbed by the reaction with the higher activation energy from $0 < \alpha < 0.2$ ($\approx$ 10 to 125 kJ mol^{-1}) [85]. For $0.2 < \alpha < 0.8$, the overall process appears to be governed by a single activation energy of $\approx$ 128 kJ mol^{-1}. The dependency then shows a decreasing contribution to the heat absorbed by the reaction with the higher activation energy [85]. The activation energy decreased from $\approx$ 128 to 0 kJ mol^{-1}.

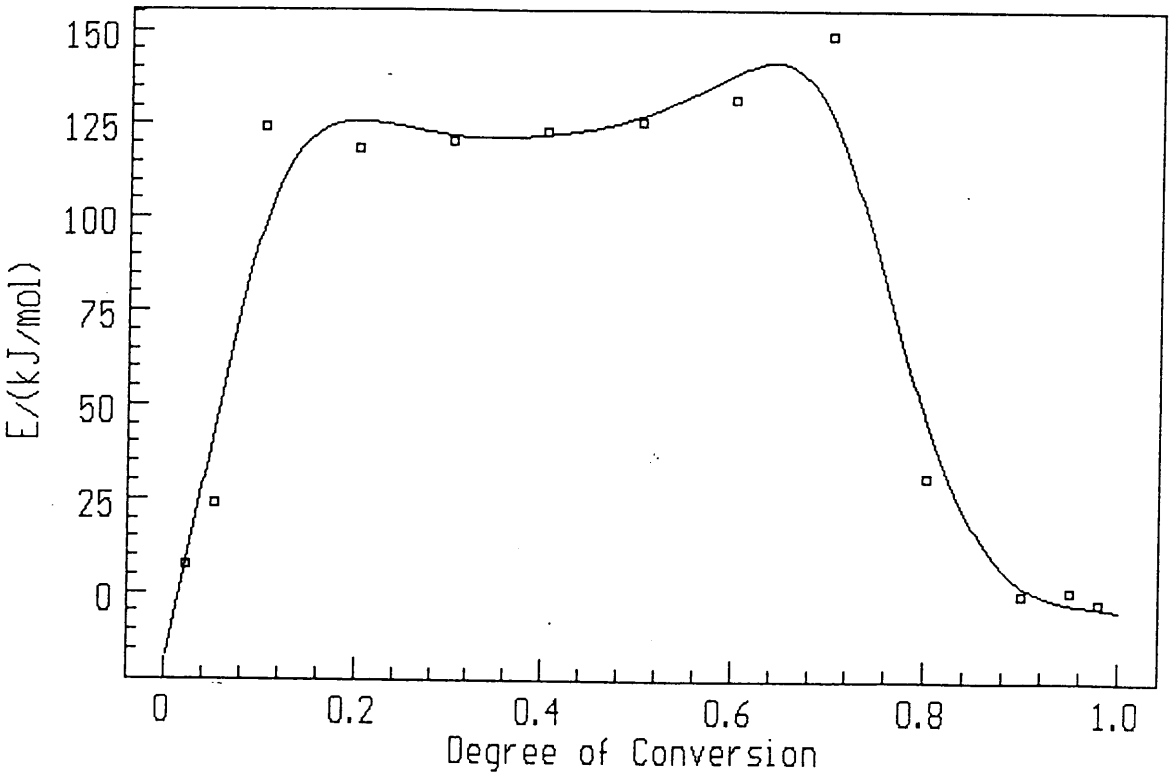

Figure 8.2.4.5 (a): Plot of E_a vs α for Lime Acres limestone in a CO_2/water-atmosphere

For $0 < \alpha < 0.2$, no kinetic model appears to fit the experimental data nor for $0.2 < \alpha < 0.8$. The isoconversional method gave an average activation energy of $\approx$ 128 kJ mol^{-1} and ln A of $\approx$ 97 for $0.2 < \alpha < 0.8$. No kinetic models appear to fit the experimental data for $0.8 < \alpha < 1.0$. The isoconversional method gives an average activation energy from $\approx$ 128 to 0 kJ mol^{-1} and ln A of $\approx$ -3 (refer to Chapter 9.2).

Table 8.2.4.1 is a summary of all the kinetic data for the decomposition of Lime Acres limestone to calcium oxide in the different atmospheres used.

Table 8.2.4.1 **Summary of the kinetic data of the thermal decomposition of Lime Acres limestone to calcium oxide in different atmospheres**

Atmosphere	Temperature Range (°C)	Fraction Decomposed	Kinetic Data from the Isoconversional Method		Kinetic Data from the Kinetic Models			
					Kinetic Model			
			E_a (kJ mol^{-1})	ln A	E_a (kJ mol^{-1})	ln A	D-W	Corr. Coeff.
Air	490 - 800	$0 < \alpha < 0.2$	50 - 330	9	no fit			
					n-th order			
		$0.2 < \alpha < 1.0$	273	11	262	11	0.042	0.9985
Air/water	500 - 820	$0 < \alpha < 0.2$	40 - 300	11	no fit			
					n-th order			
		$0.2 < \alpha < 1.0$	246	10	237	9	0.026	0.9977
					or two-dimensional phase boundary			
					233	9	0.021	0.9976
CO_2	490 - 970	$0 < \alpha < 0.2$	0 - (-50)	--	no fit			
		$0.2 < \alpha < 1.0$	(-50) - 320	--	no fit			
CO_2/air	500 - 960	$0 < \alpha < 0.2$	0 - 2500	--	no fit			
					second order			
		$0.2 < \alpha < 0.6$	2500 - 13	78	2603	115	0.195	0.9865
		$0.6 < \alpha < 1.0$	13	-3	no fit			
CO_2/water	840 - 940	$0 < \alpha < 0.2$	10 - 125	-3	no fit			
		$0.2 < \alpha < 0.8$	128	97	no fit			
		$0.8 < \alpha < 1.0$	128 - 0	-3	no fit			

Key of abbreviations used in the table: E_a = activation energy; D-W = Durbin-Watson value and Corr. Coeff. = correlation coefficient.

8.3 CALCIUM HYDROXIDE

Table 8.3 The thermal decomposition of calcium hydroxide in different atmospheres using a heating rate of 5 °C min^{-1} with sample masses between 5 - 15 mg

Atmosphere	Temperature Range (°C)	Mass Loss (%)	Mass Gain (%)	ΔH (kJ g^{-1})
Air	30 - 396 396 - 518 553 - 759	1 15 18	- - -	- 1 1
Air/H_2O	30 - 405 405 - 498 512 - 690 690 - 800	- 17 13 4	- - - -	- 1 - -
CO_2	30 - 357 357 - 805 805 - 1060	- - 53	- 26 -	- - 2
CO_2/Air	30 - 55 55 - 372 372 - 829 829 - 953	- 2 - 50	- - 20 -	- - - 1
CO_2/H_2O	30 - 314 314 - 806 806 - 919	1 - 52	- 22 -	- - 1

The calcium hydroxide is not pure as there is some calcium carbonate present as an impurity (see Chapter 7.2). The impurity influences all the results in the above table. That is why such high percentage mass losses are obtained. The theoretical percentage mass loss of calcium hydroxide decomposing to calcium oxide, is 24.3 %. The experimentally obtained mass loss in an air-atmosphere for the temperature region 396 to 518 °C, is 15 % which shows that ≈ 61 % of the sample, is $Ca(OH)_2$. There is an initial mass loss below 300 °C due to the dehydration of adsorbed water in an air-, CO_2/air- and CO_2/water-atmosphere. In the CO_2-atmosphere, there is a mass increase (figure 8.3(a)), where the formed calcium oxide (obtained from the decomposition of the calcium hydroxide), reacts with the CO_2 and forms calcium carbonate.

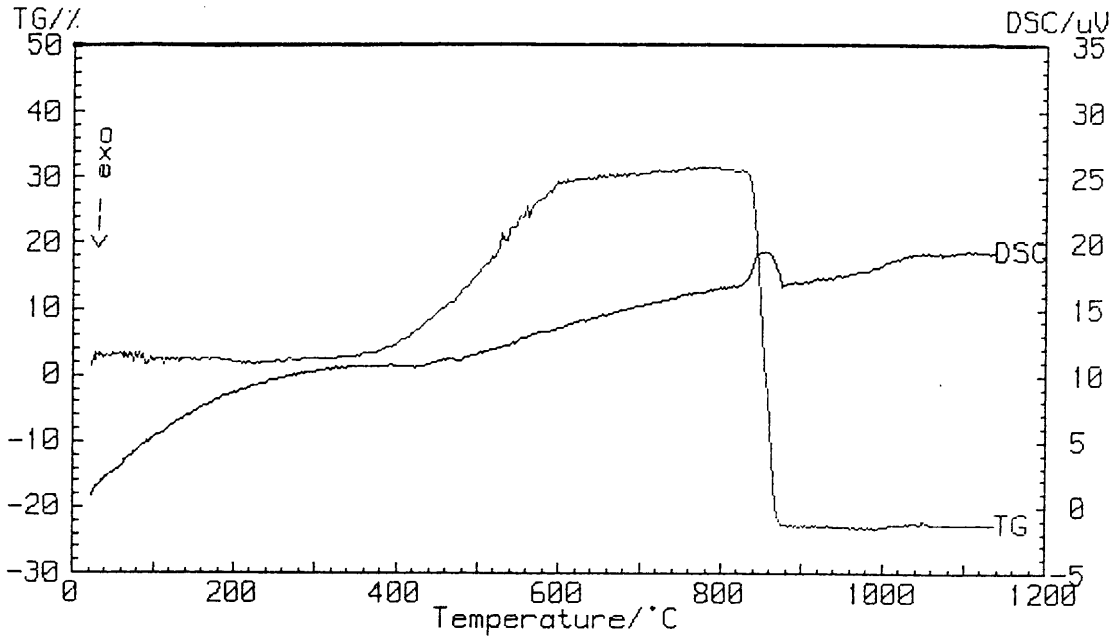

Figure 8.3 (a): **TG and DSC curves of the thermal decomposition of $Ca(OH)_2$ decomposing in a CO_2-atmosphere using a heating rate of 5 °C min^{-1}**

The mass gain is the greatest in the CO_2-atmosphere (figure 8.3 (a)) and it decreases in the CO_2/H_2O-atmosphere (figure 8.3 (b)) and the CO_2/air-atmosphere (figure 8.3 (c)). The higher mass loss in the CO_2-atmosphere is due to more calcium carbonate being formed from calcium oxide, the product of the decomposition of calcium hydroxide. The decomposition reactions that occur are the calcium hydroxide decomposing to calcium oxide, and the calcium carbonate decomposing to calcium oxide. As the product, CaO, is forming; it reacts with the CO_2 in the surrounding atmosphere to form $CaCO_3$. Thus, this leads to the increased mass loss observed at 805 - 1060 °C. The onset of the mass loss is inhibited in the CO_2-atmospheres. This indicates the strong influence of the partial pressure of CO_2 on the starting temperature of the decomposition reaction of these compounds. Thus, as the calcium hydroxide is decomposing to CaO, the CaO that is forming, is reacting with the CO_2 present to form calcium carbonate. The mass loss due to the calcium hydroxide decomposing to CaO and water is not detected.

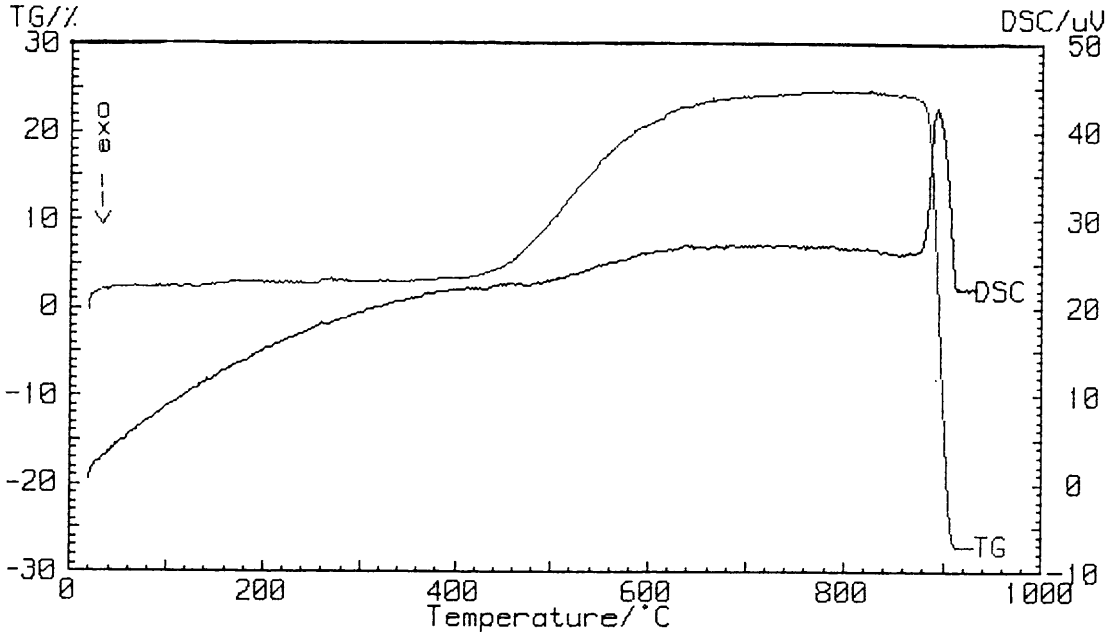

Figure 8.3 (b): TG and DSC curves of the thermal decomposition of $Ca(OH)_2$ decomposing in a CO_2/water-atmosphere using a heating rate of 5 °C min^{-1}

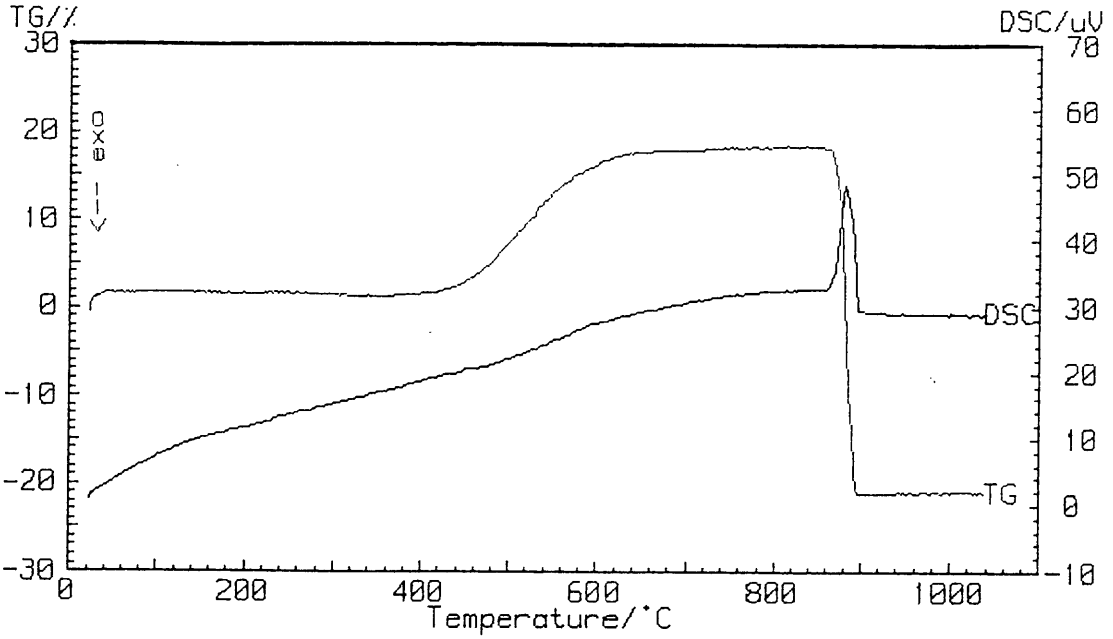

Figure 8.3 (c): TG and DSC curves of the thermal decomposition of $Ca(OH)_2$ decomposing in a CO_2/air-atmosphere using a heating rate of 5 °C min^{-1}

There is a triple-step mass loss in the air/water-atmosphere (figure 8.3 (d)) and a two-step mass loss in the air-atmosphere (figure 8.3 (e)). From figure 8.3 (d), the first mass loss of ≈ 17 % at 405 to 498 °C, corresponds to the decomposition of the calcium hydroxide to calcium oxide. The mass loss of ≈ 13 % at 512 to 690 °C could be due to the calcium hydroxide not decomposing completely in the first step to calcium oxide and there could also be an overlapping decomposition reaction of the calcium carbonate starting to decompose to calcium oxide as well. The third mass loss at 690 to 800 °C, corresponds to the decomposition of calcium carbonate to calcium oxide.

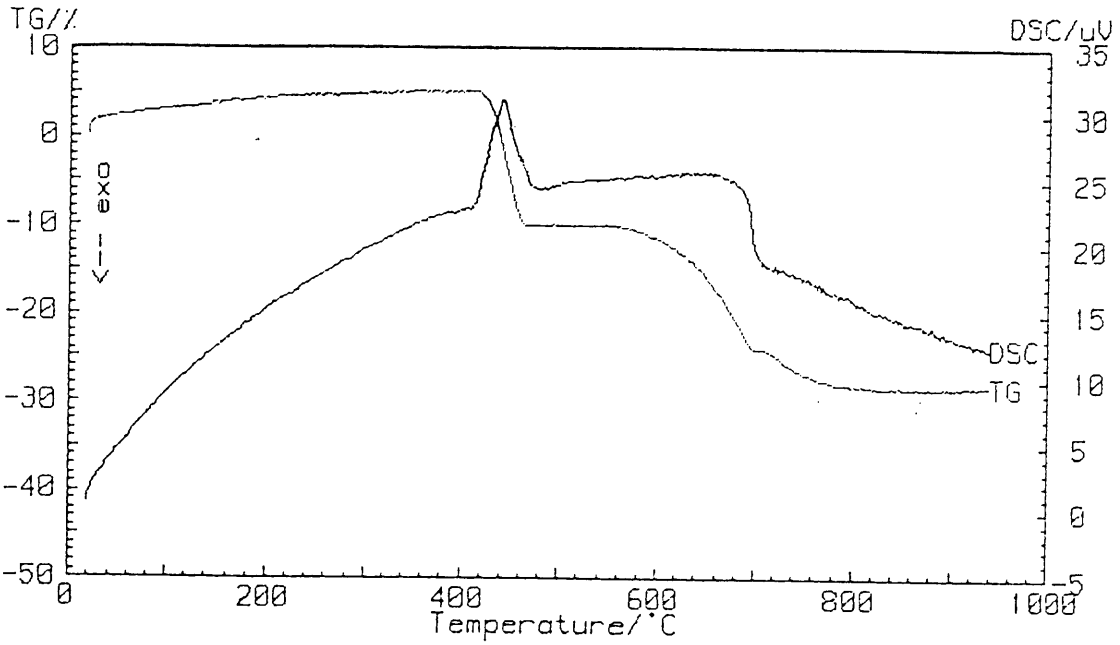

Figure 8.3 (d): **TG and DSC curves of the thermal decomposition of $Ca(OH)_2$ decomposing in an air/water-atmosphere using a heating rate of 5 °C min^{-1}**

The mass loss in the temperature region 396 to 518 °C in the air-atmosphere corresponds to the decomposition of calcium hydroxide

$$Ca(OH)_2(s) \rightarrow CaO(s) + H_2O(g).$$

The mass loss in the 553 to 759 °C temperature region could be due to the calcium hydroxide not decomposing completely in the first step to calcium oxide and there could also be an overlapping decomposition reaction of

some calcium carbonate starting to decompose to calcium oxide as well

$$CaCO_3(s) \rightarrow CaO(s) + CO_2(g).$$

The theoretical mass loss of $CaCO_3$ decomposing to CaO is 43.96%. The experimental value obtained in this temperature region is 18 % which is made up of the calcium hydroxide and possibly some calcium carbonate decomposition. If this second mass loss is only due to the calcium carbonate decomposition then it would indicate that ≈ 40 % of the sample is calcium carbonate. This is highly unlikely as the decomposition of calcium carbonate starts at a higher temperature than the 553 °C found here.

In the CO_2/H_2O-atmosphere (figure 8.3 (b)), the mass gain appears to be less than in the CO_2-atmosphere. As the calcium hydroxide decomposes to calcium oxide, there is an immediate uptake of CO_2, to form calcium carbonate. The recarbonation is ≈ 33 % in the CO_2-atmosphere and ≈ 28 % in the CO_2/H_2O-atmosphere. The partial pressure of CO_2 plays a role in the recarbonation reactions as can be seen in the reduced mass gain and mass loss values for the CO_2/air-atmospheres as compared to those obtained in the CO_2-atmosphere.

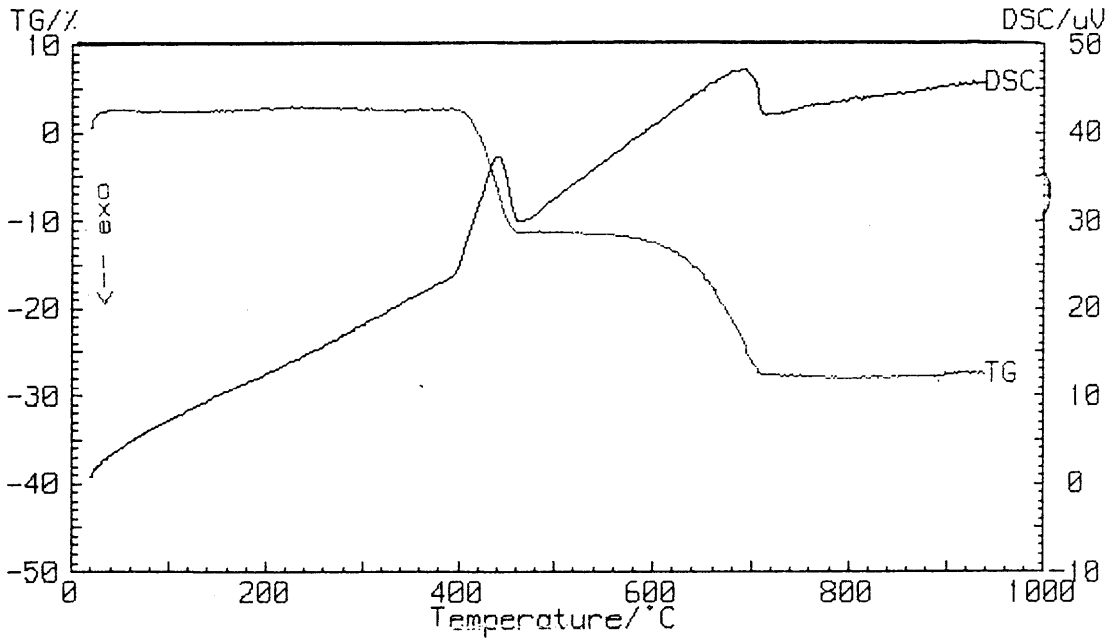

Figure 8.3 (e): **TG and DSC curves of the thermal decomposition of $Ca(OH)_2$ decomposing in an air-atmosphere using a heating rate of 5 °C min^{-1}**

8.3.1 Kinetics of the thermal decomposition of calcium hydroxide to calcium oxide in an air-atmosphere

The thermal decomposition reactions of calcium hydroxide, decomposing in an air-atmosphere, shows two mass losses. The kinetics of these two reactions are followed from 340 °C to 485 °C (which corresponds to the decomposition of the calcium hydroxide) and from 495 °C to 815 °C (which possibly corresponds to the overlapping decomposition reactions of calcium hydroxide and of the impurity, calcium carbonate, present). From figure 8.3.1 (a), it appears that the decomposition reaction from 340 °C to 485 °C does not take place via a single-step reaction. The average activation energy increases from ≈ 0 to 500 kJ mol^{-1} for $0 < \alpha < 0.2$. The ascending character of the activation energy is due to the increasing contribution made to the heat absorbed by the reaction with the higher activation energy [85].

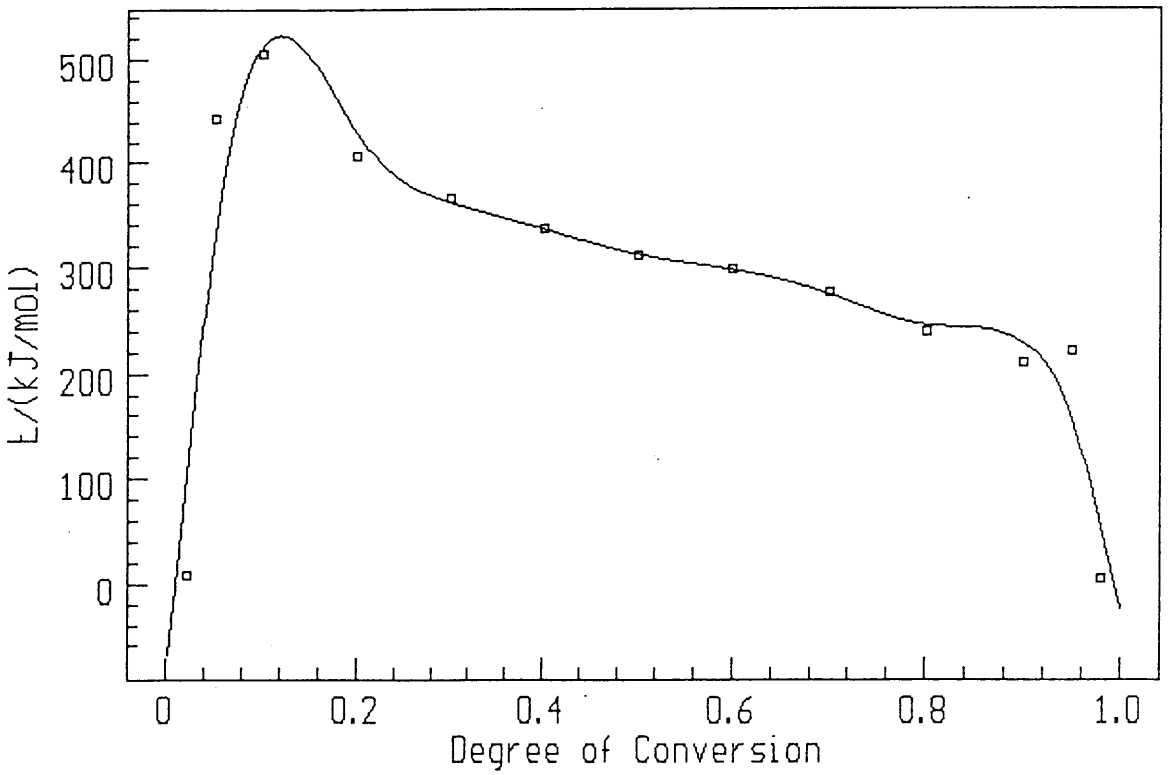

Figure 8.3.1 (a): Plot of activation energy versus fraction decomposed for the thermal decomposition reaction of calcium hydroxide to calcium oxide in an air-atmosphere from 340 °C to 485 °C

The activation energy then decreases slightly until it remains more or less constant at ≈ 369 kJ mol^{-1} for $0.3 < \alpha < 0.9$. It is concluded that a single activation energy governs the overall process rate as the activation energy remained constant as the degree of conversion changed. The activation energy then decreases from ≈ 369 to 20 kJ mol^{-1} for $0.9 < \alpha < 1.0$. Thus, it is assumed that there is a decreasing dependence on the contribution made by the reaction with the higher activation energy, to the overall reaction [85]. The kinetic models are fitted for $0 < \alpha < 0.2$, $0.2 < \alpha < 0.3$, $0.3 < \alpha < 0.9$ and $0.9 < \alpha < 1.0$.

No kinetic model is found to fit the experimental data for $0 < \alpha < 0.2$, $0.2 < \alpha < 0.3$ and $0.9 < \alpha < 1.0$.

The kinetic models which appear to fit $0.3 < \alpha < 0.9$, are the second order equation and the one-dimensional diffusion equation. The activation energy obtained for the second order equation is 415 kJ mol^{-1} with a ln A value of 29. The correlation coefficient is 0.9716 and the Durbin-Watson value is 0.140. The isoconversional method gives an activation energy of ≈ 369 kJ mol^{-1} and a ln A of ≈ 25. The one-dimensional diffusion equation gives an activation energy of 446 kJ mol^{-1}, a ln A value of 30, a correlation coefficient of 0.9405 and a Durbin-Watson value of 0.131. The second order equation gives a reasonable agreement on comparing its activation energy with that obtained from the isoconversional method and it has a better correlation coefficient. But the one-dimensional diffusion equation has a better Durbin-Watson value. The one-dimensional diffusion equation describes the mass transfer, diffusion through the product layer (CaO) and the heat transfer through the sample. The plot of the activation energy versus fraction decomposed, however, does not suggest diffusion [89]. Thus, the one-dimensional diffusion equation does not appear to fit the experimental data.

The thermal decomposition reaction from 495 °C to 815 °C, is possibly due to overlapping reactions as discussed previously. Figure 8.3.1 (b) shows that this decomposition does not take place via a single-step reaction.

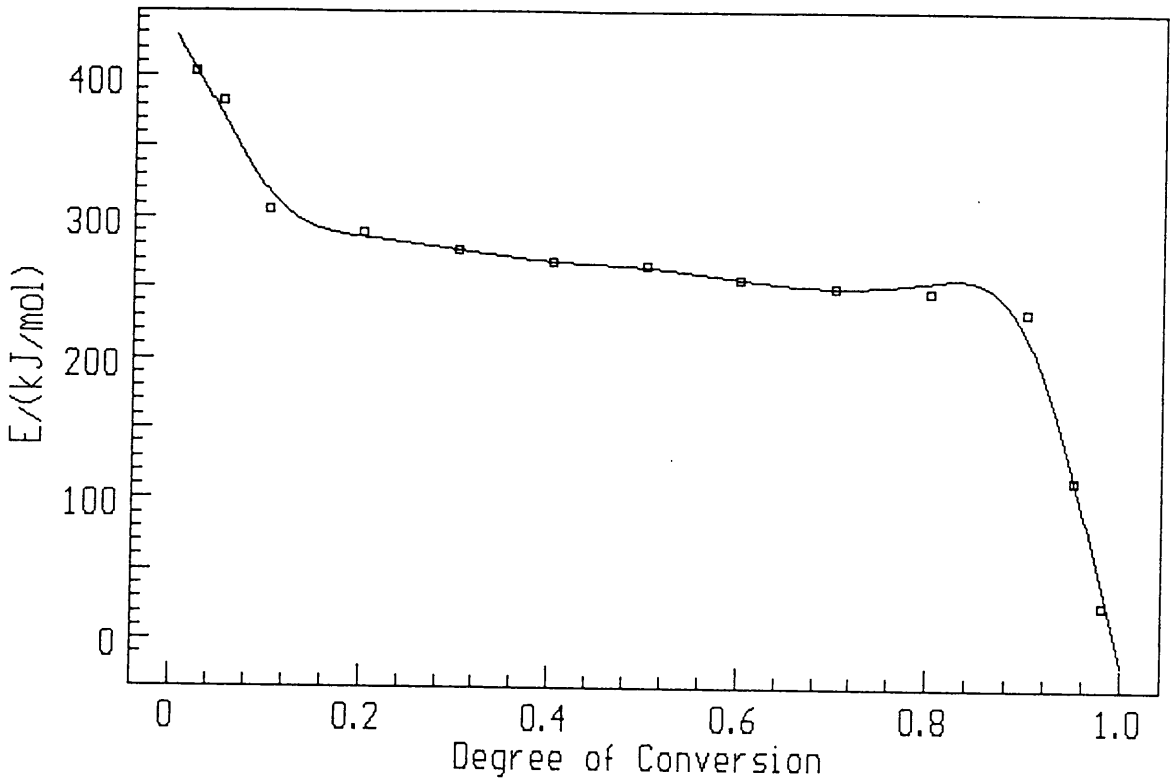

Figure 8.3.1 (b): Plot of activation energy versus fraction decomposed from 495 °C to 815 °C for calcium carbonate impurity decomposing to calcium oxide in an air-atmosphere

The activation energy decreases from ≈ 400 to ≈ 289 kJ mol^{-1} for $0 < \alpha < 0.1$, where it remains more or less constant at ≈ 289 kJ mol^{-1}. For $0.9 < \alpha < 1.0$, the activation energy decreases from ≈ 289 to ≈ 40 kJ mol^{-1}. The contribution to the overall reaction, by the reaction with the higher activation energy, decreases [85]. No kinetic models fit the experimental data for $0 < \alpha < 0.1$ and $0.9 < \alpha < 1.0$. The following kinetic models appear to fit the range $0.1 < \alpha < 0.9$: the d-dimensional Avrami-Erofe'ev equation, the first order equation (the activation energy is 245 kJ mol^{-1}, ln A value of 11; a correlation coefficient of 0.9965 and a Durbin-Watson value of 0.054) and the second order equation (with an activation energy value of 297 kJ mol^{-1}, a ln A value of 14; a correlation coefficient of 0.9933 and a Durbin-Watson value of 0.061). The best fit on comparing the correlation coefficients appears to be the d-dimensional Avrami-Erofe'ev

equation (figure 8.3.1 (c)) with an activation energy value of 267 kJ mol^{-1}, a ln A value of 12, a correlation coefficient of 0.9972 and a Durbin-Watson value of 0.069. The isoconversional method gives an activation energy value of ≈ 289 kJ mol^{-1} and a ln A value of ≈ 14. But on comparing the activation energy values, ln A values and the Durbin-Watson values, the second order equation (figure 8.3.1 (d)) appears to be a good fit.

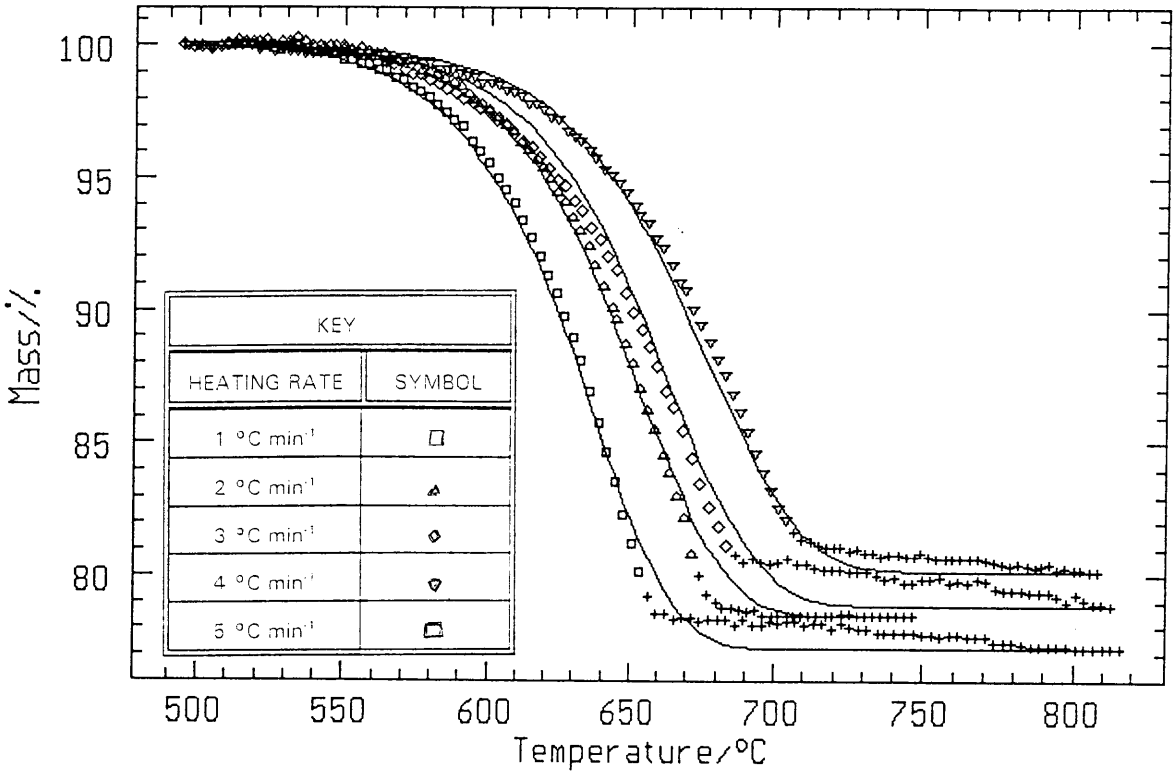

Figure 8.3.1 (c): Fitting of the d-dimensional Avrami-Erofe'ev kinetic model for the decomposition reaction at 495 to 815 °C in an air-atmosphere

There is no correlation between the kinetic data and models obtained for the decomposition reaction of pure calcium carbonate (see table 8.2.2) in an air-atmosphere and that obtained for the calcium carbonate impurity present in the calcium hydroxide. It is clear that these overlapping reactions follow a more complex mechanism.

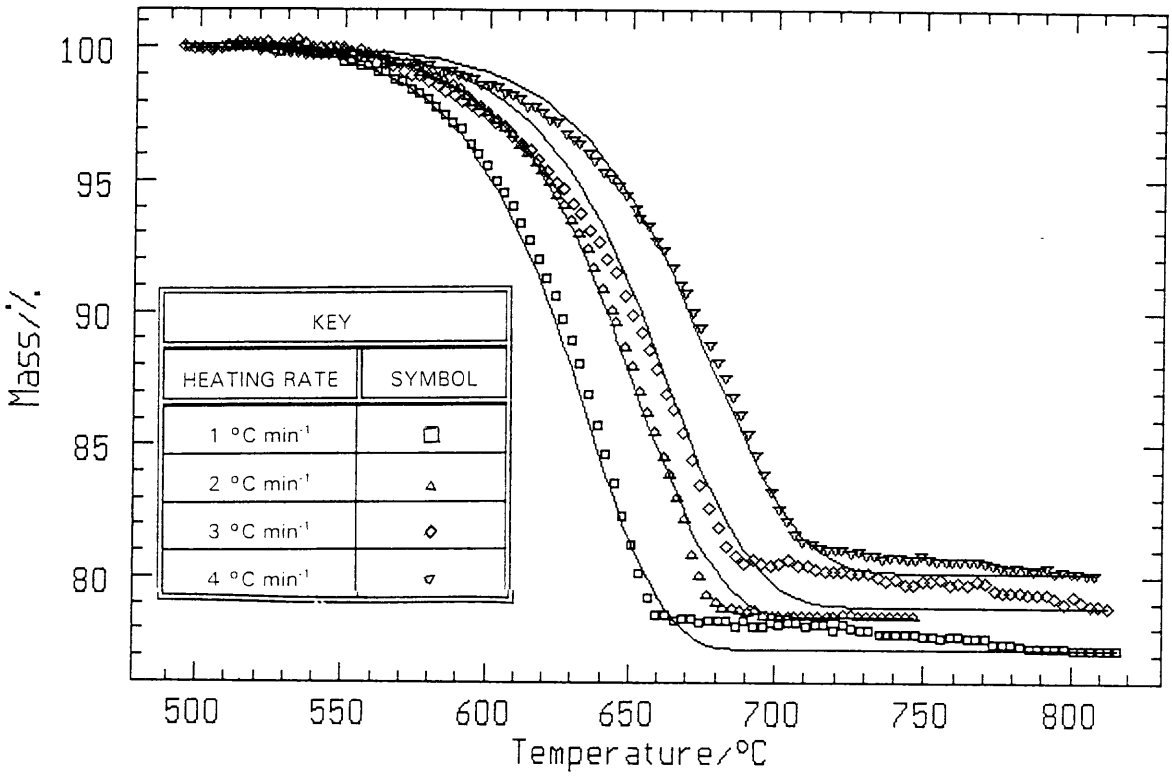

Figure 8.3.1 (d): Fitting of the second order equation for the decomposition reaction at 495 °C to 815 °C in an air-atmosphere

8.3.2 Kinetics of the thermal decomposition of calcium hydroxide to calcium oxide in an air/water-atmosphere

Figure 8.3.2 (a) shows a plot of activation energy, E_a, versus the fraction decomposed for the reactions from 345 °C to 575 °C for the first mass loss curve. The thermal decomposition of calcium hydroxide to calcium oxide appears to proceed through more than a single-step reaction. The activation energy increases from ≈ - 80 kJ mol^{-1} (refer to Chapter 9.3) to ≈ 420 kJ mol^{-1} for $0 < \alpha < 0.2$. This increase has already been discussed previously (refer to section 8.3.1). The average activation energy then remains more

or less constant at ≈ 354 kJ mol^{-1} until α = 0.8 where it decreases (see section 8.3.1) to ≈ - 60 kJ mol^{-1} (refer to Chapter 9.3). The kinetic models are fitted over the 0.2 < α < 0.8 range and the following kinetic models appear to fit: the first order with autocatalysis and the second order equation.

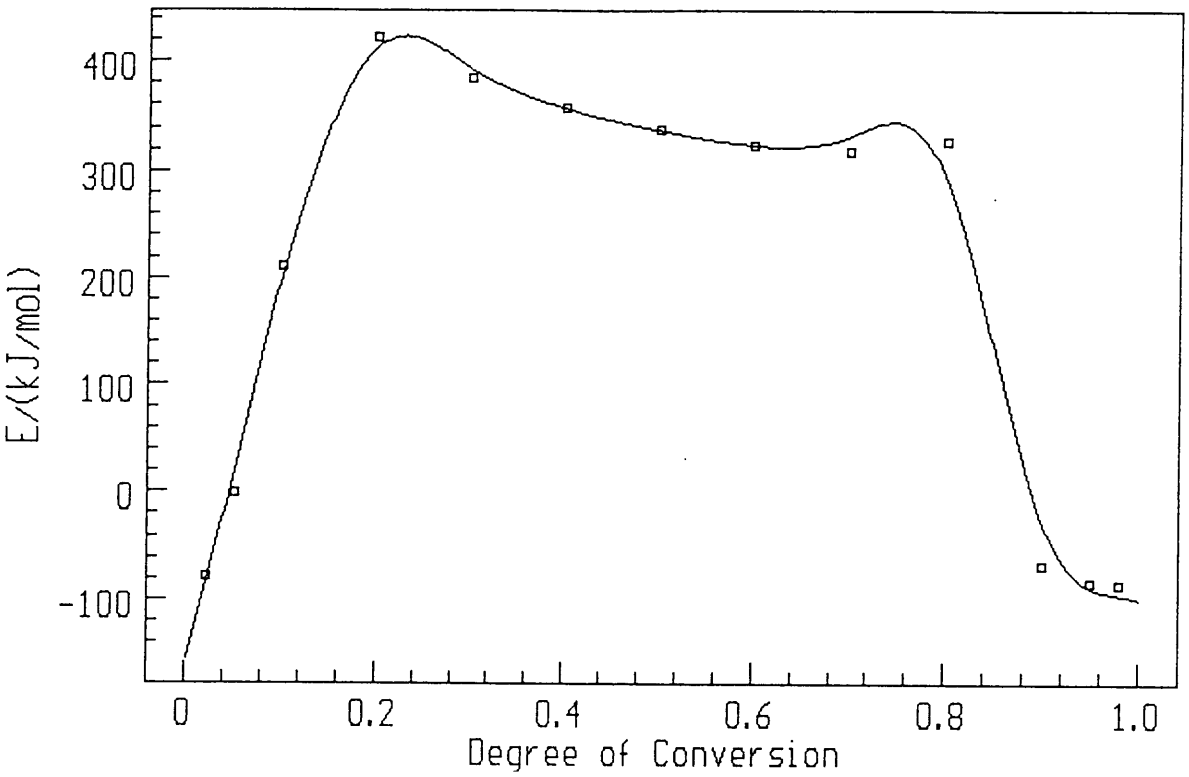

Figure 8.3.2 (a): Plot of activation energy, E_a, vs α for calcium hydroxide decomposing in an air/water-atmosphere

The isoconversional method gives an activation energy of ≈ 354 kJ mol $^{-1}$ and a ln A value of ≈ 23. Figure 8.3.2 (b) shows that the best fit of the kinetic model is the first order equation with autocatalysis with an activation energy of 344 kJ mol^{-1} and a ln A of 23. The correlation coefficient is 0.9682 and the Durbin-Watson value is 0.086.

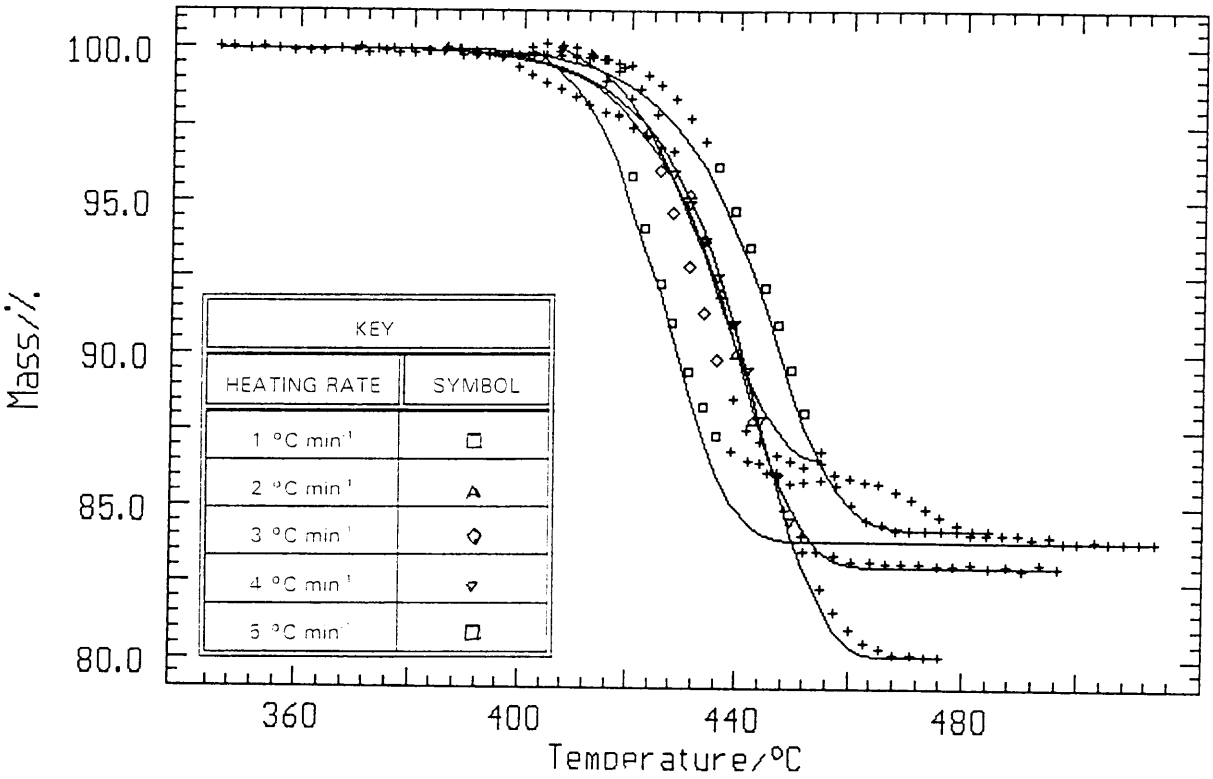

Figure 8.3.2 (b): The first order equation with autocatalysis kinetic model fitted to the experimental data of calcium hydroxide decomposing in an air/water-atmosphere

An activation energy of 430 kJ mol^{-1} and a ln A of 29 is obtained for the second order equation (figure 8.3.2 (c)). The correlation coefficient is 0.9557 and the Durbin-Watson value is 0.168. The first order kinetic model with autocatalysis implies that as the calcium hydroxide decomposes to calcium oxide, the nuclei of the calcium oxide, are forming at the sites present and by a mechanism referred to as branching. Nucleation might occur along dislocation lines.

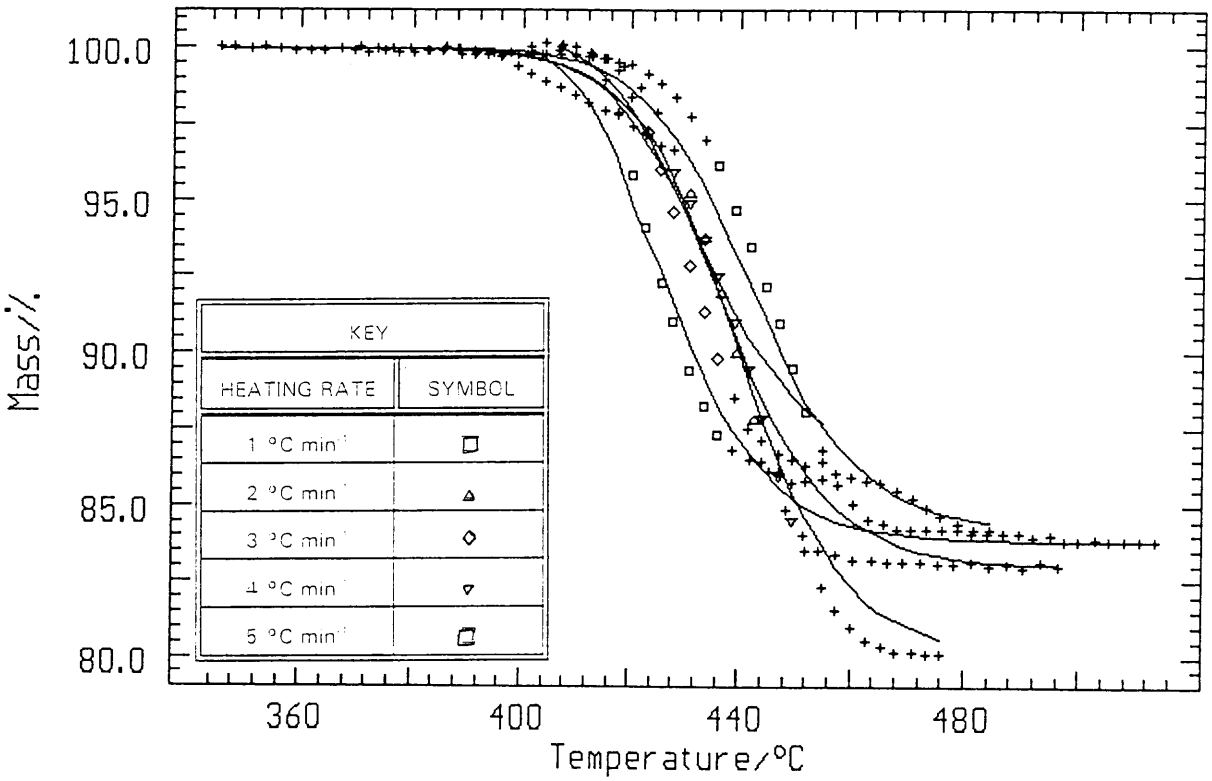

Figure 8.3.2 (c): The second order kinetic model fitted to the experimental data of calcium hydroxide decomposing in an air/water-atmosphere

For the α-range, $0 < \alpha < 0.2$, the activation energy obtained from the isoconversional method is between $\approx$ - 80 and 420 kJ mol^{-1} and a ln A value of $\approx$ 3. None of the kinetic models fit the experimental data in this range.

None of the kinetic models fit the experimental data for $0.8 < \alpha < 1.0$. The isoconversional method gives an average activation energy value of between $\approx$ - 354 to - 60 kJ mol^{-1} (refer to Chapter 9.3) and a ln A value of ≈ 3.

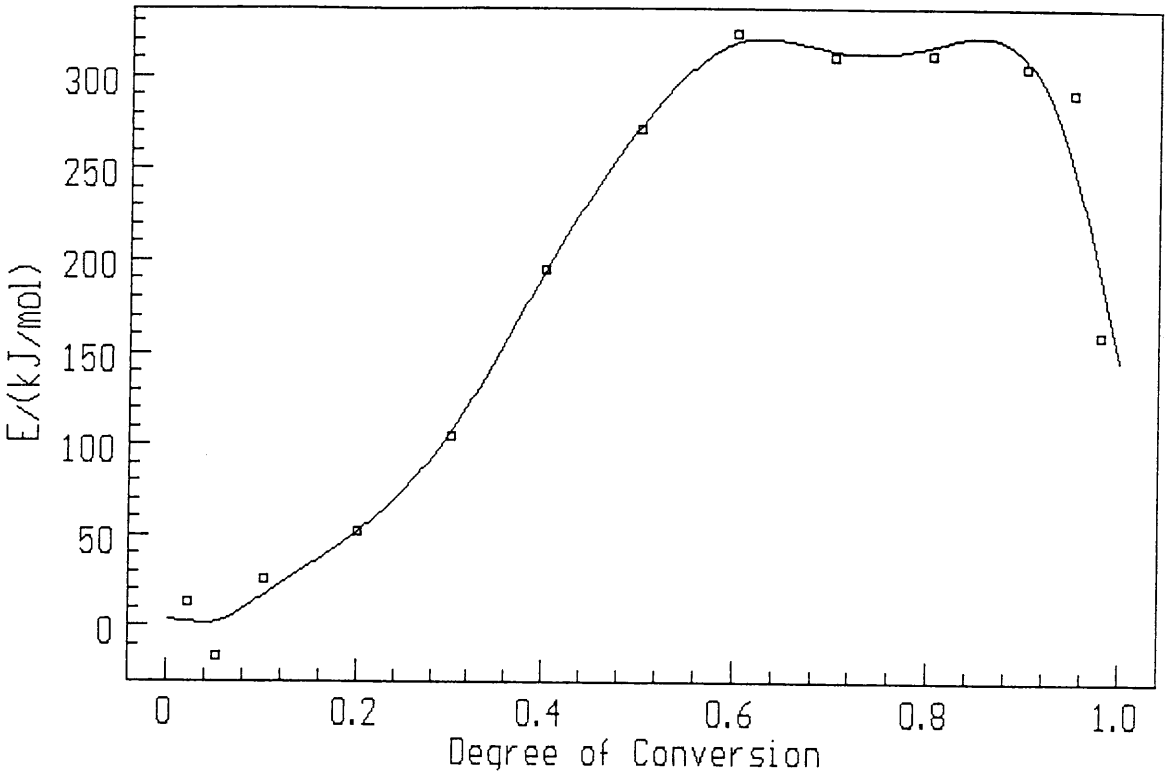

Figure 8.3.2 (d): Plot of activation energy versus fraction decomposed for calcium hydroxide decomposing to calcium oxide in an air/water-atmosphere for the second mass loss curve between 580 °C to 770 °C

The kinetic models are applied to the second mass loss curve from 580 °C to 770 °C. From figure 8.3.2 (d), it is clear that the decomposition reaction does not occur in a single step and there are possibly overlapping reactions taking place as discussed previously. For $0 < \alpha < 0.6$, none of the kinetic models fit the experimental data. The average activation energy increases from $\approx$ 0 to $\approx$ 309 kJ mol^{-1} and ln A $\approx$ 3 for $0 < \alpha < 0.6$, where it remains constant at $\approx$ 309 kJ mol^{-1} and a ln A $\approx$ 13 until $\alpha = 0.9$. The increase in activation energy indicates that the reaction with the higher activation energy makes a significant contribution to the heat absorbed [85]. On reaching the maximum, the temperature dependence of the process rate is governed by one activation energy. The best fit for $0.6 < \alpha < 0.95$, appears to be the three-dimensional diffusion equation of Ginstling-Brounshtein (figure 8.3.2 (e)).

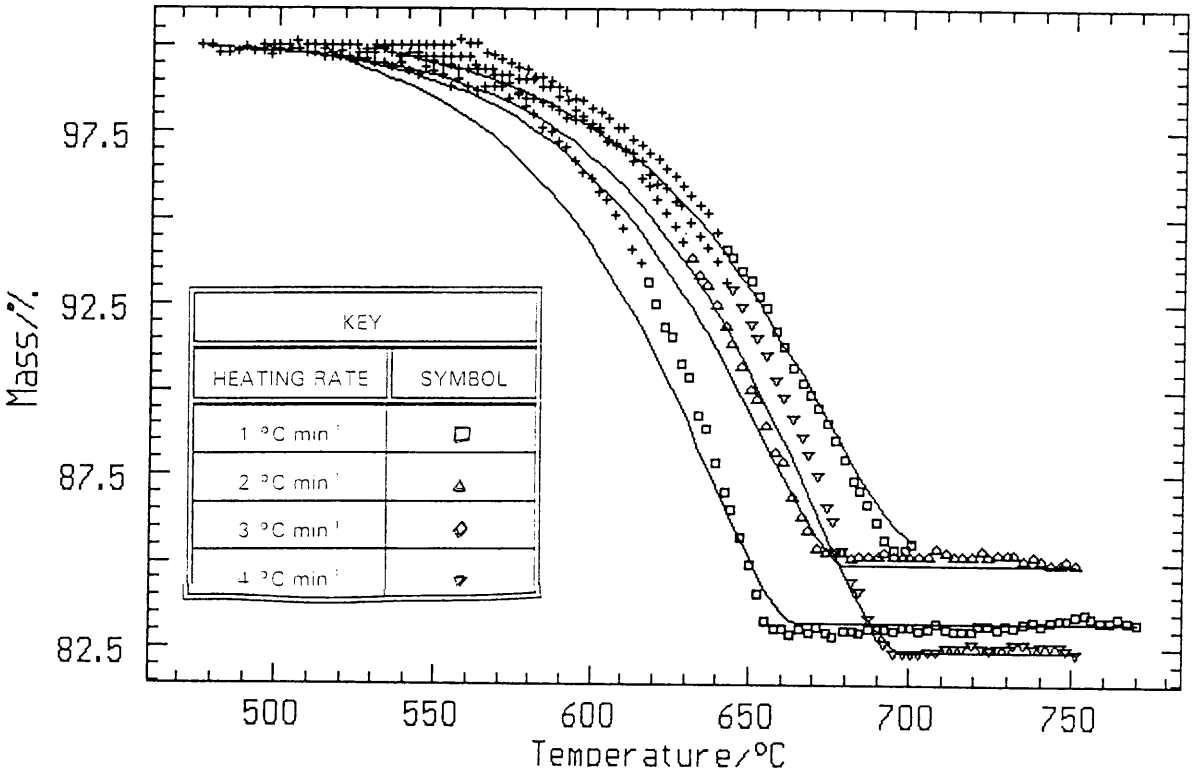

Figure 8.3.2 (e): Fitting of experimental data of the decomposition of calcium hydroxide to calcium oxide in an air/water-atmosphere with the kinetic model of the three-dimensional diffusion equation of Ginstling-Brounshtein for the second mass loss curve between 580 to 770 °C

The activation energy obtained from this kinetic model is 303 kJ mol^{-1}, ln A = 13, the Durbin-Watson value = 0.040 and the correlation coefficient is 0.9874. From the Ginstling-Brounshtein equation, it can be said that the reaction is governed by diffusion. Nucleation, growth of the nuclei and the advance of the reaction interface is dominant. No kinetic model appears to fit $0.95 < \alpha < 1.0$. The average activation energy decreases from $\approx$ 309 to $\approx$ 160 kJ mol^{-1} which indicates that the contribution made to the heat absorbed by the reaction with the higher activation energy, is decreasing [85].

There is no correlation between the kinetic data and models obtained for the decomposition reaction of pure calcium carbonate (see table 8.2.2) in an

air/water-atmosphere and that obtained for the calcium carbonate impurity present in the calcium hydroxide.

8.3.3 Kinetics of the thermal decomposition of calcium hydroxide to calcium oxide in a CO_2-atmosphere

The thermal decomposition reaction of calcium hydroxide to calcium oxide in a CO_2-atmosphere, is followed from 595 °C to 960 °C. Figure 8.3.3 (a) shows a plot of activation energy versus fraction decomposed for calcium hydroxide in a CO_2-atmosphere.

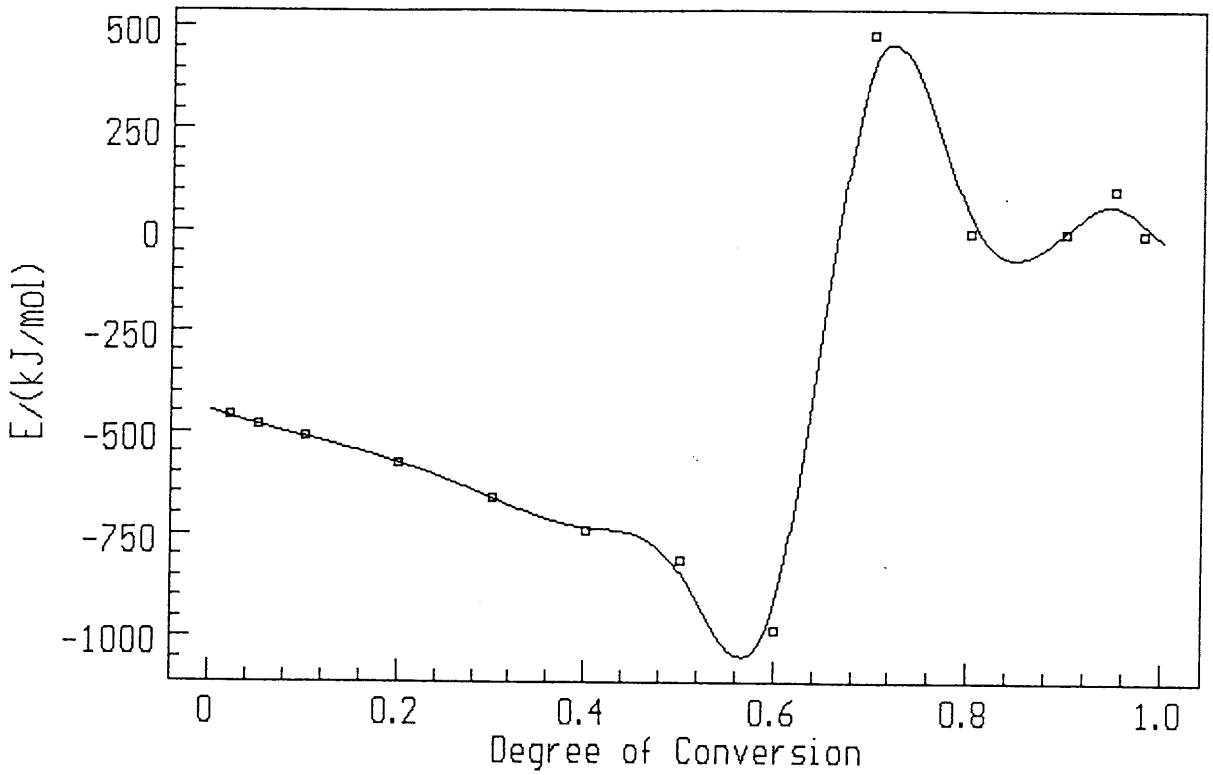

Figure 8.3.3 (a): Plot of activation energy, E_a, vs α for calcium hydroxide decomposing in a CO_2-atmosphere

From figure 8.3.3 (a), the activation energy decreases between 0 and 0.5

($\approx$ - 450 to $\approx$ - 1000 kJ mol^{-1} (refer to Chapter 9.3) and ln A $\approx$ 27) and then increases between 0.5 and 0.7 ($\approx$ - 1000 to $\approx$ 500 kJ mol^{-1}), and then decreased for 0.7 < α < 1.0 ($\approx$ 500 to $\approx$ 50 kJ mol^{-1} and ln A $\approx$ 2). None of the kinetic models appear to fit the experimental data for 0 < α < 0.5, 0.5 < α < 0.7 and 0.7 < α < 1.0.

8.3.4 Kinetics of the thermal decomposition of calcium hydroxide to calcium oxide in a CO_2/air-atmosphere

The kinetic data obtained for calcium carbonate decomposing in a CO_2/air-atmosphere from 620 °C to 970 °C, showed an increase in activation energy ($\approx$ 600 to $\approx$ 2900 kJ mol^{-1}) from 0 < α < 0.1 , then a decrease ($\approx$ 2900 to $\approx$ 1000 kJ mol^{-1}) for 0.1 < α < 0.6, after which it remains constant at an activation energy value of $\approx$ 50 kJ mol^{-1} (figure 8.3.4 (a)).

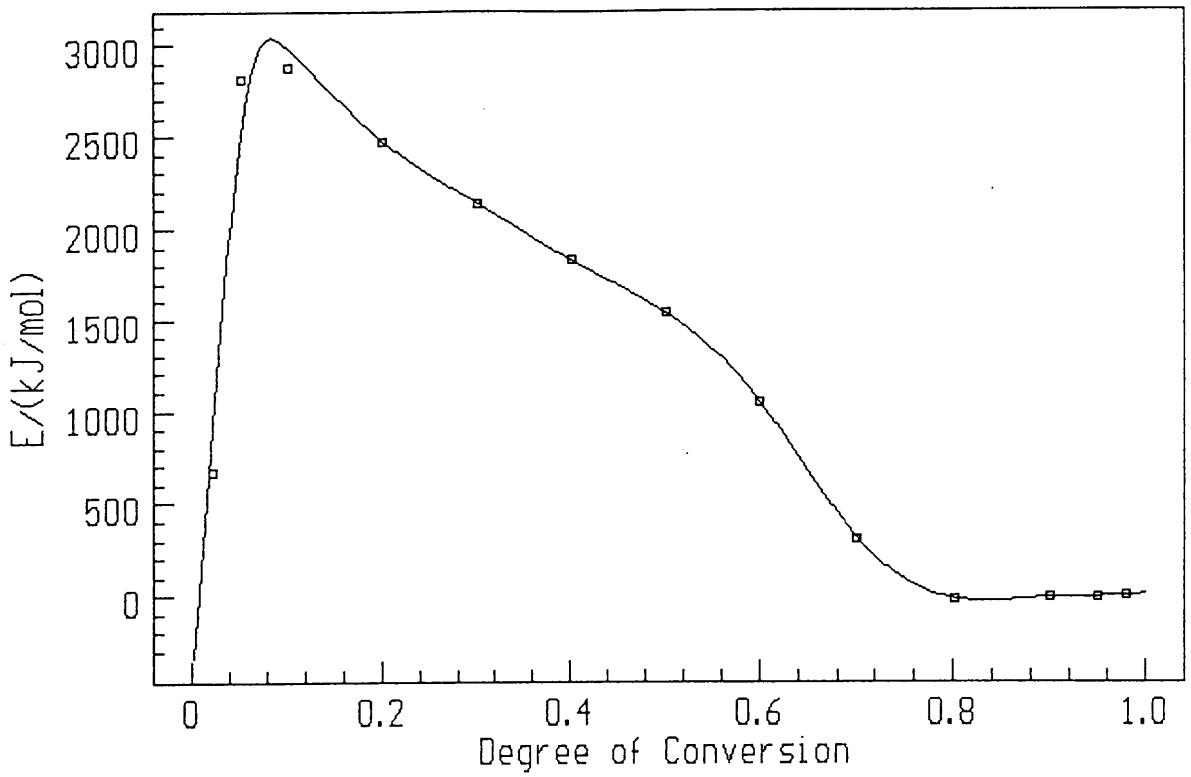

Figure 8.3.4 (a): Plot of E_a vs α for calcium hydroxide decomposing to calcium oxide in a CO_2/air-atmosphere

The various contributions that are made to the heat absorbed, is discussed

in Chapter 8.3.2.

For $0.1 < \alpha < 0.6$, the kinetic model that fits the best is the second order equation (figure 8.3.4 (b)) giving an activation energy value of 2436 kJ mol^{-1} and a ln A of 108. The correlation coefficient is 0.9608 and the Durbin-Watson value is 0.324. The average activation energy value of $\approx$ 2900 to $\approx$ 1000 kJ mol^{-1}, and a ln A value of $\approx$ 93, for $0.1 < \alpha < 0.6$ is obtained from the isoconversional method.

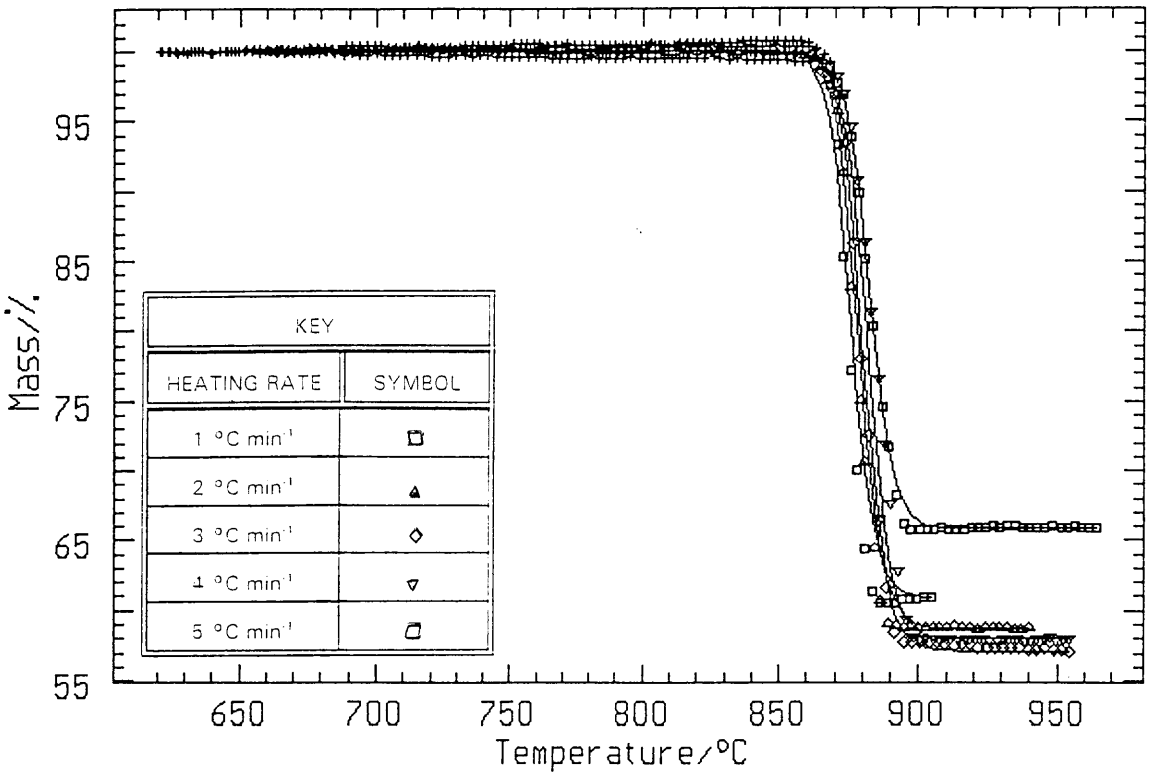

Figure 8.3.4 (b): Fitting of the second order kinetic model for calcium hydroxide decomposing to calcium oxide in a CO_2/air-atmosphere for $0.1 < \alpha < 0.6$

The decomposition reaction for $0.7 < \alpha < 1.0$ can be best described by the second order equation. The second order equation (figure 8.3.4 (c)) gives a correlation coefficient of 0.9926, a Durbin-Watson value of 0.297, an activation energy value of 2659 kJ mol^{-1} and ln A of 119. This does not compare with the average activation energy obtained of $\approx$ 50 kJ mol^{-1} and

In A ≈ -1 (refer to Chapter 9.3) from the isoconversional method in this α-range.

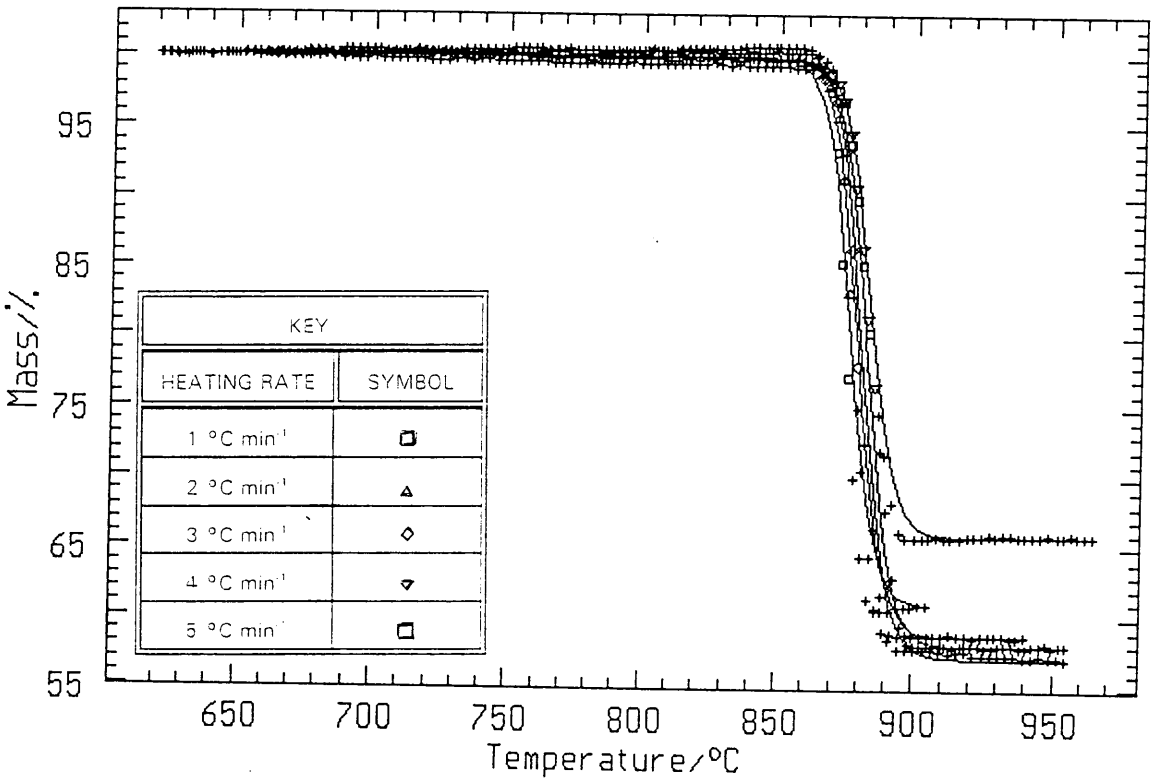

Figure 8.3.4 (c): Fitting of the second order equation for calcium hydroxide decomposing to calcium oxide in a CO_2/air-atmosphere for $0.7 < \alpha < 1.0$

8.3.5 Kinetics of the decomposition of calcium hydroxide to calcium oxide in a CO_2/water-atmosphere

From figure 8.3.5 (a), it is clear that the decomposition reaction does not occur in a single step for calcium hydroxide decomposing in a CO_2/water-atmosphere from 600 °C to 960 °C. There are at least two steps. From the shape of the plot of activation energy versus fraction decomposed, it is clear that the dependence is complex and the low activation energy with a high degree of fraction decomposed, is characteristic of the diffusion of a gas [89]. For $0 < \alpha < 0.7$, none of the kinetic models appear to fit the

experimental data. The isoconversional method gives an average activation energy of ≈ 64 kJ mol^{-1} and ln A of ≈ -1 (refer to Chapter 9.3). For 0.7 < α < 1.0, the average activation energy decreases from ≈64 to ≈0 kJ mol^{-1}. No kinetic models were found to fit the experimental data for 0.7 < α < 1.0.

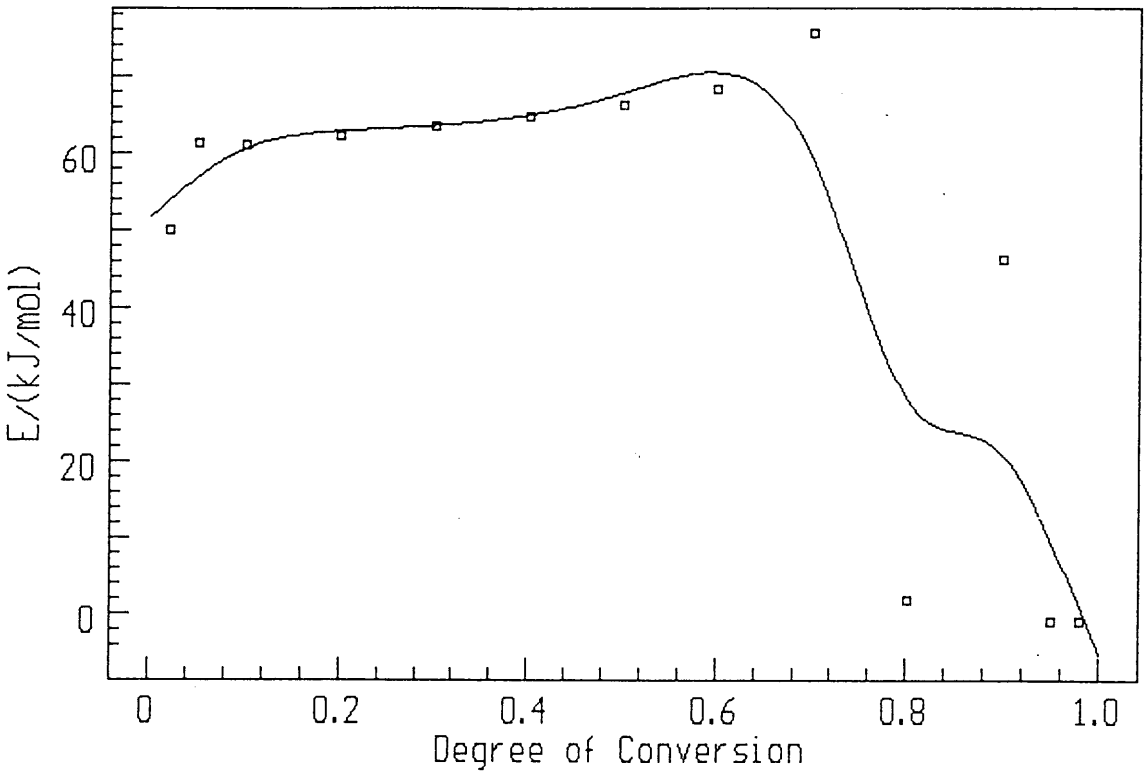

Figure 8.3.5 (a): Plot of E_a vs α for calcium hydroxide decomposing to calcium oxide in a CO_2/water-atmosphere

Table 8.3.1 is a summary of all the kinetic data for the decomposition of calcium hydroxide to calcium oxide in the different atmospheres used.

Table 8.3.1 Summary of the kinetic data of the thermal decomposition of calcium hydroxide and recarbonated CaO in different atmospheres

Atmosphere	Temperature Range (°C)	Fraction Decomposed	Kinetic Data from the Isoconversional Method		Kinetic Data from the Kinetic Models			
					Kinetic Model			
			E_a (kJ mol^{-1})	ln A	E_a (kJ mol^{-1})	ln A	D-W	Corr. Coeff.
Air	340 - 485	$0 < \alpha < 0.2$	0 - 500	-	no fit			
		$0.2 < \alpha < 0.3$	500 - 369	-	no fit			
					second order			
		$0.3 < \alpha < 0.9$	369	25	415	29	0.140	0.9716
					or one-dimensional diffusion equation			
					446	30	0.131	0.9405
		$0.9 < \alpha < 1.0$	200 - 0	-	no fit			
	495 - 815 (recarbonated CaO)	$0 < \alpha < 0.1$	400 - 289	-	no fit			
					d-dimensional Avrami-Erofe'ev			
		$0.1 < \alpha < 0.9$	289	14	267	12	0.069	0.9972
					or second order equation			
					297	14	0.061	0.9933
		$0.9 < \alpha < 1.0$	289 - 40	-	no fit			
Air/water	345 - 575	$0 < \alpha < 0.2$	(- 80) - 420	3	no fit			
					first order with autocatalysis			
		$0.2 < \alpha < 0.8$	354	23	344	23	0.086	0.9682
		$0.8 < \alpha < 1.0$	354 - (- 60)	3	no fit			
	580 - 770 (recarbonated CaO)	$0 < \alpha < 0.6$	0 - 309	3	no fit			
					Ginstling-Brounshtein equation			
		$0.6 < \alpha < 0.95$	309	15	303	13	0.040	0.9874
		$0.95 < \alpha < 1.0$	309 - 160	-	no fit			
CO_2	595 - 960	$0 < \alpha < 0.5$	(-450 to -1000)	27	no fit			
		$0.5 < \alpha < 0.7$	(-1000) - 500	-	no fit			
		$0.7 < \alpha < 1.0$	500 - 50	2	no fit			
CO_2/air	620 - 970	$0 < \alpha < 0.1$	600 - 2900	-	no fit			
					second order			
		$0.1 < \alpha < 0.6$	2900 - 1000	93	2436	108	0.324	0.9608
					second order			
		$0.7 < \alpha < 1.0$	50	-1	2659	119	0.291	0.9926
CO_2/water	600 - 960	$0 < \alpha < 0.7$	64	-1	no fit			
		$0.7 < \alpha < 1.0$	64 - 0	-	no fit			

Key of abbreviations used in the table: E_a = activation energy; D-W = Durbin-Watson value and Corr. Coeff. = correlation coefficient.

8.4 CALCIUM OXIDE

Table 8.4.1 The reactions of calcium oxide in different atmospheres using a heating rate of 5 °C min^{-1} with sample masses between 5 - 15 mg

Atmosphere	Temperature Range (°C)	Mass Loss (%)	Mass Gain (%)	ΔH (kJ g^{-1})
Air	347 - 408 402 - 536 551 - 787	5 - 4	- 2 -	2×10^{-1} - -
Air/H_2O	43 - 360 360 - 456 456 - 734	- 9 4	- - -	- 3×10^{-1} -
CO_2	79 - 285 285 - 882 882 - 954	2 - 49	- 45 -	- - 2
CO_2/Air	75 - 208 208 - 838 939 - 967	1 - 43	- 38 -	- - 2
CO_2/H_2O	33 - 75 78 - 337 337 - 516 517 - 858 864 - 927	- - - - 52	2 3 13 29 -	- - - - 1

The reactions of calcium oxide (CaO) in air-atmosphere shows two small mass losses at 347 and 551 °C due to the decomposition of the impurities, calcium hydroxide and calcium carbonate respectively, that are present (figure 8.4 (a)).

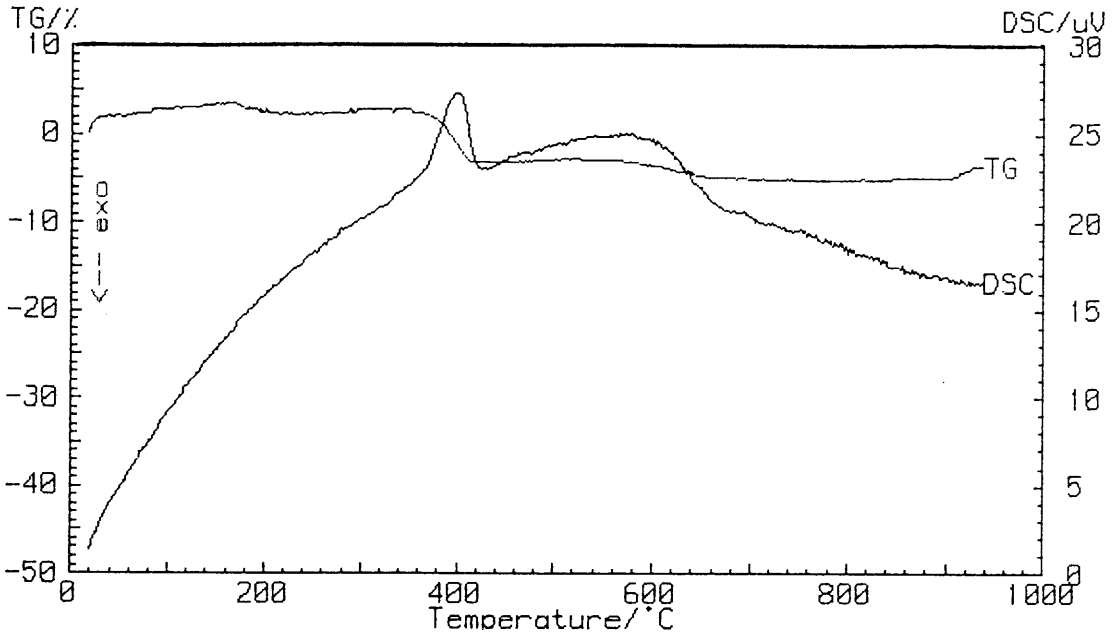

Figure 8.4 (a): **TG and DSC curves of the thermal decomposition of calcium carbonate and calcium hydroxide impurities in the CaO sample in an air-atmosphere using a heating rate of 5 °C min^{-1}**

The total mass loss in air/water-atmosphere (figure 8.4 (b)), is double the mass loss found in the air-atmosphere. This is due to the calcium oxide reacting with the water vapour to form calcium hydroxide. Theoretically, 32.1 % water vapour can be taken up but under these conditions, 5 % mass gain is observed. This indicates that ≈ 16 % of the calcium oxide, is rehydrated. On reaching the decomposition temperature of the calcium hydroxide, it decomposes to calcium oxide.

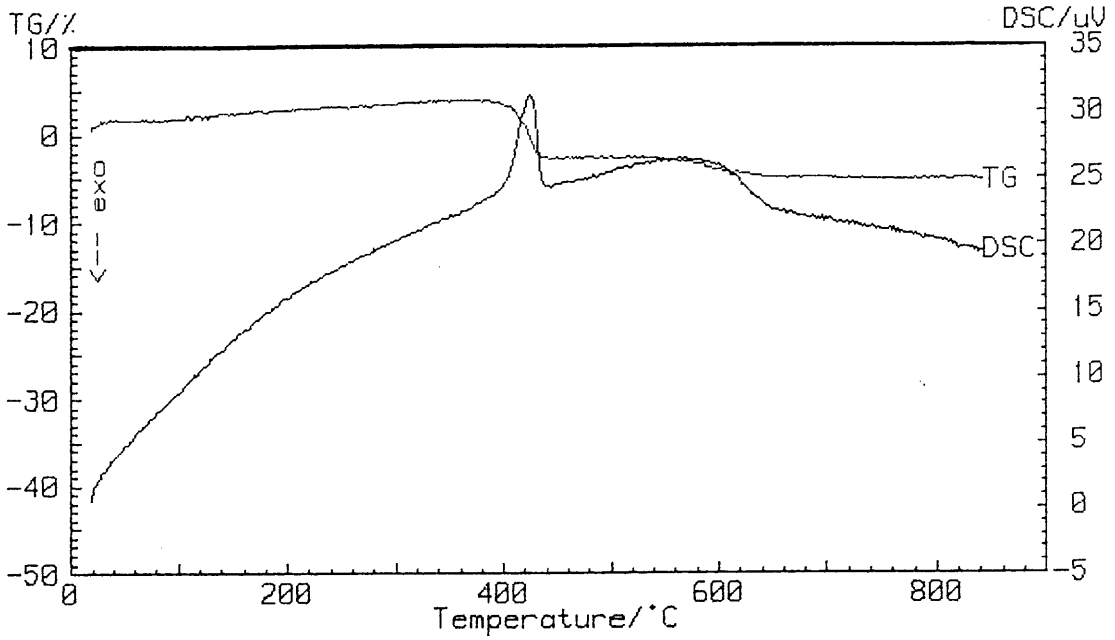

Figure 8.4 (b): **TG and DSC curves of the thermal decomposition of the impurities in the CaO sample and of the calcium hydroxide obtained via the reaction of CaO with the air/water-atmosphere using a heating rate of 5 °C min^{-1}**

The thermal reactions in a CO_2-atmosphere shows a mass loss from 79 °C due to the loss of adsorbed water. A substantial mass gain of 45 % is observed with onset at 285 °C which is due to the formation of $CaCO_3$:

$$CaO(s) + CO_2(g) \rightarrow CaCO_3(s).$$

The theoretical mass gain is 78.6 %. This indicates that ≈ 57 % of the sample is successfully recarbonated under these conditions. The total mass loss (79 °C to 954 °C) is 49 % and is due to the dehydration of some calcium hydroxide impurity present and the decarbonation of the calcium carbonate that forms (figure 8.4(b)).

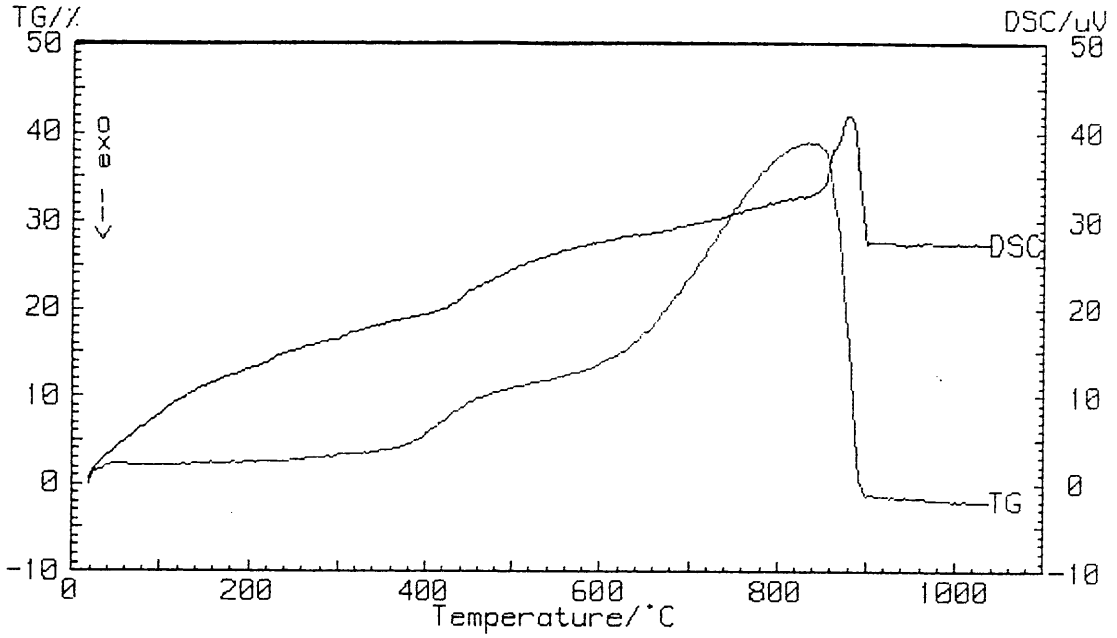

Figure 8.4(c): **TG and DSC curves of the thermal decomposition of the impurities in the CaO sample and of the calcium carbonate obtained via the reaction of CaO with the CO_2/air-atmosphere using a heating rate of 5 °C min^{-1}**

The thermal reaction of CaO in a CO_2/air-atmosphere (figure 8.4 (c)) shows the same tendencies as for a CO_2-atmosphere (figure 8.4 (d)). The only difference being that the mass loss and the mass gain is less and the onset temperatures are lower than for those in a CO_2-atmosphere. This indicates that the partial pressure of carbon dioxide plays a significant role in the recarbonation reactions.

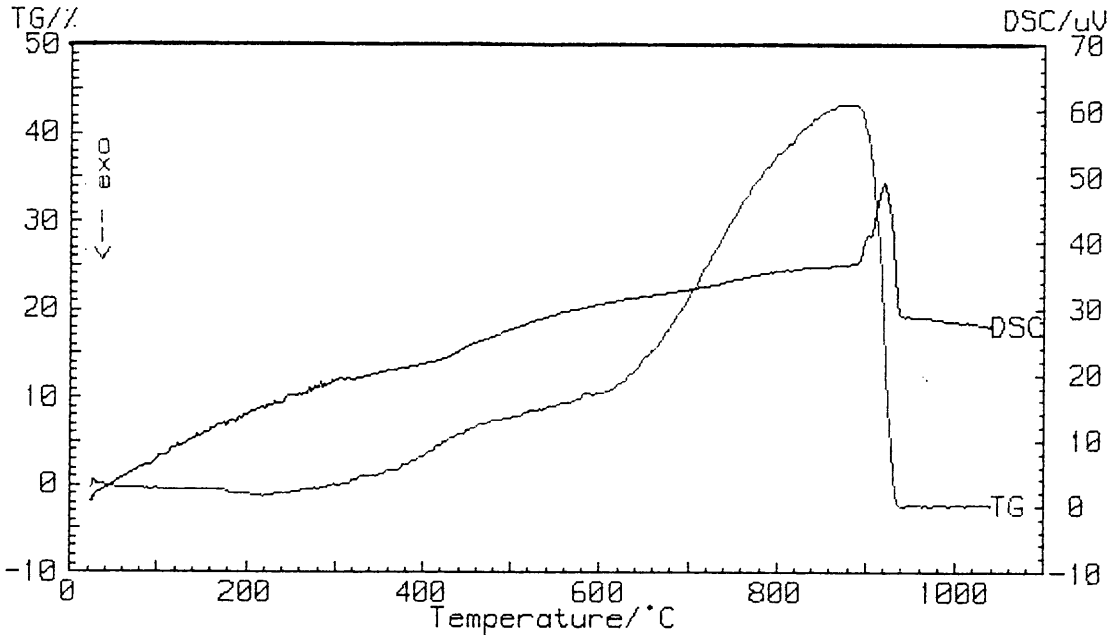

Figure 8.4(d): **TG and DSC curves of the thermal decomposition of the impurities in the CaO sample and of the calcium carbonate obtained via the reaction of CaO with the CO_2-atmosphere using a heating rate of 5 °C min^{-1}**

The mass gain curves of CaO in a CO_2/water-atmosphere (figure 8.4 (e)) differ from those found in the CO_2-atmosphere.

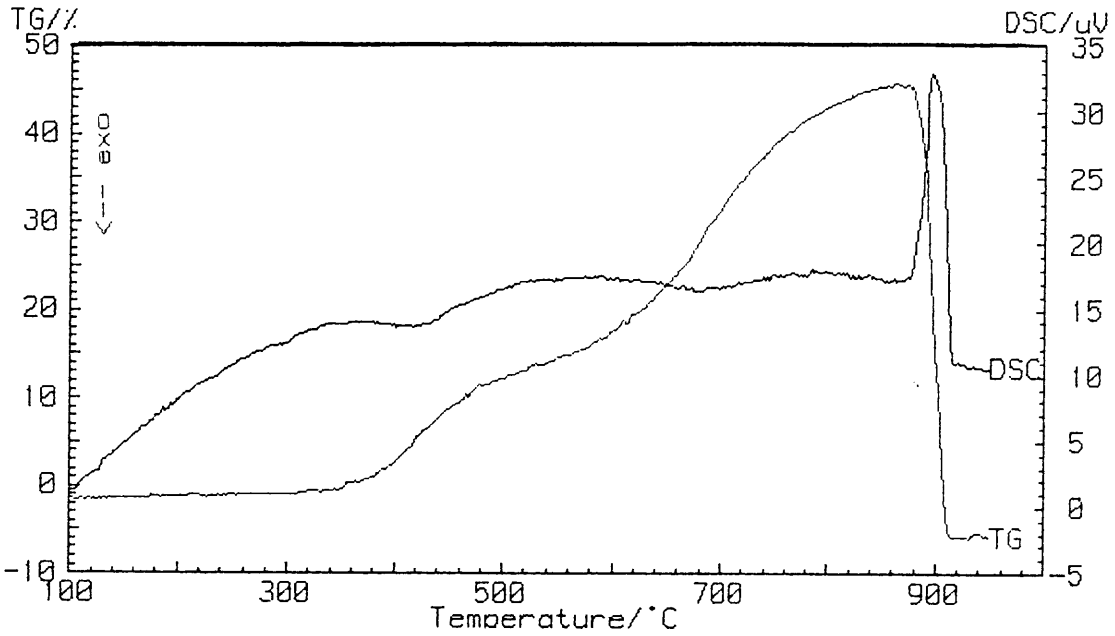

Figure 8.4(e): **TG and DSC curves of the thermal decomposition of the impurities in the CaO sample and of the calcium carbonate obtained via the reaction of CaO with the CO_2/water-atmosphere using a heating rate of 5°C min^{-1}**

In the CO_2-atmosphere, there are four mass gain steps of 2; 3; 13 and 29 % respectively at 33 °C; 78 °C; 337 °C and 517 °C onset temperatures respectively. The first mass gain steps can be due to the adsorption of water by the CaO to form $Ca(OH)_2$. The subsequent mass gain steps can be due to the reaction of CaO with the CO_2 to form $CaCO_3$. The total mass gain is ≈ 47 %. The recarbonation (≈ 60 %) appears to be more successful in the CO_2/H_2O-atmosphere than in the CO_2-atmosphere. The presence of water vapour appears to enhance the uptake of CO_2.

The total mass loss of 52 % with onset at 864 °C in the CO_2/water-atmosphere is the highest mass loss obtained for all the different atmospheres. The total mass loss is 9 % in an air-atmosphere.

8.4.1 Kinetics of the decomposition reaction of calcium carbonate obtained via the reactions of calcium oxide with an air-atmosphere

The thermogram shows two mass losses which correspond to the thermal decomposition of the impurities in the calcium oxide, namely calcium hydroxide and calcium carbonate. Figure 8.4.1 (a) shows a plot of activation energy, E_a, versus α (fraction decomposed) for the first decomposition reaction of the calcium hydroxide impurity from 310 °C to 450 °C in an air-atmosphere.

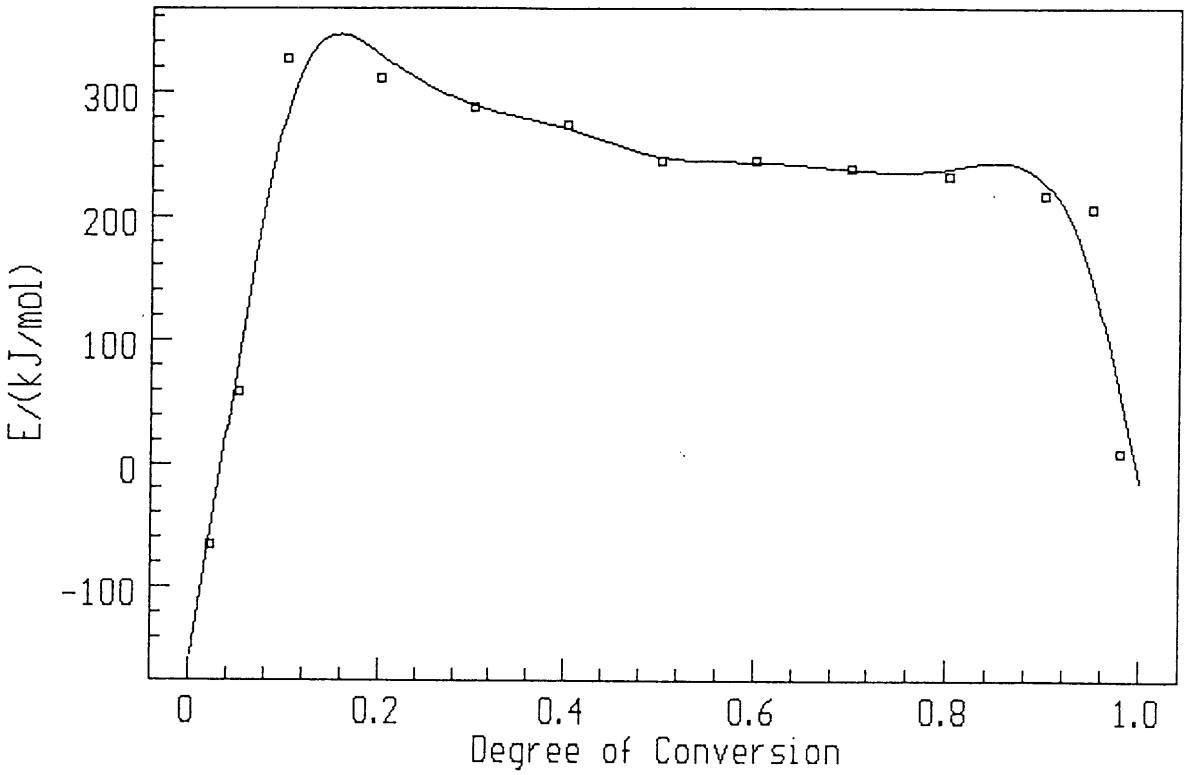

Figure 8.4.1 (a): Plot of activation energy, E_a, vs α for calcium hydroxide impurity in the calcium oxide, decomposing to calcium oxide in an air-atmosphere

It is clear that the decomposition reaction does not occur in a single step. The activation energy increases between 0 and 0.1 where it remains constant at a value of $\approx$ 259 kJ mol^{-1} until α = 0.95. The ln A value is $\approx$ 18 for $0.2 < \alpha < 0.95$. The ascending part of the dependence indicates that the reaction with the higher activation energy makes a growing contribution to the heat absorbed [85]. On reaching the maximum, the

dependence is constant indicating that the temperature dependence of the overall process rate is governed by one activation energy. The dependence then becomes descending indicating that there is a decreasing contribution of the reaction with the higher activation energy [85].

None of the kinetic models appear to give a conclusive fit for $0 < \alpha < 0.1$. The isoconversional method gives an average activation energy value varying between $\approx$ 0 to - 100 kJ mol^{-1} and a ln A value of $\approx$ 8. The kinetic model which describes the decomposition reaction the best, is the first order equation with autocatalysis kinetic model (figure 8.4.1 (b)) which gives a corresponding activation energy value of 124 kJ mol^{-1}, a ln A value of 7, a correlation coefficient of 0.9382 and a Durbin-Watson value of 1.013. The n-th order equation gives a higher activation energy value of 144 kJ mol^{-1}, a ln A value of 18, a correlation coefficient of 0.9326 and a Durbin-Watson value of 0.950.

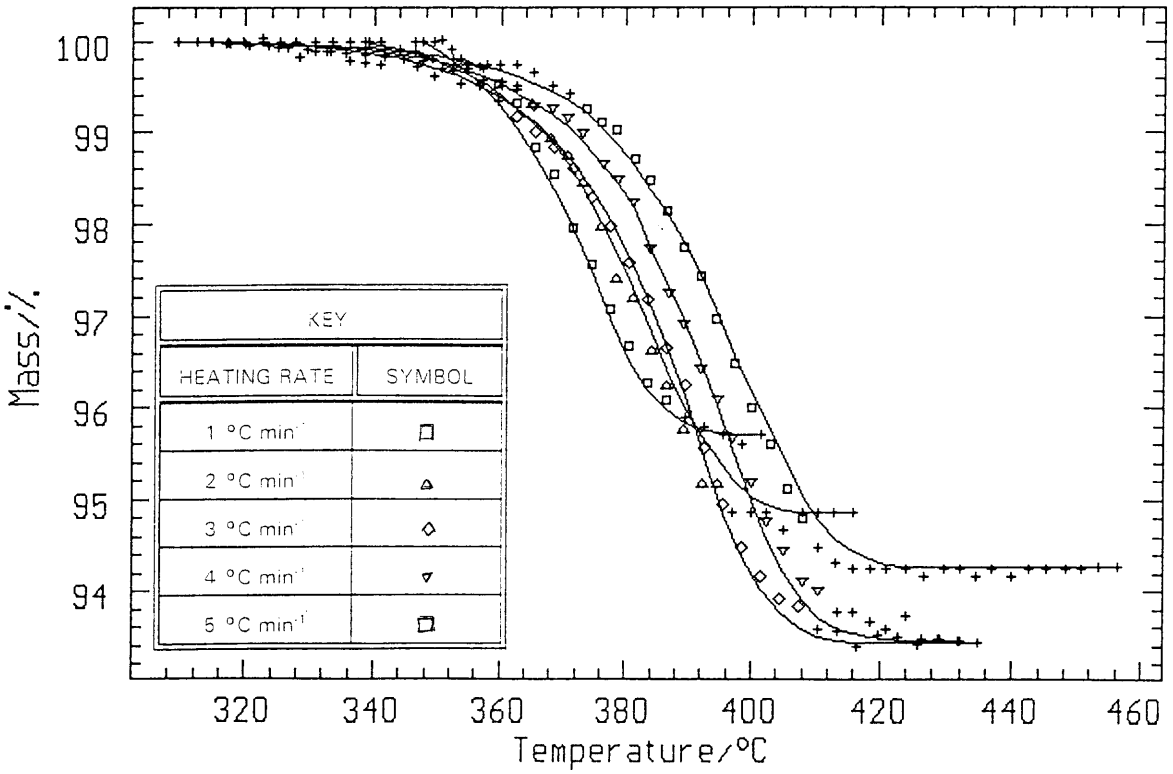

Figure 8.4.1 (b): Fitting of the first order with autocatalysis for the decomposition reaction of the calcium hydroxide impurity present in the calcium oxide for $0 < \alpha < 0.1$ in an air-atmosphere

The first order kinetic model with autocatalysis implies that as the calcium hydroxide impurity decomposes to calcium oxide, the nuclei of the calcium oxide, are forming at the sites present and by a mechanism referred to as branching.

On comparing this data to the data obtained for the "pure" calcium hydroxide in section 8.4.1, it does not correspond because it appears that the calcium hydroxide decomposes to calcium oxide via the second order kinetic model (activation energy value was 415 kJ mol^{-1} with a ln A value of 29; a correlation coefficient of 0.9716 and a Durbin-Watson value of 0.140).

The kinetic models are fitted to the α-range, $0.1 < \alpha < 0.95$, and the following models appear to fit: the Sestak-Berggren equation (correlation coefficient = 0.9960; Durbin-Watson value = 0.327; activation energy value = 211 kJ mol^{-1} and ln A value = 14) , the d-dimensional Avrami-Erofe'ev equation (correlation coefficient = 0.9959; Durbin-Watson value = 0.312; activation energy value = 212 kJ mol^{-1} and ln A value = 14), the first order with autocatalysis (correlation coefficient = 0.9957; Durbin-Watson value = 0.301; activation energy value 214 kJ mol^{-1} and ln A value = 14), the n-th order (correlation coefficient = 0.9943; Durbin-Watson value = 0.252; activation energy value of 233 kJ mol^{-1} and ln A = 16) and the two-dimensional phase boundary (correlation coefficient = 0.9928; Durbin-Watson value = 0.227; activation energy value = 211 kJ mol^{-1} and ln A value = 14). The isoconversional method gives an average activation energy value of $\approx$ 259 kJ mol^{-1} and a ln A value of $\approx$ 18. The best kinetic model fit according to the comparison of the activation energy value with that obtained from the isoconversional method (which is not reaction mechanism dependent), is the n-th order kinetic model. Figure 8.4.1 (c) is the n-th order fit and Figure 8.4.1 (d) is the Sestak-Berggren fit which gave the best correlation coefficient fit.

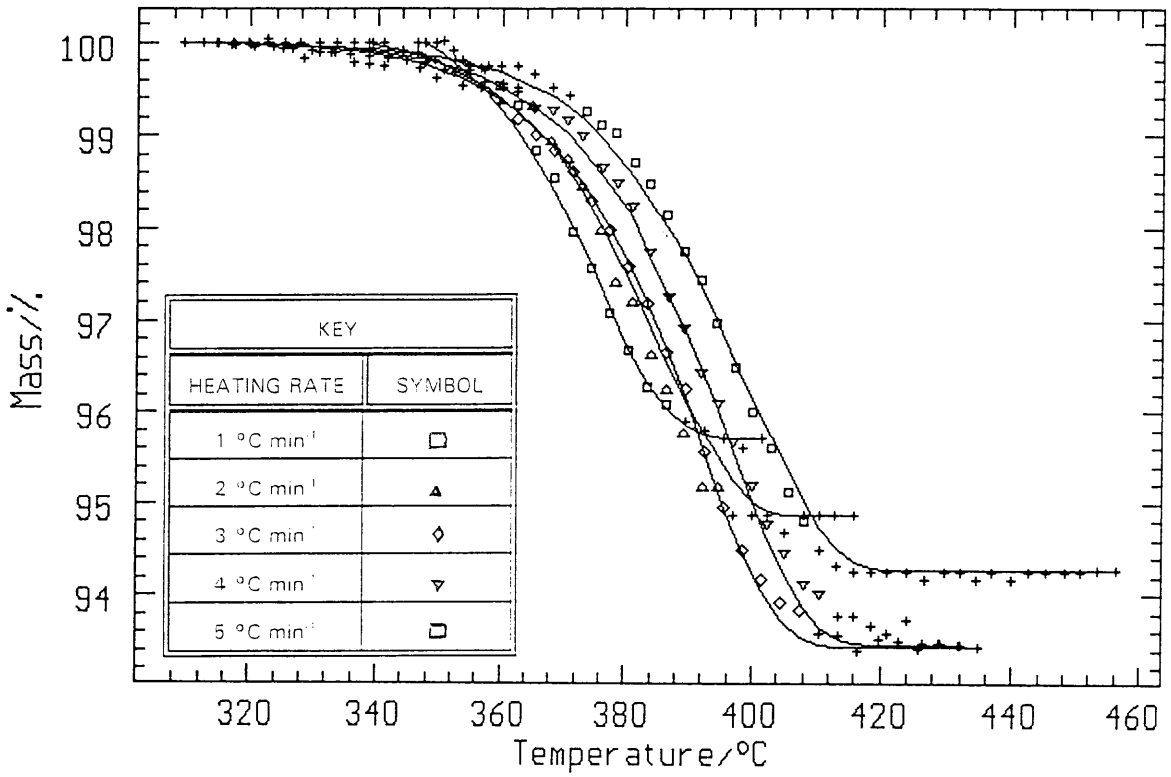

Figure 8.4.1 (c): Fitting of experimental data for $0.1 < \alpha < 0.95$ of calcium hydroxide impurity present in calcium oxide, decomposing to calcium oxide, with the kinetic model for a n-th order decomposition reaction in an air-atmosphere

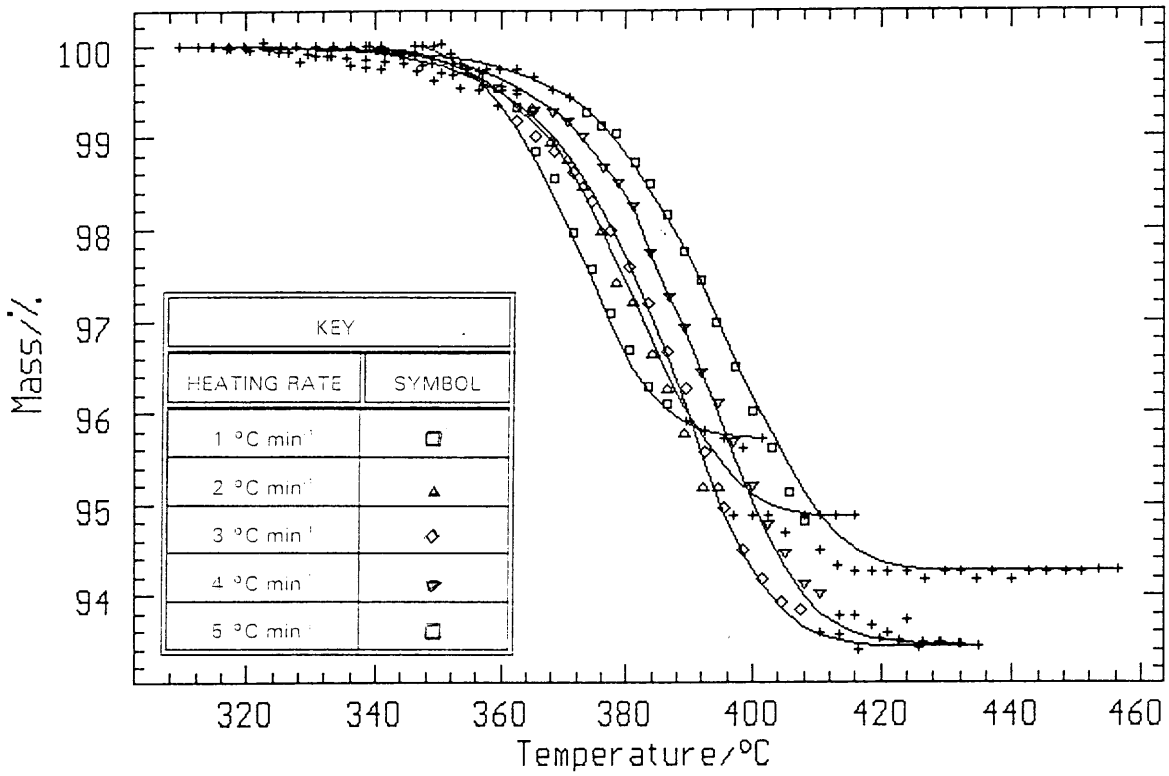

Figure 8.4.1 (d): Fitting of experimental data for $0.1 < \alpha < 0.95$ for the decomposition of the calcium hydroxide impurity present in calcium oxide, with the kinetic model for a Sestak-Berggren decomposition reaction in an air-atmosphere

The second mass loss curve which is due to the presence of calcium carbonate as an impurity in the calcium oxide. The kinetic models are fitted for the decomposition reactions from 525 °C to 700 °C. It is clear from figure 8.4.1 (e), that the decomposition reaction of the calcium carbonate does not occur in a single step. The activation energy decreases before it starts to increase until $\alpha = 0.5$, where it remains constant indicating a single-step reaction. At $\alpha = 0.95$, there is a decreasing contribution by the reaction with the higher activation energy. No kinetic models fit the range $0 < \alpha < 0.5$. The best fit over the range $0.5 < \alpha < 0.95$, is the second order equation. The activation energy obtained is 421 kJ mol^{-1} with a ln A of 23 for a correlation coefficient of 0.9594 and a Durbin-Watson value of

0.093. There is not a good correlation between the activation energy value obtained from the n-th order kinetic model and the isoconversional method (average activation energy value is ≈ 307 kJ mol^{-1} and the ln A value was ≈ 14). From section 8.2.1.1, the average activation energy recorded for $0.1 < \alpha < 1.0$ for "pure" calcium carbonate decomposing to calcium oxide, is 212 kJ mol^{-1} and ln A value of 8 using the n-th order equation with a correlation coefficient of 0.99996 and a Durbin-Watson value of 0.223.

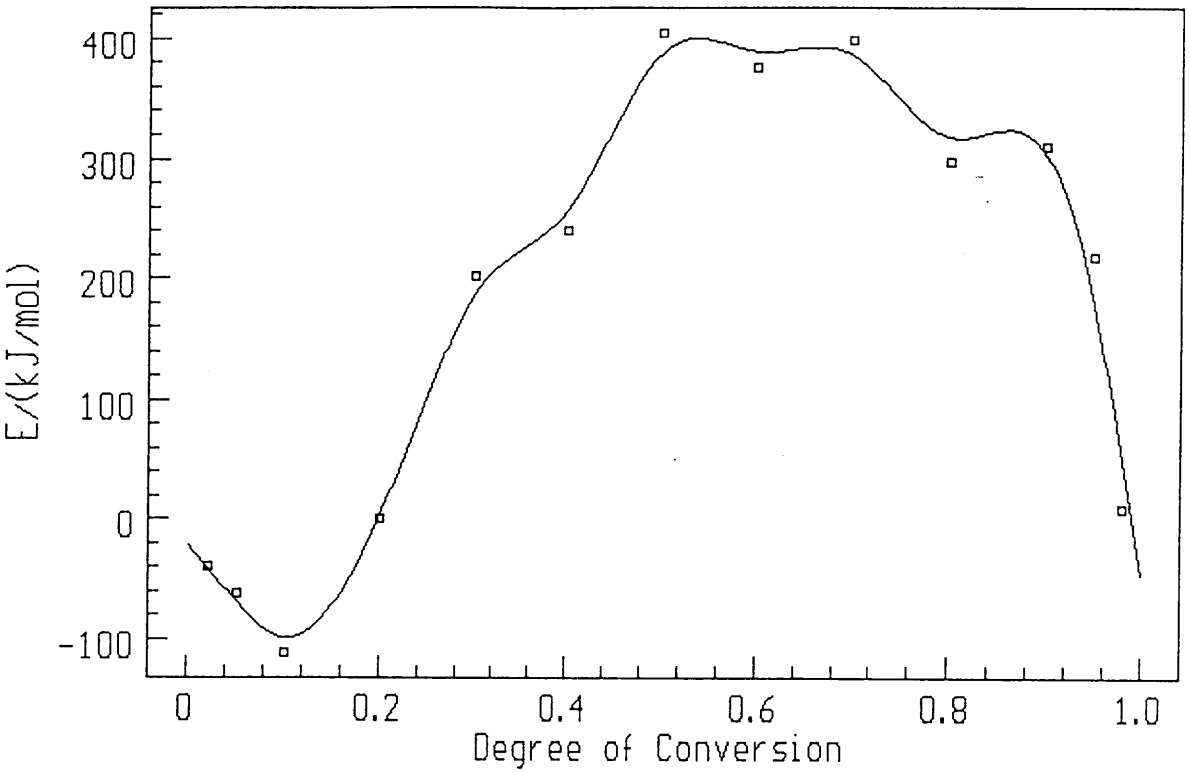

Figure 8.4.1 (e): Plot of activation energy versus fraction decomposed for the reaction of calcium oxide in an air-atmosphere for the second mass loss curve

8.4.2 Kinetics of the decomposition reaction of calcium carbonate obtained via the reactions of calcium oxide with an air/water-atmosphere

There are two mass loss curves obtained for the reaction of calcium oxide in an air/water-atmosphere. The kinetic models are fitted for the first mass loss curve from 300 °C to 450 °C. Figure 8.4.2 (a) shows a plot of activation energy, E_a, versus the fraction decomposed for this reaction. This corresponded to the decomposition of calcium hydroxide impurity present in the calcium oxide sample. The activation energy increases from ≈ 40 to ≈ 415 kJ mol^{-1} for $0 < \alpha < 0.3$. The activation energy then remains constant for $0.3 < \alpha < 0.95$ at ≈ 415 kJ mol^{-1}. The activation energy then increases slightly and then decreases to ≈ 360 kJ mol^{-1}.

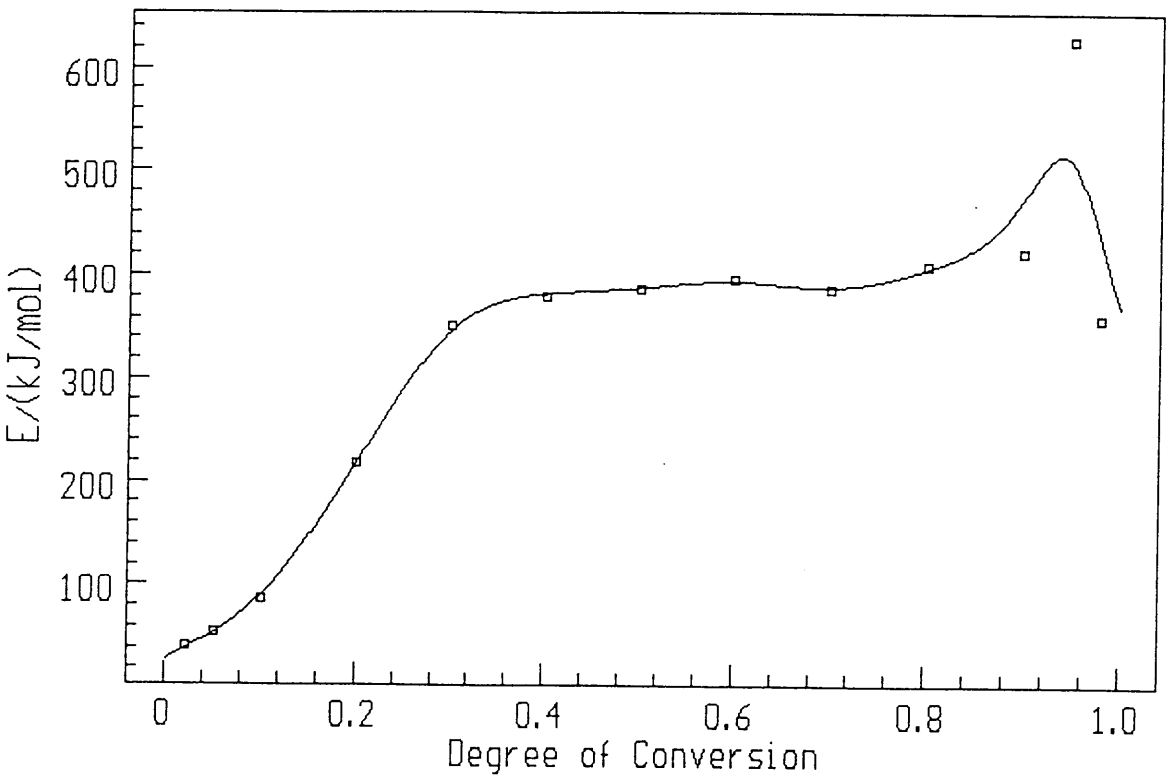

Figure 8.4.2 (a): Plot of activation energy versus fraction decomposed for the calcium hydroxide impurity present in the calcium oxide sample, decomposing in an air/water-atmosphere

The kinetic models are fitted over the $0 < \alpha < 0.3$ and $0.3 < \alpha < 0.95$ range. The best fit is the n-th order kinetic model (figure 8.4.2 (b)) for $0 <$

$\alpha < 0.3$. The correlation coefficient is 0.9455, Durbin-Watson value was 0.250, the activation energy value is 96 kJ mol^{-1} and ln A value of 4. The average activation energy ($\approx$ 40 to 415 kJ mol^{-1} and ln A value $\approx$ 4) obtained from the isoconversional method corresponds very well with that obtained from the kinetic model.

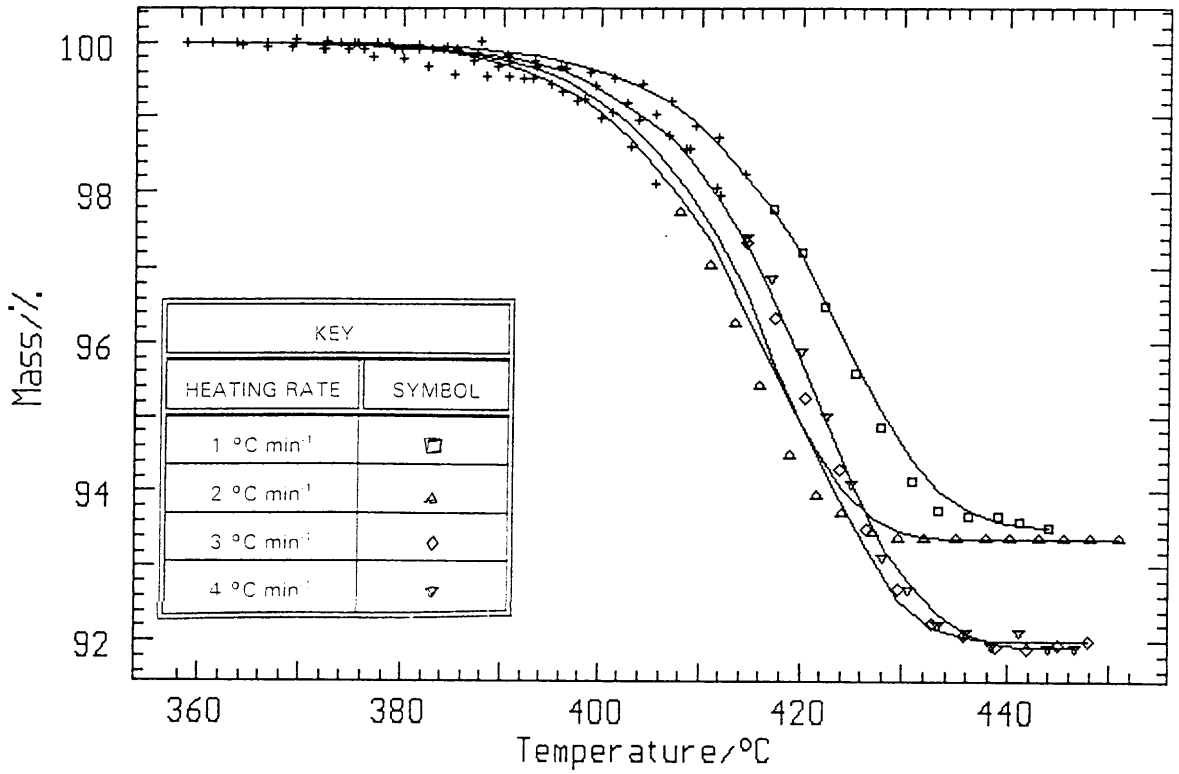

Figure 8.4.2 (b): Fitting of experimental data for $0 < \alpha < 0.2$ for the reaction of the calcium oxide in an air/water-atmosphere, with the kinetic model of the n-th order

For the α-range, $0.3 < \alpha < 0.95$, the first order equation with autocatalysis (figure 8.4.2 (c)) appears to be the best fit with an activation energy value of 412 kJ mol^{-1} and a ln A value of 29 which compare well with the average activation energy of $\approx$ 415 kJ mol^{-1} and a ln A value of $\approx$ 29, obtained from the isoconversional method. The correlation coefficient is 0.9953 with a Durbin-Watson value of 0.130.

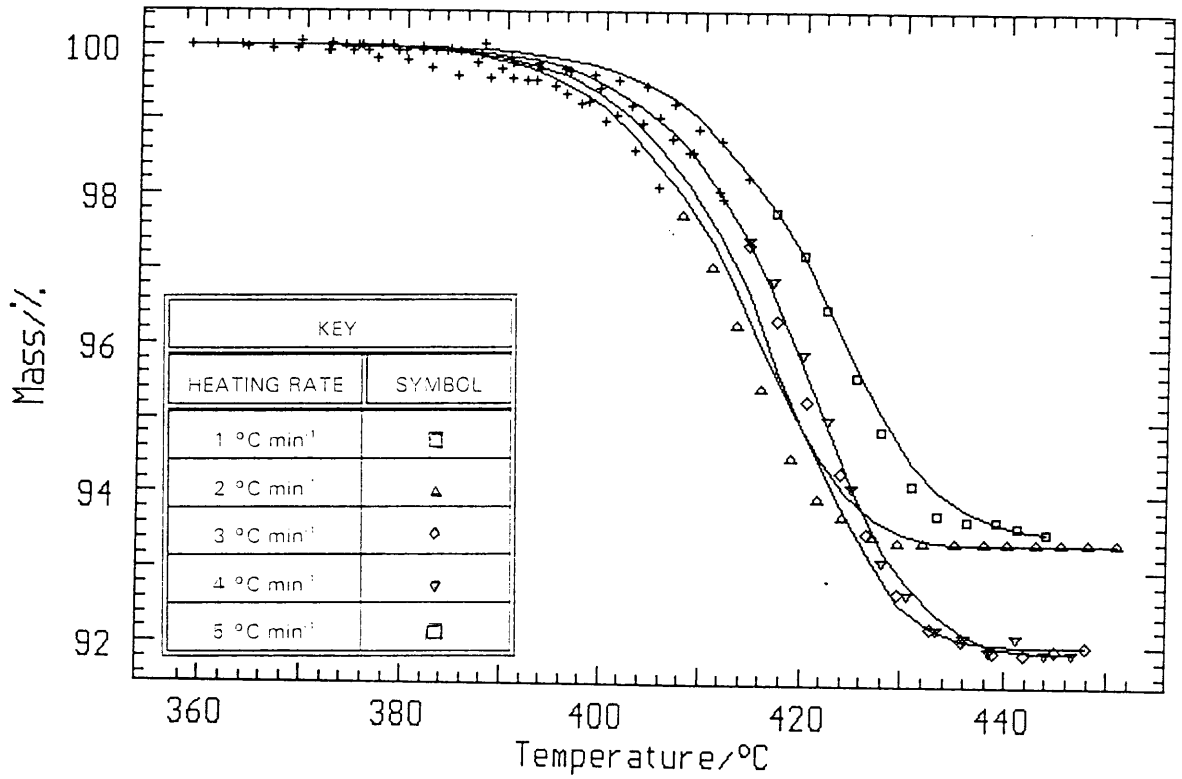

Figure 8.4.2 (c): **Fitting of experimental data for $0.3 < \alpha < 1.0$ for the reaction of the calcium oxide in an air/water-atmosphere, with the first order with autocatalysis kinetic model**

The second mass loss curve is followed over the temperature range of 470 °C to 698 °C. Figure 8.4.2 (d) shows the plot of activation energy versus fraction decomposed.

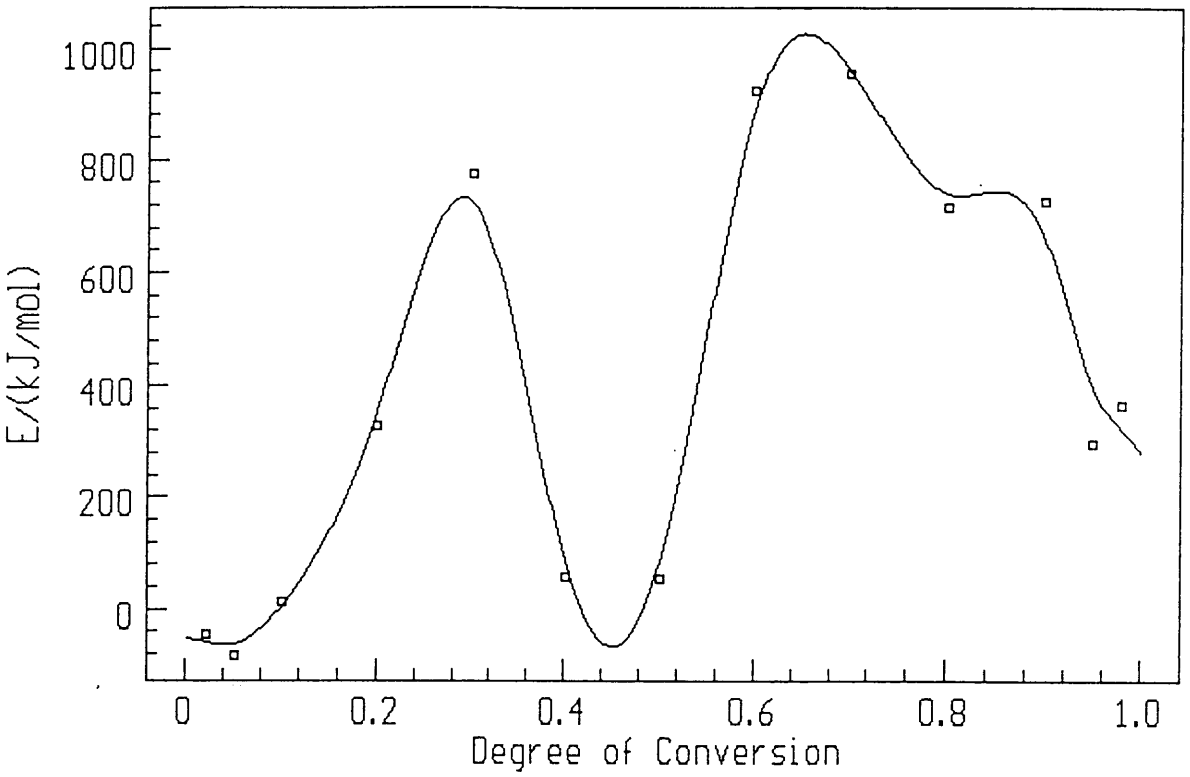

Figure 8.4.2 (d): Plot of activation energy versus fraction of calcium carbonate in calcium oxide decomposed over the temperature range from 470 °C to 698 °C in an air/water-atmosphere

The kinetic models are fitted for the range, $0 < \alpha < 0.3$, $0.3 < \alpha < 0.5$, $0.5 < \alpha < 0.7$ and $0.7 < \alpha < 1.0$. The average activation energy obtained from the isoconversional method increases from ≈ 0 to ≈ 800 kJ mol^{-1} and a ln A value of $\approx$ -2 (refer to Chapter 9.4) for $0 < \alpha < 0.3$. No kinetic models are found to fit the ranges $0 < \alpha < 0.3$ and $0.3 < \alpha < 0.5$ and $0.5 < \alpha < 0.7$. The average activation energy varies from ≈ 800 to 0 kJ mol^{-1} for $0.3 < \alpha < 0.5$ and ≈ 0 to 1000 kJ mol^{-1} for $0.5 < \alpha < 0.7$.

For the α-range, $0.7 < \alpha < 1.0$, there is a decreasing contribution made to the heat absorbed by the reaction with the higher activation energy [85]. The kinetic models which appear to fit the best are the second order equation (activation energy of 371 kJ mol^{-1}, ln A value of 20, a correlation coefficient of 0.9745 and a Durbin-Watson value of 0.056) and the three-

dimensional diffusion equation of Jander. The best fit appears to be that of Jander (figure 8.4.2 (e)). The Jander equation is a diffusion controlled equation. It appears that the diffusion of the water vapour is the rate controlling step. The activation energy value obtained is 399 kJ mol^{-1}, a ln A value of 20, a correlation coefficient of 0.9821 and a Durbin-Watson value of 0.070. The average activation energy value obtained from the isoconversional method is from ≈ 1000 to ≈ 400 kJ mol^{-1} and ln A value is ≈ 28.

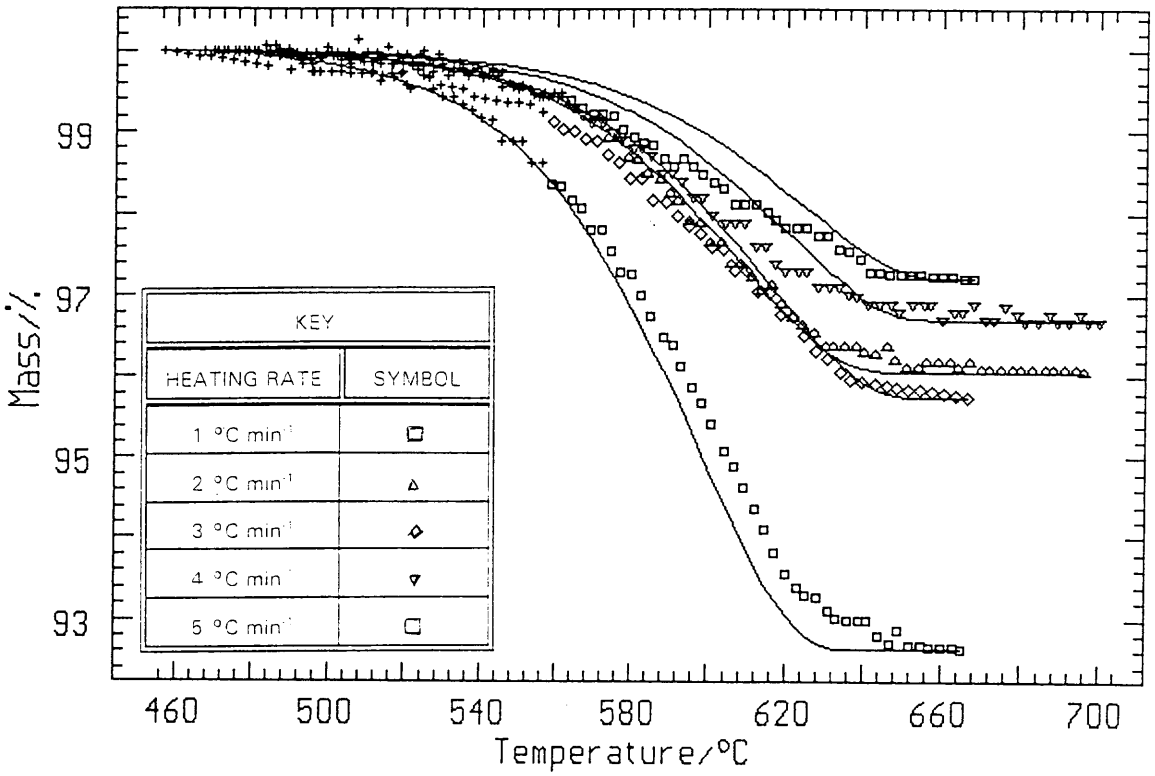

Figure 8.4.2 (e): The three-dimensional diffusion equation of Jander fitted to the experimental data for $0.2 < \alpha < 1.0$ of calcium carbonate impurity present in calcium oxide, decomposing in an air/water-atmosphere

8.4.3 Kinetics of the decomposition reaction of calcium carbonate obtained via the reactions of calcium oxide with a CO_2-atmosphere

The reactions are followed from 870 °C to 980 °C. Figure 8.4.3 (a) shows a plot of activation energy versus fraction decomposed for calcium oxide in a CO_2-atmosphere. From figure 8.4.3 (a), the activation energy increases for the α-range of 0 to 0.1 indicating that the reaction with the higher activation energy makes an increasing contribution to the heat absorbed [85]. The average activation energy increases from ≈ 550 to 901 kJ mol^{-1}.

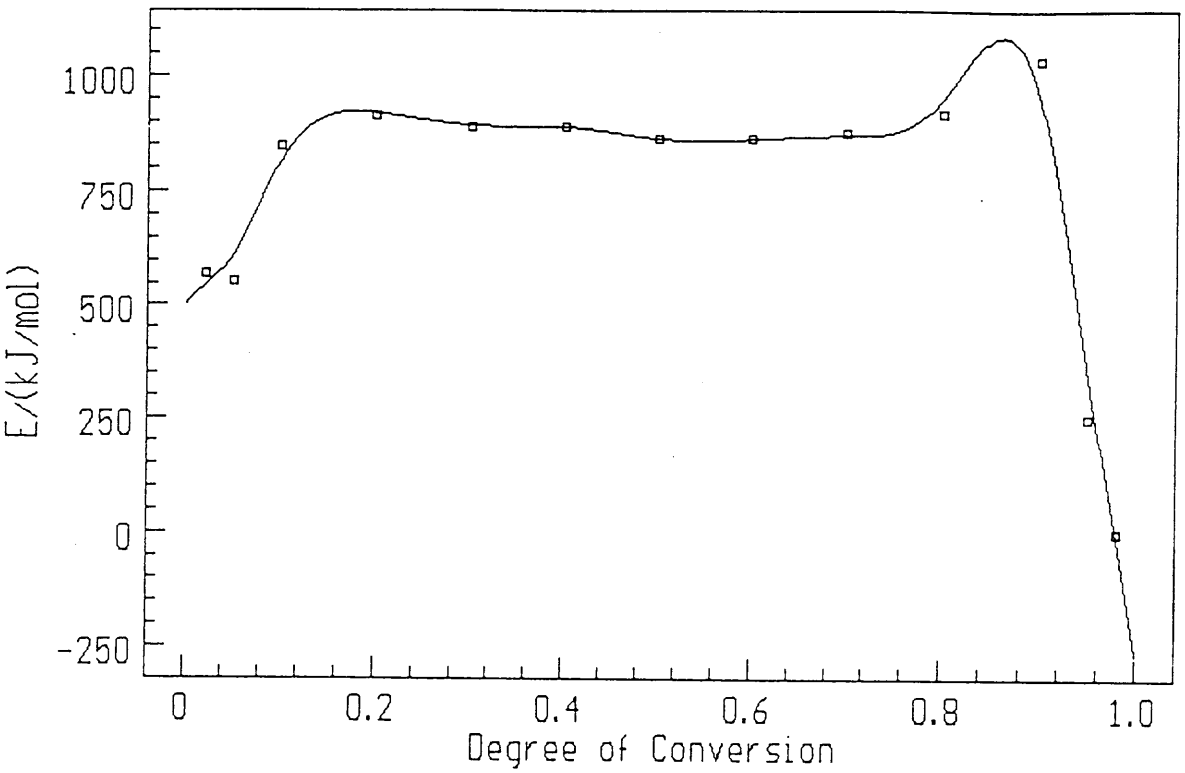

Figure 8.4.3 (a): Plot of activation energy versus fraction decomposed for CaO reacting in a CO_2-atmosphere

There the activation energy remains constant for $0.1 < \alpha < 0.9$. This constant dependence indicates that the reaction is possibly a single-step reaction with an average activation energy of ≈ 901 kJ mol^{-1}. The activation energy then increases slightly and then it decreases sharply indicating that the contribution made by the reaction with the higher activation energy, to the heat absorbed, is decreasing [85]. No kinetic

models are found to fit the ranges $0 < \alpha < 0.1$ and $0.9 < \alpha < 1.0$. The kinetic models are fitted over the α-range of 0.1 to 0.9. The average activation energy obtained from the isoconversional method is ≈ 901 kJ mol^{-1} and a ln A value of ≈ 37. The kinetic models which appear to fit are the following: the Sestak-Berggren equation, the d-dimensional Avrami-Erofe'ev equation (activation energy of 927 kJ mol^{-1}, ln A value of 38.2 ± 0.2, correlation coefficient of 0.9960 and a Durbin-Watson value of 0.111); the first order with autocatalysis (activation energy of 999 kJ mol^{-1}, ln A value of 41, correlation coefficient of 0.9957 and a Durbin-Watson value of 0.110); the n-th order equation (activation energy of 1166 kJ mol^{-1}, ln A value of 49, correlation coefficient of 0.9949 and a Durbin-Watson value of 0.128) and the two-dimensional phase boundary equation (activation energy of 1111 kJ mol^{-1}, ln A value of 46, correlation coefficient of 0.9949 and a Durbin-Watson value of 0.147).

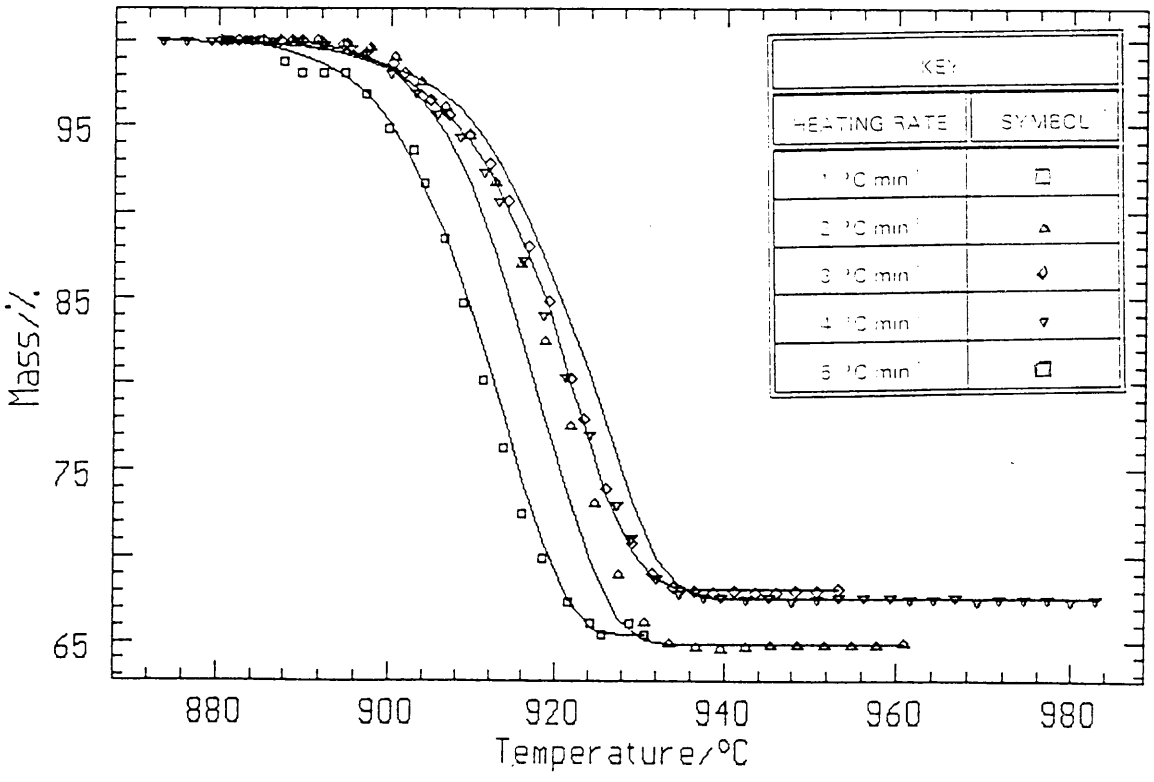

Figure 8.4.3 (b): Fitting of experimental data of the reaction of calcium oxide in a CO_2-atmosphere with the kinetic model of Sestak-Berggren for $0.1 < \alpha < 0.9$

The Sestak-Berggren equation (figure 8.3.4 (b)) appears to be the best fit, with an activation energy of 905 kJ mol^{-1}, a ln A value of 37, a correlation coefficient of 0.9959 and a Durbin-Watson value of 0.113. This fit compares favourably with the data obtained from the isoconversional method.

8.4.4 Kinetics of the decomposition reaction of calcium carbonate obtained via the reactions of calcium oxide with a CO_2/air-atmosphere

These reactions are followed from 865 °C to 940 °C. The kinetic data obtained for the reaction of calcium oxide in a CO_2/air-atmosphere shows a decrease in activation energy from ≈ - 3000 to ≈ - 4100 kJ mol^{-1} (refer to Chapter 9.4) for $0 < \alpha < 0.1$, an increase from ≈ - 4100 to ≈ - 3000 kJ mol^{-1} for $0.1 < \alpha < 0.2$, then an increase from ≈ - 3000 to ≈ 3000 kJ mol^{-1} for $0.2 < \alpha < 0.5$, after which it decreases from ≈ 3000 to ≈ 0 kJ mol^{-1} (figure 8.4.4 (a)).

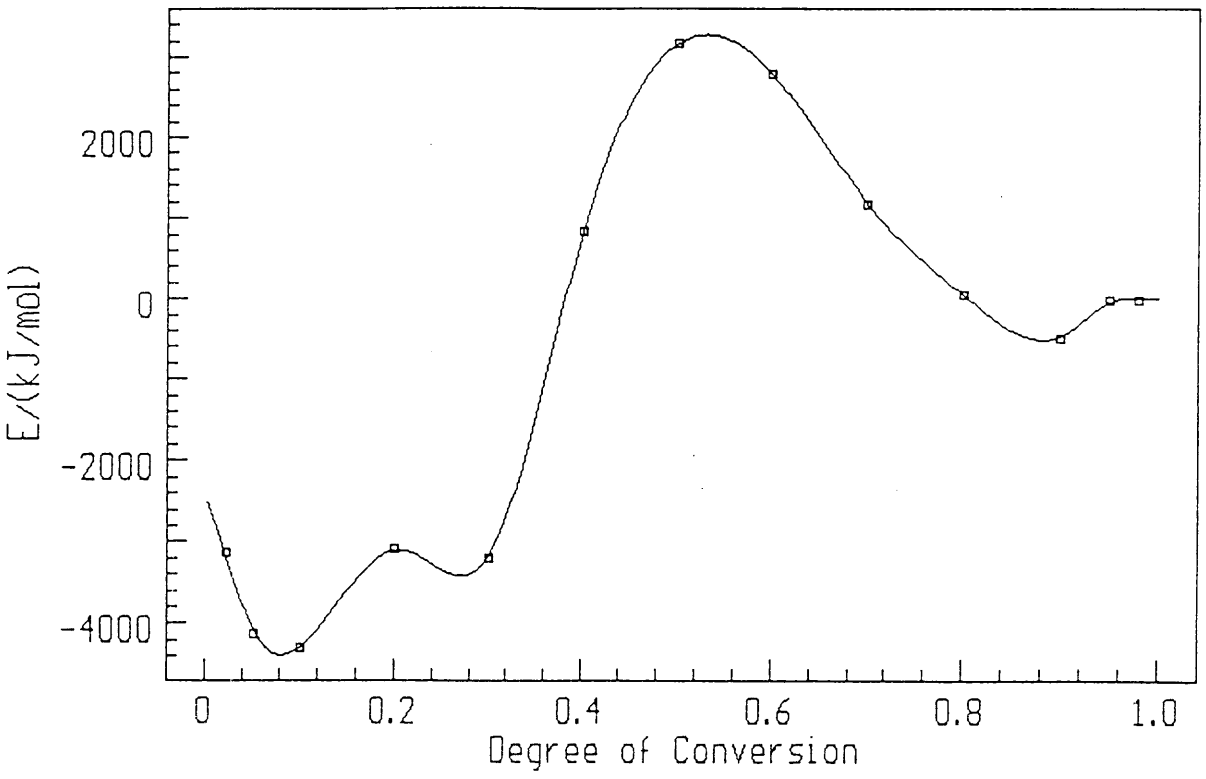

Figure 8.4.4 (a): Plot of E_a vs α for CaO in a CO_2/air-atmosphere

These large negative values for the activation energy are probably due to the fact that there are equilibrium reactions occurring especially in the CO_2-rich atmospheres. The contributions made to the heat absorbed has been discussed in Chapter 8.4.3.

No kinetic models are found to fit the ranges $0 < \alpha < 0.1$, $0.1 < \alpha < 0.2$ and $0.2 < \alpha < 0.5$.

The decomposition reaction for $0.5 < \alpha < 1.0$ can be best described by the three-dimensional diffusion equation of Jander (figure 8.4.4 (b)), with a correlation coefficient of 0.9279, a Durbin-Watson value of 0.185, an activation energy value of 2376 kJ mol^{-1} and ln A of 105. This does not compare well with the average activation energy value of $\approx$ 949 kJ mol^{-1} and ln A value of $\approx$ 46 obtained from the isoconversional method. Thus, this is not a conclusive fit.

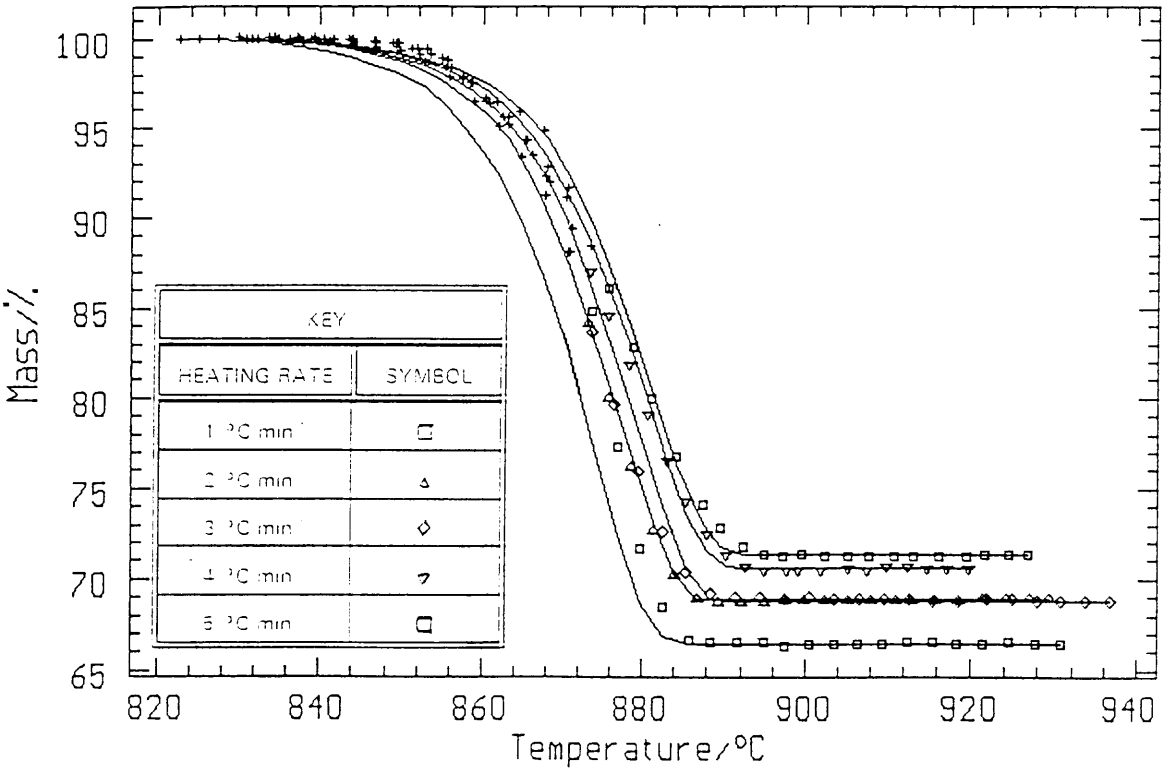

Figure 8.4.4 (b): Fitting of the three-dimensional diffusion equation of Jander for CaO in a CO_2/air-atmosphere for $0.5 < \alpha < 1.0$

8.4.5 Kinetics of the reactions of calcium oxide in a CO_2/water-atmosphere

These reactions of calcium oxide in a CO_2/water-atmosphere are followed from 850 °C to 930 °C. From figure 8.4.5 (a), it is clear that the reaction does not occur in a single step. There is an increase in activation energy from ≈ 300 to ≈ 450 kJ mol^{-1} for $0 < \alpha < 0.2$, after which the activation energy remains constant indicating a single-step reaction for $0.2 < \alpha < 0.6$. There is a decreasing contribution to the heat absorbed by the reaction with the higher activation energy for $0.6 < \alpha < 0.7$ (≈ 450 to 0 kJ mol^{-1}). The activation energy remains constant at ≈ 0 kJ mol^{-1} for $0.7 < \alpha < 0.9$ where it then increases sharply to ≈ 500 kJ mol^{-1} indicating that the reaction with the higher activation energy makes an increasing contribution to the heat absorbed [85]. For $0 < \alpha < 0.2$, $0.6 < \alpha < 0.7$ and $0.9 < \alpha < 1.0$, no kinetic models are found to fit.

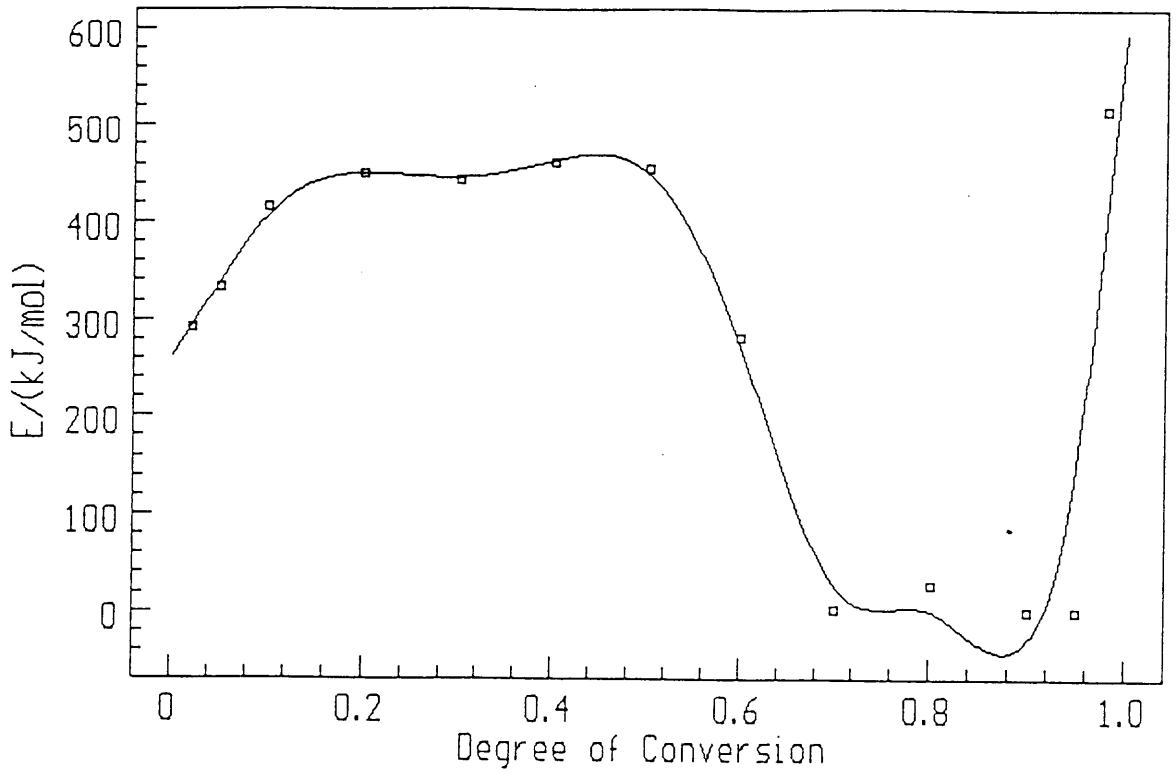

Figure 8.4.5 (a): Plot of activation energy versus fraction decomposed for CaO in a CO_2/water-atmosphere

The best fit for $0.2 < \alpha < 0.6$, appears to be the second order equation

(figure 8.4.5 (b)). It is clear from figure 8.4.5 (b) that the second order equation does not fit for $0.2 < \alpha < 0.6$. When comparing the activation energy value for the second order equation of 1497 kJ mol^{-1} and the ln A value of 65 (the correlation coefficient is 0.79997 and the Durbin-Watson value is 0.166) with those obtained from the isoconversional method (activation energy of $\approx$ 392 kJ mol^{-1} and ln A of $\approx$ 14), it is clear that this model does not fit. For $0.7 < \alpha < 0.9$, no kinetic models fit the experimental data.

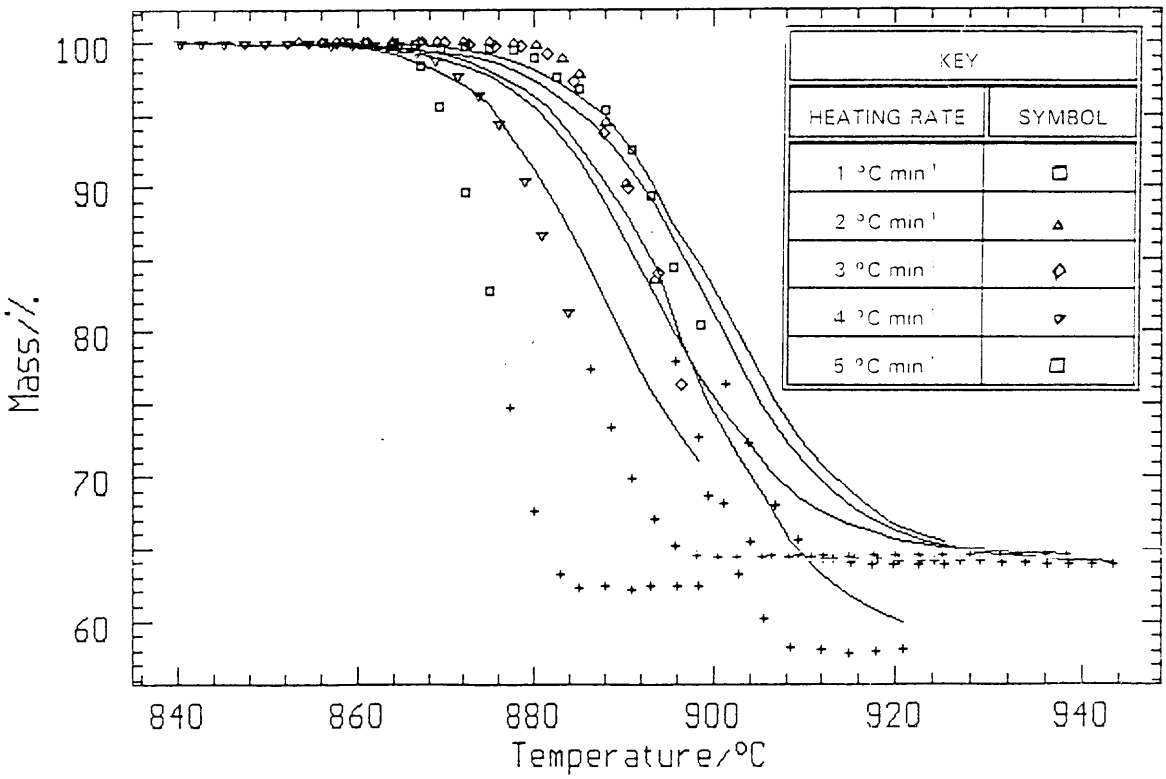

Figure 8.4.5 (b): Fitting of the second order equation for CaO reacting in a CO_2/air-atmosphere for $0.2 < \alpha < 0.6$

There was no second mass loss in the CO_2-, CO_2/air- and CO_2/water-atmospheres. The CaO reaction in these atmospheres was not followed above 950 °C. Thus, it appears that the CO_2-pressure inhibits the decomposition of calcium carbonate and thus, this decomposition reaction was not observed below 950 °C. Table 8.4.1 is a summary of all the kinetic data for the reactions of calcium oxide in different atmospheres.

Table 8.4.1 The kinetic data of the reactions of calcium oxide in different atmospheres

Atmosphere	Temperature Range (°C)	Fraction Decomposed	Kinetic Data from the Isoconversional Method		Kinetic Data from the Kinetic Models			
					Kinetic Model			
			E_a (kJ mol^{-1})	ln A	E_a (kJ mol^{-1})	ln A	D-W	Corr. Coeff.
Air	310 - 450	$0 < \alpha < 0.1$	0 - (-100)	-	no fit			
		$0.1 < \alpha < 0.95$	259	18	n-th order 233	16	0.252	0.9943
					or Sestak-Berggren 211	14	0.327	0.9960
	525 - 700	$0 < \alpha < 0.1$	(- 20) - 100	-	no fit			
		$0.1 < \alpha < 0.5$	(- 100) - 400	-	no fit			
		$0.5 < \alpha < 0.95$	350	14	second order 421	23	0.093	0.9594
Air/water	300 - 450	$0 < \alpha < 0.3$	40 - 415	4	n-th order 96	4	0.250	0.9455
		$0.3 < \alpha < 0.95$	415	29	first order with autocatalysis 412	29	0.130	0.9953
		$0.95 < \alpha < 1.0$	415 - 360	-	no fit			
	470 - 698	$0 < \alpha < 0.3$	0 - 800	-2	no fit			
		$0.3 < \alpha < 0.5$	800 - 0	-	no fit			
		$0.5 < \alpha < 0.7$	0 - 1000	-	no fit			
		$0.7 < \alpha < 1.0$	1000 - 400	28	three-dimensional diffusion equation of Jander 399	20	0.070	0.9821
CO_2	870 - 980	$0 < \alpha < 0.1$	550 - 901	-	no fit			
		$0.1 < \alpha < 0.9$	901	37	Sestak-Berggren 905	37	0.113	0.9959
		$0.9 < \alpha < 1.0$	901 - 0	-	no fit			
CO_2/air	865 - 940	$0 < \alpha < 0.1$	(-3000) - (-4100)	-	no fit			
		$0.1 < \alpha < 0.2$	(-4100) - (-3000)	-	no fit			
		$0.2 < \alpha < 0.5$	(-3000) - 3000	-	no fit			
		$0.5 < \alpha < 1.0$	3000 - 0	46	no fit			
CO_2/water	850 - 930	$0 < \alpha < 0.2$	300 - 450	-	no fit			
		$0.2 < \alpha < 0.6$	450	14	no fit			
		$0.6 < \alpha < 0.7$	450 - 0	-	no fit			
		$0.7 < \alpha < 0.9$	0	-	no fit			
		$0.9 < \alpha < 1.0$	0 - 500	-	no fit			

Key of abbreviations used in the table: E_a = activation energy; D-W = Durbin-Watson value and Corr. Coeff. = correlation coefficient.

CHAPTER NINE

CONCLUSION

9.1 GYPSUM

The dehydration of gypsum is influenced by the dehydration of impurities present in the sample and this has a marked effect on the mass loss curves. The first dehydration reaction of gypsum (pure, synthetic and natural) is the same as reported in the literature [4, 5]:

$$CaSO_4 \bullet 2H_2O\ (s) \rightarrow CaSO_4 \bullet 0.5H_2O\ (s) + 1.5H_2O\ (g)$$

All the products at the end of the first dehydration reaction of the gypsum samples also yielded some $CaSO_4 \bullet 0.15H_2O$. The end product for the second dehydration reaction for all the gypsums is the anhydrite. The calcium sulphate-water bonds appear to be relatively strong as small amounts of the compound, $CaSO_4 \bullet 0.15H_2O$, could still be observed at temperatures up to 450 °C.

It is not possible to obtain negative ln A and activation energy values because the pre-exponential factor reflects the effective collisions that occur during a reaction [88] and activation energy can only be negative if there are overlapping simultaneous reactions taking place of which one must be an equilibrium reaction. The kinetic models that are described appear to fit the experimental data but should not be regarded as a description of the mechanism of the reaction, but only as a mathematical description of the decomposition of the various compounds.

The results obtained from this study on the dehydration mechanism of pure calcium sulphate dihydrate in nitrogen-atmosphere compare with those obtained by Molony [4], Ball and Norwood [5] and Borisenko [30]. The dehydration is diffusion-controlled. The activation energies, however, do not correlate. This study obtained an activation energy of 107 kJ mol^{-1} for the

fraction, $0.1 < \alpha < 0.8$. Ball and Norwood [5] found an activation energy of $246 \geq E_a \geq 144.7$ kJ mol^{-1}.

The dehydration of gypsum in nitrogen-atmosphere appears to be controlled by the rate of nucleation and the diffusion of water vapour. This is in agreement with the literature [40, 41] but the activation energies differ. The activation energies ($94 < E_a < 101$ kJ mol^{-1}) obtained in this study for the synthetically-prepared gypsum and the natural gypsum are lower than the literature values (104 to 502 kJ mol^{-1}).

The activation energy values obtained in the air/water-atmosphere are higher (156 kJ mol^{-1} for calcium sulphate dihydrate, 114 kJ mol^{-1} for synthetic gypsum and 387 kJ mol^{-1} for natural gypsum) than in the nitrogen-atmosphere.

The rate of the decomposition reaction for natural gypsum is faster than that for pure calcium sulphate dihydrate and synthetic gypsum. This is to be expected as the surface area of natural gypsum is larger than that for pure calcium sulphate dihydrate and synthetic gypsum (refer table 7.3).

It is very important to the cement industry to control the amount of gypsum present as well as the hemihydrate content because they influence the setting times and can result in false setting, thus reducing the strength of the cement. It is clear that the atmospheric working conditions can play a vital role in the dehydration and hydration reactions of gypsum. It is found that the mathematical description of the dehydration reaction of gypsum is atmosphere dependent.

The kinetics of the dehydration of gypsum is dependent on the origin of the gypsum and on the impurities found in the various gypsum samples. Natural gypsum has less dihydrate and more hemihydrate and anhydrite present, thus the cement containing it tends to form lumps by reacting with moisture. This leads to the blockages in the silos. Thus, it is necessary to add more dihydrate to the natural gypsum or to rehydrate it.

9.2 CARBONATES

The decomposition reactions of the various limestone samples are controlled by the partial pressure of the CO_2 and by the transfer of CO_2 away from the decomposing sample. This is in accordance with that found in the literature [55]. The reported enthalpies of activation for the decomposition of calcite range from 147 to 210 kJ mol^{-1} [63; 55 respectively]. The heat of the reaction obtained in an air-atmosphere, in this study, is 204 kJ mol^{-1}. The activation energy obtained for Beestekraal , Pienaars River and Lime Acres limestone in an air-atmosphere was 249, 233 and 262 kJ mol^{-1}, respectively. The decomposition and recarbonation reactions of calcium carbonate depend on the diffusion of the CO_2 out of the sample as well as the partial pressure of the CO_2. For complete recarbonation to take place, optimum conditions, namely temperature ($\approx$ 400 °C) and a high CO_2 pressure, are required.

The negative values obtained for the ln A and activation energy for certain of the reactions is an indication of the very complex reactions that are taking place and that some of the reactions were equilibrium reactions which were dependent on the CO_2 and water vapour pressure.

The rate of decomposition for Pienaars River limestone is faster than for Beestekraal limestone, Lime Acres limestone and pure calcium carbonate. From table 7.2, the surface areas for the limestone samples decrease as follows: Pienaars River limestone > Beestekraal limestone > Lime Acres limestone > pure calcium carbonate. As the surface area increases, the rate of decomposition increases.

9.3 CALCIUM HYDROXIDE

From the reaction of calcium hydroxide in the different atmospheres, it was clear that the dehydration and rehydration (formation of calcium hydroxide) and the recarbonation (formation of calcium carbonate) depend greatly on the partial pressure of both water vapour and CO_2. The recarbonation reaction starts as soon as the calcium oxide has formed from the dehydration of calcium hydroxide.

The negative values that are obtained for ln A and the activation energy indicate that some of the reactions are equilibrium reactions. The average activation energy value obtained is higher ($\approx$ 369 kJ mol^{-1}) than the values reported in the literature [72; 73; 74; 75; 76;78; 79;80]. Chen et. al. [72] reported that the Avrami-Erofe'ev equation best describes the decomposition reaction of calcium hydroxide. This study shows that the second order equation or the one-dimensional diffusion equation best describes the decomposition reaction of calcium hydroxide.

9.4 CALCIUM OXIDE

The negative values that are obtained for ln A and activation energy for the reaction of calcium oxide with CO_2 and H_2O in different atmospheres, is also indicative of some equilibrium reactions that occur. The carbonation of the calcium oxide is dependent on the partial pressure of the water vapour and CO_2.

In conclusion, all decomposition reactions investigated during this study, have complex mechanisms, with various intermediate steps. From the activation energy versus fraction decomposed curves, it is clear that different intermediate reactions or steps play a most significant role at different temperatures. This results in preventing any general mechanistic description of the solid state decomposition reactions. The kinetic models, however, can be regarded as mathematical descriptions of the kinetics of the decomposition reactions, since statistically good fits are obtained. The

kinetic expressions had a poor fit in the final stages of the reaction and this could be attributed to a combination of effects which may include particle size, chemisorption of product gases on a residual phase, poisoning, etc. It must, however, be remembered that the conditions of the decomposition (i.e. heating rate, atmosphere, sample size, surface area) play a significant role in the kinetics of the reactions and that results obtained during this study can only be applied to reactions occurring under nearly identical conditions.

REFERENCES

1. D.G. Mantel; **The Manufacture, Properties and Applications of Portland Cements, Cement Additives and Blended Cements**, Penrose Press, PPC, Johannesburg, 1991, p.13.

2. G.C. Bye; **Portland Cement: Composition, Production and Properties,** Pergamon Press, Oxford, 1983, p.19.

3. H.F.W. Taylor; **Cement Chemistry**, Academic Press, London, 1990, p.233.

4. B. Molony and M.J. Ridge; Aust. J. Chem., 21 (4) (1968) 1063.

5. M.C. Ball and L.S. Norwood; J. Chem. Soc., 4 (1969) 1633.

6. D.G. Mantel and D.G. Liddell; World Cement, October (1988) 404.

7. F.L. Smidth; Plant Services Division; International Cement Production Seminar, Lecture 6.3 - **Chemical changes in cement during grinding and storage.**

8. R.S. Boynton; **Chemistry and Technology of Lime and Limestone**, John Wiley and Sons, New York, Second Edition, 1980, p.95.

9. D.G. Mantel; Cement Technology Course; **The Chemistry of Portland Cement**, Johannesburg, May 1995.

10. Netzsch Thermokinetic Analysis Multiple Scan, 2nd edition, Issue 5/93, Netzsch-Gerätebau GmbH, Bayern, Germany, p.2-11.

11. J. Opfermann, G. Wilke, W. Ludwig, S. Hagen, E. Kaisersberger, M. Gebhardt; Globale Analyse der Thermokinetik-ein Weg zu invarianten kinetischen Parametzern bei hoher Modellunterscheidbarkeit, Vortrag zur GEFTA-Tagung, Regensburg, 10 - 12 October 1988.

12. J. Opfermann, G. Wilke, W. Ludwig, E. Kaisersberger, M. Gebhardt, S. Hagen; Beispiele zur Anwendung der globalen Analyse. Poster zur GEFTA-Tagung, Regensburg, 10 - 12 October 1988.

13. C.H. Bamford and C.F.H. Tipper; **Comprehensive Chemical Kinetics - vol 22 - Reactions in the solid state**, Elsevier Scientific Publishing Company, Amsterdam (1980).

14. C.J. Keattch and D. Dollimore; **An Introduction to Thermogravimetry**, Second Edition, Heyden and Son Ltd (1975), p.57.

15. K.C. Kelley, J.C. Southard and C.T. Anderson; **Thermodynamic properties of gypsum and its dehydration products,** Technical Paper 625, United States Department of the Interior, Bureau of Mines, 1941.

16. P. Gay; Mineralog. Mag., 35 (1965) 347.

17. A. Fowler, H. G. Howell and K.K. Schiller; J. Appl. Chem., 18 (1968) 366.

18. J.C. Southard; U.S. Bureau of Mines, Technical Paper 625, 1941, p3.

19. W.A. Wooster; Ztschr Kristal, 94 (1936) 375.

20. P. Gallitelli; Periodica di Mineral, 4 (1933) 132.

21. Dana's System of Mineralogy; 7th edition, II, 476 (1951).

22. R.A. Kuntze; Canadian Jourval of Chemistry, 43(1965)2522.

23. S.K. Mehta; Trans. of the Indian Ceramic Society, 34 (4) (1975) 65.

24. G. Lager; Th. Armbuster, F. Rotella, J.D. Jorgensen and D.G. Hinks, Am. Mineral, 69 (9-10) (1984) 910.

25. O.W. Flörke; Neues Jahrb Mineral, 84 (1952) 189.

26. W. Grahmann; Neues Jahrb min, 1 (1920) 1.

27. D.A. Holdridge and E.G. Walker; Trans. Brit. Ceram. Soc., 66 (1967) 485.

28. J. Kazimir; Chem. zvesti, 30 (2) (1976) 160.

29. V. Satava; Silikaty, 1 (1971) 1.

30. E.M. Borisenko, Gelero Khim Reakt. Inst., Obsheh, i Neorgan Khim, Akad Nauk Belorussk SSSR, (1985) 171.

31. M.J. Ridge and B. Molony; Trans. Faraday Soc., 65 (1969) 1113.

32. S. Gregg and K. Sing; **Adsorption, Surface Area and Porosity**, Academic Press, London, 1967, p. 6.

33. H.G. McAdie; Canad. J. Chem. 42 (1964) 792.

34. J.J. Gardet, B. Guilhot and M. Soustelle; Cement and Concrete Research, 6 (1976) 697.

35. V. Satava; Proc. Int. R.I.L.E.M., (1977) 189.

36. D.G. Mantel, Cement Technology Course, **The Chemistry of Portland Cement**, PPC, Johannesburg, 1995.

37. J. Adams, W. Kneller and D. Dollimore; Thermochimica Acta, 211 (1992) 93.

38. V. Satava and J. Sestak; Anal. Chem., 45 (1) (1973) 154.

39. A.A. Khalil; Thermochimica Acta, 55 (1982) 201.

40. K. Heide; Silikattech, 7 (1969) 232.

41. M. Murat and C. Comel; Tonind Zng, 95 (1) (1971) 29.

42. A. Negro and L. Stafferi; *Sur La aneltique de deshydration de quelques varie'tes de sulfate de calcium dihydrate*, Eurogypsum, Kongress, Stockholm, 1972.

43. V. Vakhlu. P.S. Bassi and S.K. Mehta; Trans. of the Indian Ceram. Soc., 44 (2) (1985) 29.

44. J.E. Bright and M.J. Ridge Phio. Mag., 6 (1961) 441.

45. A.R. Patel and K.S. Raju; Indian J. of Pure and Appl. Physics, 7 (1969) 692.

46. R. Piéce; Science et technique de I industrie du plătre, C.A.S.T. I.N.S.A. Lyon - Villeurbanne, 20-24 Sept 1965.

47. A. Putnis, B. Winkler and L. Fernandez-Diaz; Min. Mag., 54 (1990) 123.

48. M. Murat; Proc. Int. R.I.L.E.M., M. Foucault (ed), 1977, p535.

49. A.W.D. Hills; Chem. Eng. Sci., 23 (1968) 297.

50. Hedin; NR32, Stockholm 1961.

51. O. Bowles; **Limestone and Dolomite**, U.S. Bureau of Mines, I.C. 7738 (1956) 79.

52. D. Graf and J. Lamar; Econ. Geol, 50 (1955) 639.

53. C.N. Satterfield and F. Feakes; AICHE J., 9 (1959) 115.

54. P.K. Gallagher and D.W. Johnson; Thermochimica Acta, (1973) 67.

55. D. Beruto and A.W. Searcy; J. Chem. Soc. Faraday Trans., 70 (1) (1973) 2145.

56. E.K. Powell and A.W. Searcy; Met Trans., 11B (1980) 427.

57. P.K. Gallagher and D.W. Johnson; Thermochimica Acta, 14 (1976) 255.

58. K.M. Caldwell, P.K. Gallagher and D.W. Johnson; Thermochimica Acta, 18 (1977) 15.

59. G. Narsimhan; Chem. Eng. Sci., 16 (1961) 7.

60. V.I. Koloberdin, V.N. Blinichev and V.V. Strel'tsov; Int.Chem. Eng., 15 (1975) 101.

61. C. Slonim; Z. Elektrochem., 36 (1930) 439.

62. H. Kappel and G. F. Hüttig; Kolloid Z., 91 (1940) 117.

63. H.T.S. Britton, S.J. Gregg and G.W. Winsor; Trans. Faraday Soc., 48 (1952) 63.

64. T.R. Ingraham and P. Marier; Canad. J. Chem. Eng., 41 (1963) 179.

65. J.H. Sharp and S.A. Wentworth; Anal. Chem., 41 (1969) 1614.

66. A.L. Draper and L.K. Sveum; Thermochimica Acta, 1 (1970) 345.

67. I.B. Cutler in W.D. Kingery (Ed); **The Kinetics of High Temperature Processes**, Wiley, New York, 1959, p294.

68. J.T. Lee, T.C. Keener, M. Knoderer and S.J. Khoney; Thermochimica Acta, 213 (1933) 223.

69. Z. Asaki, Y. Fukunaka, T. Nagase and Y. Kondo; Met. Trans., 5 (1974) 381.

70. J. Splichal, St. Skramovsky and J. Goll; Coll. Czech. Chem. Comm., 9 (1937) 302.

71. Ihsan Barin; "**Thermochemical Data of Pure Substances - Part I**", Second Edition, VCH Verlagsgesellschaft mbH, D - 6940 Weinheim, 1993.

72. D. Chen, X. Gao and D. Dollimore; Thermochimica Acta, 215 (1993) 65.

73. J.M. Criado and J. Morales; J. Therm. Anal., 10 (1976) 103.

74. J.N. Mayock and J. Skalny; Thermochimica Acta, 8 (1974) 167.

75. N.G. Dave and S.K. Chopra; J. Am. Ceram. Soc., 49 (1966) 575.

76. M.S. Murthy, P. Raghavendrachar and S.V. Sriram; Solar Energy, 36 (1) (1986) 53.

77. I. Fujii and K. Tsuchiya; Altern. Energy Sources, 9 (1982) 4021.

78. P.E. Halstead and A.E. Moore; J. Chem. Soc., (1957) 3873.

79. R. Sh. Mikhail, S. Brunauer and L.E. Copeland; J. Coll. Int. Sci., 21 (1966) 394.

80. D. Dollimore, G.A. Gamlen, G.R. Heal and P.F. Rodgers; Proc. Eur. Symp. Therm. Anal. 2nd, (1981) 489.

81. D. Cazorla-Amaros, J.P. Joly, A. Linares-solano, A. Marcilla-Gomis and C. Salinas-Martinez de Lecea; S. Phys. Chem., 95 (1991) 6611.

82. R.L. Blaine and P.G. Fair; Thermochimica Acta, 67 (1983) 233.

83. T. Ozawa; Bull. Chem. Soc. Jpn., 38 (1965) 1881.

84. J.H. Flynn and L.H. Wall; Polym. Lett., 4 (1966) 323.

85. S. Vyazovkin; Thermochimica Acta, 236 (1994) 1.

86. S.V. Vyazovkin, V.V. Bogdanova, I.A. Klimovtsova and A.I. Lesnikovich; J. of App. Polym. Sci., 44 (1992) 2157.

87. P.W. Atkins; **Physical Chemistry**, Oxford University Press, Oxford, Fifth Edition,1992, p878.

88. S.V. Vyazovkin and A.I. Lesnikovich; Thermochimica Acta, 165 (1990) 273.

89. S. Vyazovkin; Thermochimica Acta, 000 (1993) 1.